The Dissertation Committee for Benjamin James Andrews certifies that this is the approved version of the following dissertation:

Recharge, Decompression, and Collapse: Dynamics of Volcanic Processes

Committee:

James E. Gardner, Supervisor

William Carlson

John Lassiter

Todd Housh

Jose Luis Macias

David Mohrig

Recharge, Decompression, and Collapse: Dynamics of Volcanic Processes

by

Benjamin James Andrews, B.S., M.S.

Dissertation

Presented to the Faculty of the Graduate School of

The University of Texas at Austin

in Partial Fulfillment

of the Requirements

for the Degree of

Doctor of Philosophy

The University of Texas at Austin

May 2009

Acknowledgements

Many individuals and organizations contributed invaluable assistance to the research and writing of this dissertation. My advisor and co-author, Jim Gardner, is foremost among them. I first met Jim seven years ago when he picked me up at the Fairbanks Airport after midnight for a visit to the University of Alaska Fairbanks. Several months later, as a UAF graduate student, I went with Jim, Pavel Izbekov, and Steve Tait to Kamchatka to study Ksudach Volcano. That trip introduced me to physical volcanology field methods (techniques that often resemble hole-digging), and started me thinking about the simultaneous eruption of buoyant plumes and pyroclastic flows. Through my entire graduate career, Jim has provided insightful comments and helped me focus my research on new and exciting projects. I have found that we do not always see research questions in the same way and that Jim is not afraid to shoot down the print versions of my more speculative ideas. As a result, although my papers usually emerge from Jim's office hemorrhaging red ink, my writing has improved and I am able to explain my research to critical audiences. I am grateful to Dr. Jim Gardner for giving me field, laboratory, and teaching opportunities over the past years to become a better scientist and teacher.

My committee members have all contributed time and insights to the research that composes this dissertation. Todd Housh helped develop a routine for Laser Ablation ICP-MS analysis of strontium isotopes in plagioclase. Without his help, the first chapter of this dissertation would never have happened. Todd also taught me how to run the laser and the Isoprobe and do column chemistry, thereby giving me an appreciation of both the

fun and tedious sides of isotope geochemistry. Bill Carlson's course on thermodynamics provided a primer on, well, thermodynamics that has been useful in all aspects of my research. In addition, conversations with Bill about diffusion have helped me think about crystal residence times. Although John Lassiter's comments regarding my isotopic data have given me several headaches, they have helped to improve my laser ablation data set and my understanding of isotopic analyses. Jose Luis Macias contributed to my research on El Chichón in many ways, perhaps most importantly by helping us get samples and organizing a conference and JVGR special issue commemorating the 25th anniversary of El Chichón's 1982 eruption. That conference and publication helped me coalesce many of my ideas regarding the Chichón magmatic system. David Mohrig, the resident fluid dynamicist on my committee, helped me recognize the importance of the gradient Richardson number in characterizing length scales of entrainment and refine the eruption column model presented in Chapter 3.

Pavel Izbekov has been involved with my work at Ksudach volcano from the first trip there in 2002. His initial experiments and analyses laid the groundwork for my decompression experiments presented in Chapter 2. Larry Mack provided assistance with TIMS analysis of microdrilled samples. As the UT Geology Librarian, Dennis Trombatore provided me with excellent assistance and advice in obtaining and using images of the Mount St. Helens eruption. Kitty Milliken familiarized me with many of the quirks of the JEOL Superprobe, helping me analyze the compositions and textures of natural and experimental samples. Jose Luis Arce helped organize the El Chichón conference in San Cristobal and provided samples of many eruptions. Paul Wallace of the University of Oregon graciously allowed me to use his FTIR instrument to analyze Ksudach melt inclusions. Frank Tepley and Frank Spera provided me with valuable

reviews of the El Chichón manuscript that improved the paper in many ways. Larry Mastin gave me suggestions regarding his open-source conduit model, Conflow, which helped immensely in balancing estimates of mass flux and ascent rate in the Ksudach eruption conduit.

During my time in Texas, I have collaborated with many of fellow graduate students. Those collaborations have helped with my own research and, hopefully, with theirs. Brandon McElroy helped me develop a MatLab program to analyze the velocity field data collected with FlowJ and Ryan Ewing gave me ideas about particle sorting and helped me with ArcGIS. With those two I was also able to broaden my research interests to aeolian star dunes. Giovanni Sosa has been a great officemate and colleague to bounce ideas off of regarding magma chamber dynamics and volcanological processes. John Singleton, Kathy Goepfert, and Matt Carter, helped me sieve samples and Elke Baitis helped to prepare crystals for FTIR analysis. I hope to collaborate with many of these people in years to come.

Some of the best experiences I had as a graduate student occurred during field courses. I learned a great deal about teaching and fieldwork while working as a TA for Mark Helper at field camp. Mark and Randy Marrett showed me how to organize and run a safe and excellent field program. I look forward in future years to putting many of those lessons into practice when designing my own fieldtrips and courses.

The Jackson School of Geosciences funded my research and studies for the past 5 years through a generous support package. That support enabled me to teach laboratory and field classes, engage in my own research, and attend conferences to present my research. In addition, I was the beneficiary of Banks Scholarships, the Glenn and Martha

Vargas Endowed Presidential Scholarship, and a UT Presidential Scholarship. I am honored to have received those awards.

The National Science Foundation partially funded my research, particularly through grants EAR-0408896 (El Chichón) and EAR-0711043 (Ksudach and MSH), and recently funded my NSF Earth Sciences Postdoctoral Fellowship proposal. I am grateful to the USGS Cascades Volcano Observatory CVO and the Community Foundation of Southwest Washington for awarding me a Kleinman Research Fellowship in 2006 that enabled me to spend 3 weeks in the field at St. Helens. The Oregon Historical Society provided video of the 18 May 1980 Mount St. Helens eruption, making Chapter 3 possible.

Philip Guerrero has been a good friend and resource during the past 5 years. He has helped me navigate paperwork, the UT bureaucracy, and the rules that govern the Geology Department. With a couple of phone calls he was able to help me straighten out a delayed paycheck, turning what would have been a 2 week wait into a mere 2 hour delay. His timely emails and reminders regarding registration and deadlines saved me many times. Thank you, Philip, for helping me keep all of my ducks in a row.

My parents and my brother worked as field assistants for me during August 2006. With their help I was able to collect samples from locations I otherwise would not have reached and I thoroughly enjoyed showing them around Mount St. Helens. I would also like to thank my folks for financial support that helped me move to Texas and make rent my first month.

Willow d'Bär contributed in many small ways to my research and demonstrated how to sink one's teeth into a problem.

Lastly, I would like to thank April DeRome for her love and support during the writing of this dissertation. I don't have adequate words to describe how grateful I am to have known her during the past two years. Quite simply, April is a joy to be around and she makes me a better person.

Cheers! Go Ducks! Go Nanooks! Hook 'em!

Recharge, Decompression, and Collapse:
Dynamics of Volcanic Processes

Publication No._____

Benjamin James Andrews, Ph.D.
The University of Texas at Austin, 2009

Supervisor: James E. Gardner

Non-linear volcanic and magmatic processes control the occurrence and behavior of volcanic eruptions. Consequently, understanding the responses of volcanic systems to processes of different length scales, timescales, and magnitudes is critical to interpreting ancient deposits, understanding current eruption dynamics, and predicting future activity. Here I present the results of three studies wherein analytical geochemistry, experimental petrology, and turbulent flow analysis describe otherwise obscured volcanic processes.

Injections of new magma are common events in magma chambers. Recharging magma can change the chamber composition and temperature and may facilitate assimilation of country rock. Plagioclase phenocrysts provide an opportunity to examine recharge and assimilation processes, because their compositions are sensitive to temperature and their Sr isotopic ratios can record compositional variations in the chamber. Chemical and isotopic microanalyses of crystals from 7 eruptions of El

Chichón Volcano, Mexico, reveal that recharge and assimilation events are very common and mixing is efficient, but individual events seldom affect the entire chamber.

During every eruption, magma decompresses and ascends through a conduit from a chamber at depth to a vent at the surface. Changes in pumice textures during the 1800 ^{14}C yr BP eruption of Ksudach Volcano, Kamchatka, suggest that conduit structure changed following caldera collapse. Decompression experiments show that the post-collapse pumice decompressed at ~0.0025 MPa/s, compared to pre-collapse decompression rates of >0.01 MPa/s. By balancing those results with eruptive mass fluxes I quantify the effects of caldera collapse on a conduit, and show that collapse resulted in a conduit with a very broad base and narrow vent.

Turbulent air entrainment controls whether an eruption column rises buoyantly or collapses to generate pyroclastic flows. Through extensive re-evaluation of video and photographs of the 18 May 1980 eruption of Mount St. Helens, I report the first measurements of the turbulent velocity field of a volcanic column and show that changes in its turbulence reflect changes in eruption behavior. Those results indicate collapse was caused by a reduction in eddy size and turbulent air entrainment initiated by an increased vent size and the development of a buoyant annulus surrounding a dense, collapsing core.

Table of Contents

Introduction

Volcanic eruptions are spectacular and often devastating natural events. The character of any eruption is a product of myriad non-linear processes in the magma chamber, eruption conduit, and atmosphere. For example, whereas a small magma recharge event might be "absorbed" by a magma chamber, a larger event might trigger an eruption (e.g. Sparks et al., 1977; Pallister et al., 1992; Snyder, 2000). Or, fast magma decompression and ascent from the chamber is likely to result in explosive eruption, but slow decompression may result in effusive eruption of that same magma (e.g. Castro and Gardner, 2008; Gonnermann and Manga, 2007). Similarly, increasing the eruptive mass flux results in increased eruption plume height until a critical eruptive mass flux is exceeded, at which point the eruption column collapses and generates pyroclastic flows (e.g. Sparks, 1986). Understanding the magnitudes, length scales, and timescales of volcanic processes and the response of the system as a whole to those processes is thus required for understanding and predicting volcanic eruptions.

Our knowledge of specific volcanic processes and responses of volcanic systems to perturbations is, however, still developing. Although we know that arc magmatic systems are commonly recharged, the character and frequency of those recharge events and the thermal and compositional effects on the host magma are not fully known. During every eruption, magma ascends from a chamber at depth to the surface, but in spite of the ubiquity of this process and the controls it exerts on eruption behavior, we have a poor understanding of magma decompression and ascent rates and how they might change during an eruption. Lastly, although we recognize that turbulent air entrainment controls whether a column rises buoyant or collapses to generate pyroclastic flows, the

velocity field of an eruption column has never been described, and thus our models of eruption columns are only partly constrained by geologic observations.

This dissertation examines volcanic processes and the transient effects of those processes on the larger volcanic system through a series of three papers. The first paper examines magma recharge events at El Chichón volcano, and shows that recharge and assimilation events occur much more frequently than eruptions, and individual phenocrysts provide unique magma thermal and compositional histories. The effects of caldera collapse on magma decompression rate during the most recent caldera-forming eruption of Ksudach volcano are the focus of the second paper where I demonstrate that the conduit geometry changed during and after collapse, resulting in a greatly reduced magma decompression rate. The final paper uses the 18 May 1980 eruption of Mount St. Helens as a case study of partial eruption column collapse and presents the first quantitative descriptions of the turbulent velocity field of an eruption column.

MAGMA RECHARGE AND ASSIMILATION AT EL CHICHÓN

Magma recharge events commonly occur at arc volcanoes. Evidence of recharge and assimilation processes can be seen in oscillatory zoned phenocrysts, seismic signals, and outcrops of exhumed chambers. Indeed, recharge, assimilation, and accumulation are the processes that lead to the development of large volumes of andesitic to silicic magma, and in some instances, recharge may trigger eruptions (e.g. Sparks et al., 1977; Pallister et al., 1992). Clearly then, it is important to understand not only the composition and temperature of a recharging magma, but also the size and frequency of recharge events and their effects on the host magmatic system.

El Chichón volcano in Chiapas Mexico is uniquely suited for studies of magma recharge and assimilation because the same composition magma, stored at the same conditions, has been erupted many times over the past >8000 years. This effectively makes El Chichón a laboratory for recharge and assimilation processes. Previous workers have shown that the system is recharged by an isotopically primitive magma, but their work indicates a relatively simple history of recharge and assimilation (Tepley et al., 2000). In this dissertation, I examine the thermal and compositional histories recorded by individual plagioclase phenocrysts from multiple eruptions at El Chichón and show that each crystal in a single pumice preserves a different thermal and compositional record. Those results indicate that not only are recharge events at El Chichón much more frequent than eruptions, but different phenocrysts record the same recharge event differently according to their proximity to the recharging magma. One implication of this research is the thermal and compositional histories of individual phenocrysts are not representative of the entire magma chamber.

SYN-ERUPTIVE CHANGES IN DECOMPRESSION RATE AT KSUDACH

In every eruption, magma ascends from a chamber at depth to the surface where it erupts. Because the product of magma density, conduit area, and ascent rate is the eruptive mass flux, ascent rate strongly influences mass flux and thus the buoyancy of explosive eruption columns. Various numerical models show that rates of magma ascent and decompression and scale with conduit size, such that, all else being equal, magma ascends faster through broader conduits (Mastin and Ghiorso, 2000; Jaupart, 2000). But when eruptive mass flux changes during an eruption, what parameters change? That is, if

mass flux increases, is it because the conduit widened and ascent rate increased? In addition, how does caldera collapse affect conduit geometry and decompression rate?

The second paper in this dissertation uses the 1800 ^{14}C yr BP eruption of Ksudach volcano, Kamchatka, to examine changes in conduit geometry and ascent rate coincident with caldera collapse. The eruption provides an excellent opportunity to study syn-eruptive changes in decompression rate because the texture of erupted pumice changed at the beginning of caldera collapse. Using decompression experiments, I correlate the observed textures with decompression rate, and show that decompression slowed by a factor of ~4 after the caldera began to form. Interestingly, the mass flux did not significantly decrease at that time. Mass balance arguments thus suggest that the conduit must have widened, but a broader conduit would result in increased decompression and ascent rate. The most reasonable means of balancing mass flux and decompression rate during the post-collapse phase of eruption is to allow the conduit to be non-cylindrical. Our results provide the first description of the effects of caldera collapse on conduit geometry and suggest that conduits with broad bases and constricted upper regions may feed some eruptions.

TURBULENT DYNAMICS OF ERUPTION COLUMNS: MOUNT ST. HELENS

Every explosive eruption exits the volcanic vent denser than the atmosphere. If that erupting jet entrains and heats enough air to become buoyant before exhausting its upward momentum, it will rise buoyantly as a plume (e.g. Sparks, 1986). If the jet does not entrain enough air, it will collapse and generate devastating pyroclastic flows. We know that turbulence at the eruption column margins is responsible for air entrainment, but no quantitative descriptions have ever been made of those eddies. Moreover, because

we cannot see inside of a column, we do not understand the internal structure of eruption columns. Recent numerical models have been published that describe buoyant, non-buoyant, and partially collapsing column behavior as functions of vent radius, volatile content, or exit velocity (e.g. Neri et al., 2003; Suzuki et al., 2005; Ogden et al., 2008). Unfortunately, those models are unconstrained by observations of the turbulent structure of eruption columns.

In the final paper of my dissertation, I present quantitative descriptions of turbulence in the 18 May 1980 Mount St. Helens eruption column and relate changes in turbulence to partial column collapse. Because previous workers have described the eruption chronology (Christiansen and Peterson, 1981; Criswell, 1987) and mass fluxes (Carey et al., 1990), and numerous photographs and video of the eruption were taken, the eruption is ideal for this study. Through analysis of photographs and video, and optical flow velocimetry of select portions of video, I present measurements of the length scales (eddy size) and deviatoric velocities of the column margins during both buoyant behavior and partial column collapse. Those measurements show that eddies were larger and deviatoric velocity was lower when the column was wholly buoyant, than during partial column collapse. During partial column collapse, the eruption column width and mass flux also increased. I interpret those changes to indicate that an increase in vent radius led to partial collapse as the column developed an annular structure with a buoyant rising outer layer surrounding a denser, partially collapsing inner region. Significantly, my results suggest that complex feedbacks exist between vent size, eddy size, and column behavior, such that once collapse begins, eddy size and the rate and efficiency of air entrainment decrease.

NON-LINEAR DYNAMICS OF VOLCANIC SYSTEMS

Non-linear responses to different perturbations underlie each of the papers composing this dissertation. In each instance, I examine the response of an essentially stable system to a transient process and/or changes in boundary conditions. These papers describe instances where a system is able to buffer or absorb most perturbations, as well as instances where a significant change in behavior occurred. Although these papers will no doubt raise as many questions as they address, they help to illuminate the boundaries between different types of responses to transient volcanic and magmatic processes.

Chapter 1: Repeated Recharge, Assimilation, and Hybridization in Magmas Erupted from El Chichón as Recorded by Plagioclase and Amphibole Phenocrysts

Compositional and isotopic zoning patterns in plagioclase and amphibole phenocrysts from El Chichón record multiple cycles of country rock assimilation, magma injection, hybridization, and mixing. Laser ablation ICP-MS and electron microprobe analyses of plagioclase crystals from 7 eruptions spanning 3100 years reveal four types of zoning. These compositional and isotopic zones are often associated with textural changes observed in the crystals in thin section (e.g. sieved or patchy regions). Amphiboles are frequently zoned in Al and Si, and, in two magmas, may have clinopyroxene rims. Interestingly, most plagioclase show multiple and repeated zoning patterns. Moreover, all magmas contain all zoning patterns and textures, and crystals with substantially different sequences of zones occur within mm of one another. The most reasonable explanation for the origin of these textures is a frequently recharged chamber. Plagioclase zones with increasing anorthite contents (*An*) and decreasing $^{87}Sr/^{86}Sr$ ratios record injection by a hotter, possibly wetter, and more primitive magma (lower $^{87}Sr/^{86}Sr$ ratio). Zones with decreasing *An* and increasing $^{87}Sr/^{86}Sr$ ratios record assimilation of country rock and/or hybridization of the host and injected magmas; injection of hot magma may provide the heat for country rock assimilation. Changes in *An* without corresponding changes in $^{87}Sr/^{86}Sr$ ratio likely record slight variations in pressure or temperature during crystallization, or the far-field thermal effects of magma injection. Variations in $^{87}Sr/^{86}Sr$ ratio unaccompanied by *An* zoning record assimilation

of country rock. Amphibole zoning patterns also record periodic heating events; amphibole with clinopyroxene rims record episodes where the magma was heated beyond the amphibole stability field. Bulk compositional homogeneity and the juxtaposition of many crystals with disparate zoning patterns in single pumice require the magmatic system to be well-mixed. Strontium diffusion rates indicate that the plagioclase zoning patterns cannot have persisted at magmatic pressures and temperatures for more than ~500 years, thus cycles of injection and assimilation occur on timescales equal to or shorter than the eruption recurrence interval. Long-term compositional and isotopic homogeneity indicate that there is a balance between recharge, assimilation, and crystallization.

1.1 INTRODUCTION

Most arc stratovolcanoes erupt a range of magma compositions (Gardner et al., 1995a; Hobden et al., 1999; Volynets et al., 1999). Because bulk composition of any given magma reflects the cumulative effects of crystallization, country rock assimilation, and magmatic recharge, changes in that composition may be used to study the net rates or volumes at which magmatic processes operate (e.g. DePaolo, 1981; Spera and Bohrson, 2004; Zellmer et al., 2005). There are, however, problems with using bulk composition to describe the details of magmatic history. Primarily, because bulk composition represents the net result of different magmatic processes, it can be difficult to identify and quantitatively describe the effects of a particular process (e.g. magma recharge), particularly if the magma is completely hybridized. Secondly, bulk compositional studies can do little to elucidate the magmatic histories of volcanoes that display relatively long-term compositional homogeneity (Tepley et al., 2000).

Fortunately, because the isotopic composition of magmas can be changed by only recharge and assimilation (and not fractional crystallization), and those two processes may be expected to have different effects (e.g. recharge by a primitive magma might decrease bulk $^{87}Sr/^{86}Sr$, whereas assimilation of continental crust should increase $^{87}Sr/^{86}Sr$), isotopically zoned crystals may preserve a record of assimilation and recharge events (Tepley et al., 1999; Tepley et al., 2000; Davidson et al., 2001; Ramos et al., 2005). Moreover, a separate record of crystallization, assimilation, and recharge is recorded in compositionally zoned phenocrysts because major and trace element compositions of the crystallizing phenocrysts are strong functions of melt temperature and composition (e.g. Tsuchiyama, 1983; Holland and Blundy 1994; Gardner et al., 1995b; Bachman and Dungan, 2002; Cortes et al., 2005; Holtz et al., 2005). Using isotopic and elemental crystal zonation patterns I have tried to elucidate the magmatic history of El Chichón Volcano, a volcano that has erupted magmas that have changed little compositionally and isotopically for at least the past 3100 years (McGee et al., 1987; Espindola et al., 2000; Tepley et al., 2000; Macias et al., 2003; *this work*).

I combine bulk compositional and isotopic analyses with plagioclase and hornblende zonation patterns from 7 different eruptions, spanning at least 3100 years (Tilling et al., 1984; Espindola et al., 2000). All magmas erupted are trachyandesitic, with variations of only ~2 wt% SiO_2, ~0.3 wt% MgO, and <0.4 wt% K_2O, and essentially homogeneous isotopic ratios (Tilling et al., 1984; Espindola et al., 2000; Tepley et al., 2000; Macias et al., 2003; *this work*). Despite that relative homogeneity, plagioclase phenocrysts exhibit complex internal zonations in anorthite content (*An*) and $^{87}Sr/^{86}Sr$ ratios. I speculate that recharge by relatively hot, primitive magma or assimilation of radiogenic crust and then subsequent magma hybridization and circulation can explain

the observed zoning patterns. Interestingly, multiple zonation patterns are found within single crystals, and crystals with very different zonation patterns occur millimeters apart within the same pumice, indicating the El Chichón magmatic system has been recharged numerous times and is well-mixed. Recharge events are likely responsible for most mixing within the system. Rates of recharge-driven convection are substantially faster ($\sim 10^{-5}$ m/s) than settling velocities of plagioclase or hornblende phenocrysts ($<10^{-6}$ m/s) (Huppert and Sparks, 1980; Snyder, 2000; Turcotte and Schubert, 2002), and thus the phenocrysts are transported with and record the thermal and compositional histories of the hybridizing magmas. Significantly, there appears to be a balance between recharge and assimilation rates, as has been suggested by some models (e.g. Spera and Bohrson, 2004).

1.2 Geologic Setting and Eruptive History

El Chichón Volcano, a complex of domes and associated pyroclastic deposits, located in the Chiapanecan Volcanic Arc of southeastern Mexico (Figure 1.1), has been actively erupting trachyandesitic magmas for at least the past 0.3 My (Duffield et al., 1984; Rose et al., 1984; McGee et al., 1987; Tilling et al., 1987; Espindola et al., 2000; Tepley et al., 2000; Table 1.1). Juvenile rocks are dominated by mm-scale (or larger) plagioclase and hornblende phenocrysts. Clinopyroxene is present in most samples, and anhydrite was observed in pumice erupted in 1982 (McGee et al., 1987). The volcano is inferred from regional geology and crustal xenoliths to overly Jurassic to Miocene carbonates, sandstones, and evaporites, although almost none crop out in the area around El Chichón (Tepley et al., 2000). The Sr and Nd isotopic compositions of these and other country rocks are distinct from magmas erupted at El Chichón (Figure 1.2).

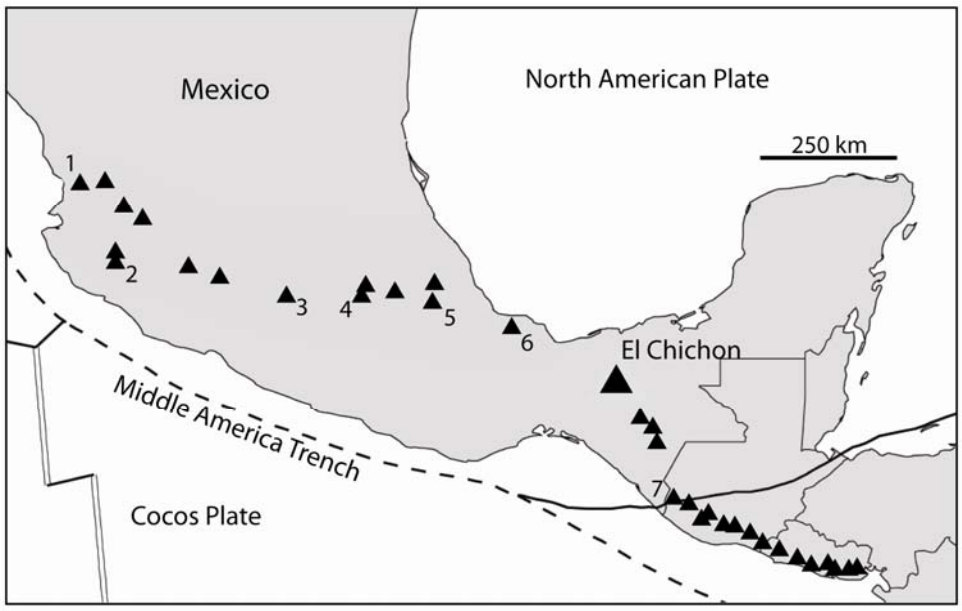

Figure 1.1. Locations of El Chichón Volcano and other Mexican and Central American volcanoes: 1) Ceboruco, 2) Colima, 3) Nevado de Toluca, 4) Popocatepetl, 5) Pico de Orizaba, 6) San Martin, and 7) Tacana.

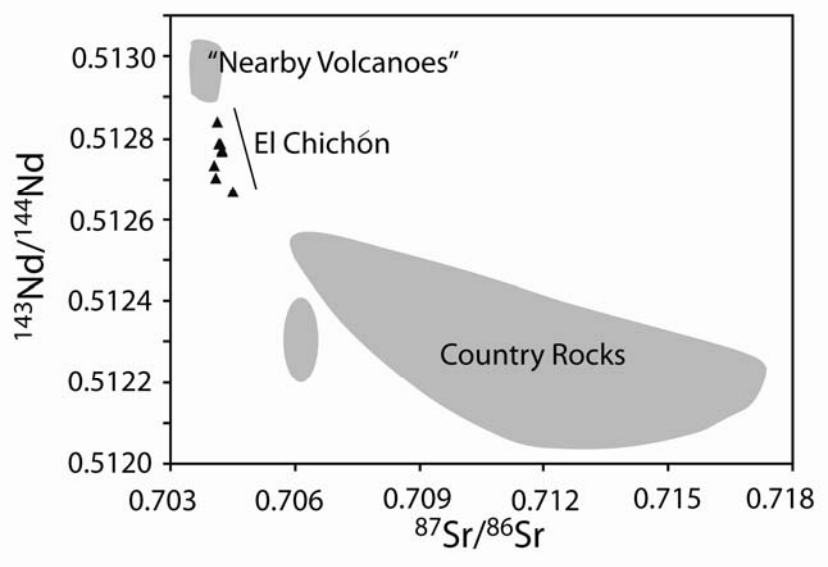

Figure 2.2. Whole-rock Sr and Nd isotopic ratios of El Chichón, nearby volcanics, and country rocks. The country rock types include evaporites, marls, sandstones, arenites, and granodiorites. Data for country rocks and "nearby volcanics" are from Tepley et al., 2000.

Table 1.1. Phase assemblages and elemental compositions of El Chichón samples. Mineralogies are reported as modal percent, major elements as weight percent (normalized to 100), and trace elements as ppm. Ages are presented in y.B.P. (except for Unit A, in years A.D.) and are from Espindola et al. (2000).

	A	B	C	D	E	F	J
Age	-1982	550	900	1250	1500	1600	3100
Plagioclase	9	10	5	8	30	20	10
Amphibole	3	3	4	3	8	8	8
Clinopyroxene	1	1.5	1	1.5	3	6	2.5
Oxides	1	1	1	<1	1	2	2
Biotite	-	-	-	1.5	-	-	-
SiO_2	57.86	56.28	56.32	58.33	58.18	57.18	56.92
Al_2O_3	18.51	19.34	19.82	18.42	18.12	18.41	18.63
TiO_2	0.676	0.741	0.671	0.665	0.693	0.699	0.731
FeO	6.01	6.52	5.36	5.82	6.17	6.33	6.42
MnO	0.183	0.193	0.207	0.18	0.184	0.175	0.196
MgO	2.26	2.47	2.48	2.16	2.21	2.39	2.46
CaO	7.32	7.57	7.31	7.09	7.14	7.68	7.53
K_2O	4.1	3.92	4.15	4.12	4.22	4.2	3.99
Na_2O	2.76	2.48	2.55	2.78	2.75	2.61	2.63
P_2O_5	0.341	0.359	0.364	0.337	0.337	0.337	0.365
Ni (XRF)	7	7	14	9	10	9	10
Cr (XRF)	7	10	8	9	10	10	11
V (XRF)	176	193	161	169	179	186	191
Ga (XRF)	22	23	21	23	23	22	22
Cu (XRF)	14	27	260	24	11	23	18
Zn (XRF)	77	79	165	78	75	77	86
La	30.03	30.18	25.5	31.47	29.86	30.91	28.41
Ce	57.5	57.22	47.03	57.39	56.41	58.8	54.15
Pr	7	6.57	5.45	6.48	6.47	7.11	6.24
Nd	27.05	26.56	22.22	26.08	26.23	27.54	25.67
Sm	5.59	5.81	4.99	5.56	5.77	5.62	5.77
Eu	1.6	1.6	1.45	1.6	1.62	1.6	1.68
Gd	4.64	4.86	4.4	4.61	4.76	4.67	4.91
Tb	0.68	0.73	0.68	0.68	0.72	0.69	0.73
Dy	3.88	4.17	4.03	3.95	4.15	3.99	4.2
Ho	0.78	0.83	0.81	0.79	0.82	0.81	0.83
Er	2.15	2.25	2.19	2.16	2.24	2.18	2.28
Tm	0.32	0.33	0.32	0.32	0.33	0.33	0.33
Yb	2.05	2.14	2.08	2.03	2.1	2.03	2.09
Lu	0.34	0.34	0.33	0.33	0.34	0.33	0.34
Ba	775	712	633	777	765	756	741
Th	9.27	9.49	7.7	9.59	9.34	8.63	8.53
Nb	12.84	14.52	11.77	14.64	14.92	12.69	13.85
Y	20.7	22.73	22.58	21.86	22.5	20.67	22.72
Hf	3.61	3	2.99	3.63	3.64	3.48	3.51
Ta	0.94	1	0.81	1.02	1.03	0.94	0.96
U	2.87	2.84	2.62	2.91	2.84	2.56	2.51
Pb	8.68	9.08	7.38	8.96	7.45	6.91	7.57
Rb	81.5	69.1	66.1	87.7	83.5	75	72.2
Cs	3.84	3.28	3.12	4.02	3.03	3.41	3.34
Sr	1006	984	846	970	945	1052	968
Sc	10.2	10.9	8.7	9.8	9.6	11.4	11.1

The Holocene has been a period of active volcanism at El Chichón with at least 12 explosive eruptions occurring in the past 7700 years (Espindola et al., 2000; Figure 2.3). Pyroclastic deposits comprising a series of block-and-ash flow, surge, and ash flow deposits are the bulk of the stratigraphic sequence at El Chichón (Figure 1.3). Eruptions that have been dated by Espindola et al. (2000) show a recurrence interval of ~700 years (<400 since 3700 yr.BP.). The only two pumice falls present in the Holocene sequence are Units B (550 yr.BP.) and A (1982 A.D.) (Espindola et al., 2000, Figure 1.3).

Previous workers have described the complex compositional and textural zoning patterns in plagioclase phenocrysts erupted from El Chichón (Belkin et al., 1984; McGee et al., 1987; Tepley et al., 2000). Anorthite contents range from ~An_{35} to ~An_{85}; compositional changes occur as both small magnitude oscillatory variations on the order of 2-5 mol% An, and larger magnitude (10-40 mol% An) spikes (McGee et al., 1987). Interestingly, those calcic zones also contain abundant melt and gas inclusions (McGee et al., 1987). Belkin et al. (1984) and McGee et al. (1987) interpret the zoning patterns to reflect repetitive fluctuations in the volatile pressure (ΔP on the order of 100MPa) resulting from stirring of the magma chamber, assimilation of volatile-rich country rock (e.g. salt domes or evaporites), and possibly eruption. Alternatively, Tepley et al. (2000) suggest the zoning patterns record repeated cycles of magma recharge and assimilation. Regardless of model, the ubiquity of zoning in all erupted products indicates that the same processes have been underway at El Chichón for the past 0.3 My (McGee et al., 1987; Tepley et al., 2000).

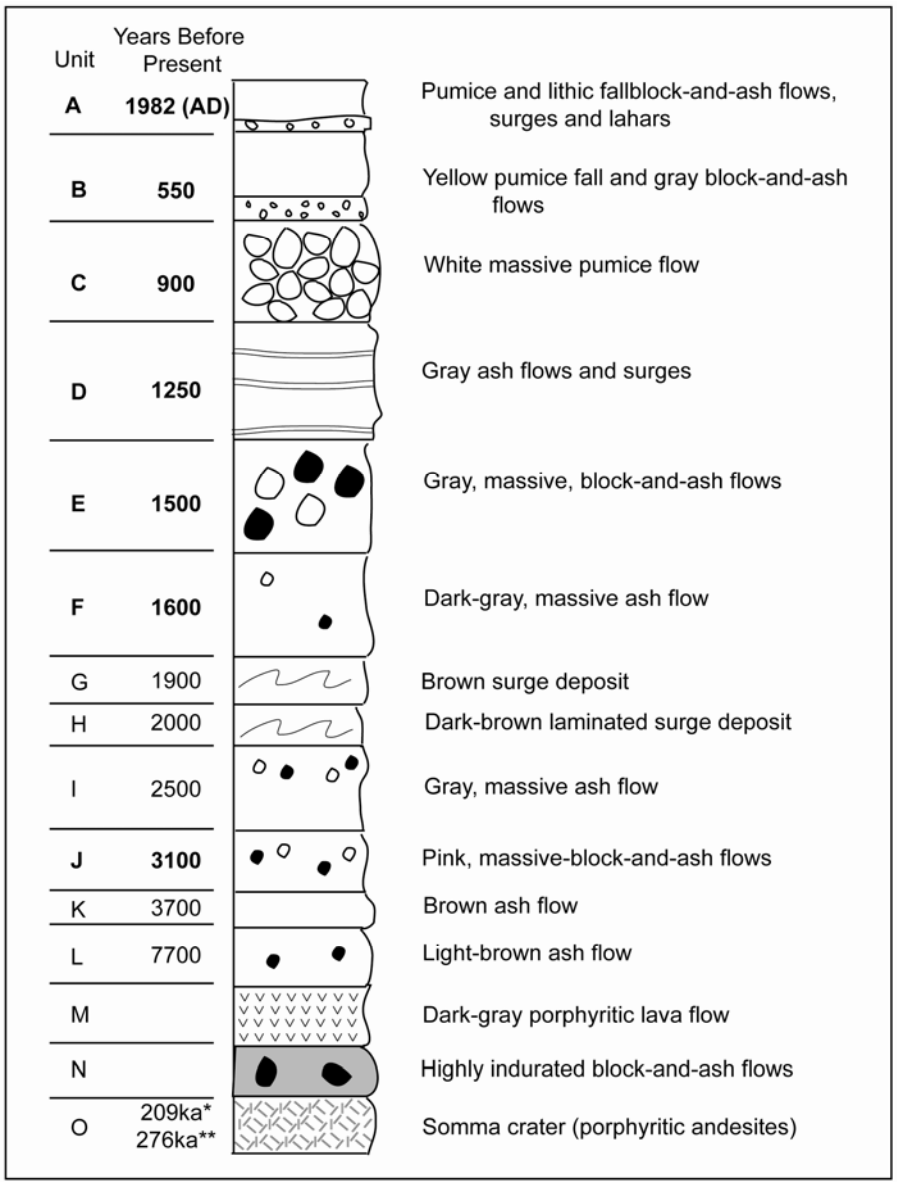

Figure 1.3. Simplified El Chichón stratigraphic column adapted from Espindola et al. (2000). Additional ages (*, **) are from Damon and Montesinos (1978) and Duffield et al. (1984). Samples used in this study indicated by bold text for Unit and Age.

1.3 SAMPLES AND ANALYTICAL TECHNIQUES

Samples used in this study are a suite of rocks representing 7 eruptions from the past 3100 years (Figure 1.3). A large juvenile clast was collected from deposits of each eruption. That sample was then split into three pieces, one piece used for bulk compositional analysis, one for bulk isotopic analysis, and the final for sectioning. Polished 100-μm-thick sections were made of each sample for electron microprobe and laser ablation ICP-MS analysis.

1.3.1 Whole Rock Analyses

Bulk samples were analyzed by X-Ray Fluorescence (XRF) and Inductively-Coupled Plasma Mass Spectrometer (ICP-MS) for major and trace elements at the GeoAnalytical Lab at Washington State University. Bulk Sr, Nd, and Pb isotopic analyses were conducted using a multi-collector, magnetic sector ICP-MS (IsoProbe) at the University of Texas at Austin Department of Geological Sciences. Sr, Nd, and Pb were separated from the crushed whole rock samples following the ion chromatographic techniques described in Housh and McMahon (2000). The samples were run as solutions in 2% HNO_3 using an Aridus microconcentric desolvating nebulizer sample introduction system on the IsoProbe. Analytical uncertainties are reported in Table 1.2.

Table 1.2. Whole-rock isotopic compositions of El Chichón samples. Uncertainties are reported as 2 standard deviations. Ages are presented as years B.P., except for Unit A (years A.D.).

	A	B	C	D	E	F	J	Uncertainty
Age	1982 A.D.	550	900	1250	1500	1600	3100	
$^{87}Sr/^{86}Sr$	0.70406	0.704191	0.704155	0.704256	0.704231	0.704101	0.704213	0.000019
$^{143}Nd/^{144}Nd$	0.512734	0.512786	0.512788	0.512769	0.512773	0.512703	0.512786	0.000015
$^{206}Pb/^{204}Pb$	18.7696	18.7748	18.7695	18.7828	18.7955	18.7841	18.7823	0.0042
$^{207}Pb/^{204}Pb$	15.599	15.602	15.597	15.599	15.607	15.601	15.603	0.0057
$^{208}Pb/^{204}Pb$	38.523	38.519	38.507	38.519	38.553	38.541	38.529	0.015

Nd and Sr were measured in static, multicollection mode on a Micromass IsoProbe multicollector, magnetic sector ICP-MS. ^{147}Sm, ^{83}Kr, and ^{85}Rb were monitored to correct for the isobaric interferences at ^{144}Nd, ^{86}Sr, and ^{87}Sr, respectively. I applied a phenomenological correction to account for mass-dependent instrumental fractionation of Nd and Sr (Wombacher and Rehkämper, 2003; Beard and Albarède, 2004), with $^{146}Nd/^{144}Nd = 0.7219$ and $^{86}Sr/^{88}Sr = 0.1194$, respectively. An in-house Nd standard (UTAmes Nd) was used as the primary fractionation standard for Nd. This standard has been calibrated against Shin Etsu Nd ($^{143}Nd/^{144}Nd = 0.512120$) with a resulting value for UTAmes of $^{143}Nd/^{144}Nd = 0.512090 +/- 0.000017$ (2σ). For Sr, Eimer and Amend Sr was used as the primary fractionation standard ($^{87}Sr/^{86}Sr = 0.708032$). Shin Etsu and JNdi were measured as secondary standards for the Nd runs, and NBS 987 was measured as a secondary standard for the Sr runs. The results were: Shin Etsu $^{143}Nd/^{144}Nd = 0.512115 +/- 0.000020$ (2σ, n= 6), JNdi $^{143}Nd/^{144}Nd = 0.512112 +/- 0.000022$ (2σ, n=6) and NBS987 $^{87}Sr/^{86}Sr = 0.710233 +/- 0.000039$ (2σ, n=22).

Pb was measured in static, multicollection mode on the IsoProbe after being spiked with Tl. ^{202}Hg was monitored to correct for an isobaric interference on ^{204}Pb. The data were corrected for mass fractionation using $^{205}Tl/^{203}Tl = 0.418918$. The standard NBS 981 was measured throughout the course of these analyses. The data have been

adjusted to the values for Galer and Abouchami (1998) for NBS 981. Twenty-three measurements of NBS 981 resulted in the following: $^{206}Pb/^{204}Pb$ = 16.9402 +/- 0.0042 (2σ), $^{207}Pb/^{204}Pb$ = 15.4962 +/- .0056 (2σ), and $^{208}Pb/^{204}Pb$ = 36.7081 +/- .0154 (2σ). Procedural blanks using the IsoProbe are: Nd: 40-50 pg, Sr: 41-100 pg, and Pb: 40-50 pg.

1.3.2 Electron Microprobe Analyses

Major element analyses of minerals were collected using a JEOL JXA-8200 "Superprobe" Electron Microprobe (EPMA) at the University of Texas at Austin Department of Geological Sciences. All analyses were collected using a 15 kV, 10 nA beam; plagioclase analyses were collected with a focused beam, whereas amphibole analyses were collected with a 10 μm defocused beam. The start and end of plagioclase transects were located using Back-Scattered Electron (BSE) images collected with the EPMA; transect analyses were collected every 5 μm. BSE images were subsequently used to locate laser transects and describe plagioclase textures.

1.3.3 Isotopic Microanalyses

Laser Ablation ICP-MS (LA-ICP-MS) analyses were collected using the IsoProbe and a New Wave LUV-213 nm frequency quintupled Nd-YAG laser. Isotopes ^{88}Sr, ^{87}Sr, ^{86}Sr, ^{85}Rb, ^{84}Sr, and ^{82}Kr were analyzed in static acquisition mode. ^{87}Sr and ^{86}Sr were corrected for isobaric interferences from ^{87}Rb and ^{86}Kr, respectively. A large homogeneous plagioclase megacryst from a mafic alkali basalt, GTO-05-6b2, was used as a LA-ICP-MS standard. Five spots from the megacryst were sampled by microdrilling, and the powders were processed to separate Sr following the procedures of

Housh and McMahon (2000). The Sr samples were run as solutions in 2% HNO_3 using an Aridus microconcentric desolvating nebulizer sample introduction system on the IsoProbe in static multicollection mode. The data were corrected for mass fractionation using a modified general power law with Eimer and Amend Sr as the primary fractionation standard. Four analyses of NBS 987 during this course of analyses gave $^{87}Sr/^{86}Sr$ = 0.710254 +/- 0.000038 (2σ). The five analyses from GTO-05-6b gave the following results: 0.703489, 0.703476, 0.703455, 0.703425, and 0.703489; the mean of those five analyses is 0.703467 +/- 0.000054 (2σ). It is estimated that each sampled spot contained 400-800 ng Sr.

LA-ICP-MS analyses were collected by either scanning the laser across the sample surface, thereby continuously sampling a track, or by discretely sampling a series of spots following a core to rim transect. The signal intensity was optimized with the laser pulsing a 30 μm spot at 10 Hz, with a 5 μm/s scan speed (0 μm/s for spots), and 100-150 J/cm^2 fluence. The depth of the laser tracks was measured using a petrographic microscope equipped with a focus drive linear encoder and found to be ~70 μm. Backgrounds were collected immediately before each track analysis. Track analyses were collected with 1 second integrations for n cycles, where n depends on the track length. All integrations with $^{85}Rb/^{86}Sr > 0.1$ were discarded. I applied a 6-point running average to the data (equivalent to 30 μm traversed by the laser at 5 μm/sec, which is equal to one laser beam diameter), and then added 15 μm errors bars to the spatial component of the running average; the data have a spatial resolution between 30 and 50 μm. Mass fractionation was first corrected using an exponential law. Following those corrections, I found that LA-ICP-MS $^{87}Sr/^{86}Sr$ ratios of standard GTO-05-6b2 were systematically higher than those measured by TIMS; in the previously published version

of this work, the LA-ICP-MS track analyses were not properly corrected (Andrews et al., 2008). Although some of that disparity may be the result of collecting backgrounds when the plasma was not loaded, the differences are not fully understood. To resolve those problems, final data processing was accomplished with an empirical correction. First, the exponentially-corrected $^{87}Sr/^{86}Sr$ ratios of standard GTO-05-6b2 were plotted against the exponentially-corrected $^{88}Sr/^{86}Sr$ ratios. The data were then linearly regressed to find the nominal $^{88}Sr/^{86}Sr$ ratio, $^{88}Sr/^{86}Sr^*$, that resulted in $^{87}Sr/^{86}Sr = 0.703467$. LA-ICP-MS transects of El Chichón plagioclase were corrected by linearly regressing a given transect's $^{87}Sr/^{86}Sr$ ratios to $^{88}Sr/^{86}Sr^*$ (determined from GTO-05-6b2); the slope upon which an analysis is regressed is specific to each analysis. Further description of this procedure is presented in Appendix 2.

LA-ICP-MS spot analyses were collected with 1 second integrations for 45 seconds following a 5 second pre-ablation of the sample. Backgrounds were collected for 90 seconds before every 2-9 analyses by ablating a semiconductor-grade blank Si wafer containing no Rb or Sr; this method of background measurement loaded the plasma. Mass fractionation was first corrected using an exponential law. As with the transect analyses, the exponentially-corrected LA-ICP-MS $^{87}Sr/^{86}Sr$ ratios of spot analyses were higher for standard GTO-05-6b2 than those measured by TIMS. Final data processing was accomplished with an empirical correction. First, exponentially-corrected $^{87}Sr/^{86}Sr$ ratios of GTO-05-6b2 were plotted against exponentially-corrected $^{88}Sr/^{86}Sr$ ratios. Those ratios were found to not vary systematically within a single spot analysis, but analyses from a single day define a systematic variation in $^{87}Sr/^{86}Sr$ with $^{88}Sr/^{86}Sr$. Analyses from each day were regressed to find that day's nominal $^{88}Sr/^{86}Sr$ ratio, $^{88}Sr/^{86}Sr^*$, that resulted in $^{87}Sr/^{86}Sr = 0.703467$. During processing of those data and data

from a second standard described below, I found that the slope upon which data are regressed is proportional to ^{88}Sr signal. That relation allows for correction of each analysis as a function of ^{88}Sr signal and $^{88}Sr/^{86}Sr^*$. Further description of this procedure is presented in Appendix 2.

GTO-05-6b2 was measured by LA-ICP-MS following approximately every other crystal using the methods outlined above. Corrected LA-ICP-MS track analyses of that megacryst yield $^{87}Sr/^{86}Sr$ ratios of 0.70380 ± 0.00018 (2σ). Corrected LA-ICP-MS spot analyses of GTO-05-6b2 megacryst yield $^{87}Sr/^{86}Sr$ of 0.70345 ± 0.0015 (2σ, n=52), and individual analyses have internal precision of ±0.0006 (2 s.e.).

A large, homogeneous labradorite megacryst, OR-Labr, was used as a secondary standard for LA-ICP-MS spot analyses. The crystal was sampled in 5 spots by microdrilling, and the powders were processed to separate Sr following the procedures of Housh and McMahon (2000). The samples were analyzed using a ThermoFinnigan Triton Thermal Ionization Mass Spectrometer (TIMS) at the University of Texas at Austin. The five TIMS analyses of OR-Labr gave the following results: 0.70400, 0.70388, 0.70372, 0.70389, and 0.70405; the mean of those five analyses is 0.70391 ±0.00026 (2σ). Eight LA-ICP-MS spot analyses of OR-Labr yield an average $^{87}Sr/^{86}Sr$ composition of 0.7039 ±0.0011 (2σ) (Appendix 2). Although the LA-ICP-MS analyses are systematically lower than the TIMS analyses, thus indicating a possible overcorrection of mass fractionation, they are within LA-ICP-MS analytical uncertainty. As a result, although a less empirical data processing technique is desirable, the techniques described above provide a working method of processing LA-ICP-MS analyses.

Given that Tepley et al. (2000) report a range in $^{87}Sr/^{86}Sr$ ratios of 0.7039-0.7054, and the LA-ICP-MS signal variation in tracks across GTO-05-6b2 is a significant fraction of that range, differentiation of analytical "noise" from "real" zonation in LA-ICP-MS track analyses can present a significant challenge. I minimized this problem by collecting at least two core-to-rim tracks from each plagioclase phenocryst, located as closely as possible. Comparisons of the two tracks with BSE images and photomicrographs of the phenocrysts allow us to correlate the transects, resulting in recognition of "real" zoning and spatial resolution on the order of 50 μm. LA-ICP-MS analyses of 55 μm diameter spots collected beside the analysis tracks on selected crystals indicate the transects accurately record the magnitudes and positions of isotopic zoning in plagioclase (Figure 1.4). I report the LA-ICP-MS data by plotting either both tracks or a series of spot analyses.

I have estimated uncertainties in LA-ICP-MS track analyses by correlating transect pairs and measuring the differences between track analyses. The standard deviation of the difference in $^{87}Sr/^{86}Sr$ ratio between transects ranges from 0.0002 to 0.0007, and is similar to the standard error of six 1-second integrations of track analyses, typically ±0.0004. Uncertainties in track analyses are reported as ±0.0005, equal to 2 standard errors of the 6-point running mean. The uncertainties of spot analyses are reported as 2 standard errors of the measured $^{87}Sr/^{86}Sr$ ratios, typically ±0.0005. Notably, those LA-ICP-MS analytical uncertainties are 2-4 times greater than those reported by Davidson et al. (2001). This is a result of calculating the uncertainties using the methods described above instead of using a theoretical uncertainty based upon counting statistics.

As the empirical corrections described above should make clear, there are several unresolved problems concerning the LA-ICP-MS techniques described in this paper. A

more thorough understanding of those problems will hopefully improve LA-ICP-MS precision and accuracy. The following summary of techniques and problems is presented to aid future workers. Backgrounds for track analyses were collected on-peak with non-loaded plasmas. Track analyses of plagioclase commonly had negative ^{82}Kr signals and significant ^{85}Rb signals ($^{85}Rb/^{86}Sr > 0.05$), that resulted in significant interference corrections. I interpret those signal intensities to derive from improper measurement of backgrounds. When measuring the spot analyses, I attempted to remedy those problems with background characterization by collecting the on-peak backgrounds with a loaded plasma. This had the effect of reducing the ^{82}Kr signal to essentially zero, but it also reduced the ^{85}Rb signal to consistently negative voltages. That negative Rb signal indicates an improper measurement of the background; El Chichón plagioclase contain enough Rb that $^{85}Rb/^{86}Sr$ ratios should commonly be between 0 and 0.05.

The problems with Kr and Rb measurement can likely be solved by a different method of measuring backgrounds. One possible solution is to measure the backgrounds at half-masses. This would allow for a measurement of the noise in each detector. Sample analyses would then measure the total signal intensities at masses 82, 84, 85, 86, 87, and 88. Rather than trying to subtract away the interferences of Kr and Rb using on-peak backgrounds, the interferences can be fully calculated and corrected. I expect that this approach will improve analytical accuracy and precision. Additional discussion of this technique and background interferences is presented in Appendix 2.

1.4 RESULTS

1.4.1 Mineralogies and Whole-Rock Compositions

Plagioclase (up to ~5 mm long) is the most abundant phenocryst in all samples, ranging from <10 vol.% to >20 vol.% (Table 1.1). Plagioclase nearly always has euhedral rims, but shows a wide range of interior textures (Figure 1.5). All samples contain highly sieved and/or patchy zoned plagioclase phenocrysts, as well "clean" phenocrysts, whose interiors may be optically zoned but lack other textural irregularities. In addition, Units C, E, F, and J contain numerous plagioclase with interiors that are almost entirely sieved (Figure 1.5).

Roughly equant brown hornblende (up to 1 mm) is the next most common phenocryst in all samples, with abundances as high as 15 vol.%. Some hornblende have faint, optically visible zones, ~50 μm thick along their rims (Figure 1.5). Some hornblende in Units C, E, F, and J have sieve-like, irregularly textured interiors and zones (Figure 1.5). In addition, sieved hornblende in Units E and F are occasionally mantled by green augite 50 μm thick (Figure 1.5). Interestingly, hornblende with such textural irregularities occur within 100 μm of euhedral hornblende (Figure 1.5). Moreover, these strongly zoned hornblende occur in the same samples as the thoroughly sieved plagioclase.

Augite is about half as abundant as hornblende in most samples (except M, in which augite is absent). Augite is green, and typically forms subhedral to euhedral rods

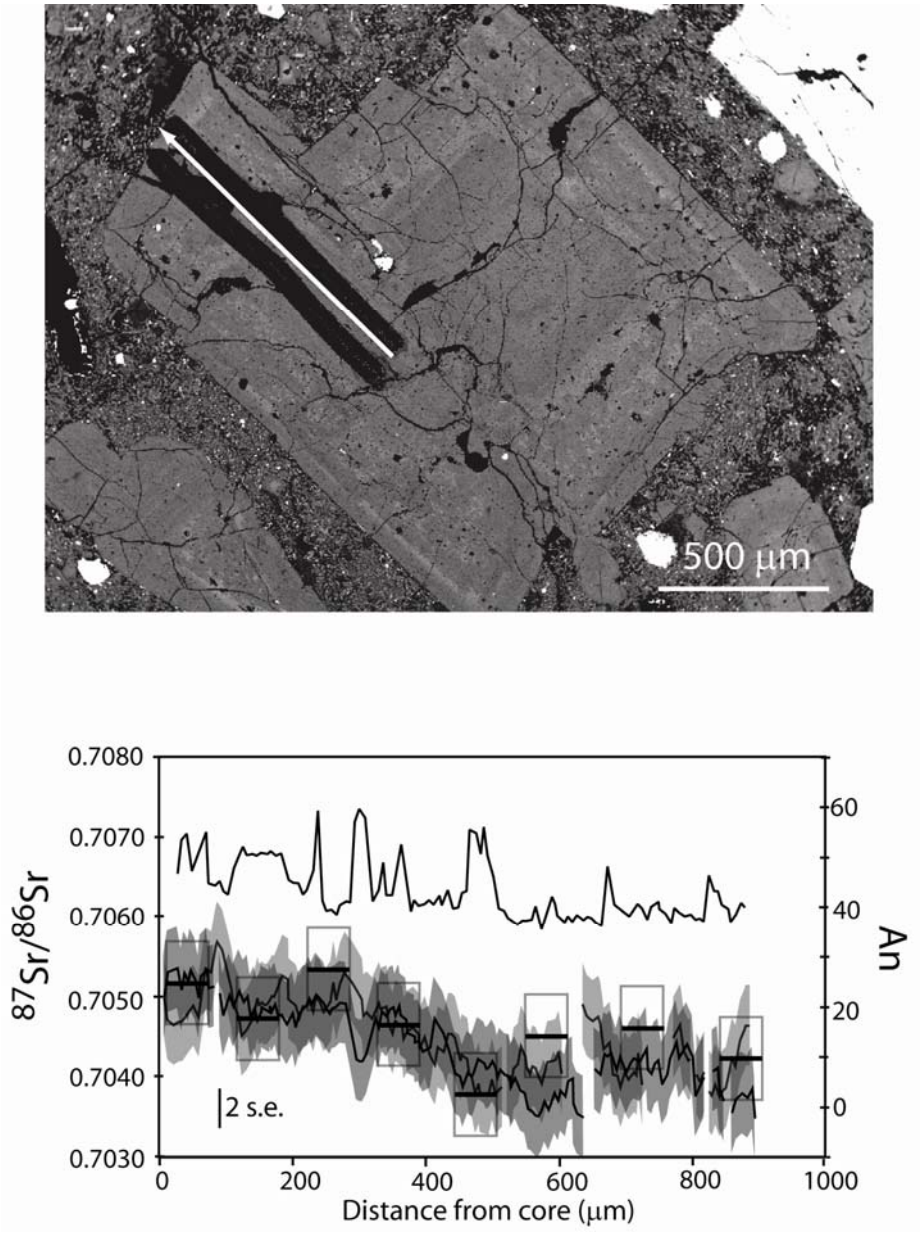

Figure 1.4. LA-ICP-MS analyses and *An* content of a Unit E plagioclase phenocryst. Dark lines with gray shading indicate $^{87}Sr/^{86}Sr$ ratios as measured along two parallel transects (gray regions tracking each line show 15 μm error in the spatial component of the data and ±2 s.e. of $^{87}Sr/^{86}Sr$ ratios); results of LA-ICP-MS spot analyses are shown with solid bars and 1 s.e. error boxes. Spot analyses verify the zoning pattern recorded by LA-ICP-MS transects; boxes show 2 s.e. in $^{87}Sr/^{86}Sr$ measurement. *An* content is indicated by the solid black line with no gray shading.

and prisms, which may be up to 0.5 mm long. Where augite mantles hornblende, it frequently pseudomorphs after hornblende (Figure 1.5).

Minor minerals include magnetite, apatite, and titanite, which occur in every sample, and biotite. Magnetite typically occurs as euhedral cubes up to 200 μm in size. Biotite is only observed in Unit D, where it occurs as euhedral crystals up to 800 μm. Anhydrite was observed in samples erupted in 1982.

All rocks are potassic trachyandesites (Table 1.1), and all plot near the shoshonite-latite boundary on a total alkali-silica diagram (LeBas et al., 1986). The most striking feature is how little compositional variation is present between samples spanning 3100 years. For example, silica content varies by only ~2 wt.%, MgO by 0.32 w.t%, and K_2O by 0.39 wt.%. Trace elements concentrations also show very little variation between samples; Unit C is the exception to this pattern in that it contains approximately an order of magnitude higher Cu (260 versus 11-27 ppm), and twice as much Ni and Zn as the other Units.

Whole-rock isotopic analyses of all samples reveal a slight decrease in radiogenic components with time, from high values of ~0.70425 ($^{87}Sr/^{86}Sr$) and ~18.795 ($^{206}Pb/^{204}Pb$) to low values of ~0.7040 and ~18.77 (Figure 1.6**,** Table 1.2). Isotopic compositions appear to be trending toward those of the "nearby volcanoes," as discussed by Tepley et al. (2000) (Figure 1.3).

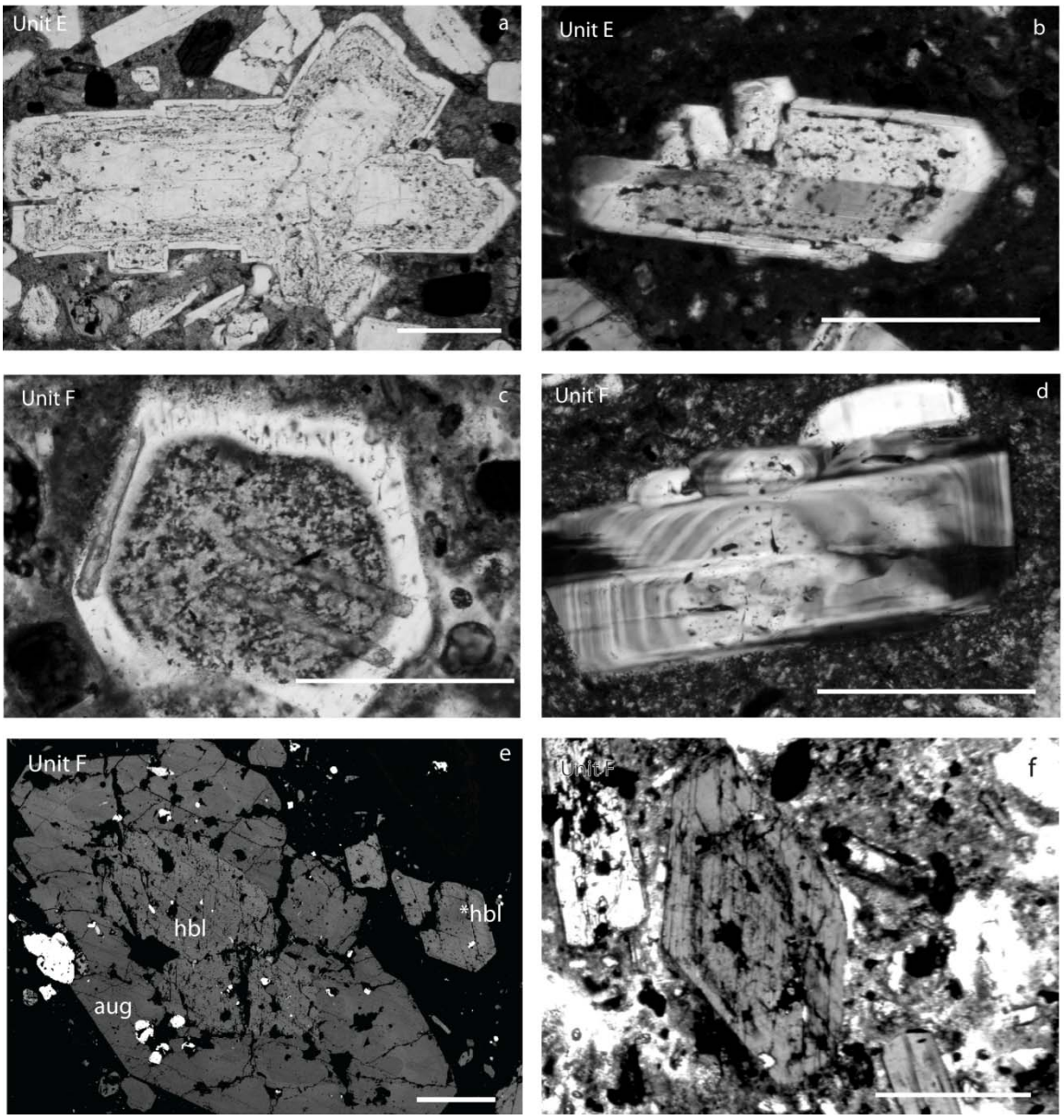

Figure 1.5. Photomicrographs of plagioclase and hornblende. Plagioclase zoning patterns range from crystals with relatively clean cores and rims but strongly sieved intermediate zones (a and b), to those whose cores are completely sieved (c), to those with oscillatory zoning (d). Hornblende may be mantled by augite (e) or occur as euhedral crystals that may (f) or may not (star in e) be zoned. Interestingly, hornblende with substantially different textures occur within ~100 μm of one another (e). Scale bar is 500 μm in all photographs.

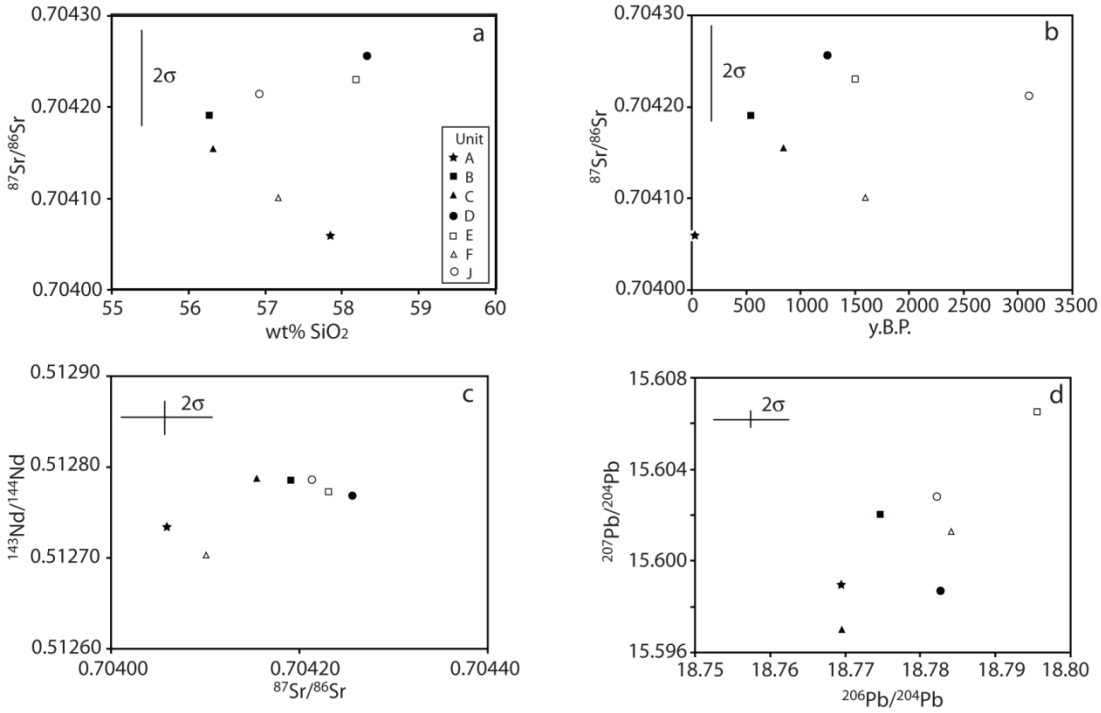

Figure 1.6. Variation in Sr, Nd, and Pb whole rock isotopic ratios. El Chichón samples do not display a systematic variation of $^{87}Sr/^{86}Sr$ with respect to SiO2 (a). There is, however, a general decrease in $^{87}Sr/^{86}Sr$ ratio with time, specifically from 3100 to 1600 yr.BP and from 1500 yr. BP to 1982 A.D. (b). Nd and Sr isotopic ratios do not appear to be covariant (c). $^{207}Pb/^{204}Pb$ and $^{206}Pb/^{204}Pb$ ratios generally correlate (d), and decrease from the oldest to youngest Units (Table 2.2).

1.4.2 Plagioclase Isotope Stratigraphy

Plagioclase phenocrysts are complexly zoned with compositions ranging from ~An_{30} to >An_{70}. Rim compositions, however, are typically ~An_{40}, but range from An_{30} to An_{60}. Interestingly, individual samples can contain the entire range in rim compositions. Changes in *An* across two adjacent zones may vary from ~1 to >25 mol% An. Plagioclase phenocrysts often contain dissolution surfaces, patchy zones, and sieve textures (Figure 1.5), all of which frequently herald large-amplitude changes in *An* content (Figures 1.7). Many of the larger amplitude compositional changes

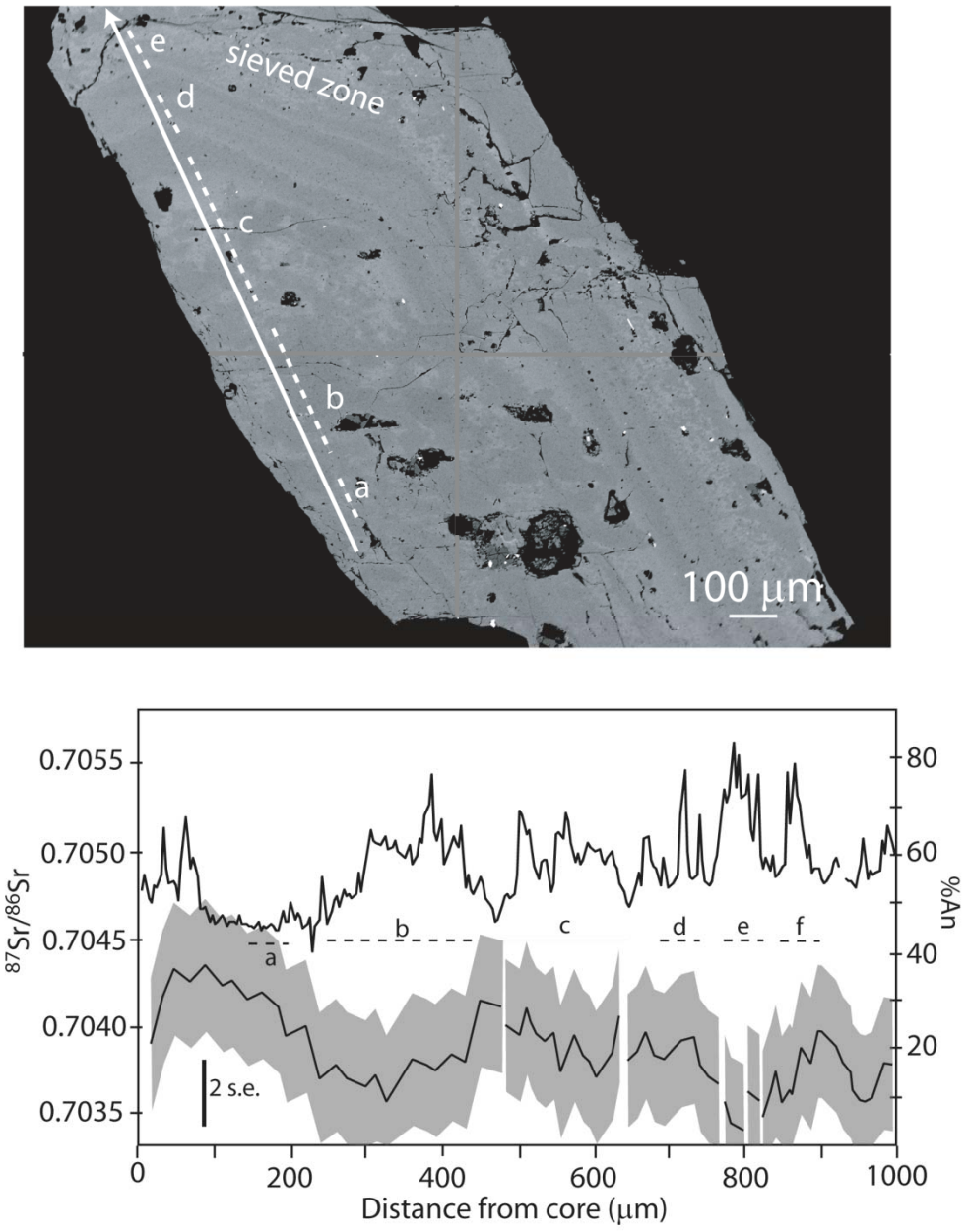

Figure 1.7. Core-to-rim transect across a Unit E plagioclase. *An* is indicated by the upper line and $^{87}Sr/^{86}Sr$ ratios by the black line and gray 2 s.e. uncertainty. In general, the plagioclase displays Type I and II zoning. Type IV zoning, however, occurs in regions a, as a decrease in $^{87}Sr/^{86}Sr$ ratio, and f, as changes in $^{87}Sr/^{86}Sr$ ratio that do not appear to correlate with changes in An. Type III zones superimposed on Type I and II zones appear in regions b, c, d, and e.

occur as "step functions" rather than smooth transitions. Thicknesses of individual zones generally correspond with the change in *An* content; for example, a change in composition from An_{40} to An_{70} is often associated with a wider high-An zone than that associated with a variation from An_{45} to An_{50} (Figure 1.7); the same relationship holds for zones with decreases in An.

All analyzed plagioclase are complexly zoned in Sr isotopic composition (Figures 1.4, 1.7, and 1.8). For most crystals, the "average" $^{87}Sr/^{86}Sr$ ratio is ~0.7040, but departures from that ratio may be positive or negative, and typically have magnitudes of up to ~0.0015, a range substantially greater than that between bulk analyses. The length scale of compositional zones varies from ~30 μm (our minimum spatial resolution) to ~200 μm (Figures 1.4, 1.7, and 1.8). As with *An* zoning, the boundaries in Sr isotopic zoning frequently appear to be "step functions" rather than smooth transitions, and frequently accompany textural and compositional zoning (Figures 1.7 and 1.8).

When combining all of our plagioclase data I recognize four types (I-IV) of zoning patterns. Type I zones have increasing *An* content and decreasing $^{87}Sr/^{86}Sr$ ratios, often with changes of >10 mol.% *An* and >0.001 $^{87}Sr/^{86}Sr$ (Figure 1.7). Although such zones may be as thin as 30 μm, they are typically wider than 100 μm; relatively longer wavelength decreases in $^{87}Sr/^{86}Sr$ ratio accompanying spikes in *An* content may be an artifact of the laser spot size. Patchy, sieved, or dissolution textures are often present in these zones, particularly in their inner part. Type II zones have increasing $^{87}Sr/^{86}Sr$ ratios and decreasing *An* content (Figure 1.7). The amplitudes of Type II zones are similar to those of Type I, but the Type II zones are generally thicker than those of Type I (Figure 1.7). Type I and II zoning patterns are often associated. Although adjacent Type I and II

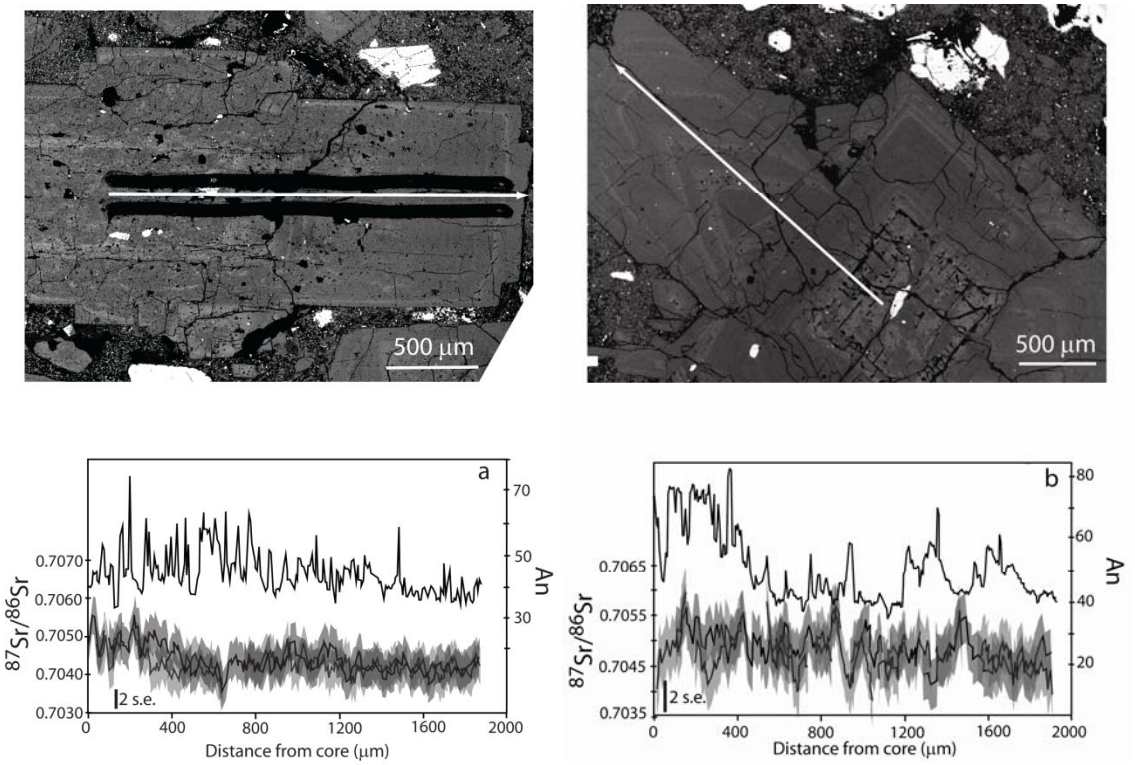

Figure 1.8. Representative core-to-rim EPMA and LA-ICP-MS transects across Unit E (a and b), Unit C (c), and Unit A (d) plagioclase. *An* indicated by solid line and $^{87}Sr/^{86}Sr$ ratios by dashed lines with a gray region representing the range in measured values. Plagioclase with significant Type III zones and three major Type I and II zoning pairs (a). Plagioclase with Type III and IV zoned core and Type I and II zoning in the outer ~800 μm (b).

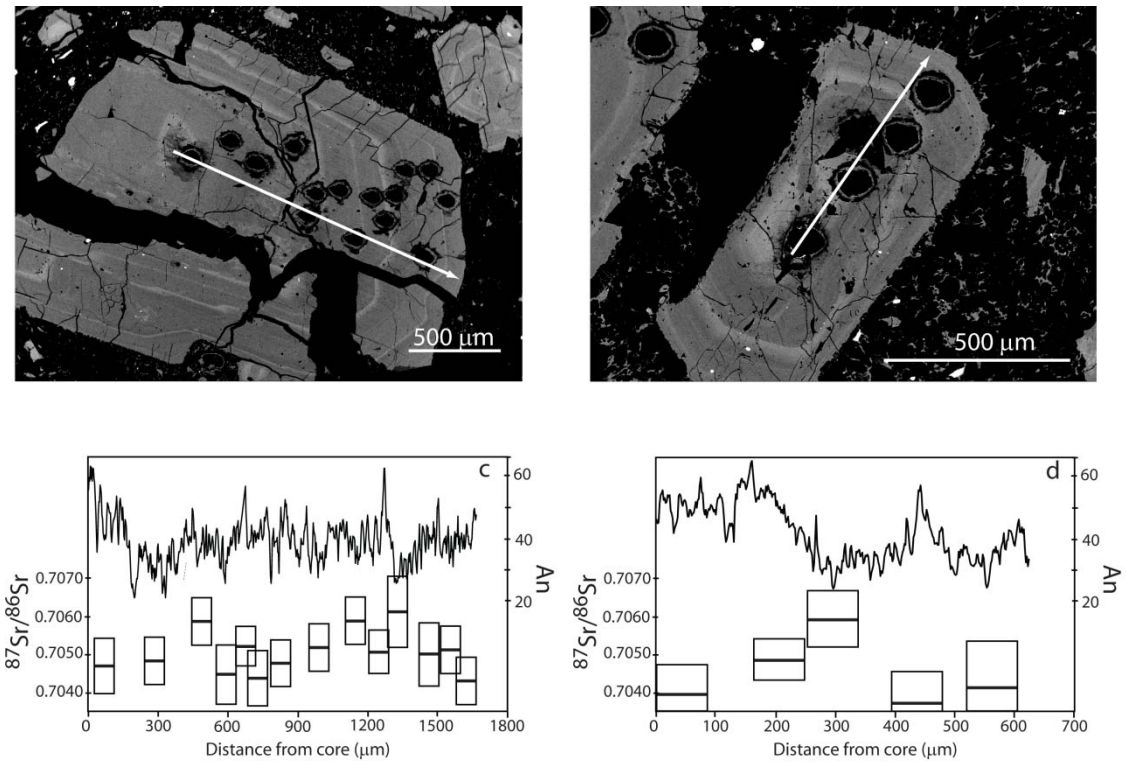

Figure 1.8. (continued) Representative core-to-rim EPMA and LA-ICP-MS transects across Unit C (c) and Unit A (d) plagioclase. Crystal with Type II zoning in the core, Type I zoning ~600 and ~1200 μm from the core, and high frequency Type III zoning superimposed on a Type IV zoning trend from ~800-1200 μm (c). Plagioclase with Type II zoning in the core, and a pair of Type I and II zones at distances of 350-600 μm from the core (d).

zones generally have similar amplitudes, their wavelengths may differ, and thus coupled type I-II pairs occur as both symmetric and asymmetric sets (Figures 1.4, 1.7, and 1.8). Interestingly, the largest amplitude changes in *An* in Type I or II zones, up to 30 mol.%, are similar to the total range in plagioclase rim compositions, but the largest variations in Sr isotopic composition (~0.0020) are greater than observed rim variations (Figure 1.8).

Type III zones have variations in *An* content only (Figures 1.7 and 1.8). Although these zones may vary by as much as 25 mol.% *An*, most are <10 mol.%. Type III patterns occur more frequently than other types, have shorter wavelengths (as small as 10 μm), and frequently can occur within broader Type I and II zones (thus the *An* content changes through a series of steps or oscillations). It should be noted, however, that the frequent occurrence of Type III zones may be an artifact of differences in the laser and EPMA spot sizes. Type IV zones have variation in $^{87}Sr/^{86}Sr$ ratio with no corresponding change in *An* (Figure 1.7). These zones generally have length scales of <70 μm and $^{87}Sr/^{86}Sr$ ratio variations of <0.001, both of which are generally smaller than those seen in Type I and II zones. Type IV zoning is the least common of the four zoning types.

Plagioclase contain multiple zones, and repeated zoning types. For example, one crystal from unit E contains multiple pairs of Type I and II zones, and another unit E plagioclase shows several Type IV zones (Figure 1.8). It is important to note that there appears to be no particular pattern in which zonings occur within a given sample. For example, crystals in Unit B do not all show the zoning sequences (or even sequences near their rims), and thus there is no unique crystal isotope signature for unit B. Some of the El Chichón plagioclase show greater amplitude Sr isotopic variation in their cores versus rims, whereas others show the opposite (Figure 1.8). Moreover, the same variety of zoning patterns occurs in all eruptions. All samples have phenocrysts that contain large and small amplitude Type I and II zones, very short wavelength Type III changes in *An* content, and infrequent Type IV zones. Phenocrysts with lower-An rims generally display lower amplitude and longer wavelength *An* variation than crystals with higher-An rims (Figure 1.8). Although there is little variation in average Sr isotopic composition between crystals with these two patterns, the former group is more likely to display Type

IV zoning, whereas crystals with high-An rims show a greater degree and higher amplitude of Types I and II zoning.

1.4.3 Amphibole Compositional Zoning

Representative hornblende analyses are presented in Table 1.3. Zoned as well as homogeneous crystals are present in all eruptions. In optically zoned, "clean" hornblende, the principle difference between core and rim compositions is in Al_2O_3 and SiO_2 contents, with concentrations varying by as much as 2 wt.%. Similar variation is present in hornblende with sieve textures or mantled by augite. Interestingly, these substitutions do not always occur in the same sense within single samples, indeed hornblende with high-Al cores and others with high-Si cores occur within the same pumice.

1.5 DISCUSSION

1.5.1 Origin of Zoning in Plagioclase

Type I zones are those with sharply increasing *An* content and decreasing $^{87}Sr/^{86}Sr$ ratios. Because of their decreasing $^{87}Sr/^{86}Sr$ ratios, these zones require that the plagioclase comes into contact with less radiogenic melt than with what it was previously in contact. In addition, the increase in *An* content indicates that the new melt was compositionally less evolved and possibly hotter and/or wetter. The common occurrence of dissolution and patchy regions at the inner part of the zones supports a hotter melt (e.g. Tsuchiyama and Takahashi, 1983; Tsuchiyama, 1985; Nakamura and Shimakita, 1998; Tepley et al., 2000). I thus suggest that Type I zones record the injection of hot, less

Table 1.3 Representative hornblende core and rim compositions. All analyses collected with a 15 kV, 10 nA beam with a 10 μm spot size.

Unit			*SiO_2*	*Al_2O_3 TiO_2*	*FeO*	*MgO*	*MnO*	*CaO*	*Na_2O*	*K_2O*	*Total*
A	Core	39.63	12.13	2.49	18.05	10.24	0.56	11.84	1.95	1.48	98.38
	Core	39.35	12.25	2.5	17.74	10.48	0.45	11.84	1.86	1.53	98.02
	Rim	40.06	11.32	2.5	18	10.58	0.47	11.62	1.91	1.51	97.96
	Core	40.97	11.69	2.64	16.46	11.22	0.47	12.17	1.92	1.57	99.41
	Rim	40.64	11.49	2.74	17.4	10.92	0.5	12.3	1.95	1.6	99.58
B	Core	41.04	10.93	2.06	17.81	10.12	0.61	11.19	1.86	1.36	96.98
	Rim	40.45	11.25	2.44	17.98	9.87	0.55	11.28	1.96	1.41	97.21
	Core	40.52	12.5	1.95	14.95	11.17	0.29	11.53	1.98	1.38	96.26
	Rim	40.19	11.65	2.7	15.62	10.47	0.56	11.46	2.06	1.34	96.05
C	Core	40.66	11.98	2.43	16.79	10.83	0.53	11.86	2.05	1.54	98.71
	Rim	39.84	12.68	2.55	15.78	11.34	0.42	11.97	2.23	1.34	98.18
	Core	40.94	12.76	2.06	16.81	10.92	0.56	11.87	1.93	1.63	99.46
	Rim	38.99	15.36	2.23	14.17	11.91	0.27	12.25	2.42	1.18	98.79
D	Core	42.12	11.08	1.54	18.24	10.53	0.59	11.92	1.9	1.12	99.04
	Rim	40.96	11.57	2.01	18.06	10.12	0.62	11.77	1.99	1.58	98.78
	Core	40.9	12.19	1.67	18.34	10.01	0.63	11.73	1.88	1.38	98.71
	Rim	41.42	11.68	1.42	18.13	10.05	0.7	11.79	1.99	1.28	98.46
E	Core	42.6	11.29	1.5	18.38	10.25	0.64	11.58	1.95	1.17	99.35
	Rim	39.91	12.91	2.56	17.55	10.3	0.54	11.69	2.26	1.34	99.06
	Core	42.44	10.92	1.54	18.33	10.31	0.63	11.66	1.96	1.32	99.11
	Rim	40.83	11.84	2.43	16.43	10.56	0.48	11.83	1.91	1.5	97.85
F	Core	39.87	13.26	2.22	17.46	10.33	0.5	11.77	1.84	1.44	98.69
	Rim	40.52	11.56	2.53	17.71	10.29	0.55	11.8	1.78	1.51	98.33
	Core	40.18	11.88	1.92	20.04	9.61	0.53	11.75	1.91	1.35	99.18
	Rim	40.46	10.71	1.89	17.81	10.22	0.55	11.66	1.55	1.51	96.36
J	Core	41.16	11.74	2.15	17.84	10.19	0.6	11.89	2.08	1.54	99.3
	Rim	40.12	15.27	2.19	14.43	11.98	0.19	12.08	2.12	1.17	99.56
	Core	41.3	11.89	1.95	17.4	10.48	0.7	11.62	1.94	1.52	98.84
	Rim	40.38	12.65	2.57	17.93	10.19	0.51	11.55	2.05	1.55	99.38

radiogenic magmas. Plagioclase near the recharging magma experiences an increase in temperature that may result in possible resorption of the original phenocryst rim (Figure 1.9). As the recharging and host magmas hybridize, new, more anorthitic plagioclase grows on the phenocryst; this new rim has a lower $^{87}Sr/^{86}Sr$ ratio than the previous, inner zone.

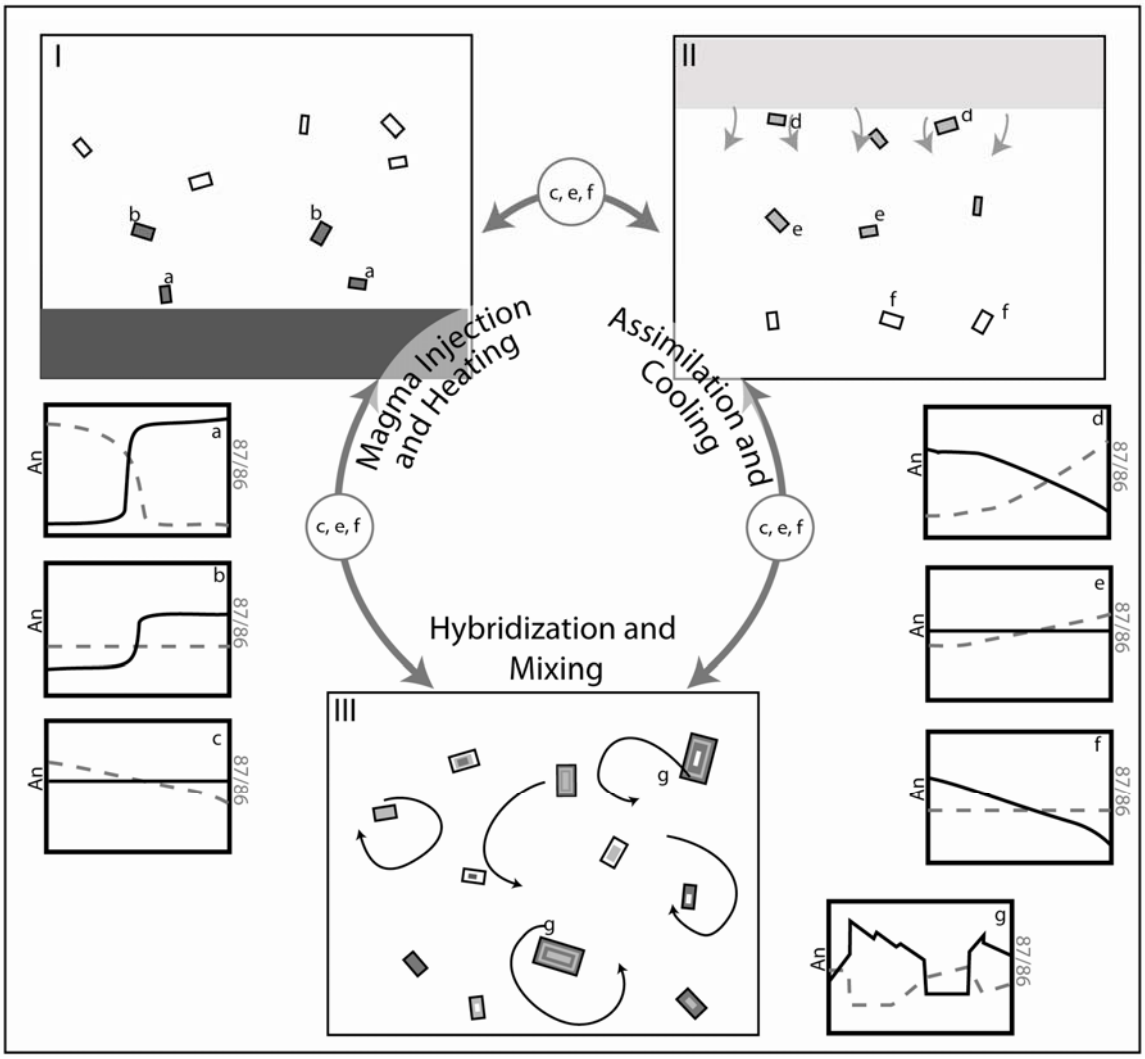

Figure 1.9. Diagram showing formation of different zoning types. In figure A, interval 1, crystals a, b, and c all crystallize with invariant An and 87Sr/86Sr ratios. As hotter, more primitive magma (dark gray) is injected in interval 2, crystal a is engulfed by the intruding magma and forms a Type I zone. Crystal b, on the other hand, is far enough from the intruding magma that it experiences an increase in temperature, but no change in isotopic composition, and c is far enough away that it remains entirely unchanged. During interval 3, the two magmas hybridize (light gray), producing a Type II zone in crystal a, and lowering the isotopic ratio of b. Crystal c remains far enough from the intrusion that it records only very minor changes in *An* and $^{87}Sr/^{86}Sr$ ratio. (cont. on next page)

Figure 1.9 (continued). Interval 1 of figure B is identical to that of figure A. In interval 2, however, assimilation of country rock (gray) begins to occur and is recorded by the crystal closest to the wall (d) as a Type II zone. In interval 3, host magma contaminated by country rock penetrates further into the chamber recorded as a type II zone in crystal e, and eventually, as a small amplitude Type IV zone in crystal f. It is important to consider the processes depicted in figures A and B together, such that the heat required for assimilation of wall-rock (B) may be provided by a hot intruding magma (A). Furthermore, mixing of the system will move crystals through the chamber resulting in a single crystal, for example, perhaps developing Type I zones in one magma injection, and Types II, III, or IV in a later event when the crystal is farther from the injection.

Type II zones have decreasing *An* content and increasing $^{87}Sr/^{86}Sr$ ratios. The change in isotopic ratios requires that the composition of the crystallizing melt became more radiogenic. The accompanying decrease in *An* content suggests the melt must also became more evolved and possibly cooler and/or dryer. As noted earlier, Type II zones frequently occur in contact with an inner Type I zone. Thus two processes, hybridization and assimilation, may result in Type II zones. In the first, following a recharge event, after a Type I zone forms, the magmas may continue to hybridize, such that the comparatively hotter, more primitive hybrid mixes further with the host magma resulting in cooling and a gradual return to the original $^{87}Sr/^{86}Sr$ ratios (Figure 1.9). This scenario results in growth of a rim with decreasing *An* content and increasing Sr isotopic ratio. Such a scenario assumes that the injection is relatively small compared to the existing magma body. The second scenario envisions that Type II zones could form through assimilation of radiogenic country rock. The sedimentary and metamorphic rocks presumed to underlie El Chichón are more radiogenic than the El Chichón magmas (Figure 1.2; Tepley et al., 2000). Assimilation of such rocks would cool the magma,

resulting in more albitic plagioclase (Spera and Bohrson, 2004). If Type II zones represent assimilation, then coupled Type I and II zones may indicate that frequent injections of hot magma provides the heat necessary for the chamber to partially melt and ingest wall rock.

Changes in *An* content unaccompanied by Sr isotopic variations (Type III zones) record a change in either temperature or melt composition. Increases greater than ~10 mol.% most likely reflect heating of the chamber. Given that replenishment by comparatively hotter magma is the only way a chamber may be significantly heated, but Type III zones do not have isotopic changes, positive Type III zones may record crystallization near a recharging magma where the thermal, but not compositional, effects manifest (Figure 1.9). Crystallization resulting from cooling is the most reasonable explanation for Type III zones with similar amplitude decreases in *An* content. Smaller changes in *An* content (e.g. < 5 mol.%) are likely the result of circulation or convection through a magma chamber with minor variations in temperature, or the result of differential plagioclase growth kinetics of Ca, Na, Al, and Si (although it should be noted that this latter mechanism is unlikely to produce zoning with amplitudes greater than 2 mol.% An, Ginibre et al., 2002).

Type IV zones, with changes in only Sr isotopic ratios, require a change in melt composition without a concomitant change in bulk composition or temperature. These zones are likely related to injection of new magma or assimilation of wall rock and formation of Type II zones. At some time following injection or assimilation, the contaminated, hybridizing magma is mixed back into the main host body of magma (Figure 1.9). During this process, the host magma temperature may not change significantly, but, the isotopic composition of the host magma will trend toward that of

the hybrid, while that of the hybrid magma will trend toward that of the host. Thus Type IV record the far-field effects of country rock magma injection and country-rock assimilation.

How long do crystals reside at El Chichón? In particular, do the complex zoning patterns present in plagioclase phenocrysts represent multiple cycles of recharge, hybridization, assimilation, and crystallization between eruptions, or are eruptions also recorded in these zoning patterns? Sr isotopic diffusion profiles provide one means of estimating the maximum residence time of a particular crystal. Ramos et al. (2005) used this technique in examining isotopic disequilibria between plagioclase phenocrysts and melt in the Columbia River Basalts. Here I apply it to the El Chichón Type I zones.

Given that Type I zones are likely the result of rapid changes in temperature and isotopic composition, I approximate their initial shapes as step functions. With time, this profile will relax such that the $^{87}Sr/^{86}Sr$ ratio of the inner side decreases and the outer side increases. The length over which the profile relaxes is a function of Sr diffusivity, time, and temperature. Using measured *An* contents, temperatures of 800˚-830˚C (Macias et al., 2003; Andrews et al., 2005), and reasonable estimates of a compositionally and thermally dependent diffusion coefficient of Sr in plagioclase ($\sim 10^{-18}$ to 3×10^{-20} m^2/s; Giletti and Casserly, 1994), I calculate plagioclase residence times as short as 50 years, and as long as 500 years (Carslaw and Jaeger, 1959). Although this range is quite large, its upper end is similar to the eruption recurrence interval for El Chichón. These residence times are similar to those calculated for other intermediate composition arc volcanoes (Costa et al., 2003; Zellmer et al., 2003; Gioncada et al., 2005), and predict Stokes settling length scales of <70 m for plagioclase and ~150 m for amphibole. Significantly, the maximum residence times do not permit single crystals to record

significant portions of the Holocene eruption history of El Chichón, as suggested by previous work (Belkin et al., 1984; McGee et al., 1987; Tepley et al., 2000). It should be noted that the sharpness in Sr diffusion profiles is actually lessened by the smoothing technique employed with the LA-ICP-MS Sr data, and thus our time estimates are maximums.

1.5.2 Origin of Zoning in Hornblende

Hornblende displays a range of textures, most notably some brown hornblendes in Units F and J have prominent sieved cores or dissolution textures and may be rimmed by augite. Formation of sieved cores, dissolution textures, and augite rims require that the crystal be removed from its stability conditions, either by heating or coming into contact with a drier magma (Browne et al., 2003). Compositional zoning in hornblende also requires changes in magma temperature or composition (Holland and Blundy, 1994; Bachman and Dungan, 2002). But given that only Al and Si compositions vary significantly, compositional changes are unlikely to have formed the rims on hornblende, and instead the rims most likely record thermal changes. Applying the hornblende-plagioclase thermometer of Holland and Blundy (1994) to our hornblende compositions and using plagioclase rim compositions (An_{40} to An_{50}), indicates core-to-rim temperature variation of ~60˚ in most samples. Interestingly, these temperature variations may be positive or negative. The greatest temperature variations are positive and are recorded in Units F and J (up to 100˚C), both of which contain sieved hornblendes. The augite rims on hornblende in Units E and F indicate an increase in melt temperature beyond the hornblende stability field (Browne et al., 2003).

The most reasonable explanation for the formation of the textures and zoning in hornblende is similar to that for plagioclase. Zoned hornblende record heating events resulting in zoning and/or dissolution (Browne et al., 2003). If the heating event is small enough, additional, more Al-rich zones are grown. If the event is larger, hornblende may undergo dissolution prior to growth of new hornblende. In instances where the heating is extreme, the magma is heated beyond hornblende stability and augite forms. These two textures could form in the same event, and thus the augite-mantled hornblende formed very near an injecting magma (analogous to plagioclase Type I zones) whereas non-mantled crystals formed farther from the injection (analogous to Type III zones). The negative core-to-rim temperatures likely record mixing of amphiboles from the comparatively hot hybrid with the cooler host magma. This mixing process is further indicated by the occurrence of euhedral hornblende within ~100 μm of sieved and/or mantled hornblende.

1.5.3 Repeated Cycles of Recharge, Assimilation, and Hybridization

Any model describing the origin of various zoning patterns in plagioclase phenocrysts at El Chichón must explain independent (Types III and IV zoning) and coupled (Types I and II zoning) variations in major elements and Sr isotopic compositions. Thermal events recorded in amphibole textures and compositional zoning need to be explained. Furthermore, the model must be able to generate multiple zoning types in single crystals and thoroughly mix these different crystals together before erupting. Lastly, long-term bulk compositional homogeneity must be maintained. With those conditions and processes in mind, I propose a model that incorporates repeated

recharge, assimilation, hybridization, and "passive" crystallization to explain the zoning patterns observed at El Chichón.

When hot, isotopically primitive magma intrudes into the host magma, crystals near the contact or in the mixing are heated greatly; this increase may be sufficient to produce dissolution, patchy, or sieve textures in plagioclase (and hornblende) (Figure 1.9). As the injecting and host magmas mix, more anorthitic plagioclase with lower $^{87}Sr/^{86}Sr$ ratios grow on the existing plagioclase phenocrysts (Type I zones). As mixing continues, the hybrid cools and begins to take on the $^{87}Sr/^{86}Sr$ ratio of the host magma, depending on the relative proportions of host and intruding magmas. Plagioclase with decreasing *An* and increasing $^{87}Sr/^{86}Sr$ ratio grows on the phenocryst producing Type II zones and hornblende may record a decrease in temperature. The frequent occurrence of Type I zones followed by Type II zones suggests this process is common at El Chichón. This recharge and hybridization process can also produce Type III zones in plagioclase and Al-Si zoning in hornblende. The thermal fluxes during these cycles in injection are sufficient to heat parts of the chamber to ~60˚C or greater and are the likely source of heat for partial melting of wall rock. Plagioclase and hornblende near enough to experience the thermal result of recharge without encountering the injected or hybridizing magma will grow zones with increasing *An* or Al, respectively.

As the host magma is in contact with the wall rock, it will heat and assimilate the wall rock (Figure 1.9). Crystals in magma interacting most strongly with the wall rock will acquire Type II zones. When this contaminated magma mixes back into the host magma, crystals in the host may develop Type IV zones.

The presence of multiple and repeated zoning types within individual crystals indicates that recharge, assimilation, and crystallization events occur repeatedly prior to

eruption. Considering that multiple zoning types occur within each crystal, those crystals must have circulated through the magma body. Given crystal residence times, these cycles of recharge, assimilation and crystallization must occur during periods of <500 years. Further evidence of residence times on the order of the eruption recurrence interval is seen in the crystal populations and textures. Although certain events may have large impacts on the system (e.g. thoroughly sieved plagioclase and hornblende mantled by augite both record significant heating), these textures appear only periodically, thus it is unlikely that the crystals are from a long-lived crystal mush.

The disparities in zoning patterns in crystals found in the same pumice indicate each crystal experienced a different sequence of processes. But, as discussed above, a single event can be responsible for different zoning patterns. Given the length scales over which hybridization, assimilation, and cooling occur (meters to 10's-100's of meters), it is impossible for these crystals to have grown "in place" (i.e. only mm apart). Instead, these crystals must have nucleated and grown far apart, before mixing and melt homogenization were complete (Figure 1.9).

Thermally driven mixing keeps the chamber well-mixed as the rates of convection are at least an order of magnitude faster than settling velocities of the crystals ($>10^{-5}$ m/s compared with $<10^{-6}$ m/s; Huppert and Sparks, 1980; Snyder, 2000; Turcotte and Schubert, 2002). The difference in settling and mixing rates indicates that phenocrysts are effectively coupled to the melt and thus record local changes in melt composition and temperature. For phenocrysts with disparate zoning patterns and similar rims to erupt in the same pumice, melt homogenization and mixing must finish only shortly before eruption. Given the infrequent occurrence of mafic enclaves or other magmatic inclusions at El Chichón, melt homogenization must be quite efficient (Tepley et al.,

2000). Using our data and the plagioclase growth rates calculated by Larsen (2005) (4×10^{-10} to 65×10^{-10} cm/s) I estimate that each eruption occurred weeks to months after homogenization. This supports earlier work by Macias et al. (2003) proposing that recharge triggered the 550 y.B.P. eruption, but suggests that not all recharge events trigger an eruption.

Interestingly, there appears to be a balance between the rates of recharge, assimilation, and crystallization at El Chichón over at least the past 3100 years. Consider that despite crystals recording Sr isotopic variations >0.002, the bulk isotopic compositions have varied by <0.0004. Thus although there is a slightly decreasing trend in radiogenic components with time, this change is insignificant compared with the recharge and assimilation processes underway. Moreover, despite numerous recharge events, and crystallization and fractionation processes, the magmas erupted from El Chichón have maintained the same latite-shoshonite composition and mineral assemblages over more than 3100 years. One way to interpret these data is that the recharging magmas are the heat source for wall rock assimilation, thus during the Holocene repeated pulses of less radiogenic Sr introduced by injected magmas have been offset by assimilated radiogenic Sr.

The maintenance of this balanced system may indicate that the changes recorded in plagioclase crystals were induced by comparatively small volume events, such that the entire chamber did not experience significant changes in bulk properties. This interpretation is supported by EC-E'RAχFC models indicating, not surprisingly, that large recharge volumes result in more substantial thermal, chemical, and isotopic changes to the system (Spera and Bohrson, 2004). Small volume events also facilitate the contemporaneous growth of different zoning types in different parts of the chamber. The

highly sieved plagioclase and hornblendes common in units C, E, F, and J may record larger volume recharge events that affected a greater portion of the chamber.

Our model is thus similar to that of Tepley et al. (2000) in that zoning is dominantly a function of changes in temperature and melt composition initiated by recharge rather than fluctuations in volatile pressure as proposed by earlier research (Belkin et al., 1984; McGee et al., 1987). In addition, I agree with suggestions that the same processes have operated at El Chichón during at least the last 3100 years, and possibly the entire eruptive history of the volcano (Tepley et al., 2000). Significantly, however, because our estimates of phenocryst residence times are shorter than or equal to the eruption recurrence interval, individual crystals cannot record the entire magmatic history at El Chichón. Our model thus requires numerous small volume recharge pulses between eruptions instead of infrequent, eruption-triggering, large volume recharge events.

1.6 CONCLUSIONS

Plagioclase and hornblende phenocrysts at El Chichón record multiple cycles of small volume magma recharge and assimilation during the past 3100 years. Sr isotopic zonation is unlikely to persist in plagioclase at magmatic temperatures for more than ~500 years, thus the multiple recharge events recorded in numerous crystals indicate the recharge and assimilation cycles are shorter than the eruptive occurrence interval. The diversity of crystal zoning patterns found within each eruption indicates that different zoning types may form contemporaneously and that the system is very well mixed. This hybridization process maintains an effectively steady-state balance between recharge and assimilation such that the long term compositional effects of assimilation and recharge

are roughly equal and El Chichón's bulk chemical and isotopic composition has remained essentially constant over the past 3100 years.

Chapter 2: Effects of Caldera Collapse on Conduit Dimensions and Magma Decompression Rate: An Example from the 1800 ^{14}C yr BP Eruption of Ksudach Volcano, Kamchatka, Russia

Caldera collapse changes volcanic eruption behavior and mass discharge. Many models of caldera formation predict that those changes in eruption dynamics result from changes in conduit and vent structure during and after collapse. Unfortunately, no previous studies have quantified or described how conduits change in response to caldera collapse. Changes in pumice texture coincident with caldera formation during the 1800 ^{14}C yr BP KS_1 eruption of Ksudach Volcano, Kamchatka, provide an opportunity to constrain magma decompression rates before and after collapse and thus estimate changes in conduit geometry. Prior to caldera collapse, only white rhyodacite pumice with few microlites and elongate vesicles were erupted. Following collapse, only gray rhyodacite pumice containing abundant microlites and round vesicles were erupted. Bulk compositions, phase assemblages, phenocryst compositions, and geothermometry of the two pumice types are indistinguishable, thus the two pumice types originated from the same magma. Geothermobarometry and phase equilibria experiments indicate that magma was stored at 100-125 MPa and 895±5°C prior to eruption. Decompression experiments suggest microlite textures observed in the white pumice require decompression rates of >0.01 MPa s^{-1}, whereas the textures of gray pumice require decompression at ~0.0025 MPa s^{-1}. Balancing those decompression rates with eruptive mass discharges requires conduit size to have increased by a factor of ~4 during caldera collapse. Slower ascent through a broader conduit following collapse is also consistent with the change from highly stretched vesicles present in white pumice to round vesicles

in gray pumice. Numerical modeling suggests that the mass discharge and low decompression rates during the Gray Phase require the post-collapse conduit to have a very broad base and narrow upper region.

2.1 INTRODUCTION

Calderas form during voluminous eruptions, when a volcanic edifice collapses into an emptying magma chamber. Observations of modern eruptions and interpretations of ancient deposits indicate that collapse is frequently accompanied by increased mass discharge and a change from dominantly buoyant, Plinian behavior to generation of dominantly non-buoyant pyroclastic flows (Sigurdsson and Carey, 1989; Scott et al., 1996; Andrews et al., 2007). Such observations have been incorporated into models of caldera formation that predict both increased mass discharge and pyroclastic flow generation after collapse (Bacon, 1983; Druitt and Sparks, 1984; Hildreth and Mahood, 1986; Suzuki-Kamata et al., 1993; Wilson and Hildreth, 1997; Lipman, 2000). Those models, primarily developed for very large eruptions, describe initial activity at a single vent, initiation of collapse after a small (~10%) fraction of magma is erupted, and the opening of multiple or ring vents during and after collapse (Bacon, 1983; Druitt and Sparks, 1984; Hildreth and Mahood, 1986; Suzuki-Kamata et al., 1993; Wilson and Hildreth, 1997; Lipman, 2000). The increased number and size of those vents, and the conduits that supply them, is believed to accommodate the increased mass discharge (e.g. Wilson and Hildreth, 1997). Contrary to such general models, caldera collapse likely occurs relatively late in eruptions of more modest volume (~10 km^3 magma, DRE), after ~3/4 of the magma or more has been expelled (Gardner and Tait, 2000; Roche and Druitt, 2001; Andrews et al., 2007). Interestingly, although pyroclastic flow generation may

increase following caldera collapse in those smaller eruptions, mass discharge does not necessarily increase (Gardner and Tait, 2000; Andrews et al., 2007).

Absent from most studies of caldera-forming eruptions are quantitative descriptions of changes in conduit geometry following collapse or thorough examinations of the effects of collapse on magma ascent rate. Understanding changes in conduit geometry and magma ascent rate is critical to interpreting changes in their product, mass discharge. Moreover, because magma ascent may be driven by buoyancy, overpressure in the chamber, or some combination of those forces, and is strongly affected by conduit size (Druitt and Sparks, 1984; Jaupart, 2000; Mastin and Ghiorso, 2000; Mastin, 2002), balancing mass discharge, conduit geometry, and magma ascent rate can provide insight into changes in subsurface structure following caldera collapse.

Here, I quantify changes in decompression and ascent rate during caldera collapse and infer changes in conduit structure by comparing textures of decompression experiments with measured changes in groundmass textures within pumice erupted during the KS_1 caldera-forming eruption of Ksudach volcano. That eruption, ~1800 ^{14}C yr BP, occurred in four phases, and caldera collapse happened after ~65% of the total eruptive volume was ejected. Mass discharge remained relatively constant or decreased slightly following collapse (Andrews et al., 2007). My work shows that a change in pumice color from white to gray coincident with caldera collapse (Andrews et al., 2007) reflects changes in vesicle texture, and those differences and increased microlite number densities reflect a reduced decompression rate. Interestingly, the balance between mass discharge, conduit size, and decompression rate suggests that although the conduit base widened significantly following collapse, upper regions of the conduit narrowed.

2.1.1 KS1 Eruption Background

The ~1800 ^{14}C yr BP KS_1 eruption deposited ~8.5 km^3 of compositionally uniform rhyodacite magma (dense rock equivalent, DRE) along much of the length of the Kamchatka Peninsula (Figure 2.1) (Braitseva et al., 1996; Andrews et al., 2007). A complete description of the eruption and its deposits can be found in Andrews et al. (2007). In summary, the eruption can be subdivided into four phases based on mass discharge, lithic concentration, and pumice color. During the Initial Phase, mass discharge doubled from $5x10^7$ to 10^8 kg s^{-1} and 1-1.4 km^3 of magma (DRE) was erupted. Mass discharge during the Main Phase increased to 2-$6x10^8$ kg s^{-1} and 4.5-5.5 km^3 of magma (DRE) was deposited. Although the Lithic Phase deposits are volumetrically small, ~0.2 km^3 magma (DRE), mass discharge remained relatively high during this phase, 1-$4x10^8$ kg s^{-1}. Gray Phase mass discharge did not change significantly from the previous two phases, remaining at 2-$3x10^8$ kg s^{-1}, and 2.0-2.5 km^3 of magma (DRE) was erupted.

Eruption rates of accidental lithics and the concentration of those lithic fragments in fall deposits vary substantially with the eruption phases. During the Initial Phase, approximately 0.2 km^3 of accidental lithics were erupted at rates of 0.5-$2.0x10^7$ kg s^{-1}, resulting in fall deposits with up to ~20 wt.% lithics. The eruption rate of lithics during most of the Main Phase was 1-$2x10^7$ kg s^{-1}, as nearly 0.5 km^3 of lithics were ejected to produce fall deposits with generally <10 wt.% lithics. Lithic Phase fall deposits contain >50 wt.% lithics, reflecting the eruption of ~0.3 km^3 of lithics at rates of 2-$7x10^7$ kg s^{-1}. Lithic eruption rates during the Gray Phase decreased to 0.5-$1.0x10^7$ kg s^{-1}, as approximately 0.25 km^3 of lithics were erupted, resulting in fall deposits with ~10 wt.% lithics.

Collapse of Ksudach Caldera V (Figure 2.1) likely began during the Lithic Phase (Andrews et al., 2007). The deposits represent eruption of a single magma and pumice color thus indicates the timing of eruption relative to caldera collapse: careful and thorough inspection shows that no gray pumice were erupted before and no white pumice after the start of the Gray Phase (Andrews et al., 2007). In addition, caldera formation caused an increase in the eruption of pyroclastic flows: during the Main Phase, ~1/3 of the eruptive mass discharge fed flows, whereas ~2/3 of the Gray Phase mass discharge supplied pyroclastic flows (Andrews et al., 2007).

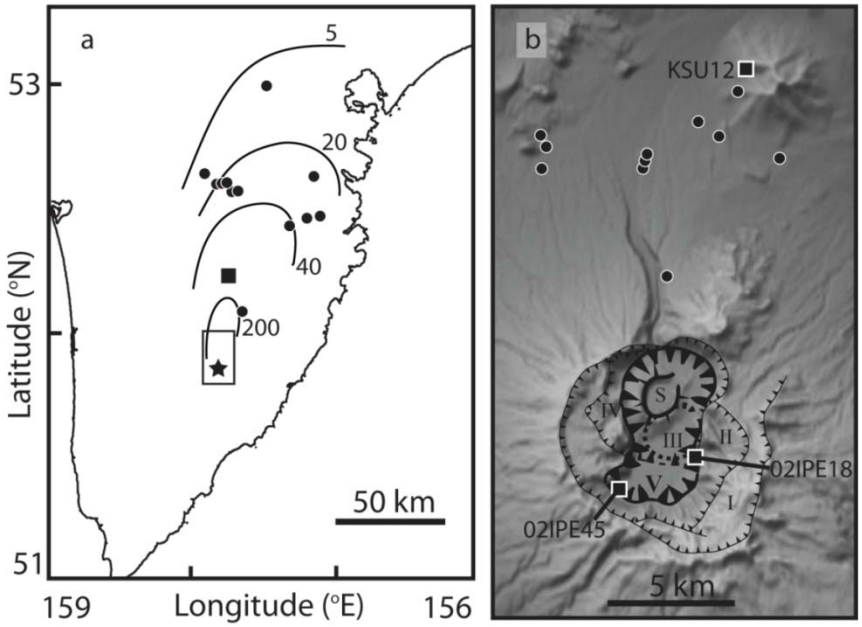

Figure 2.1. Location of Ksudach volcano in southern Kamchatka. a) Cumulative deposits from the KS1 eruption are dispersed over much of Kamchatka along a NNE depositional axis (Andrews et al., 2007). b) The 1800 ^{14}C KS_1 eruption formed Caldera V, the youngest of five nested calderas (I-V) in the Ksudach massif; recent activity has been focused at Shtuybel cone, S (after Braitseva et al., 1996). Sample sites from Andrews et al. (2007) are shown with black circles, locations of samples used in this study are indicated by black boxes (location KSU23 in a, and locations 02IPE18, 02IPE45, and KSU12 in b).

2.2 EXPERIMENTAL AND ANALYTICAL METHODS

2.2.1 Phase Equilibria Experiments

Samples of pumice were collected from near the southern caldera rim and at locations ~11 km NNE and ~50 km N of the caldera (Figure 2.1). Bulk chemical analyses were collected for Initial Phase pumice 02IPE45 and Gray Phase pumice 02IPE18. Thin sections were made of those samples and additional thin sections were prepared from Initial, Main, Lithic, and Gray Phase pumice for glass, phenocryst, and textural analysis. A portion of sample 02IPE45 was gently crushed to a <50 μm powder for use as starting material in phase equilibria and decompression experiments.

Phase equilibria experiments were prepared by sealing powder in 2-mm O.D. $Ag_{70}Pd_{30}$ tubing with sufficient deionized H_2O to ensure that all experiments were water saturated ($P_{total}=P_{H2O}$). Those experiments were conducted in externally heated Waspalloy pressure vessels with nickel filler rods and pressurized with H_2O at a range of temperatures and pressures (Table 2.1). Oxygen fugacity during the experiments is estimated at approximately one log unit (±0.5) above the Ni-NiO (NNO) buffer curve. All experiments were quenched by first cooling the pressure vessels with forced air, and then immersing them in water. After each experimental run, the sample was mounted in epoxy on a glass slide and polished for analysis. Stable phases were identified using a petrographic microscope and electron microprobe.

One high-temperature phase equilibria experiment, K-22B, was conducted in an externally heated TZM pressure vessel pressurized with argon. Oxygen fugacity for that experiment was fixed at NNO by loading Ni metal and NiO powders into a 4-mm $Ag_{70}Pd_{30}$ tube also loaded with a 2-mm $Ag_{70}Pd_{30}$ tube containing the sample and sufficient deionized water to ensure saturation of the experiment. The presence of both

Table 2.1 Phase equilibria and decompression experimental conditions. Initial material for experiments was either crushed white pumice 02IPE45, or a previously run experiment. Stable mineral phases are indicted by ox (Fe-Ti oxides), px (pyroxene), or plg (plagioclase). Plagioclase composition is indicated by anorthite content, for example An_{30} denotes plagioclase with 30 mol% anorthite; uncertainties in anorthite content are estimated to be 1 mol%. Crystallinity of microlite phases present in decompression experiments, but in concentrations <0.1 vol.% are denoted *tr*. Number densities, N_V, are presented in mm^{-3}. All decompression experiments were quenched at 20 MPa. Experiments marked with an asterisk (e.g. KD-1*) were used as starting material for subsequent experiments, and hence have no decompression rate. Uncertainties in N_v are 1 standard deviation. (Table is continued on next page.)

Run	Initial Material	Duration (hours)	P_i (MPa)	T (°C)	Stable Phases	dP/dt (MPa/s)	Fe-Ti oxides vol.%	N_V	Pyroxene vol.%	N_V	Plagioclase vol.%	N_V
K-1R	*02IPE45*	92	100	900	gl, ox, px, plg (An_{43})	--	--	--	--	--	--	--
K-2	*02IPE45*	96	100	750	gl, ox, px, plg	--	--	--	--	--	--	--
K-3	*K-1R*	96	100	800	gl, ox, px, plg (An_{30})	--	--	--	--	--	--	--
K-4	*K-2*	96	100	800	gl, ox, px, plg (An_{29})	--	--	--	--	--	--	--
K-5	*K-1R*	96	100	850	gl, ox, px, plg (An_{35})	--	--	--	--	--	--	--
K-6	*K-2*	96	100	850	gl, ox, px, plg (An_{38})	--	--	--	--	--	--	--
K-7	*K-1R*	96	100	875	gl, ox, px, plg (An_{35})	--	--	--	--	--	--	--
K-8	*K-2*	96	100	875	gl, ox, px, plg (An_{37})	--	--	--	--	--	--	--
K-10	*02IPE45*	96	100	950	gl, ox, px	--	--	--	--	--	--	--
K-11A	*K-1R*	95	200	900	gl, ox, px	--	--	--	--	--	--	--
K-11B	*K-1R*	95	200	900	gl, ox	--	--	--	--	--	--	--
K-12A	*K-6*	236	200	850	gl, ox, px	--	--	--	--	--	--	--
K-12B	*K-1R*	236	200	850	gl, ox, px	--	--	--	--	--	--	--
K-13	*K-7*	233	100	850	gl, ox, px, plg (An_{36})	--	--	--	--	--	--	--
K-14	*02IPE45*	162	50	900	gl, ox, px, plg (An_{37})	--	--	--	--	--	--	--
K-15	*02IPE45*	364	50	850	gl, ox, px, plg (An_{31})	--	--	--	--	--	--	--
K-16	*K-11A*	389	250	850	gl, ox, px	--	--	--	--	--	--	--
K-17	*K-1R*	294	150	875	gl, ox, px	--	--	--	--	--	--	--
K-18A	*K-1R*	183	200	875	gl, ox, px	--	--	--	--	--	--	--
K-18B	*K-8*	183	100	875	gl, ox, px, plg (An_{40})	--	--	--	--	--	--	--
K-19	*02IPE45*	120	100	900	gl, ox, px, plg (An_{45})	--	--	--	--	--	--	--
K-20	*02IPE45*	209	50	875	gl, ox, px, plg (An_{36})	--	--	--	--	--	--	--
K-21	*K-14*	141	100	900	gl, ox, px, plg (An_{38})	--	--	--	--	--	--	--
K-22A	*K-15*	96	100	850	gl, ox, px, plg (An_{30})	--	--	--	--	--	--	--
K-22B	*K-19*	118	100	925	gl, ox, px	--	--	--	--	--	--	--
K-23	*K-11A*	94	150	825	gl, ox, px, plg (An_{36})	--	--	--	--	--	--	--
K-24	*02IPE45*	96	150	825	gl, ox, px, plg (An_{37})	--	--	--	--	--	--	--

Table 2.1 (continued).

Run	Initial Material	Duration (hours)	P_i (MPa)	T (°C)	Stable Phases	dP/dt (MPa/s)	Fe-Ti oxides vol.%	Fe-Ti oxides N_V	Pyroxene vol.%	Pyroxene N_V	Plagioclase vol.%	Plagioclase N_V
KD-1*	*02IPE45*	96	150	890	gl, ox, px	--	*tr*	$3.6x(\pm2)10^4$	0.3	$1.3(\pm0.5)x10^3$	0	0
KD-2	*KD-1*	--	150	890	--	0.05	0.1	$1.1x(\pm1)10^6$	0.1	$6.5(\pm3)\ x10^4$	0	0
KD-3	*KD-1*	--	150	890	--	0.01	0.3	$5.1x(\pm2)10^5$	0.1	$6.0\ (\pm3)x10^4$	0.2	$1.0(\pm1)x10^2$
KD-4*	*02IPE45*	96	100	890	gl, ox, px, plg	--	0.3	$1.3x(\pm1)10^5$	0.6	$3.8\ x(\pm1)10^4$	2.2	$2.9(\pm1.4)x10^3$
KD-5	*KD-1*	--	150	890	--	0.005	0.2	$5.4x(\pm3)10^5$	0.3	$1.3\ x(\pm0.7)10^4$	*tr*	$1.9(\pm0.2)\ x10^4$
KD-6	*KD-1*	--	150	890	--	0.001	0.3	$2.4x(\pm1)10^5$	1.3	$1.2\ x(\pm0.4)10^5$	6.9	$1.5(\pm1)\ x10^5$
KD-7	*KD-1*	--	150	890	--	0.0025	0.3	$4.4x(\pm2)10^5$	0.5	$1.6\ x(\pm0)10^4$	*tr*	$9.8(\pm2)\ x10^2$
KD-8*	*K-1R*	96	75	900	gl, ox, px, plg (An_{39})	--	0.3	$5.0x(\pm0.9)10^5$	0.8	$1.4\ x(\pm1)10^5$	6.9	$6.3(\pm1)\ x10^5$
KD-9*	*K-19*	96	75	875	gl, ox, px, plg (An_{36})	--	0.5	$3.2x(\pm2)10^5$	0.9	$2.9\ x(\pm1)10^5$	2.7	$1.\ 2(\pm0.7)\ x10^6$
KD-10*	*02IPE45*	96	100	890	--	--	0.2	$1.5x(\pm1.5)10^5$	0.3	$1.9\ x(\pm1)10^5$	0.5	$7.8(\pm5)\ x10^4$
KD-11	*KD-9*	--	75	875	--	0.0025	2.3	$8.0x(\pm4)10^5$	5	$1.5\ x(\pm0.5)10^6$	11.8	$2.0\ (\pm0.7)x10^6$
KD-12	*KD-8*	--	75	900	--	0.0025	0.4	$3.4x(\pm1)10^5$	1.4	$3.7\ x(\pm1)10^5$	2.7	$1.1\ (\pm0.6)x10^6$
KD-13	*KD-10*	--	100	890	--	0.0025	0.3	$4.1x(\pm0.9)10^5$	1	$2.9\ x(\pm0.6)10^5$	3.9	$2.8\ (\pm1)x10^5$
KD-14*	*02IPE45*	96	125	900	gl, ox, px	--	0.1	$1.4x(\pm0.5)10^4$	*tr*	$5.2\ x(\pm1)10^3$	0	0
KD-15	*KD-10*	--	100	890	--	0.001	0.2	$2.0x(\pm0.7)10^5$	0.6	$2.1\ (\pm1)x10^5$	6.7	$2.4\ (\pm1)x10^5$
KD-16	*KD-14*	--	125	900	--	0.001	0.3	$5.0x(\pm2)10^4$	0.2	$1.5\ x(\pm1.5)10^4$	1	$2.0\ (\pm2)x10^4$
KD-17*	*02IPE45*	96	100	890	gl, ox, px, plg	--	*tr*	$8.2x(\pm2)10^4$	0.2	$7.3x(\pm2)10^4$	0	0
KD-19	*KD-17*	--	100	890	--	0.01	0.7	$1.7x(\pm0.7)10^5$	0.5	$3\ x(\pm1)10^3$	13.4	$5.0(\pm5)\ x10^2$
KD-20	*KD-17*	--	100	890	--	0.005	0.5	$1.3x(\pm0.7)10^5$	0.8	$8\ x(\pm4)10^3$	0.2	$3.5(\pm1.5)\ x10^4$

Ni and NiO at the conclusion of the experiment indicates oxygen fugacity was fixed during the run.

To verify phase stabilities, three pairs of reversal experiments were conducted to verify phase stabilities: for a given pressure and temperature, aliquots of one sample equilibrated at higher pressure and/or temperature and one at lower pressure and/or temperature, were reloaded and sealed in 2-mm O.D. $Ag_{70}Pd_{30}$ tubes with sufficient deionized water for saturation and run at the given conditions. The presence of the same phase assemblages and phase compositions in the two experiments is considered to indicate phase stability at the given conditions. All reversal experiments were conducted in Waspalloy pressure vessels with nickel filler rods pressurized with H_2O.

2.2.2 Decompression Experiments

Starting materials for decompression experiments were prepared by loading crushed pumice into 2-mm O.D. $Ag_{70}Pd_{30}$ tubes and then annealing the sample at starting

P-T conditions for at least 96 hours. Groups of experiments were decompressed from different initial conditions (Table 2.1). An aliquot of each starting material was prepared for analysis of microlite textures at initial P-T conditions. Other aliquots of each starting material were reloaded into $Ag_{70}Pd_{30}$ tubes for decompression and held at initial temperature and pressure (+4 MPa) for 2 hours. Decompression was accomplished in multiple increments of 5 MPa using a hand operated pressure intensifier; each pressure drop occurred in less than 5 seconds. The decompression rate was calculated by dividing that 5 MPa decrease by the time between pressure drops; for example, lowering pressure every 1000 seconds results in a decompression rate of 0.005 MPa s^{-1}. All samples were decompressed to 20 MPa and quenched with forced air and then immersion in water. That final pressure approximates the pressure estimated from bulk vesicularities and initial water contents of the white and gray pumice assuming closed-system degassing. Pressure and vesicularity are related with the expression

$$Ves = \frac{\frac{X_{v,P}RT}{P}}{\frac{X_{v,P}RT}{P} + \sum X_i V_i + X_{H2O,P}V_{H2O,P}}$$

Eq. 2.1

in which *Ves* is the volume fraction of vesicles; R is the universal gas constant; T is temperature in K; X_i and V_i are the anhydrous mole fractions and molar volumes of all oxide species in the melt (from Spera, 2000); $X_{H2O,P}$ and $V_{H2O,P}$ are the mole fraction and molar volume of H_2O dissolved in the melt at pressure P, as calculated using the method of Moore et al. (1998). The number of moles of H_2O vapor at a given pressure, $X_{v,P}$, is calculated from the difference of the initial mole fraction of H_2O dissolved in the melt and $X_{H2O,P}$.

2.2.3 Compositional Analyses

Mineral and glass compositions were analyzed with JEOL JXA-8200 and Cameca SX-50 electron microprobes at the University of Texas at Austin and the University of Alaska Fairbanks Departments of Geological Sciences. All analyses were conducted using a 15 kV, 10 nA beam; mineral analyses were conducted with a focused beam, whereas glass analyses were conducted with a 10-μm defocused beam. Analyses were processed using JEOL and Probe For Windows software. Sodium migration in glasses was monitored and corrected using the volatile correction program within Probe For Windows. Comendite glass KN-18 was used to monitor any drift during glass analyses.

Crystals from lightly crushed white (02IPE45) and gray (02IPE18) pumice were selected for melt inclusion analysis. Crystals containing melt inclusions were mounted in orthodontic resin, glued to slides with thermoadhsive Crystalbond® 509, and polished until the inclusions of interest were intersected. The Crystalbond® 509 was then reheated, allowing the crystals to be flipped and reattached to the slide. The opposite sides of the crystals were then polished so that melt inclusions were doubly-intersected and doubly-polished. Immediately prior to FTIR analysis, the orthodontic resin surrounding each crystal was dissolved with acetone; the crystals were then cleaned with ethanol.

Melt inclusion compositions were measured with Fourier Transform Infrared spectroscopy (FTIR) and then electron microprobe. Those samples were analyzed with a ThermoElectron Nicolet Nexus 670 FTIR in the Department of Geological Sciences at the University of Oregon. All analyses were conducted using transmission of white light through a KBr window. For each spectrum, 250 to 1000 scans were collected with a resolution of 4 cm^{-1}. FTIR spectra were examined at 3550 cm^{-1} wavenumbers for total

H_2O. No CO_2 was detected in any inclusion. Measured IR absorbances were converted to water concentrations using the methods of Stolper (1982), Newman et al. (1986), and Zhang et al. (1997). Absorptivity of 76 L mol^{-1} mm^{-1} was used for the 3550 cm^{-1} absorption band. Inclusion thicknesses were measured by mounting the crystals on a pin and examining them on edge, in oil, under a microscope; the error associated with this technique is ±2 μm.

2.2.4 Textural Analyses

Bulk vesicularities of samples were measured using the method of Gardner et al. (1996). The wet and dry masses of 15 pumice each from Main and Gray Phase fall samples KSU-23H and KSU-23A were measured with a pycnometer, and those measurements were converted to bulk pumice densities, ρ_t. The vesicularity was then calculated using

$$Ves = \left(1 - \frac{\rho_t}{\rho_g}\right)$$

Eq. 2.2

by assuming a solid, vesicle-free density, ρ_g, of 2350 kg/m^3. The precision of this technique is estimated to be <0.03, based upon repeated measurements of the same sample.

Vesicle sizes and shapes were quantified through image analysis of back-scattered electron (BSE) images obtained with the electron microprobe. Grayscale images were converted to black and white images showing vesicles and solids. The areas and dimensions of vesicles were then measured using ImageJ. Vesicle aspect ratios were

calculated as the ratio of the long and short axes, *l* and *b*, respectively. Equivalent vesicle radii, *a*, were calculated as:

$$a = \sqrt{lb}$$

Eq. 2.3

Capillary numbers of vesicles, *Ca*, were calculated using the relation of Hinch and Acrivos (1980):

$$\frac{l}{a} = 3.45\sqrt{Ca}$$

Eq. 2.4

Microlite textures of natural and experimental samples were quantified with analysis of BSE images. Plagioclase, Fe-Ti oxide, pyroxene, and plagioclase microlites were outlined manually in each image and their sizes and area measured using ImageJ. Because of their similar appearance in BSE images, orthopyroxene and clinopyroxene were not differentiated, nor were ilmenite and titanomagnetite. Areal crystal number densities, N_A, were calculated using

$$N_A = \sqrt{\frac{n}{A}}$$

Eq. 2.5

where *n* is the number of crystals of a particular phase counted in area *A* of glass only (Hammer et al., 1999). Three-dimensional number densities, N_V, were calculated from the two-dimensional measurements as

$$N_V = \sqrt{\frac{{N_A}^3}{\phi}}$$

Eq. 2.6

where crystallinity, ϕ, is defined as the fraction of the vesicle-free image occupied by the microlite phase of interest.

For samples with three-dimensional microlite number densities of ≤1000 mm^{-3}, N_V was also measured directly using a petrographic microscope by counting the number of crystals in a known area and measuring the thickness of the sample. Because that technique counts crystals within a volume and does not extrapolate two-dimensional number densities into three dimensional values, the technique has greater precision in measuring N_V at low number densities. This greater precision occurs because number densities calculated with the three-dimensional method are directly proportional to the number counted, whereas the values calculated with the two-dimensional technique are proportional to the number counted raised to the 3/2 power. Because the starting materials for decompression experiments contain microlites, number densities of decompression experiments were calculated as the difference of N_V measured in the decompression experiment and N_V of the experiment's starting material.

2.3 RESULTS

2.3.1 Natural Compositions

The KS_1 white and gray pumice are both rhyodacite with 71.5 – 72.1 wt.% SiO_2, have nearly identical alkali concentrations (5.2 – 5.3 wt.% Na_2O and 1.4 wt.% K_2O), and differ by less than 0.1 wt.% in Al_2O_3 concentrations (Table 2.2). Trace element concentrations are similarly indistinguishable with, for example, 178-180 ppm Sr and 1.40-1.41 ppm Eu in both pumice. With few exceptions, the KS_1 white and gray pumice compositions differ by less than 5% (relative to each other).

Both white and gray pumice contain the same phenocryst assemblage: plagioclase, clinopyroxene, orthopyroxene, titanomagnetite, and ilmenite, in order of

decreasing abundance, where phenocrysts are defined as crystals larger than 20 μm. Plagioclase composes ~3 vol.% of the rock (vesicle-free) and occurs as 300-600 μm tabular crystals. Those crystals are frequently twinned and concentrically zoned, and often host glass inclusions. Most zones are An_{40}-An_{50} in composition, but can range from ~An_{35} to ~An_{60}, and are generally 20-50 μm in width. Rim compositions are An_{40}-An_{42}.

Clinopyroxene occurs generally as 200-400 μm prismatic phenocrysts and composes ~1 vol.% of the vesicle-free rocks. Those crystals are green and optically unzoned. Orthopyroxene is present in a similar abundance and occurs as 200-400 μm brown prisms. Occasional glass inclusions are hosted by pyroxene crystals, but less frequently than in plagioclase. Clinopyroxene is typically ~$En_{38}Fs_{21}Wo_{40}$, and orthopyroxene is typically ~$En_{56}Fs_{41}Wo_{28}$ (Table 2.2).

Titanomagnetite and ilmenite are the least abundant phenocryst phases and together compose <1 vol.%. Those two oxides occur as equant, euhedral crystals ~100 μm in size. Titanomagnetite and ilmenite crystals are occasionally found in contact. Titanomagnetite compositions are typically ~35 mol.% ulvospinel; ilmenite phenocrysts range in composition from 76-85 mol.% ilmenite (Table 2.2).

Matrix glass compositions of the two pumice types are also very similar (Table 2.2). All matrix glass is rhyolitic, with SiO_2 concentrations of 74.1(±0.1) wt.% and Na_2O concentrations of 5.0(±0.1) wt.%. Both pumice contain 2.7(±0.3) wt.% FeO and 2.3(±0.2) wt.% CaO.

Table 2.2 Representative whole rock, glass, and mineral compositions of KS_1 white and gray pumice. Representative analyses (oxides in weight percent) of bulk (WR), matrix glass (MG), melt inclusion (MI), plagioclase, clinopyroxene. Melt inclusions contain 3.8-4.4 wt.% H2O, whereas matrix glass is nearly anhydrous. Mineral analyses are presented for plagioclase (plg), clinopyroxene (cpx), orthopyroxene (opx), ilmenite (ilm), and titanomagnetite (mt). All analyses are given as weight percent oxides. Total iron is reported as FeO*. Uncertainties in microprobe analyses are indicated as ($\pm 1\sigma$) for each element. Whole rock compositions were analyzed with XRF at Washington State University. Matrix glass, melt inclusions, and minerals were analyzed with electron microprobe.

Sample	**SiO_2**	**Al_2O_3**	**TiO_2**	**FeO***	**MnO**	**CaO**	**MgO**	**K_2O**	**Na_2O**	**Cr_2O_3**	**Total**
uncertainty	0.26	0.17	0.05	0.15	0.04	0.05	0.02	0.1	0.16	0.01	
White											
WR	71.48	14.54	0.449	3.14	0.142	2.84	0.78	1.37	5.18	--	100
MG	74.12	13.50	0.32	2.70	0.14	2.22	0.49	1.41	5.10	--	100
MI	73.39	13.13	0.27	2.5	0.14	1.67	0.14	1.24	3.22	--	100
plg	53.76	29.18	0.02	0.62	--	11.92	0.05	0.08	5.08	--	100.64
cpx	52.37	1.44	0.33	11.27	0.82	13.75	19.75	0.29	--	--	100.03
opx	52.79	0.62	0.18	23.91	1.86	19.39	1.35	0.03	--	--	100.12
ilm	--	0.16	44.78	48.28	1.21	--	2.44	--	--	0.04	98.43
mt	--	1.91	12.28	78.2	0.94	--	1.42	--	--	0.02	99.09
Gray											
WR	72.14	14.45	0.448	2.94	0.37	2.54	0.95	1.36	2.25	--	100
MG	73.98	13.44	0.36	2.79	0.13	2.46	0.54	1.33	4.96	--	100
MI	72.6	13.87	0.42	2.47	0.13	1.78	0.32	1.19	2.8	--	100
plg	54.94	28.37	0.04	0.55	--	11.08	0.03	0.06	5.23	--	100.3
cpx	52.71	1.05	0.24	12.69	1.11	13.95	18.43	0.28	--	--	100.47
opx	52.79	0.62	0.18	23.91	1.86	19.39	1.35	0.03	--	--	100.12
ilm	--	0.31	40.77	51.09	0.83	--	3.19	--	--	0.03	98.55
mt	--	1.96	12.12	79.57	0.96	--	1.5	--	--	0.02	100.58

Glass inclusions hosted by phenocrysts from white and gray pumice are compositionally indistinguishable and rhyodacitic in composition (Table 2.2). Although SiO_2 concentrations do not vary substantially between inclusions, water concentrations range from ~1.5 – 8 wt.%. Most of that range is likely a result of post-entrapment host

crystallization and leaking during decompression and eruption. Excluding inclusions with anomalously high and low water concentrations, the most reasonable pre-eruption water contents recorded by the inclusions are 4.4(±1.0) and 3.8(±0.9) wt.% H_2O (±1 e.s.d.) for the white and gray pumice, respectively.

2.3.2 Natural Vesicle and Microlite Textures

Both white and gray pumice have bulk vesicularities within 1 estimated standard deviation, 78.2±3.8 and 75.2±3.3 vol.%, respectively. Equivalent radii of vesicles in white and gray pumice are indistinguishable, 50(±15) μm for both. Interestingly, however, the two pumice types have different vesicle shapes (Figure 2.2). Vesicles in white pumice are more elongate: aspect ratios are typically >2:1 and can be >10:1 in white pumice, compared to vesicle aspect ratios <5:1 in gray pumice (Figure 2.3).

More and larger microlites (crystals smaller than 20 μm) are present in gray pumice than in white (Figure 2.2), resulting in much higher microlite crystallinity of the gray pumice, ~25%, than the white, <1%. Microlite number densities for plagioclase, pyroxene (clinopyroxene and orthopyroxene), and magnetite ± ilmenite are orders of magnitude higher in gray pumice

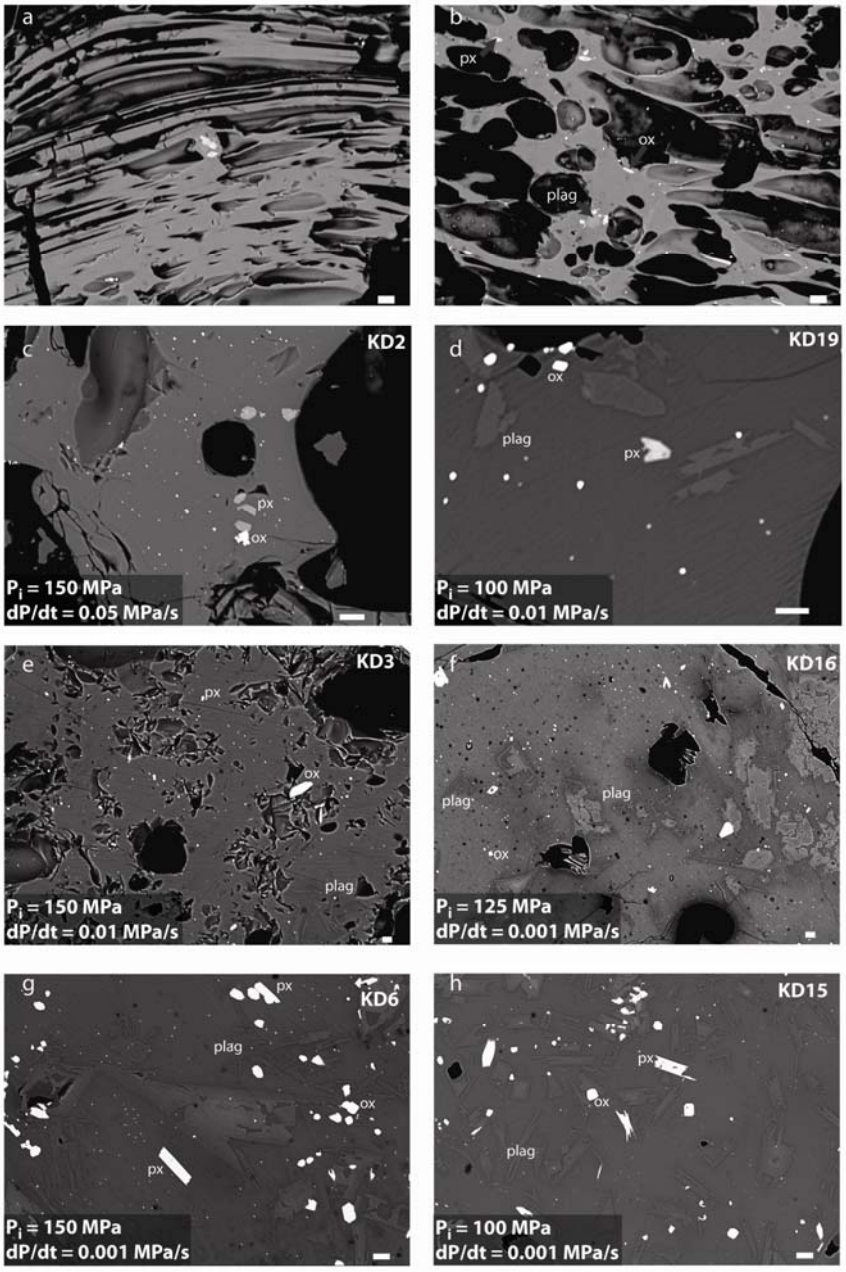

Figure 2.2. Representative textures of KS_1 pumice and decompression experiments. a) White pumice are composed of microlite-free glass. Vesicles in white pumice are commonly have elongate and have aspect ratios >10:1. b) In contrast, gray pumice contain abundant oxide (ox), pyroxene (px), and plagioclase (plag) microlites. Vesicles in gray pumice are generally round with aspect ratios <3:1. (continued on next page)

Figure 2.2 (continued) In experiments KD-2 (c), KD-3 (e), and KD-6 (g), decompressed from initial pressures Pi=150 MPa, microlitenumber density and size increase as decompression rate slows from 0.05 to 0.001 MPa s^{-1}, such that although no plagioclase microlites are present in KD-2, a few swallow-tail plagioclase microlites are present in KD-3, and abundant swallow-tail and skeletal plagioclase microlites are present in KD-6. Variations in starting pressures also affect microlite textures. Comparison of experiments KD3 and KD-19 (d), both decompressed at 0.01 MPa s^{-1}, indicates that experiments decompressed from a higher initial pressure nucleate fewer microlites, and those microlites have more prominent swallow-tail morphologies. Comparison of experiments KD-6, KD-16 (f), and KD-15 (h), all decompressed at 0.001 MPa s^{-1}, suggests that microlite habit is also a function of initial pressure, in that the experiments decompressed from 125 and 150 MPa contain both skeletal and swallow-tail plagioclase microlites whereas KD-15, P_i=100 MPa, contains dominantly swallow-tail plagioclase microlites. The white scale bars in all images are 10 μm.

(Table 2.3). That difference is most apparent in plagioclase, where $2(\pm1)x10^6$ mm^{-3} are present in gray pumice, whereas $1(\pm1)x10^2$ mm^{-3} are present in white pumice. Pyroxene and Fe-Ti oxides are present in densities of ~$4x10^6$ mm^{-3} in gray pumice and 1-$3x10^5$ mm^{-3} in white pumice. Total microlite number densities are approximately ~$4x10^5$ and ~$1.3x10^7$ mm^{-3} for white and gray pumice, respectively. All uncertainties in microlite number densities are reported as ±1 standard deviation.

Size distributions of plagioclase microlites in gray pumice have modes of 2.0 μm, and are positive skewed (Figure 2.4). In contrast, what few plagioclase microlites are present in white pumice are all smaller than 2 μm. Pyroxene size distributions are coarser in gray pumice than in white, 2.0 μm compared to 1.0 μm, but have similar skewness of 1.4-1.7 μm (Figure 2.4). Iron-titanium oxides distributions in both pumice types have 1-μm modes and are positively skewed (Figure 2.4).

Table 2.3. Microlite textures of KS_1 white and gray pumice. Volumetric number densities, N_v, are presented in mm^{-3}. Measurements are presented as the range of the average value plus and minus 1 standard deviation. Presented values represent the average of analyses collected from 29 BSE images of white pumice and 10 BSE images of gray pumice collected at magnifications of 500-1000x.

	Oxide N_v	**Pyroxene** N_v	**Plagioclase** N_v
White	$2(\pm1)x10^5$	$2(\pm1)x10^5$	$1(\pm1)x10^2$
Gray	$4(\pm3)x10^6$	$4(\pm3)x10^6$	$2(\pm1)x10^6$

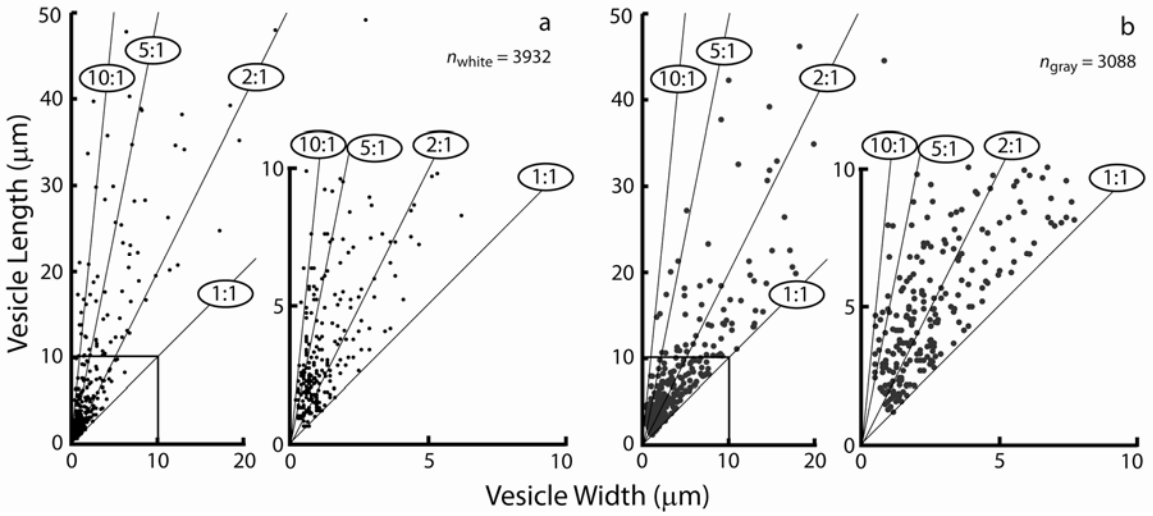

Figure 2.3. Vesicle sizes in white and gray pumice. Vesicles in white pumice (a) are typically more elongate than those in gray pumice (b). Although the two populations overlap, most vesicles in white pumice have aspect ratios (long : short) greater than 2:1 (and as high as ~20:1), whereas most vesicles in gray pumice have aspect ratios less than 5:1. Aspect ratios of vesicles are indicated by diagonal lines extending from the origin, e.g. 2:1.

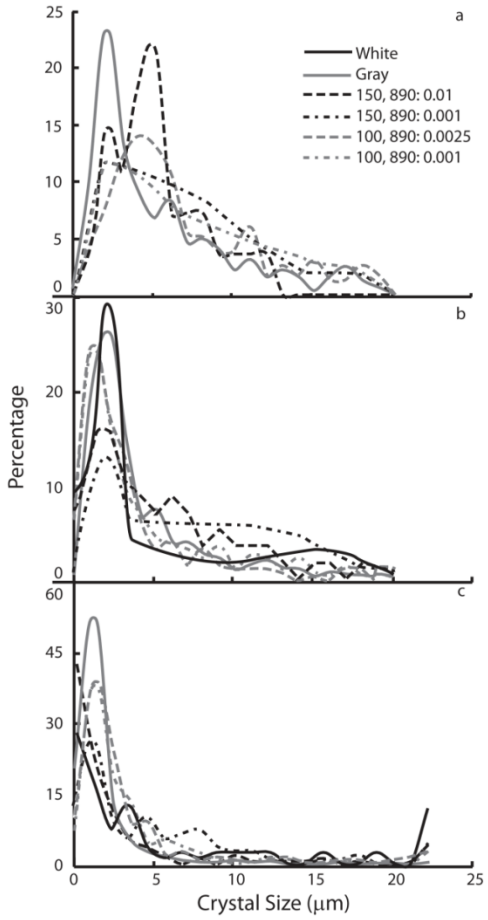

Figure 2.4. Microlite size distributions of natural pumice and representative decompression experiments. a) Plagioclase microlites are nearly absent in white pumice, whereas gray pumice have unimodal distributions with a mode at ~2 μm. In decompression experiments, plagioclase microlites have unimodal distributions that coarsen and develop tails as initial pressure and decompression rate decrease. b) Pyroxene microlites have unimodal distributions with prominent modes at 2 μm. As initial pressure decreases, those modes become more prominent. c) Oxide microlites in experimental samples have unimodal distributions with most crystals smaller than 2 μm. As decompression rate and initial pressure decrease, skewness of the distributions increases. The number of microlites composing each distribution are 0, 420, 23, 235, 357, and 774 plagioclase; 165, 897, 29, 117, 242, and 334 pyroxene; and 61, 495, 167, 112, 177, and 218 Fe-Ti oxide in white pumice, gray pumice, 150 MPa 0.01 MPa s^{-1}, 150 MPa 0.001 MPa s^{-1}, 100 MPa 0.0025 MPa s^{-1}, and 100 MPa 0.001 MPa s^{-1} samples, respectively.

2.3.3 Geothermometry of Natural Samples

Geothermometry of Fe-Ti oxide pairs was determined using the iron recalculation method of Stormer (1983) and the algorithm of Anderson and Lindsley (1988). Temperature estimates were limited to touching pairs of titanomagnetite and ilmenite grains; Mg and Mn contents of those pairs indicates they are in equilibrium (Bacon and Hirschmann, 1988). In addition, application of the program QUILF to electron microprobe analyses of Fe-Ti oxides, clinopyroxene, and orthopyroxene indicates equilibrium among all Fe-Ti-Mg phases (Anderson et al., 1993). Analyses of 12 oxide pairs from white pumice and 8 pairs from gray pumice indicate overlapping temperatures of 891±8 °C (±1 e.s.d.) for the white and 897±6 °C (±1 e.s.d.) for the gray pumice. Consideration of white and gray oxide pairs together yields equilibrium temperatures of 895±5 °C (±1 e.s.d.). Those analyses also indicate oxygen fugacities of $\sim 10^{-11.5}$ bars, or approximately $\log(f_{O2})$ = NNO+1.

2.3.4 Experimental Phase Equilibria

At all pressures and temperatures examined, silicate melt (glass) and Fe-Ti oxides are stable (Figure 2.5). No distinction was made between titanomagnetite and ilmenite for determination of phase stabilities. As expected, both plagioclase and pyroxene become stable as water pressure and/or temperature decreases. For example, at 200 MPa, plagioclase and pyroxene are stable only below 825 °C and 875 °C, respectively, whereas at 100 MPa they are both stable above 900 °C.

Plagioclase varies systematically in composition with temperature and pressure (Figure 2.5). For example, at 100 MPa, anorthite content of plagioclase increases from An_{30} to An_{43} as temperature increases from 800 to 900 °C. Anorthite content increases by

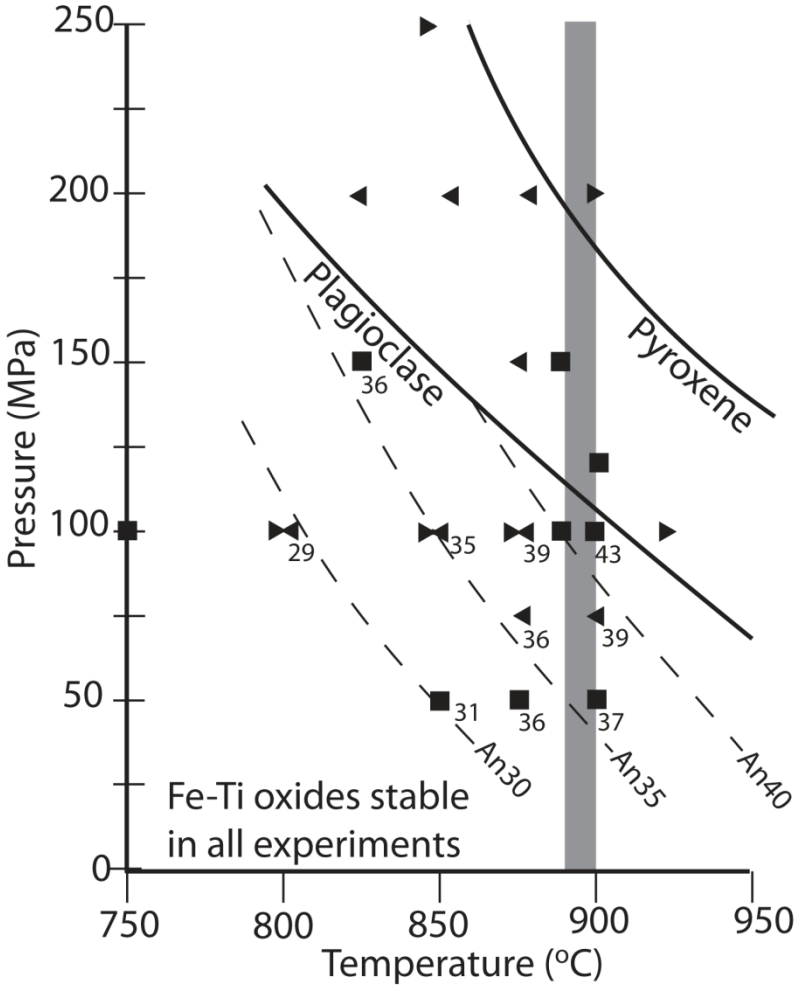

Figure 2.5. KS_1 phase equilibria. The phase assemblage of Fe-Ti oxides, clinopyroxene, orthopyroxene, and plagioclase (~An_{42}) is stable at conditions of 100-125 MPa and ~895 °C. Fe-Ti oxide equilibrium temperatures of 895±5 °C are indicated by the shaded box. Right and left pointing triangles indicate melting and crystallization experiments, respectively. Anorthite contents of plagioclase in crystallization and "straight-in" experiments are labeled; dashed lines contour those data and indicate anorthite content. Experiments are listed in Table 2.2.

~5 mol.% *An* over a pressure range of ~50 MPa: at 850 °C plagioclase of composition An_{30} and An_{35} is stable at 50 and 100 MPa, respectively.

Glass compositions vary systematically with temperature. Iron and calcium concentrations increase with temperature: at 100 MPa, FeO increases linearly from 1.5 wt.% to 2.75 wt.% and CaO increases from 1.25 to 2.4 wt.% as temperature increases from 800 to 925 °C. Silica concentration decreases with increasing temperature: in samples run at 100 MPa, silica concentration decreases from 75 wt.% to 69 wt.% as temperature increases from 800 to 925 °C. Variation of glass compositions with pressure is less dramatic. In general, iron and calcium concentrations increase by ~0.5 wt.% as pressure increases from 100 to 200 MPa. Silica concentration decreases by 1-2 wt.% as pressure increases from 100 to 200 MPa.

2.3.5 Decompression Experiments

2.3.5.1 Decompression from 150 MPa at 890 °C

Five experiments were decompressed from 150 MPa at 890°C (Figure 2.6). The starting material for those experiments contained no plagioclase, $1.3(\pm0.5)x10^3$ mm^{-3} pyroxene, and $3.6(\pm2.0)x10^4$ mm^{-3} Fe-Ti oxide microlites. Experiments decompressed at 0.05 MPa s^{-1} nucleate no plagioclase. As decompression rate decreases from 0.010 to 0.001 MPa s^{-1}, plagioclase density increases from $1.0(\pm1.0)x10^2$ to $1.5(\pm1.0)x10^5$ mm^{-3}. Pyroxene number densities do not vary substantially with decompression rate and are 10^4 to 10^5 mm^{-3}. The number densities of Fe-Ti oxides decrease from $1.0(\pm0.5)x10^6$ mm^{-3} at 0.050 MPa s^{-1} to $1.3(\pm0.4)x10^5$ mm^{-3} at 0.001 MPa s^{-1}.

The mode of plagioclase microlite size is 2-4 μm in all experiments where present, but the distribution of sizes becomes more positively skewed as decompression rate decreases (Figure 2.4). Pyroxene size distributions, on the other hand, are affected

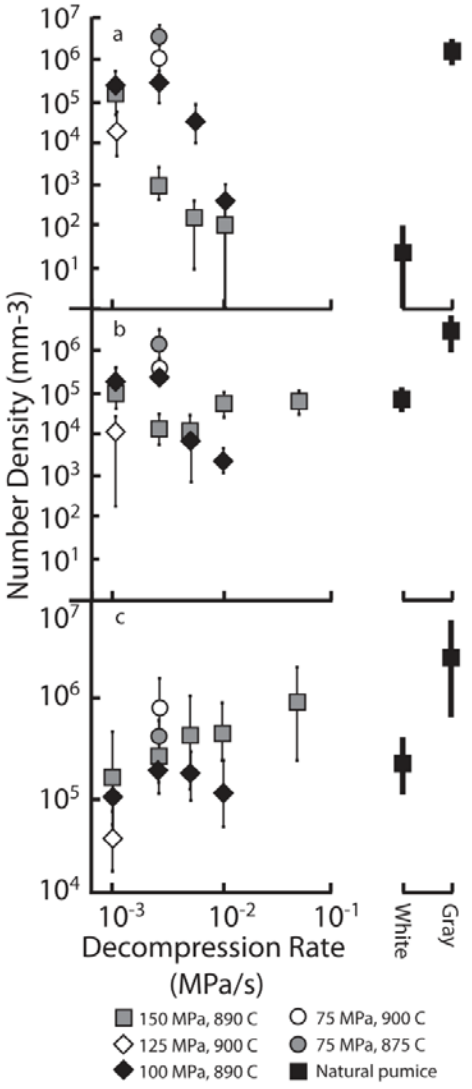

Figure 2.6. Variation in microlite N_V with decompression rate. a) Volumetric number densities of plagioclase increase with decreasing decompression rate. Experiments run at lower temperatures or initial pressures have higher plagioclase number densities. b) Volumetric number densities of pyroxene increase with decreasing decompression rate for experiments decompressed from 100 MPa, but are relatively constant in experiments initiated from 150 MPa. c) Oxide number densities decrease with decreased decompression rate in experiments initiated from 150 MPa, but do not change significantly in experiments decompressed from 100 MPa. Error bars are one standard deviation.

more complexly by decompression rate (Figure 2.4). As decompression rate decreases from 0.050 to 0.005 MPa s^{-1}, the mode coarsens from 1-2 to 4-6 μm and skewness increases from 0.7 to 1.0 μm. As decompression rate is further reduced, to 0.005 MPa s^{-1}, the mode decreases to 3.5 μm and skewness increases to 1.6 μm. At decompression rates of 0.0025 and 0.001 MPa s^{-1}, the mode is <2 μm and skewness decreases to <0.5 μm. Over the range in decompression rates, the mode in Fe-Ti oxide microlite size remains ~1 μm, but skewness of the distributions decreases systematically from 5.5 μm at 0.050 MPa s^{-1} to 1.4 μm at 0.001 MPa s^{-1} (Figure 2.4).

2.3.5.2 Decompression from 100 MPa at 890 °C

Four experiments were decompressed from 100 MPa at 890 °C (Figure 2.6). The initial material for those experiments contained $7.8(\pm5.0)x10^4$ mm^{-3} plagioclase, $1.9(\pm1.0)x10^5$ mm^{-3} pyroxene, and $1.5(\pm1.5)x10^5$ mm^{-3} Fe-Ti oxide microlites. Plagioclase number density increases from $5.0(\pm5.0)x10^2$ to $2.4(\pm1)x10^5$ mm^{-3} as decompression rate decreases from 0.010 to 0.001 MPa s^{-1}. Pyroxene number density increases from $3.0(\pm1.0)x10^3$ to $2.9(\pm0.6)x10^5$ mm^{-3} as decompression rate decreases. Similarly, Fe-Ti oxide number densities increase from $1.3(\pm0.5)x10^5$ to $4.1(\pm0.7)x10^5$.

The modes of plagioclase size distributions increase from 1-2 to 4-6 μm as decompression rate decreases (Figure 2.4). Skewness of those distributions decreases from 1.0 to 0.6 μm. The mode of pyroxene microlite sizes increases from 1 μm at 0.010 MPa s^{-1} to 3 μm at 0.005 MPa s^{-1}, but as decompression decreases further, the skewness increases from 0.6 to >1.4 μm, and the mode returns to 1 μm (Figure 2.4). Skewness of Fe-Ti oxide size distributions decreases systematically from 3.7 to 2.3 μm as

decompression rate slows from 0.010 to 0.001 MPa s^{-1}, but the modes of those distributions remain ~1 μm (Figure 2.4).

2.3.5.3 Decompression from 125 MPa at 900 °C

One experiment was decompressed from 125 MPa at 900 °C (Figure 2.6). The initial material for that experiment contained no plagioclase, 5.2(±1.0)x10^3 mm^{-3} pyroxene, and 1.4(±0.5)x10^4 mm^{-3} Fe-Ti oxides. The experiment decompressed at 0.001 MPa s^{-1} contains 0-4x10^4 mm^{-3} plagioclase and 0-3x10^4 mm^{-3} pyroxene. The number density of Fe-Ti oxides is the lowest measured in any experiment, 3-7x10^4 mm^{-3} (Figure 2.6). The size distributions of plagioclase and pyroxene microlites are very broad and have no recognizable modes. The size distribution of Fe-Ti oxide microlites has a mode of 1 μm, skewness of 2.3, and is similar in appearance to experiments decompressed at 0.0025 MPa s^{-1} from 150 MPa and 890 °C.

2.3.5.4 Decompression from 75 MPa

Two experiments were decompressed at 0.0025 MPa s^{-1} from 75 MPa at temperatures of 875 and 900 °C (Figure 2.6). The starting materials for those experiments contained 1.2(±0.7)x10^6 mm^{-3} plagioclase, 2.9(±1.0)x10^5 mm^{-3} pyroxene, and 3(±2)x10^5 mm^{-3} Fe-Ti oxide microlites at 875 °C, and 6.3(±1.0)x10^5 mm^{-3} plagioclase, 1.4(±1.0)x10^5 mm^{-3} pyroxene, and 5.0(±0.9)x10^5 mm^{-3} Fe-Ti oxide microlites at 900°C. The 875 °C experiment contains more plagioclase microlites than does the 900 °C experiment: 2.0(±0.7)x10^6 compared to 1.1(±0.6)x10^6 mm^{-3} (Figure 2.6). Pyroxene microlite number densities decrease from 1.5(±0.5)x10^6 mm^{-3} at 875 °C to

4.0(±1.0)x10^5 mm^{-3} at 900 °C (Figure 2.6). Fe-Ti oxides show a similar pattern, decreasing from densities of 8.0(±4.0)x10^5 to 3.4(±1.0)x10^5 mm^{-3} as temperature increases (Figure 2.6**)**. The modes of plagioclase size increases from 1.8 to 2.4 μm as temperature increases from 875 to 900 °C, and skewness decreases from 1.3 to 1.0 μm. In contrast, pyroxene modes decrease from 4.0 to 1.9 μm and skewness increases from 1.4 to 2.4 μm. Fe-Ti oxide size distribution modes decrease from 2.7 to 1.9 μm and skewness increases from 0.9 to 1.0 μm.

2.4. DISCUSSION

2.4.1 Eruption of A Single Magma During the KS_1 Eruption

Many eruptions tap multiple magmas (Hildreth, 1983; Pallister et al., 1996; Hammer et al., 1999). Often those compositional differences give rise to color contrasts and provide a means of recognizing different magma types in the field. Following that line of reasoning, the KS_1 white and gray pumice could be easily interpreted as originating from two different magmas. That interpretation would be wrong, however, as several lines of evidence indicate a single magma erupted to produce the KS_1 white and gray pumice. First, bulk compositions of the white and gray pumice are indistinguishable. Second, phase assemblages and phenocryst and matrix glass compositions are the same. Compositions of coexisting minerals indicate that both the white and gray pumice originated from the same magma with the same pressure, temperature, and oxygen fugacity. Third, glass inclusions from white and gray pumice contain overlapping water concentrations and, using the model of Moore et al. (1998), indicate saturation pressures of 110-150 MPa. Assuming a temperature of 895 °C from

geothermometry, the natural phase assemblage is stable at pressures less than 125 MPa, where plagioclase stability begins. Compositions of plagioclase rims from experiments run at 100 MPa and 900 °C are most consistent with the compositions of natural samples, further constraining storage conditions of the rhyodacite. At pressures of 100 MPa, experimental glass compositions become more siliceous and less calcic than natural matrix glass as temperature drops below 875 °C. It is highly unlikely that two magmas of the same composition and stored at the same conditions existed simultaneously and in isolation from one another beneath the Ksudach edifice prior to the KS_1 eruption. Instead, the most reasonable explanation is that the white and gray pumice originated from a single magma stored at 110-125 MPa, equivalent to a depth of 4-5 km, and 895(±5) °C.

2.4.2 Decompression Rates of KS_1 Pumice

Given that the only differences between the white and gray pumice are textural, and the two pumice types are aliquots of the same magma, I suggest that those differences result from different decompression and ascent rates during the eruption. That the gray pumice contains more microlites indicates it decompressed more slowly than the white pumice. The decompression experiments in this study provide a quantitative estimate for decompression rates of the white and gray pumice.

White pumice are characterized by plagioclase number densities $<5x10^2$ mm^{-3} and pyroxene and Fe-Ti oxide densities of $1\text{-}4x10^5$ mm^{-3}. Plagioclase number densities of experiments decompressed from 150 or 100 MPa at rates equal to or greater than 0.01 MPa s^{-1} correspond well with the natural samples; all experiments decompressed at slower rates produce plagioclase number densities that far exceed those of white pumice.

Number densities of pyroxene microlites in experiments decompressed from 150 MPa are all less than the natural samples, but experiments decompressed slower than 0.005 MPa s^{-1} from 100 MPa reproduce the values found in white pumice. Pyroxene microlites are less abundant in the experiment decompressed at 0.001 MPa from 125 MPa, whereas the experiments decompressed at 0.0025 MPa from 75 MPa both contain more pyroxene microlites than do natural samples. Fe-Ti oxide number densities of all decompression experiments, except that initiated at 125 MPa, are in agreement with the natural value.

In white pumice, pyroxene microlite size distributions within white pumice are positively skewed and have a mode of 2 μm, Fe-Ti oxide distributions are unimodal with most crystals <2 μm and no crystals larger than 8 μm; insufficient plagioclase are present for reliable size distributions. Experiments decompressed from 150 MPa have either the appropriate mode (at 0.01 MPa s^{-1}) or skewness (at 0.005 MPa s^{-1}) but not both. In contrast, the sample decompressed at 0.001 MPa s^{-1} from 100 MPa reproduces both the mode and skewness of the size distribution. Fe-Ti oxide size distributions of all experiments except those decompressed from 75 MPa are more positively skewed than the natural samples, but the modes of all experiments except those decompressed from 75 MPa compare are similar to the natural samples.

In gray pumice, plagioclase microlites are present in densities of ~$2x10^6$ mm^{-3}, and pyroxene and Fe-Ti oxide microlites occur in densities of ~5-$6x10^6$ mm^{-3}. Experiments decompressed at 0.0025 MPa s^{-1} from 100 MPa reproduce the natural plagioclase number densities, as do experiments decompressed from 75 MPa; all other experiments contain fewer plagioclase than the natural samples. The only experiment containing pyroxene in densities comparable to gray pumice is the sample decompressed at 0.0025 MPa s^{-1} from 75 MPa at 875 °C. Fe-Ti oxide number densities of all but the

slowest (0.001 MPa s^{-1}) experiment decompressed from 150 MPa correspond well with those of the gray pumice, as do experiments decompressed at 0.0025 MPa s^{-1} from 100 and 75 MPa.

Size distributions of plagioclase and pyroxene microlites in gray pumice have 2-μm modes and skewness of 1.2 and 1.7 μm. Fe-Ti oxide distributions have modes of 1 μm and no microlites coarser than 6 μm. Plagioclase size distributions of experiments decompressed at 0.001 and 0.0025 MPa s^{-1} from 100 MPa reproduce the natural size distribution, as does the experiment decompressed at 0.0025 MPa s^{-1} from 75 MPa at 875 °C. Samples decompressed at ≤0.0025 MPa s^{-1} from 100 MPa and 890 °C have pyroxene size distributions that fit the natural samples. The experiment decompressed at 0.0025 MPa s^{-1} from 75 MPa and 900 °C also reproduces the gray pyroxene size distributions. Fe-Ti oxide size distributions of experiments decompressed at 0.0025-0.005 MPa s^{-1} from 150 and 100 MPa correspond well with the natural size distributions; the experiment decompressed at 0.001 MPa from 125 MPa and 900 °C also reproduces the natural distribution. Experiments decompressed at slower rates or from lower initial pressures contain Fe-Ti oxide size distributions that are either less positively skewed or coarser than the natural distributions.

Based on results of decompression experiments and pre-eruptive storage conditions of 895 °C and 110-125 MPa, the most reasonable decompression rate for the white pumice is ≥0.01 but <0.10 MPa s^{-1}. Experiments decompressed at those rates reproduce plagioclase number densities in agreement with white pumice. Fe-Ti oxide number densities also support those decompression rates. Decompression experiments and pre-eruptive storage conditions indicate gray pumice most likely decompressed at 0.0025 MPa s^{-1}. Experiments decompressed at that rate from 100 MPa reproduce gray

pumice plagioclase number densities and sizes, pyroxene sizes, and Fe-Ti oxide number densities and sizes. Insufficient plagioclase densities are present at faster decompression rates, and slower rates fail to produce the observed microlite size distributions.

2.4.3 Changes in Ascent Rate Coincident with Caldera Collapse

The change from white to gray pumice occurred immediately after the Lithic Phase, when caldera collapse is thought to have begun (Andrews et al., 2007). Thus the reduction in magma decompression rate occurred immediately after caldera formation began. That timing poses two important and related questions: why did decompression rate decrease, and why was that decrease coincident with caldera collapse?

Change in either the driving pressure or conduit dimensions could result in a reduced decompression rate. I assume that decompression occurs primarily in the conduit during ascent, and that decompression in the chamber at depth is insignificant. That assumption is valid for several reasons. The magnitude of the change in decompression rate and its timing strongly argue against chamber-pressure reduction as the cause of slowed ascent. Notably, Druitt and Sparks (1984) suggested that caldera formation occurs when chamber overpressure is relieved and the edifice collapses. Although I do not rule out overpressure of the KS_1 magma chamber, bleeding off the maximum possible overpressure that crustal rocks can sustain, 25 MPa (Druitt and Sparks, 1984), would result in a maximum reduction in decompression rate of ~25% (e.g. 0.01 MPa s^{-1} reducing to 0.0075 MPa s^{-1}); significantly less than the observed ~75% decrease (0.01 MPa s^{-1} to 0.0025 MPa s^{-1}). Moreover, their model predicts that collapse should occur relatively early, not after ~2/3 of the magma has erupted. Total decompression time required to produce the observed textures in gray pumice is ~8-11

hours, which is substantially less than the >32 hours that elapsed between the start of the eruption and the onset of erupting gray pumice.

By assuming that decompression occurs primarily during ascent, ascent velocity is the ratio of decompression rate to the lithostatic pressure gradient

$$u = \frac{\frac{dP}{dt}}{\frac{dP}{dz}}$$

Eq. 2.7

The reduced decompression rate recorded by Gray Phase groundmass textures thus reflects a ~75% reduction in ascent velocity.

Vesicle textures record strain in the magma during decompression and ascent and support a reduced ascent rate during the Gray Phase. The capillary number, Ca, provides a means of estimating shear rates through the equation:

$$Ca = \frac{aG\mu}{\Gamma}$$

Eq. 2.8

where a is the non-deformed bubble radius, G is shear rate, μ is melt viscosity, and Γ is surface tension (e.g. Rust and Manga, 2002). Because the white and gray pumice formed from the same magma, viscosity and surface tension may be treated as equals in comparison of the two vesicle populations. Thus variation in the capillary number between the two pumice types is the result of changes in either equivalent vesicle radius or shear rate. As the equivalent radius is known for each vesicle, the relative shear rates recorded by each vesicle may be estimated.

Assuming surface tension of 0.15 N m^{-1} (from extrapolation of the hydrous rhyolite data presented by Mangan and Sisson, 2005) and viscosity of ~10^5 Pa s calculated using the methods of Spera (2000), the average shear rates recorded by all

measured vesicles are ~4.3x10^{-7} s^{-1} and ~2.9x10^{-7} s^{-1} in the white and gray pumice, respectively. If only the 5% of vesicles with the largest capillary numbers are considered, the white pumice record ~50% higher shear rates than the gray, 2.8(±1)x10^{-6} s^{-1} compared to 1.8(±1)x10^{-6} s^{-1}. Those higher shear rates are consistent with faster ascent of the white pumice compared to the gray pumice.

2.4.4 Changes in Conduit Geometry Coincident with Caldera Collapse

A simple estimation of conduit area, A, can be made from mass discharge using

$$A = \frac{\frac{dM}{dt}}{\rho u}$$

Eq. 2.9

where dM/dt is the eruptive mass discharge, ρ is magma density, and u is average ascent velocity (from Equation 2.7). Comparison of mass discharges and ascent velocities of the Main and Gray Phases indicate that the conduit size increased by a factor of ~4 following the initiation of caldera collapse. Such a relation is, however, a simplification and ignores the dependence of ascent rate on conduit size and shape (Jaupart, 2000; Mastin and Ghiorso, 2000; Mastin, 2002).

Numerical models offer a more sophisticated method of balancing conduit size, mass discharge, and decompression rate (Mastin and Ghiorso, 2000; Mastin, 2002). Such models are required are useful in considering eruption conduits, because volatile exsolution during magma ascent results in increased viscosity, that in turn necessitates increased vertical pressure gradients in the flow to conserve mass. Numerical models iteratively solve for an equilibrium state that accounts for the effects of viscous drag from the conduit walls on the feedbacks between magma pressure, volatile content, magma

viscosity, and pressure gradient. The program Conflow allows examination of the effects of conduit geometry on mass discharge and decompression rate (Mastin and Ghiorso, 2000; Mastin, 2002), and thus estimates of conduit geometries during the Main and Gray Phases by comparing model runs with estimated mass discharges and experimental decompression rates. For the simulations discussed below, I calculated the average decompression rate from

$$\frac{dP}{dt} = \frac{\Delta P}{\sum \frac{z_i - z_{i-1}}{u_i}}$$

Eq. 2.10

where ΔP and z_i are the total pressure drop and distance ascended through step i, and u_i is the velocity of that step. The average decompression rate of any given model run is taken as the average dP/dt (Equation 2.9) calculated from the base of the conduit up to when the model flow reaches a vesicularity of 70% (the fragmentation point in Conflow).

The mass discharge of the Main Phase can be modeled by a single cylindrical conduit with a diameter of 120-150 m (Figure 2.7). The decompression rate within that conduit is 0.30 MPa s^{-1} to 0.35 MPa s^{-1}. Both of those rates are significantly higher than the estimated minimum decompression rate for white pumice, 0.01 MPa s^{-1}. If decompression rate is solved for, decompression rates of 0.01 MPa s^{-1} are modeled if conduit diameter is 20 m. Such a size, however, results in a mass discharge more than 2 orders of magnitude less than that of the Main Phase.

If non-cylindrical conduits are considered, then a single, tapering conduit can simultaneously accommodate the required mass discharge and approach the minimum decompression rate estimated for the Main Phase (Figure 2.7). Modeling indicates that a single conical conduit with a basal diameter of ~400 m and a vent diameter of 100 m can

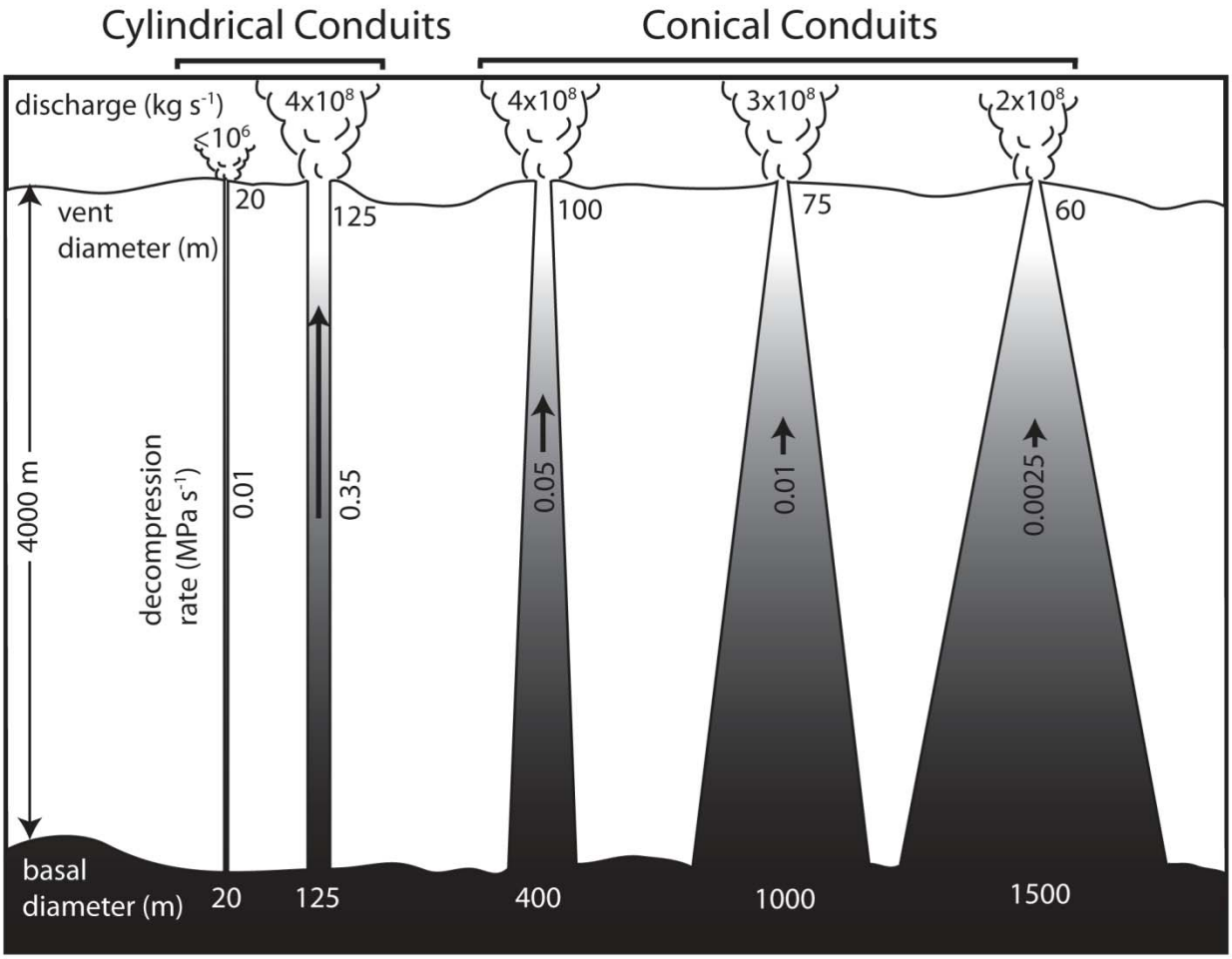

Figure 2.7. Effects of conduit geometry on magma decompression rate and mass discharge. Cylindrical conduits can either satisfy the magma decompression rate or mass discharge for the Main or Gray phases of eruption, but cannot simultaneously satisfy both. Conduits with tapering geometries can accommodate the Main and Gray phase decompression rates and mass discharges. The figure is drawn to scale.

accommodate a mass discharge of ~$4x10^8$ kg s^{-1} with a decompression rate of ~0.05 MPa s^{-1} (Figure 2.7). If the conduit base is broadened to 1000 m, and the vent is constricted to

75 m, mass discharge remains >$3x10^8$ kg s^{-1}, and decompression rate slows to ~0.01 MPa s^{-1} (Figure 2.7). More conical geometries fail to predict the required mass discharge and/or predict decompression rates that are too low.

The Gray Phase mass discharge can be modeled by a single cylindrical conduit with a diameter of 100-130 m. The decompression rate within such a conduit, ~0.2 MPa s^{-1}, however, is two orders of magnitude greater than that estimated from decompression experiments, 0.0025 MPa s^{-1}. It is thus unlikely that a single cylindrical conduit fed the Gray Phase. Cylindrical conduits with diameters <20 m predict decompression rates approaching those of the Gray Phase, but the mass discharges through those conduits are two orders of magnitude too low (Figure 2.7).

The presence of multiple conduits during the Gray Phase is one way to solve simultaneously for mass discharge and decompression rate, but this solution seems unlikely for several reasons. First, the Gray Phase mass discharge requires approximately 100 conduits with 20-m diameters to operate simultaneously during the eruption phase. Such a large number is unreasonable because those conduits would have to be near enough to one another that they all fed the same Plinian column, but far enough apart that they did not coalesce, as coalescence would result in an increase in decompression rate. Furthermore, it is unlikely that such a large number of conduits could remain active for the duration of the Gray Phase without conduit heterogeneities leading to the widening of some conduits and increases in decompression rate. Similarly, were all of those conduits to coalesce into a ring-dike, it is hard to imagine that dike maintaining a uniform aperture throughout the Gray Phase, and far more likely that magma ascent would become focused along certain segments, leading to changes in mass discharge and/or decompression rate.

A single conduit can model the Gray Phase mass discharge and decompression rate if it has a conical geometry (Figure 2.7). A conical conduit that tapers from 1200-1600 m at its base to a vent of ~60 m can simultaneously accommodate the required mass discharge and decompression rate. If mass discharge is evenly distributed among two, three, or four conduits, those conduits still require basal diameters of ~1000 m and vent diameters of ~40 m. Conduits with larger vents generate decompression rates and mass discharges too high for the Gray Phase, whereas conduits with wider bases appear unreasonable given the size of Ksudach Caldera V.

Modeling results thus indicate that a cylindrical (150 m diameter) to conical conduit, with a base as wide as 1000 m and a vent as narrow as 75 m, fed the Main Phase (Figure 2.7). Following the initiation of caldera collapse, the conduit developed a more conical geometry as the conduit base widened to 1200-1600 m, and the upper regions constricted to ~60 m (Figure 2.7).

It is not surprising that conduit geometries for the KS_1 Main and Gray Phases differ dramatically, because caldera collapse should alter the subsurface structure of the volcano. What is interesting is that concomitant with broadening of the conduit base, the upper regions of the conduit narrowed. Those conduit changes and the large increase in the amount of accidental lithics erupted during the Lithic Phase provide insight into the mechanism of caldera collapse.

Any model of caldera collapse during the KS_1 eruption must account for constriction of the upper regions of the conduit while broadening of the conduit base (Figure 2.8). I propose that prior to eruption, pressure built in the chamber, fracturing the wall rock until a fracture propagated to the surface to become the eruption conduit. Further fracturing of wall rock along the conduit and the roof of the chamber occurred

during pre-collapse phases of eruption. Collapse began during the Lithic Phase, as the weakened roof of the chamber and lower regions of the conduit broke apart and were partly ejected. Although the 0.3 km^3 of lithics ejected during the Lithic Phase represents only ~25% of the total amount of lithics, they were erupted at a rate 3-10 times greater than during any other phase of eruption. That substantial increase in erosion represents the fracturing that occurred as the edifice began to collapse. Caldera collapse thus resulted in a conduit with a broad base and a narrow top. Although collapse may have continued into the Gray Phase, the conduit geometry was largely set by the end of the Lithic Phase.

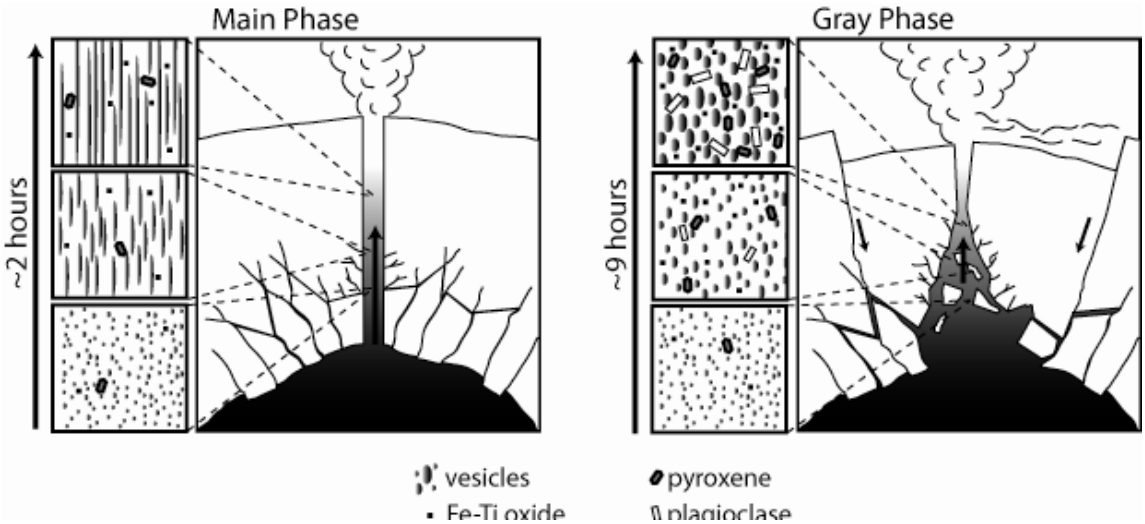

Figure 2.8. Caldera collapse and development of a tapering conduit. Prior to eruption, pressure in the chamber fractured the surrounding wall rock until a fracture propagates to the surface and becomes the conduit. During the Initial and Main Phases of eruption, relatively rapid ascent through that conduit (~2 hours total decompression time) exerted high shear rates and produced pumice with highly stretched vesicles, few oxide and pyroxene microlites, and no plagioclase microlites. Fracture of the conduit walls and base continued as magma was withdrawn from the chamber. Collapse began during the Lithic Phase as the thoroughly fractured conduit walls and base of the conduit broke apart and were ejected. That expulsion of lithics both broadened the conduit base and allowed caldera collapse to occur, resulting in constriction of the upper conduit regions. The Gray Phase conduit thus had a broad base and narrow top that reduced average magma decompression, ascent, and shear rates, and produced pumice with round vesicles and abundant microlites.

Chapter 3: Turbulent dynamics of the 18 May 1980 Mount St. Helens eruption column

Volcanic eruption columns that fail to entrain and heat enough air to become buoyant collapse and generate devastating pyroclastic flows. Turbulent eddies along the column margins entrain and mix air into the column interior, allowing the column to become buoyant. Currently, the turbulent velocity field of volcanic eruption columns is unknown, and therefore numerical models of eruption columns remain untested against geologic observations. Through extensive re-evaluation of video and photographs of the 18 May 1980 eruption of Mount St. Helens, I report the first measurements of the turbulent velocity field of a volcanic column. During the buoyant, B2, phase of eruption, eddies along the column margins were larger and the deviatoric component of velocity was lower than during partial column collapse in the B3 phase of eruption. I propose that the turbulent structure of the column margins reflects the thickness and velocity gradients of the fraction of the column in communication with the atmosphere. Thus eddy size scales with the column radius when the entire column becomes buoyant, whereas eddy size is controlled by the thickness of a buoyant annulus surrounding a dense, collapsing core during periods of partial column collapse.

3.1 INTRODUCTION

When a volcanic eruption column exits the vent as a momentum jet, it is ~5-8 times denser than the ambient atmosphere (Sparks, 1986; Woods, 1995). Heating and expansion of turbulently entrained air substantially reduces the bulk column density (Sparks, 1986; Woods, 1995), and if the column entrains enough air, it will rise buoyantly as a plume. If, however, the column fails to entrain enough air before it loses its upward

momentum, it will collapse and generate pyroclastic flows. Direct observations of recent eruptions indicate a single vent can simultaneously produce a buoyant plume and non-buoyant pyroclastic flows if portions of the column remain non-buoyant at the top of the momentum jet (Christiansen and Peterson, 1981; Criswell, 1987; Scott et al., 1996). The processes of air entrainment thus control whether a column rises buoyantly, or partially or completely collapses.

Turbulence generated by shear between the column margins and the atmosphere is responsible for air entrainment. Eddies along column margins entrain air from the atmosphere, and eddies throughout the column mix that air into the column interior. Because air is entrained from the column margins, column density is radially heterogeneous, with a dense core and less dense margins. The turbulent dynamics of entrainment and mixing control the magnitude of density heterogeneities and whether they persist to the top of the momentum jet.

Some numerical studies use large eddy simulations to model turbulent air entrainment (e.g. Neri et al., 2003). Other numerical models treat entrainment as a constant-rate process with different effective entrainment rates for buoyant and collapsing columns (e.g. Suzuki et al., 2005), an approach validated by experimental measurements of entrainment in jets with reversing buoyancy (Kaminski et al., 2005). Importantly, however, those models are unconstrained by quantitative descriptions of turbulence in eruption columns and, as a result, do not fully consider the turbulent dynamics of entrainment.

In this study, I describe the turbulent length scales and deviatoric velocities during buoyant behavior and partial collapse of the 18 May 1980 eruption column of Mount St. Helens. Because direct observation of column interiors is impossible, I focus on the

column margins. The data presented in this chapter data show that the turbulent length scale decreased and deviatoric velocity increased during partial column collapse, and that turbulent dynamics of the column reflect and may control changes in air entrainment.

3.2 MOUNT ST. HELENS BACKGROUND

The 18 May 1980 eruption of Mount St. Helens (MSH) allows an almost unique opportunity to evaluate plume dynamics of Plinian-style eruptions because of the extensive body of recorded images and video. After its well known avalanche and directed blast, the eruption lasted for ~8 hours, which has been divided into four phases (Table 3.1) (Waitt and Dzurisin, 1981; Criswell et al., 1987; Carey et al., 1990). Between ~9:00 AM and 12:15 PM (B1 and B2 phases; all times local and approximate), a buoyant plume with mass flux of up to 1.3×10^7 kg/s was established above the vent (Figure 3.1a). Between 12:15 PM and 4:25 PM (B3 phase), mass flux increased to an average of 4.4×10^7 kg/s and the eruption column almost wholly collapsed, with ~90% of the mass flux generating pyroclastic flows directed out of the crater to the north, yet a significant buoyant plume remained over the vent (Figure 3.1b). Dominantly buoyant behavior resumed between 4:30 PM and 6 PM (B4 phase) when mass flux decreased to 1.6×10^7 kg/s. Radar observations indicate that column height grew during the B2 phase (from 15 to 18 km), and remained relatively steady through the B3 phase (~14 km) (Carey et al., 1990).

Table 3.1. Mass fluxes of Mount St. Helens 18 May 1980 eruption (Carey et al., 1990). *PF* indicates average mass flux of pyroclastic flows generated during B3 phase.

	Time	Column Height (km)	Mass flux (kg/s)
B1	0900-1100	15.4	6.3×10^6
B2	1100-1215	15-18	1.3×10^7
B3	1215-1625	13-16	3.9×10^6
			4.0×10^7 *(PF)*
B4	1625-1715	16-19	1.6×10^7

-

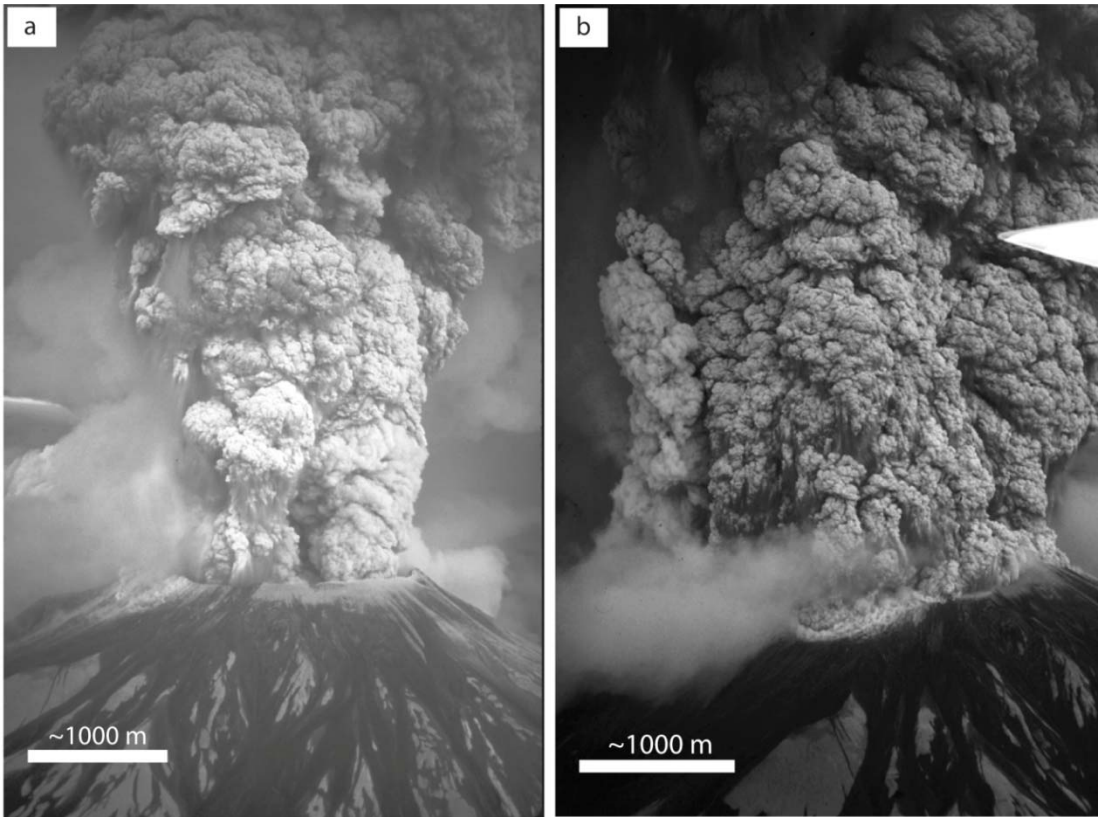

Figure 3.1. a) Photograph of the dominantly buoyant B2 eruption column showing large, discrete eddies that do not fill the entire crater. b) During partial column collapse, the B3 eruption column is covered in small, tightly spaced eddies and fills the entire crater. Photographs by D. Swanson, USGS.

3.3 METHODS

Using photographs and digitized video of the eruption, I characterized the eruption column by measuring eddy sizes and the velocity field of the column margins. Photographs taken throughout the B2 and B3 phases indicate that eddy size and column appearance did not vary significantly throughout either phase. Sizes of 200 eddies were measured from photographs and individual video frames of the B2 eruption phase, and 194 were measured from the B3 phase. Eddy sizes were measured as the lateral distance across the large cauliform structures on the surface of the eruption column. Flow-J, an Image-J plug-in that measures the velocity field by tracking pixel intensities through a stack of images (Abramoff et al., 2000), was used to characterize the surfacial velocity field of the eruption column. From those velocity fields, I measured the average vertical velocity component, u, and the deviatoric component of velocity, u', the latter of which may be thought of as the characteristic eddy spin rate. Integral length scales of those velocity fields, which provide a statistical measurement of the largest structures within the velocity field, were calculated using two-point autocorrelations (Bernard and Wallace, 2002). Uncertainties in eddy size, integral length scale, and velocity measurements are reported as ±1 standard deviation. Additional descriptions of methodology and error analysis are provided in Appendix 5.

3.4 RESULTS

The B2 eruption column is characterized by eddies with mean diameters of 560 (±180) m, frequently separated from one another by several hundred meters (Figures 3.1 & 3.2). The mean rise speed of eddies, $\bar{u}$, is 50 (±10) m/s. The deviatoric component velocity field, u', ranges from 55 to 85 m/s (Figure 3.2). Rising eddies often shed

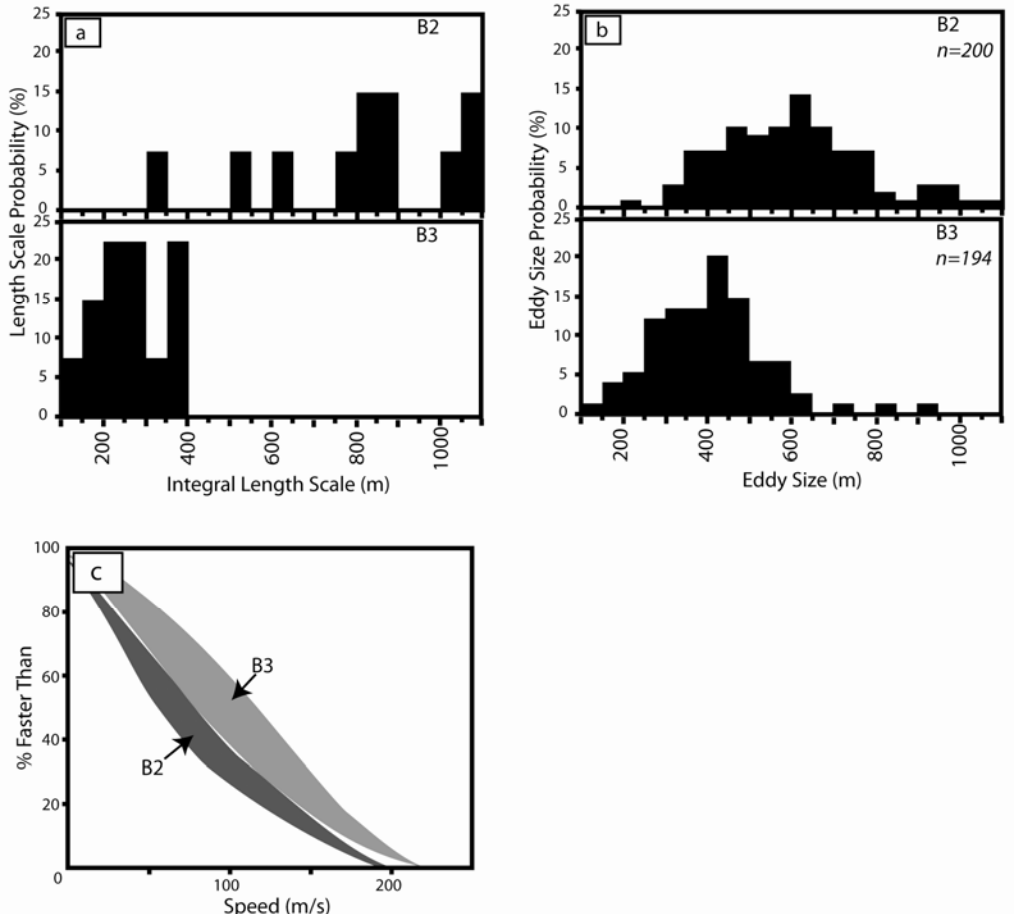

Figure 3.2. a) Integral length scales of the column margins during the B2 phase are much larger than those measured during the B3 phase (Table 3.2). b) Eddy sizes measured from still photographs and video frames; *n* indicates the number of eddies measured for each eruptive phase (Table 3.2). c) Deviatoric velocity components for the B2 and B3 eruptive phases shown as the probability of any point moving faster than the given speed (Table 3.2). The gray regions indicate ±1 standard deviation.

curtains of sedimenting pyroclasts, and the ash and vapor contents of the column appear heterogeneous, as strong color variations are present (Figure 3.1). Most striking is a large, white (steam-rich) cloud that remains slightly inside the south rim of the crater,

suggesting a non-circular column cross section. Because the inside of the 1.9 km diameter crater rim is visible in many of the photographs, column diameter during the B2 phase appears to have been 1.5 ± 0.1 km at the rim elevation ~700 m above the vent.

Table 3.2. Length scales and deviatoric velocities along column margins. Length scales are from photographs, L, and velocity field autocorrelations, Λ. Uncertainties in L are reported as ±1 standard deviation.

	Eddy size (m)		Deviatoric velocity (m/s)
	L	Λ	u'
B2	560±180	300-1000	55-85
B3	370±130	150-400	75-120

When the B3 eruption column was mainly collapsing in the afternoon, it was uniformly covered by tightly spaced eddies with average diameters of 370 (±130) m (Figures 3.1 & 3.2). Interestingly, eddy rise speed along the margins remained ~50 (±10) m/s. The deviatoric velocity components range from 75 to 120 m/s (Figure 3.2). Little sedimentation was observed from rising eddies. Strong color heterogeneities are not present, likely indicating relatively uniform ash and vapor contents of the column margins. The column occupied the entire crater, occasionally spilling over to shed minor pyroclastic flows down the west, south, and east flanks, suggesting a circular column cross-section at least 1.9 km in diameter at the elevation of the rim. In general, the column margins were buoyant, little sedimentation was observed from rising eddies, and most of the pyroclastic flows were directed to the north, indicating that pyroclastic flow generation is unlikely to have occurred through collapse of the column margins.

3.5 DISCUSSION

Any model describing the switch from buoyant plume to partial collapse during the 18 May 1980 MSH eruption should account for changes in turbulent dynamics and the observed increase in total mass flux (but decreased buoyant mass flux). Furthermore, the model must allow for a return to wholly buoyant behavior, as occurred during the final B4 phase of eruption. I will address those requirements by examining eddy size, because that size scales with vent radius and exit velocity, and inversely with column density (Bernard and Wallace, 2002). Importantly, the product of those three parameters is the eruptive mass flux.

The time-averaged radial velocity profile of a turbulent jet is approximately Gaussian, and at sufficient distances downstream from the vent, that profile governs the length scale of turbulence (Bernard and Wallace, 2002). Because the initial scale of the velocity profile is determined by vent radius, the largest eddies should scale with vent radius. Eddy size decreased 560 to 370 m between the B2 and B3 phases, implying vent radius shrank by ~50%. Such a reduction would, all else remaining equal, result in mass flux dropping by a factor of about four, contrary to the observed three-fold increase in mass flux (Table 3.1). Therefore, the observed turbulence cannot be linked solely to changes in vent radius.

Shear between the high-velocity jet and ambient atmosphere is the principal cause of turbulence in the eruption column, and in incompressible flows the length scale of turbulence scales with this velocity as does the deviatoric velocity (Bernard and Wallace, 2002). Thus, all else being equal, a fast jet should have larger, faster eddies than does a slow jet. The two-fold decrease in eddy size between the B2 and B3 phases argues for a reduction in jet velocity. Such a decrease is inconsistent with the observed increases in

eddy rotation speed and total mass flux. Therefore, a decreased jet velocity cannot be the sole cause of changes in turbulent dynamics.

Lastly, the turbulent length scale is inversely proportional to the density of the jet (Bernard and Wallace, 2002). Smaller eddy sizes in the afternoon could suggest that the column density increased by a factor of ~two. An increased column density would be consistent with increased mass flux and, indeed, many previous workers have attributed column collapse during B3 to density (Christiansen and Peterson, 1981; Klug and Cashman, 1994). Several lines of evidence, however, argue against an increased column density. First, if decreased eddy size reflects increased column density (thus increased mass flux is solely caused by increased jet density), then the width of the column should not change between the B2 and B3 phases. Instead, the column radius at the rim elevation increased 20%, from 1.5 ± 0.1 to 1.9 ± 0.2 km, suggesting that either column density decreased or the initial column radius increased. Second, there are no substantial differences in the grain-size distributions and compositions of pyroclastic material erupted during the B2, B3, and B4 phases (Appendix 4). Those data imply that if an increase in column density were coincident with column collapse, then that increase would have resulted from decreased exsolved gas content. Magmas with differing volatile contents were erupted on 18 May: mafic dacite exsolved ~4.6 wt.% H_2O and silicic andesite exsolved >4 wt.% H_2O, but those exsolved volatile contents were diluted by lithics to ~2.8 and >2 wt.% water, respectively (Carey and Sigurdsson, 1985; Rutherford et al., 1985; Klug and Cashman, 1994). Point counting of pyroclastic fall and flow deposits indicates that the proportion of silicic andesite in the eruption column, however, never exceeded 10 wt.%, and thus exsolved gas content did not decrease more than 0.1 wt.%. The resulting <1% increase in column density is insufficient to explain

the observed ~50% reduction in eddy size. Although it is difficult to fully assess the effects of increased column density on deviatoric velocity, it is unlikely that a <1% increase in density could increase deviatoric velocity by ~40%.

Differences in *u'* of the B2 and B3 phases also offer insight to the structure of the column. The deviatoric velocity is a strong function of both the initial jet velocity and radial gradients in velocity. There is no evidence indicating increased exit velocity during B3, thus I consider it most likely that the radial gradient in velocity increased while the column was partially collapsed. That suggests that the time-averaged velocity profile of the column was not Gaussian.

Changes in either vent radius, jet velocity, or density alone thus cannot explain the observed changes in turbulence and eruption dynamics. Because partial collapse requires the column to segregate into two sections, one of which is buoyant while the other remains dense and collapses, I propose that during partial collapse, the column segregates into an outer annulus, which is in turbulent communication with the atmosphere, and a dense core, which is effectively isolated from the atmosphere (Figure 3.3). The key factor in this model is that the annular scale R_b sets the velocity profile, which determines the turbulence scale, and thus R_b, and not the total column radius R, controls the size of eddies in the column margin, air entrainment, and consequently the buoyant mass flux (Figure 3.3). Conduit flow modeling (Mastin and Ghiorso, 2000) and observed mass fluxes suggest that the vent radius increased from ~25 m during B2 to ~37 m during B3. If I assume that the bulk density of the buoyant annulus is less than that of the atmosphere, then changes in column diameter and mass-balance arguments indicate that R_b at the rim elevation was ~200 m during B3 and the dense core was composed, in roughly equal proportions, by the upward jet and downward, pyroclastic flow-generating

return flow. At the start of the B4 phase, R decreased to ~27 m. Eddies efficiently entrained air throughout that narrower column, permitting a return to dominantly buoyant eruption behavior.

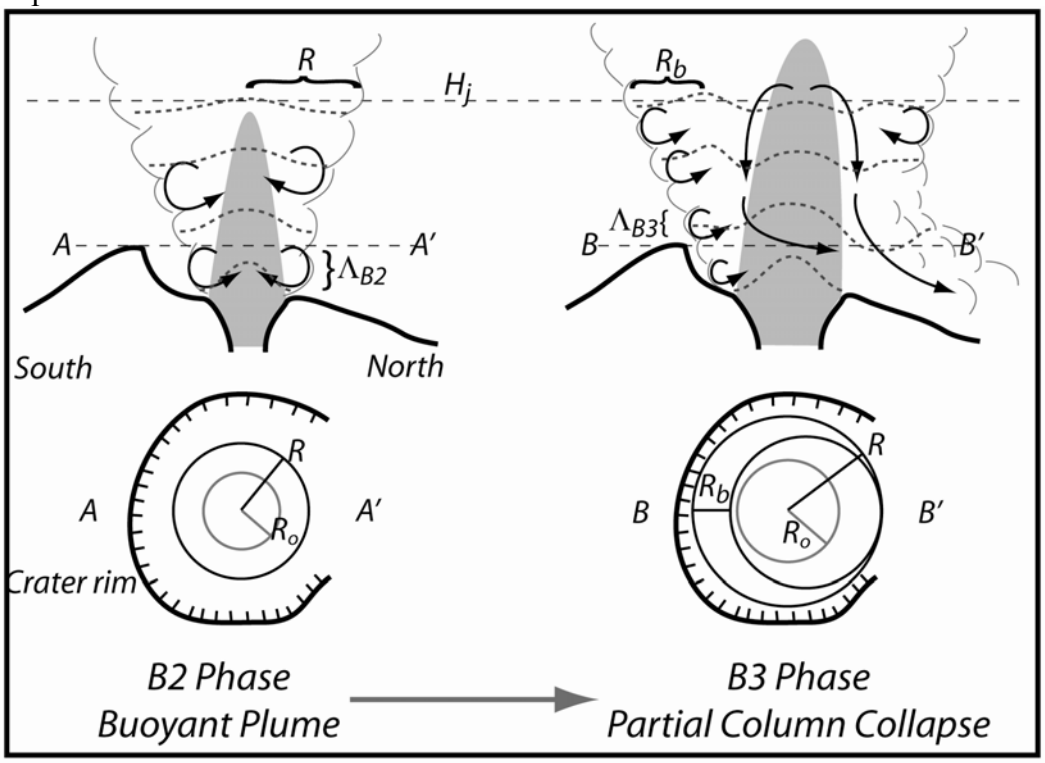

Figure 3.3. Heterogeneous model for column partial collapse. During the B2 eruption phase, eddy size, Λ_{B2}, is controlled by plume radius, R, which is set by vent radius R_o. B2 phase eddies can efficiently entrain air throughout the column before the top of the momentum jet, H_j. As vent radius, R_o, widens in the B3 phase, air is no longer entrained throughout the column, leading to segregation of a buoyant annulus, with size R_b, and dense core. Although R is still a function of R_o, R_b controls eddy size, Λ_{B3}. Partial collapse of the core creates a downward flow along the inner boundary of the annulus. This flow intensifies turbulence in the annulus, further reduces R_b, and inhibits entrainment into the core during the B3 phase. Once partial collapse is initiated, crater geometry directs flows to the north, and the annulus acquires an asymmetric shape. Time-averaged velocity profiles are shown at different heights as dotted gray lines in the cross section. Plume dimensions in map view are indicated for elevations A-A' and B-B' indicated in cross section.

Differences in turbulence thus show that a widened vent led to column collapse between morning and afternoon. Collapse occurred when *R* became too large for eddies to effectively entrain air through the column. Once collapse began, the dynamics of the jet changed significantly. Collapse of the core generated a downward flow of material that effectively increased the core radius and inhibited air entrainment. The velocity profile of the jet was no longer roughly Gaussian, but more likely a profile with positive velocities along the buoyant margins and in the center, and negative velocities inboard of the buoyant annulus (Figure 3.3). The modified profile produced higher *u'* and likely resulted in more local air entrainment, but the smaller eddy size inhibited mixing deep into the column, and thus the bulk entrainment rate decreased.

If I assume atmospheric densities, α, of 1.25 kg/m^3, and column densities, ρ, of 1 kg/m^3 for the buoyant B2 column and B3 annulus, and 2 kg/m^3 for the B3 column interior, then I may calculate gradient Richardson numbers, *Ri*, with the expression

$$Ri = abs\left(\frac{g\frac{\rho-\alpha}{\Lambda}}{\alpha\left(\frac{u'}{\Lambda}\right)^2}\right)$$

Eq. 3.1

using measured values of *u'* and Λ. Gradient Richardson numbers <0.25 indicate likely mixing between the column and atmosphere, whereas values >0.25 indicate little mixing. I calculate B2 phase *Ri*≈0.20 and B3 phase *Ri*≈0.15. These values indicate mixing during both the B2 and B3 phases but, significantly, entrainment during the latter was restricted to a smaller region: the buoyant annulus. Interestingly, *Ri* gives insight to stable annulus size and termination of the feedback between smaller eddy size and increased column collapse. Presumably, as the column begins to collapse, large eddies mixing air into the column interior cannot lower density sufficiently to prevent collapse. That higher density

results in increased *Ri* number, inhibiting mixing and leading to increased column collapse. As collapse progresses, eddy size, entrainment rate, and *Ri* decrease and turbulence intensifies until $Ri \leq 0.25$ and conditions stabilize. The B2 and B3 *Ri* thus reflect stable conditions during wholly buoyant and partially collapsed column behavior.

That the B3 phase erupted the lowest buoyant mass flux of the eruption, despite erupting the highest total mass flux, indicates preferential partitioning of mass into pyroclastic flows and substantial reduction in the total amount of air entrained. Reduced air entrainment into the column resulted from two processes. First, decreased eddy size reduced the volume of air entrained by the column and restricted mixing to the buoyant annulus. Second, the crater geometry directed pyroclastic flows from the collapsing column interior almost exclusively to the north, leading to a more or less continuous disruption in the buoyant annulus and further reducing the column volume in communication with the atmosphere. As a result, the total amount of entrained air (proportional to buoyant mass flux) decreased despite a greater total column surface area (proportional to *R*) through which to entrain air. The gradient Richardson numbers of the column margins were similar, $Ri \approx 0.2$, during full buoyancy and partial collapse, and likely controlled the size of the buoyant annulus during partial collapse. Our model confirms and explains previous observations of decreased entrainment efficiency in partially collapsing columns (Kaminski et al., 2005; Suzuki et al., 2005) and explains how mass within the eruption column is segregated into the buoyant plume and non-buoyant pyroclastic flows.

Our model has ignored the effects of compressible flow dynamics, specifically shockwaves, on turbulence generation within the column. Although Ogden et al. (2008) have shown that overpressured jets may have significantly different dynamics than

pressure-balanced jets, two lines of evidence argue against the importance of shockwave generation in restricting the turbulent length scale and reducing air entrainment at MSH. First, no shockwaves in the column are observed in video of the B2 or B3 eruption phases, such as those seen in the 1992 eruption of Spurr (McGimsey and Dorava, 1994). Second, there is no evidence of higher exsolved volatile content supporting increased exit velocity or overpressure at the vent during the B3 phase.

Conclusions

The papers composing this dissertation describe and discuss volcanic processes from the magma chamber to the atmosphere. The common theme underlying those papers are complex, non-linear responses to events that are, in essence, rather simple. For example, we expect that recharge by a hot, isotopically primitive magma will increase the host magma temperature, change its isotopic composition, and possibly result in assimilation of wall rock. Those results do occur, but detailed examination of the processes shows that some portions of the magma experience far greater compositional and thermal excursions than others, and thus the timescales and length scales of magma recharge and mixing must be considered. To further illustrate the importance of those scales, consider that although a large recharge event might trigger an eruption, a dozen small events might accumulate a larger volume of magma, but never trigger an eruption; the dynamic boundary, in this case triggering an eruption, is never crossed in that second scenario. Interestingly, many volcanic processes occur near such dynamic boundaries, but extrapolations of laboratory or modeling results may not accurately describe processes on both sides of a behavioral divide. Interpreting ancient volcanic systems and predicting future eruptions thus requires not only knowledge of specific volcanic processes, but also knowledge of where dynamic boundaries lie in parameter space.

The phenocryst textures at El Chichón show that magma recharge can be very common and not necessarily trigger eruption. That research also demonstrates that each phenocryst provides a distinct record of magma chamber history, consequently the thermal and compositional history of a chamber is not likely recorded by a single crystal. Although this work provides constraints on the frequency, temperature, and composition

of recharging magmas, it does not yet constrain the volumes or length scales of recharge events. I expect that length scales of recharge processes can be estimated if a large enough set of phenocrysts is examined and correlated. Once the size of recharge events is known, then more detailed models of chamber dynamics will arise. Those models should allow for an assessment of minimum chamber size based upon the zoning patterns of large sets of phenocrysts, and enable prediction of the critical recharge rates, temperatures, and compositions that trigger eruption.

The Ksudach KS_1 pumice record changes in decompression rate and a change in conduit structure resulting from caldera collapse. It is not particularly surprising that conduit size changed during caldera collapse, but it is interesting that the conduit likely developed a broad base and constricted upper region. This indicates that the conduit geometry, and not just its radius, must be considered in assessing mass flux and decompression rate. In general, we should probably expect changes in decompression rate and conduit geometry to accompany caldera collapse. One interesting test of that hypothesis would be to examine the groundmass textures of pre-collapse and post-collapse pumice from a different volcano. Quantitative knowledge of how conduit structure changes during collapse will improve our understanding of caldera-forming eruption dynamics.

Observations of the Mount St. Helens eruption column indicate turbulence along the column margins reflects changes in eruption behavior and reduced air entrainment. Those results also indicate that segregation of the column into a buoyant annulus surrounding a dense core during partial collapse results in decreased air entrainment and thus a decreased buoyant mass flux. That implication is interesting because it shows that the turbulent length scale controls the rate and efficiency of air entrainment and it

provides an explanation for the reduced entrainment rates described by other workers (e.g. Kaminski et al., 2005). In the near future, I plan to quantitatively relate entrainment rates to turbulence. Although the research in this dissertation quantitatively describes column behavior in wholly buoyant and partially collapsed eruption regimes, it does not describe the critical conditions for partial collapse. I expect those conditions can be predicted numerically using the turbulent length scales and deviatoric velocities from this dissertation as boundary conditions.

Appendix 1: El Chichón Phase Compositions

Analyses were collected using a JEOL JXA-8200 electron microprobes at The University of Texas at Austin Department of Geological Sciences. All analyses are reported as weight percent oxides. Plagioclase compositional transects are reported in Appendix 2.

Table A1.1. Electron microprobe standards and secondary standards.

	Na2O	MgO	Al2O3	SiO2	K2O	CaO	TiO2
Glass	Albite	Kak. Hbl.	VG	LPGL	Orthoclase	VG2	Ilmenite
Plagioclase	Albite	--	An50	Orthoclase	Orthoclase	An100	--
Amphibole	Kak. Hbl.	Kak. Hbl.	Kak. Hbl.	Kak. Hbl.	Kak. Hbl.	Kak. Hbl.	Kak. Hbl.

	MnO	Cr2O3	FeO	SrO	Secondary
Glass	Ilmenite	--	VG2	--	KN18
Plagioclase	--	--	Fayalite	Sr Glass	An50
Amphibole	Mn Garnet	--	Kak. Hbl.	--	Kak. Hbl.

Sample: El Chichon
Phase: Glass

Conditions: 15 kV, 10 nA, 10 μm

Sample	Na2O	MgO	Al2O3	SiO2	K2O	CaO	TiO2	MnO	FeO	SO3	Cl	Total
Uncertainty	0.05	0.02	0.09	0.23	0.03	0.03	0.02	0.04	0.17	0.00	0.01	
Unit A	3.56	0.16	16.77	64.67	4.86	1.54	0.20		1.53	0.09	0.33	93.63
Unit A	3.77	0.20	16.29	64.06	5.20	1.49	0.20	0.16	1.55	0.07	0.26	93.18
Unit A	3.18	0.18	17.06	66.42	4.83	1.58	0.23	0.07	1.31	0.08	0.28	95.14
Unit A	3.75	0.15	18.83	61.28	3.74	3.55	0.15	0.04	1.14	0.08	0.21	92.88
Unit B	2.44	0.18	17.24	70.79	2.36	1.55	0.23	0.09	1.57	0.07	0.25	96.70
Unit B	2.38	0.17	16.87	70.82	2.25	1.52	0.18		1.41	0.09	0.26	95.89
Unit B	2.44	0.18	17.24	70.79	2.36	1.55	0.23	0.09	1.57	0.07	0.25	96.70
Unit B	2.38	0.17	16.87	70.82	2.25	1.52	0.18		1.41	0.09	0.26	95.89
Unit B	3.94	0.13	18.21	64.63	3.76	2.72	0.19	0.12	1.28	0.08	0.22	95.23
Unit B	3.04	0.16	15.92	65.12	3.84	1.60	0.23	0.13	1.32	0.09	0.25	91.62
Unit B	3.52	0.12	16.64	62.57	5.09	1.58	0.20	0.06	1.55	0.07	0.23	91.57
Unit C	3.87	0.20	16.57	67.61	5.10	1.46	0.25	0.01	1.52	0.11	0.23	96.88
Unit C	3.65	0.19	15.93	65.95	4.89	1.51	0.20	0.14	1.40	0.11	0.25	94.15
Unit C	4.01	0.19	16.14	67.26	4.98	1.79	0.20	0.09	1.30	0.19	0.23	96.33
Unit C	3.68	0.19	16.01	66.34	4.90	1.48	0.19	0.09	1.63	0.34	0.26	95.05
Unit C	2.83	0.17	17.31	62.58	4.36	1.56	0.17	0.12	1.23	0.09	0.25	90.61
Unit D	2.83	0.13	15.91	70.10	2.58	1.33	0.18	0.06	1.26	0.07	0.27	94.64
Unit D	2.62	0.13	16.12	71.18	2.86	1.29	0.20	0.12	1.15	0.07	0.26	95.92
Unit D	2.93	0.11	16.45	71.40	2.60	1.51	0.20	0.12	1.16	0.07	0.25	96.75
Unit D	3.24	0.12	14.95	68.40	4.42	1.17	0.16	0.16	1.24	0.07	0.27	94.14
Unit D	3.34	0.26	15.49	69.94	4.38	1.28	0.19	0.10	1.32	0.07	0.24	96.54
Unit D	3.34	0.26	15.49	69.94	4.38	1.28	0.19	0.10	1.32	0.07	0.24	96.54
Unit D	3.24	0.12	14.95	68.40	4.42	1.17	0.16	0.16	1.24	0.07	0.27	94.14
Unit D	2.83	0.13	15.91	70.10	2.58	1.33	0.18	0.06	1.26	0.07	0.27	94.64
Unit D	2.62	0.13	16.12	71.18	2.86	1.29	0.20	0.12	1.15	0.07	0.26	95.92
Unit D	2.93	0.11	16.45	71.40	2.60	1.51	0.20	0.12	1.16	0.07	0.25	96.75
Unit E	6.32	0.02	18.86	59.60	6.17	1.48	0.19	0.07	0.28	0.06	0.05	93.09
Unit E	4.68	0.20	18.10	65.82	3.47	2.75	0.18	0.07	0.97	0.08	0.14	96.42
Unit E	3.26	0.10	15.42	68.30	3.62	1.32	0.21	0.08	0.92	0.07	0.24	93.47
Unit F	3.71	0.02	15.51	72.72	3.99	0.94	0.23	0.03	0.79	0.06	0.07	98.04
Unit F	2.50	0.05	13.34	75.12	4.36	0.23	0.27	0.02	0.85	0.05	0.08	96.86
Unit F	3.48	0.01	14.26	73.13	3.55	0.80	0.25	0.02	0.85	0.06	0.08	96.49
Unit F	3.89	0.01	15.43	72.22	5.33	0.93	0.28	0.03	0.79	0.06	0.07	99.01
Unit F	4.27	0.06	16.17	70.38	6.26	0.82	0.19	0.10	0.71	0.06	0.07	99.06
Unit F	4.05	0.05	16.38	70.49	5.66	1.08	0.18	0.03	0.75	0.06	0.07	98.77
Unit F	5.05	0.12	17.80	66.21	5.52	1.61	0.11	0.04	0.77	0.07	0.15	97.40
Unit F	3.88	0.04	16.10	69.77	6.15	0.84	0.22	0.01	0.85	0.05	0.10	97.99
Unit F	5.03	0.06	18.12	69.93	5.55	1.49	0.14	0.03	0.81	0.05	0.06	101.25
Unit F	4.99	0.07	17.74	69.85	4.81	1.83	0.17	0.07	0.83	0.05	0.07	100.45
Unit J	3.98	0.01	19.05	65.35	10.06		0.05	0.01	0.35	0.06	0.06	98.96
Unit J	3.95	0.25	15.66	67.45	4.90	1.73	0.25	0.05	1.19	0.08	0.20	95.73

Sample: El Chichon
Phase: Amphibole

Conditions: 15 kV, 10 nA, 10 μm

Sample		Na2O	MgO	Al2O3	SiO2	K2O	CaO	TiO2	MnO	FeO	Total
Uncertainty		0.12	0.22	0.13	0.22	0.03	0.12	0.19	0.03	0.12	
Unit C	CHI-9510	2.05	10.83	11.98	40.66	1.54	11.86	2.43	0.53	16.79	98.67
Unit C	CHI-9510	2.09	10.39	11.87	40.86	1.61	11.77	2.48	0.52	17.52	99.10
Unit C	CHI-9510	1.96	10.34	11.73	40.87	1.62	11.82	2.35	0.49	17.47	98.64
Unit C	CHI-9510	2.23	11.34	12.68	39.84	1.34	11.97	2.55	0.42	15.78	98.14
Unit C	CHI-9510	2.17	12.06	13.49	40.40	1.52	12.17	1.97	0.33	14.08	98.19
Unit C	CHI-9510	1.99	10.52	11.91	40.58	1.59	11.74	2.46	0.54	17.34	98.67
Unit C	CHI-9510	2.05	10.70	11.93	40.60	1.58	11.76	2.53	0.52	17.15	98.81
Unit C	CHI-9510	1.99	10.58	11.71	40.82	1.56	11.78	2.51	0.53	16.73	98.21
Unit C	CHI-9510	2.14	10.89	11.80	40.92	1.57	11.70	2.38	0.54	16.83	98.75
Unit C	CHI-9510	1.98	11.36	11.89	40.71	1.44	11.68	2.79	0.53	15.44	97.82
Unit C	CHI-9510	2.06	10.43	12.46	40.28	1.64	11.73	2.56	0.47	16.98	98.61
Unit C	CHI-9510	2.05	10.57	12.07	40.27	1.63	11.89	2.54	0.54	16.71	98.26
Unit C	CHI-9510	2.12	10.78	12.17	40.82	1.64	11.84	2.64	0.56	16.64	99.21
Unit C	CHI-9510	2.18	10.74	12.63	42.00	1.74	11.49	2.54	0.48	15.86	99.66
Unit C	CHI-9510	1.93	10.92	12.76	40.94	1.63	11.87	2.06	0.56	16.81	99.46
Unit C	CHI-9510	2.10	11.69	13.85	40.20	1.41	12.07	2.17	0.38	14.84	98.71
Unit C	CHI-9510	2.08	10.42	12.34	40.11	1.67	11.74	2.37	0.48	16.77	97.98
Unit C	CHI-9510	2.19	13.26	15.37	39.90	1.21	12.57	1.79	0.14	12.39	98.81
Unit C	CHI-9510	2.26	13.25	14.88	40.05	1.18	12.40	2.00	0.19	12.37	98.58
Unit C	CHI-9510	2.26	12.66	15.16	39.58	1.22	12.41	1.91	0.22	13.57	98.98
Unit C	CHI-9510	2.42	11.91	15.36	38.99	1.18	12.25	2.23	0.27	14.17	98.79
Unit C	CHI-9510	2.34	11.18	15.30	38.70	1.20	12.22	2.18	0.31	15.62	99.03
Unit D	CHI-9615	1.98	10.32	11.33	41.11	1.25	11.90	1.70	0.67	17.58	97.84
Unit D	CHI-9615	1.90	10.53	11.08	42.12	1.12	11.92	1.54	0.59	18.24	99.04
Unit D	CHI-9615	2.11	10.18	11.74	41.36	1.29	11.80	1.80	0.69	18.70	99.67
Unit D	CHI-9615	1.99	10.12	11.57	40.96	1.58	11.77	2.01	0.62	18.06	98.68
Unit D	CHI-9615	2.01	10.34	11.55	41.59	1.25	11.61	1.64	0.62	17.67	98.26
Unit D	CHI-9615	1.88	10.01	12.19	40.90	1.38	11.73	1.67	0.63	18.34	98.71
Unit D	CHI-9615	1.80	9.68	12.02	41.05	1.42	11.66	1.86	0.57	19.12	99.18
Unit D	CHI-9615	1.79	10.60	11.18	42.61	1.11	11.78	1.48	0.69	17.81	99.05
Unit D	CHI-9615	1.74	10.46	11.69	41.63	1.20	11.67	1.38	0.63	17.94	98.34
Unit D	CHI-9615	1.99	10.05	11.68	41.42	1.28	11.79	1.42	0.70	18.13	98.46
Unit D	CHI-9615	1.88	9.45	12.38	40.26	1.31	11.89	1.92	0.62	18.30	98.00
Unit D	CHI-9615	1.98	10.27	11.48	41.88	1.30	11.88	1.78	0.58	17.20	98.34
Unit D	CHI-9615	1.82	10.44	11.65	41.29	1.39	11.78	1.97	0.61	18.13	99.09
Unit D	CHI-9615	1.96	9.89	12.92	40.31	1.40	11.73	2.06	0.63	18.20	99.09
Unit D	CHI-9615	1.99	11.20	11.18	41.53	1.35	11.67	2.09	0.77	16.94	98.73
Unit D	CHI-9615	1.87	10.14	11.43	41.54	1.30	11.64	1.75	0.69	17.35	97.69
Unit D	CHI-9615	1.84	11.21	10.91	42.60	1.14	11.68	1.58	0.65	16.76	98.37
Unit D	CHI-9615	1.98	10.08	11.05	41.56	1.38	11.72	1.96	0.60	18.22	98.55
Unit D	CHI-9615	1.85	10.96	9.85	42.66	1.18	11.80	1.71	0.68	17.03	97.70
Unit D	CHI-9615	1.97	10.21	10.92	41.28	1.37	11.79	1.98	0.54	18.64	98.69
Unit D	CHI-9615	1.88	10.22	11.43	41.39	1.36	11.76	1.96	0.65	18.92	99.56
Unit D	CHI-9615	1.94	9.87	11.45	41.20	1.49	11.65	2.00	0.58	19.42	99.61
Unit D	CHI-9615	1.93	10.88	11.42	41.32	1.56	11.87	2.08	0.60	17.63	99.29
Unit D	CHI-9615	1.87	10.60	10.91	41.75	1.42	11.89	2.11	0.58	18.10	99.23
Unit D	CHI-9615	1.83	10.24	11.33	40.79	1.52	11.77	2.04	0.62	18.35	98.48
Unit E	CHI-9516	1.95	10.25	11.29	42.60	1.17	11.58	1.50	0.64	18.38	99.35
Unit E	CHI-9516	1.94	10.57	11.40	42.51	1.20	11.72	1.64	0.59	18.05	99.61
Unit E	CHI-9516	2.00	10.34	11.34	42.08	1.26	11.73	1.58	0.61	17.97	98.89
Unit E	CHI-9516	1.99	9.77	11.44	41.05	1.48	11.58	2.24	0.61	17.81	97.95
Unit E	CHI-9516	2.26	10.30	12.91	39.91	1.34	11.69	2.56	0.54	17.55	99.06

Sample		Na2O	MgO	Al2O3	SiO2	K2O	CaO	TiO2	MnO	FeO	Total
Unit E	CHI-9516	1.96	10.31	10.92	42.44	1.32	11.66	1.54	0.63	18.33	99.11
Unit E	CHI-9516	1.99	10.64	10.70	42.57	1.24	11.63	1.63	0.73	17.99	99.12
Unit E	CHI-9516	1.90	10.86	10.57	42.93	1.31	11.62	1.32	0.61	17.84	98.96
Unit E	CHI-9516	2.01	10.30	11.72	41.21	1.49	11.86	2.10	0.62	18.04	99.34
Unit E	CHI-9516	1.92	10.42	11.45	41.44	1.57	11.64	2.31	0.54	17.75	99.03
Unit E	CHI-9516	1.91	10.56	11.84	40.83	1.50	11.83	2.43	0.48	16.43	97.82
Unit E	CHI-9516	1.92	10.56	11.28	42.08	1.27	11.75	1.49	0.58	17.41	98.34
Unit E	CHI-9516	1.91	10.34	11.49	41.34	1.49	11.85	2.09	0.71	17.77	98.99
Unit E	CHI-9516	1.93	10.07	11.90	41.01	1.57	11.87	1.98	0.60	18.81	99.75
Unit E	CHI-9516	2.13	10.30	12.16	40.93	1.52	11.87	2.38	0.54	17.33	99.16
Unit E	CHI-9516	2.11	10.41	11.67	41.15	1.55	11.83	2.21	0.56	16.98	98.47
Unit E	CHI-9516	2.02	9.98	12.47	40.12	1.48	11.89	2.22	0.59	18.14	98.90
Unit E	CHI-9516	1.95	10.22	11.77	41.10	1.53	11.82	2.04	0.66	18.51	99.60
Unit E	CHI-9516	1.88	10.00	11.98	40.44	1.62	11.80	2.16	0.58	18.06	98.50
Unit E	CHI-9516	1.80	10.06	11.45	41.13	1.47	11.71	2.01	0.66	18.45	98.74
Unit E	CHI-9516	2.08	10.70	11.76	40.94	1.51	11.89	2.43	0.56	17.12	98.99
Unit E	CHI-9516	1.91	10.62	11.70	41.17	1.50	11.77	2.25	0.49	17.36	98.77
Unit J	CHI-9514	2.08	10.19	11.76	41.16	1.54	11.89	2.15	0.60	17.84	99.21
Unit J	CHI-9514	1.93	10.29	11.74	41.16	1.63	11.82	2.14	0.58	18.10	99.41
Unit J	CHI-9514	2.06	10.12	11.74	41.06	1.58	11.83	2.20	0.62	18.12	99.32
Unit J	CHI-9514	2.04	10.75	11.53	41.69	1.48	11.93	2.27	0.63	16.98	99.29
Unit J	CHI-9514	1.92	10.87	11.63	41.79	1.42	11.73	2.40	0.64	16.98	99.37
Unit J	CHI-9514	1.90	10.16	11.83	41.54	1.55	11.60	2.31	0.59	18.03	99.50
Unit J	CHI-9514	2.12	11.98	15.27	40.12	1.17	12.08	2.19	0.19	14.43	99.54
Unit J	CHI-9514	2.26	12.23	14.62	40.58	1.12	12.04	2.12	0.14	14.81	99.90
Unit J	CHI-9514	2.18	12.02	14.78	40.51	1.11	12.00	2.19	0.23	14.46	99.47
Unit J	CHI-9514	1.91	10.19	12.01	41.02	1.61	11.73	1.94	0.61	17.57	98.59
Unit J	CHI-9514	1.89	10.28	12.27	41.38	1.65	11.48	2.30	0.59	17.16	98.99
Unit J	CHI-9514	1.91	10.12	12.10	41.37	1.61	11.46	2.17	0.54	17.34	98.61
Unit J	CHI-9514	1.98	10.39	11.82	41.42	1.66	11.61	2.18	0.63	17.71	99.39
Unit J	CHI-9514	1.94	10.42	11.92	41.46	1.66	11.66	2.11	0.64	17.74	99.54
Unit J	CHI-9514	1.79	10.35	11.98	41.67	1.61	11.78	2.25	0.63	17.50	99.53
Unit J	CHI-9514	1.96	10.09	11.74	41.28	1.65	11.64	2.14	0.61	17.76	98.85
Unit J	CHI-9514	1.81	9.93	11.81	41.28	1.67	11.55	2.31	0.55	17.80	98.71
Unit J	CHI-9514	1.98	10.08	11.91	41.42	1.69	11.56	2.10	0.65	18.52	99.92
Unit J	CHI-9514	1.86	10.10	11.95	41.35	1.66	11.73	2.06	0.63	17.70	99.03
Unit J	CHI-9514	1.82	9.79	11.83	41.31	1.65	11.58	2.12	0.60	17.72	98.40
Unit J	CHI-9514	1.92	10.02	11.78	41.19	1.67	11.68	2.04	0.62	18.15	99.07
Unit J	CHI-9514	1.75	10.11	11.88	41.36	1.65	11.60	2.21	0.56	17.55	98.66
Unit J	CHI-9514	2.23	10.92	15.28	39.47	1.30	12.03	1.96	0.35	15.56	99.09
Unit J	CHI-9514	1.82	9.12	10.94	33.27	1.21	16.69	1.98	0.32	12.93	88.28
Unit J	CHI-9514	2.08	10.48	12.35	41.20	1.57	11.77	2.62	0.48	17.50	100.06
Unit J	CHI-9514	1.96	10.08	12.03	41.21	1.62	11.71	2.49	0.51	17.10	98.69
Unit J	CHI-9514	2.14	9.93	12.13	41.19	1.68	11.60	2.30	0.59	17.91	99.46
Unit J	CHI-9514	2.03	10.34	11.98	41.26	1.63	11.66	2.53	0.62	17.15	99.19
Unit J	CHI-9514	1.94	10.48	11.89	41.30	1.52	11.62	1.95	0.70	17.40	98.79
Unit J	CHI-9514	1.76	10.26	11.56	41.85	1.45	11.56	1.98	0.61	17.92	98.94
Unit J	CHI-9514	1.81	10.16	11.20	41.86	1.47	11.70	1.84	0.68	18.14	98.86
Unit J	CHI-9514	1.65	10.24	10.98	41.64	1.53	11.60	1.73	0.75	18.34	98.48
Unit J	CHI-9514	1.85	10.46	10.37	42.45	1.40	11.51	1.58	0.73	17.54	97.89
Unit J	CHI-9514	2.05	10.19	12.65	40.38	1.55	11.55	2.57	0.51	17.93	99.37
Unit J	CHI-9514	2.16	10.11	12.27	40.97	1.61	11.63	2.57	0.47	16.62	98.42

Core to rim transect of Unit J amphibole

Sample		Na2O	MgO	Al2O3	SiO2	K2O	CaO	TiO2	MnO	FeO	Total
Unit J	CHI-9514	1.88	10.23	11.55	42.29	1.23	11.66	1.63	0.70	18.43	99.60
Unit J	CHI-9514	1.99	9.90	12.31	41.54	1.35	11.66	1.54	0.72	18.76	99.76
Unit J	CHI-9514	1.82	9.95	12.06	41.80	1.35	11.57	1.55	0.69	18.57	99.35
Unit J	CHI-9514	1.86	9.86	11.94	42.00	1.34	11.54	1.48	0.67	18.50	99.19
Unit J	CHI-9514	1.83	10.02	11.80	41.59	1.23	11.55	1.61	0.70	18.00	98.32
Unit J	CHI-9514	2.08	10.23	11.59	42.02	1.27	11.46	1.44	0.65	18.16	98.89
Unit J	CHI-9514	1.85	9.86	12.05	41.28	1.34	11.65	1.44	0.67	18.68	98.81
Unit J	CHI-9514	1.92	9.85	12.08	41.49	1.37	11.58	1.47	0.62	18.88	99.26
Unit J	CHI-9514	1.83	9.87	11.93	41.59	1.33	11.54	1.56	0.68	18.19	98.52
Unit J	CHI-9514	1.84	10.17	12.07	41.73	1.29	11.48	1.53	0.72	18.35	99.18
Unit J	CHI-9514	1.94	9.85	11.90	41.63	1.31	11.63	1.52	0.76	17.93	98.47
Unit J	CHI-9514	2.06	9.96	12.17	41.62	1.37	11.75	1.52	0.60	18.41	99.46
Unit J	CHI-9514	1.82	10.21	11.86	41.44	1.29	11.55	1.38	0.62	18.37	98.54
Unit J	CHI-9514	1.79	9.95	11.88	40.65	1.26	11.40	1.60	0.73	18.22	97.49
Unit J	CHI-9514	2.01	9.76	12.14	41.40	1.34	11.71	1.52	0.62	18.62	99.12
Unit J	CHI-9514	1.78	9.95	12.00	41.36	1.29	11.64	1.39	0.67	18.35	98.42
Unit J	CHI-9514	1.86	9.90	12.11	41.72	1.28	11.60	1.65	0.71	18.87	99.70
Unit J	CHI-9514	1.83	9.77	12.02	41.43	1.24	11.52	1.45	0.60	18.09	97.96
Unit J	CHI-9514	1.87	9.90	11.55	41.22	1.15	11.47	1.45	0.65	17.91	97.16
Unit J	CHI-9514	1.91	9.87	11.69	42.42	1.19	10.96	1.31	0.61	17.25	97.20
Unit J	CHI-9514	1.85	9.60	12.13	41.26	1.22	11.42	1.45	0.72	18.14	97.80
Unit J	CHI-9514	2.03	10.08	12.21	41.91	1.21	11.68	1.51	0.76	18.16	99.56
Unit J	CHI-9514	2.07	9.81	11.99	42.06	1.18	11.60	1.52	0.71	17.56	98.49
Unit J	CHI-9514	2.01	10.04	12.08	41.92	1.21	11.58	1.66	0.66	17.85	99.01
Unit J	CHI-9514	1.87	9.14	11.64	38.53	1.10	14.30	1.69	0.58	17.14	95.99
Unit J	CHI-9514	2.04	10.30	11.79	41.55	1.11	11.68	1.92	0.74	17.95	99.07
Unit J	CHI-9514	1.92	10.72	11.01	42.72	1.08	11.65	1.97	0.62	17.37	99.06
Unit J	CHI-9514	1.82	10.78	10.82	42.66	1.10	11.69	1.77	0.66	17.05	98.34
Unit J	CHI-9514	1.92	10.27	11.24	41.94	1.19	11.62	1.67	0.59	17.56	97.99
Unit J	CHI-9514	1.91	10.53	11.47	41.70	1.21	11.66	1.56	0.62	17.67	98.32
Unit J	CHI-9514	1.92	10.38	11.79	41.55	1.30	11.71	1.84	0.56	18.20	99.24
Unit J	CHI-9514	1.92	10.27	11.74	41.74	1.28	11.65	1.70	0.67	17.89	98.86
Unit J	CHI-9514	1.98	10.88	11.31	42.12	1.16	11.61	1.65	0.60	18.10	99.40
Unit J	CHI-9514	1.86	10.76	11.18	42.34	1.19	11.62	1.74	0.69	17.12	98.49
Unit J	CHI-9514	1.96	10.63	11.42	42.16	1.26	11.65	1.59	0.57	17.82	99.07
Unit J	CHI-9514	1.83	10.76	11.29	42.03	1.28	11.71	1.80	0.66	17.06	98.40
Unit J	CHI-9514	1.83	10.61	11.07	42.93	1.28	11.75	2.01	0.61	17.05	99.13
Unit J	CHI-9514	1.89	10.96	11.10	42.64	1.28	11.82	1.73	0.62	17.25	99.29
Unit J	CHI-9514	1.85	10.74	11.27	42.57	1.33	11.64	1.91	0.65	17.34	99.29
Unit J	CHI-9514	1.89	10.67	11.41	42.00	1.34	11.67	1.89	0.58	17.39	98.83
Unit J	CHI-9514	1.86	10.13	11.81	41.43	1.44	11.68	2.21	0.63	17.21	98.38
Unit J	CHI-9514	2.01	10.37	11.93	41.32	1.47	11.67	2.06	0.59	17.31	98.72
Unit J	CHI-9514	2.01	10.48	11.75	41.28	1.52	11.65	1.92	0.62	17.34	98.55
Unit J	CHI-9514	1.85	10.41	11.75	41.08	1.50	11.69	2.05	0.53	17.43	98.30
Unit J	CHI-9514	1.82	10.29	11.72	41.55	1.58	11.64	2.09	0.59	17.74	99.01
Unit J	CHI-9514	1.82	9.74	11.87	41.10	1.64	11.70	2.05	0.61	18.05	98.58
Unit J	CHI-9514	1.94	9.41	11.87	41.20	1.65	11.46	2.28	0.58	18.99	99.39
Unit J	CHI-9514	2.12	10.15	12.18	40.52	1.64	11.55	2.66	0.57	17.54	98.92
Unit J	CHI-9514	1.90	10.07	12.08	40.90	1.57	11.70	2.44	0.48	17.48	98.60
Unit J	CHI-9514	2.12	10.68	12.08	40.87	1.56	11.70	2.22	0.47	16.99	98.66
Unit J	CHI-9514	1.96	9.96	12.24	40.80	1.65	11.64	2.65	0.60	17.68	99.17
Unit J	CHI-9514	3.41	5.53	15.00	52.46	2.64	7.88	1.38	0.34	10.49	99.13
Unit J	CHI-9514	2.00	0.04	8.90	32.94	1.92	1.18	0.14	0.02	0.82	47.95
Unit J	CHI-9514	0.72	0.28	2.52	13.58	0.66	0.92	0.10	0.06	0.61	19.44
Unit J	CHI-9514	2.29	0.10	9.66	43.08	3.34	0.91	0.17	0.03	0.92	60.49
Unit J	CHI-9514	0.24	0.02	1.74	9.14	0.63	0.33	0.04	0.03	0.23	12.40
Unit J	CHI-9514	2.54	0.08	10.71	42.52	3.05	1.34	0.16	0.05	0.92	61.37
Unit J	CHI-9514	1.62	0.20	6.91	27.55	1.91	1.09	0.11	0.01	0.81	40.22
Unit J	CHI-9514	0.54	0.20	2.87	13.61	1.01	0.27	0.10	0.03	0.37	18.99
Unit J	CHI-9514	1.28	0.16	9.42	44.80	3.28	0.75	0.17	0.07	0.89	60.83
Unit J	CHI-9514	1.48	0.10	7.38	27.40	1.56	1.09	0.07	0.06	0.84	39.97

Continuation of Unit J transect

Sample		Na2O	MgO	Al2O3	SiO2	K2O	CaO	TiO2	MnO	FeO	Total
Unit J	CHI-9514	1.38	0.48	7.34	41.41	2.68	3.29	0.13	0.08	0.96	57.75
Unit J	CHI-9514	0.97	0.13	5.85	29.15	2.20	0.81	0.10	0.05	0.50	39.74
Unit J	CHI-9514	3.02	0.13	14.71	52.35	3.37	2.12	0.14	0.05	1.03	76.91
Unit J	CHI-9514	3.69	0.00	30.80	51.59	0.26	12.96	0.03	0.00	0.58	99.91
Unit J	CHI-9514	2.10	10.10	12.22	41.01	1.60	11.55	2.60	0.47	17.97	99.62
Unit J	CHI-9514	2.08	10.25	12.05	40.32	1.62	11.56	2.31	0.52	17.69	98.40

Appendix 2: El Chichón Plagioclase Transects

Major element compositions were analyzed with a JEOL JXA-8200 electron microprobes at The University of Texas at Austin Department of Geological Sciences. All analyses are reported as weight percent oxides. Calibration and secondary standards are listed in Appendix 1.

Laser Ablation ICP-MS (LA-ICP-MS) analyses were collected using the IsoProbe and a New Wave LUV-213 nm frequency quintupled Nd-YAG laser. Isotopes ^{88}Sr, ^{87}Sr, ^{86}Sr, ^{85}Rb, ^{84}Sr, and ^{83}Kr were analyzed using static acquisition mode. Preliminary mass fractionation was corrected using an exponential fractionation law. Following correction for mass fractionation, the $^{87}Sr/^{86}Sr$ ratios were found to be systematically high; to resolve that problem, I used a secondary, empirical correction based on LA-ICP-MS analyses of standard GTO-05-6b2, and variation of $^{87}Sr/^{86}Sr$ ratio with $^{88}Sr/^{86}Sr$ ratio and ^{88}Sr signal intensity.

Exponentially-corrected track analyses, collected by continuously sampling from core to rim, show a negative correlation between corrected $^{87}Sr/^{86}Sr$ and $^{88}Sr/^{86}Sr$ ratios (Figure A2.1). That negative correlation indicates overcorrection of mass fractionation; some of that overcorrection may be the result of measuring backgrounds using a non-loaded plasma. Secondary correction of track data is made by considering $^{87}Sr/^{86}Sr$ ratios as a linear function of $^{88}Sr/^{86}Sr$ ratios for standard GTO-05-6b2 (Figure A2.2). Because the nominal $^{87}Sr/^{86}Sr$ ratio is known from TIMS analyses (0.703467), those data

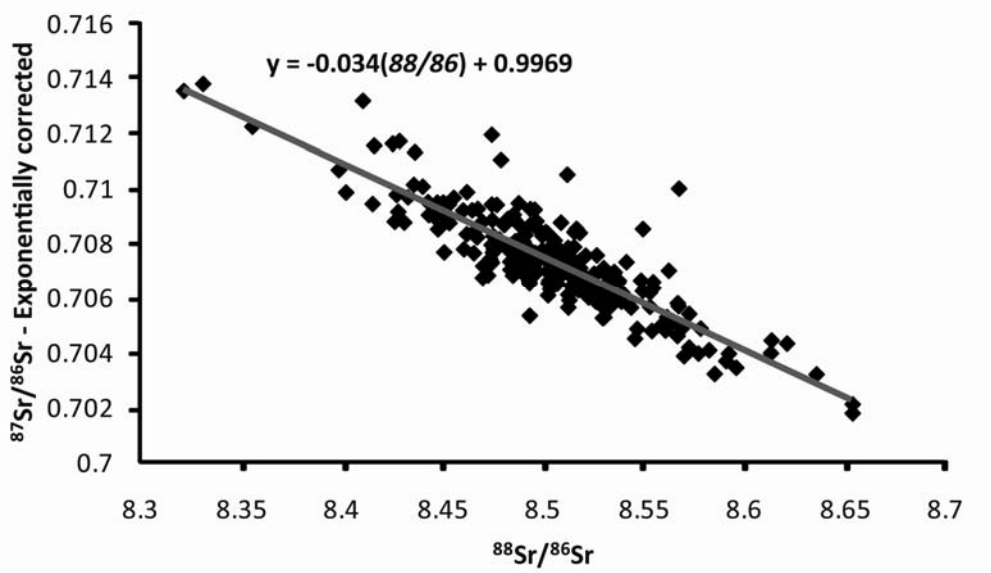

Figure A2.1. Exponentially-corrected $^{87}Sr/^{86}Sr$ versus $^{88}Sr/^{86}Sr$ for a track analysis of El Chichón Unit E plagioclase. The data may be linearly regressed along a best-fit line to empirically correct the analyses.

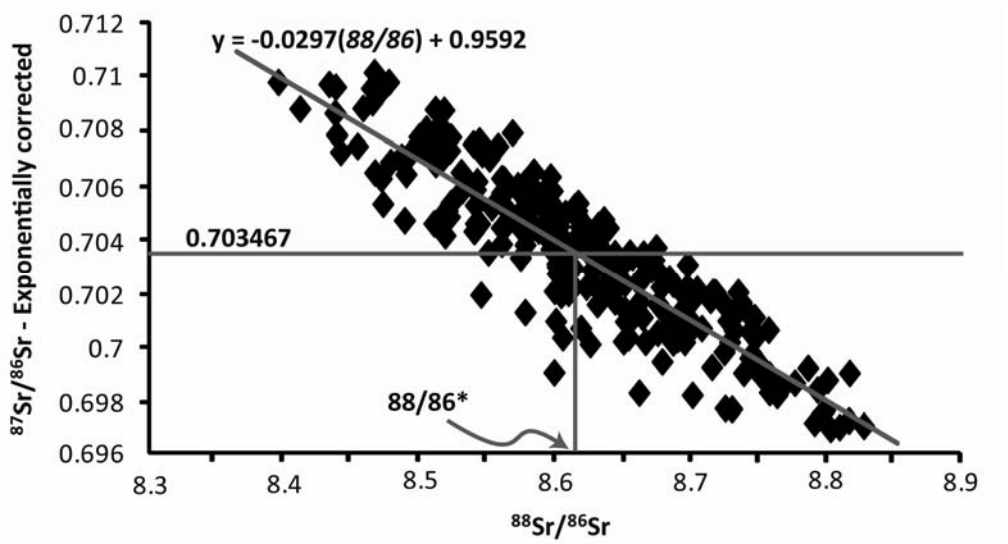

Figure A2.2. Exponentially-corrected $^{87}Sr/^{86}Sr$ versus $^{88}Sr/^{86}Sr$ for a track analysis of GTO-05-6b2. Linear regression of the data to the TIMS measured ratio of 0.703467 yields an $^{88}Sr/^{86}Sr$ ratio, 88/86*, for regression of unknown analyses.

may be regressed along the best-fit line to a single $^{88}Sr/^{86}Sr$ ratio, *88/86**, such that $^{87}Sr/^{86}Sr = 0.703467$. Secondary correction of unknown samples is made by regressing their data along the best-fit slope (determined from each analysis, e.g. Figure A2.2) to *88/86**. Following secondary processing, the corrected $^{87}Sr/^{86}Sr$ ratios have lower absolute values and improved standard errors (Figure A2.3).

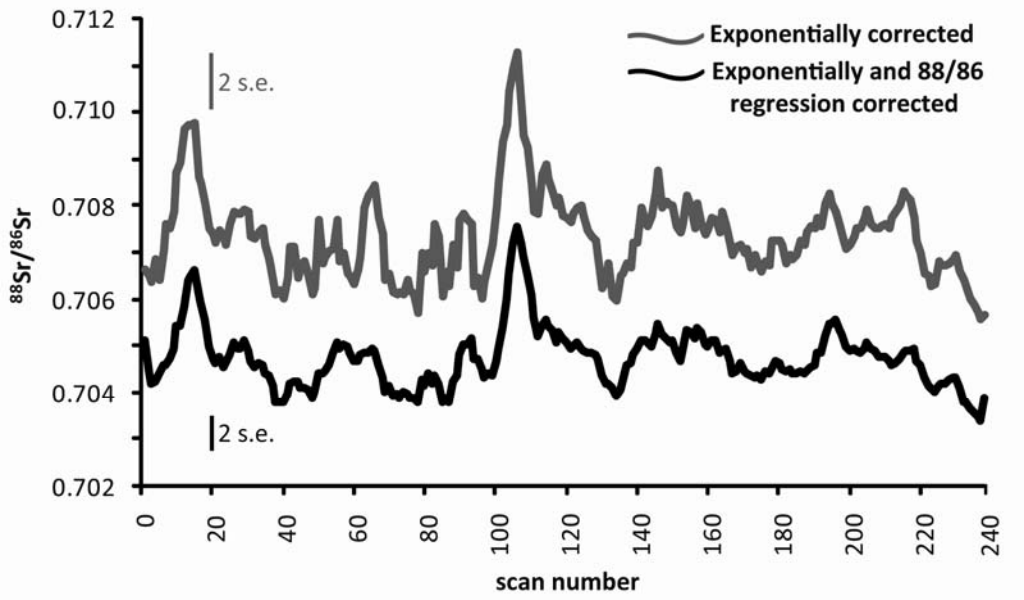

Figure A2.3. Comparison of a Unit E plagioclase transect analysis with and without regression correction.

Exponentially-corrected spot analyses of standard GTO-05-6b2 are significantly higher than the nominal value (Table A2.1). Because the blanks for spot analyses were collected with a loaded plasma, a slightly different correction procedure was used than with track analyses. First, exponentially-corrected $^{87}Sr/^{86}Sr$ ratios were plotted against

$^{88}Sr/^{86}Sr$ ratios from each day's analyses of GTO-05-6b2. Those data were linearly regressed to a single $^{88}Sr/^{86}Sr$ ratio, *88/86**, such that $^{87}Sr/^{86}Sr = 0.703467$ (Figure A2.4). A similar regression of OR-Labr analyses shows that the slope of the regression is

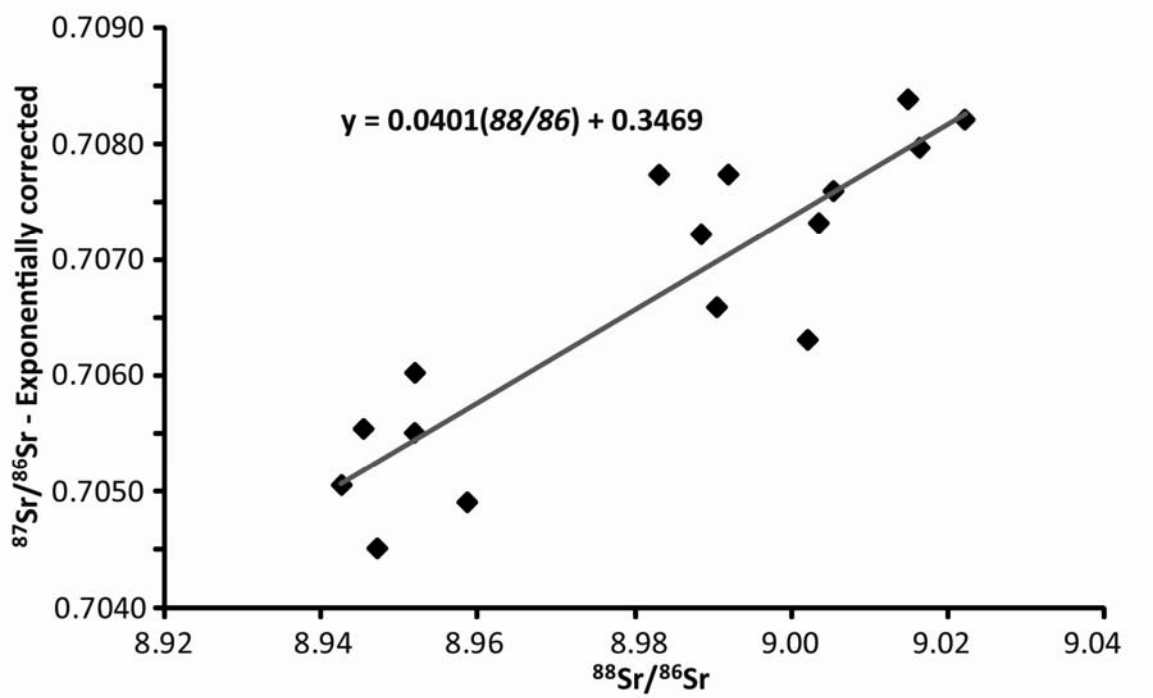

Figure A2.4. Exponentially-corrected $^{87}Sr/^{86}Sr$ versus $^{88}Sr/^{86}Sr$ ratios for spot analyses of GTO-05-6b2 collected during a single day. The ratios may be regressed to determine an $^{88}Sr/^{86}Sr$ ratio, 88/86*, for regression of unknown analyses. The slope of the regression, 0.0401 for these data, is proportional to the ^{88}Sr signal intensity.

proportional to ^{88}Sr signal (Figure A2.5), such that analyses with lower ^{88}Sr intensities should be regressed with a shallower slope. The function describing regression slope is determined by dividing the GTO-05-6b2 regression slope by the average intensity of ^{88}Sr in those analyses of GTO-05-6b2. Unknown analyses are corrected by regressing the data along a slope proportional to their 88Sr intensity to *88/86**.

It should be noted that the corrections described in this appendix are empirical. Significantly, the problems that these corrections attempt to remedy are likely related to the method in which backgrounds were measured. Specifically, early analyses (track

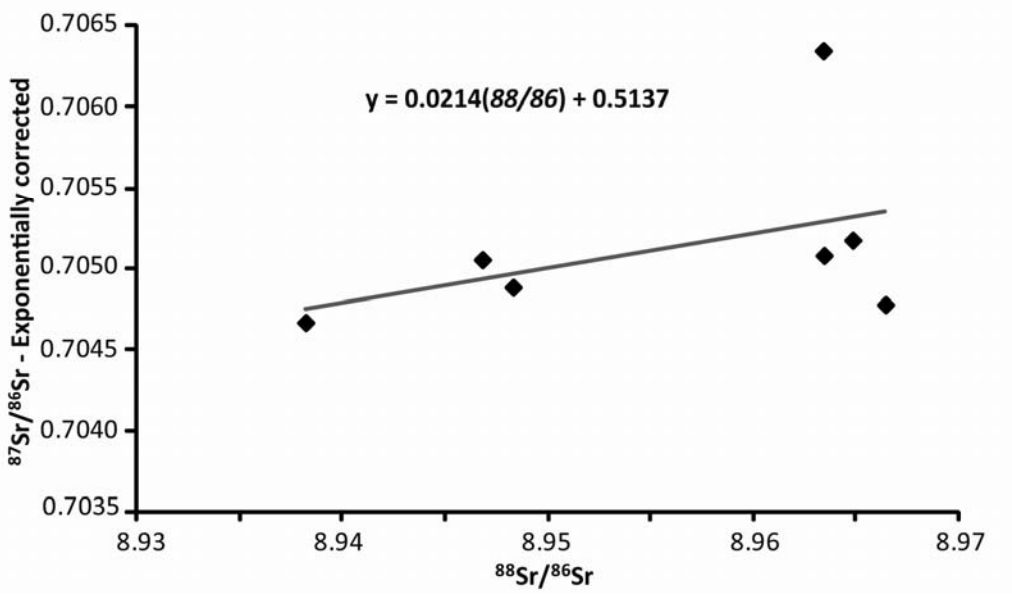

Figure A2.5. Exponentially-corrected $^{87}Sr/^{86}Sr$ versus $^{88}Sr/^{86}Sr$ ratios for OR-Labr. The slope of the regression is proportional to the signal voltage. Thus these analyses, with average ^{88}Sr intensities of ~0.1 V, define a slope approximately half that of the GTO-05-6b2 analyses in Figure A2.4 which had average ^{88}Sr intensities of ~0.2 V.

analyses) measured on-peak backgrounds with a non-loaded plasma. That technique resulted in negative ^{82}Kr intensities during track analyses. Thus correction for Kr interferences on Sr produced an increased ^{86}Sr signal. Moreover, there was significant analytical noise in the measurements of 82Kr and 85Rb. All of those effects contributed to uncertainty in the data. During spot analyses, I collected backgrounds with a loaded plasma in an attempt to properly measure the on-peak backgrounds and not collect

unknown analyses with negative ^{82}Kr voltages. This approach succeeded in that the ^{82}Kr signals during spot analyses were not consistently negative: the background corrected ^{82}Kr voltages average within one standard deviation of zero. Unfortunately, the ^{85}Rb signal behaves similarly, thus making correction for ^{87}Rb interference on ^{87}Sr very difficult. Moreover, the noise in the ^{82}Kr and ^{85}Rb signals during spot analyses were significant and greatly contribute to uncertainties in measurement of the $^{87}Sr/^{86}Sr$ ratio. Future LA-ICP-MS Sr isotopic analyses should explore different methods of collecting backgrounds. One possible method would be to measure detector backgrounds with the flight tube closed. In this approach, the backgrounds would be quite small (the noise in the detector when it should be measuring "zero"), and thus all measured Kr, Rb, and Sr signals would be used, and not the signals minus a background plasma signal (loaded or non-loaded).

Table A2.1. LA-ICP-MS spot analyses of standard GTO-05-6b2. Exponentially corrected analyses are systematically higher than the TIMS-measured 87Sr/86Sr ratio of 0.703467. Regression-corrected analyses are within analytical uncertainty of the TIMS measurement.

				Exponentially-corr					Regression-corr
Date:	88/86*	slope	Sample	87Sr/86Sr	88Sr/86Sr	V 88	n	2 s.e.	87Sr/86Sr
31-Mar-09	8.9	0.21*V88	GTO6b2 1	0.70492	8.95851	0.1998	42	0.00051	0.70246
			GTO6b2 2	0.70452	8.94698	0.2431	41	0.00053	0.70212
			GTO6b2 3	0.70507	8.94242	0.2367	40	0.00059	0.70296
			GTO6b2 4	0.70555	8.94522	0.2487	43	0.00047	0.70319
			GTO6b2 5	0.70552	8.95177	0.2268	42	0.00048	0.70305
			GTO6b2 6	0.70603	8.95182	0.2531	34	0.00049	0.70328
			GTO6b2 7	0.70774	8.98311	0.1602	31	0.00083	0.70495
			GTO6b2 8	0.70839	9.01500	0.1563	37	0.00075	0.70461
			GTO6b2 9	0.70822	9.02228	0.1809	35	0.00066	0.70357
			GTO6b2 11	0.70632	9.00215	0.1811	40	0.00060	0.70243
			GTO6b2 12	0.70723	8.98850	0.1845	42	0.00056	0.70380
			GTO6b2 13	0.70660	8.99052	0.1929	43	0.00065	0.70293
			GTO6b2 15	0.70733	9.00357	0.1539	38	0.00108	0.70398
			GTO6b2 16	0.70798	9.01649	0.1583	40	0.00061	0.70410
			GTO6b2 17	0.70760	9.00544	0.1705	44	0.00054	0.70383
			GTO6b2 18	0.70774	8.99198	0.2049	43	0.00053	0.70379
		Average		**0.70667**					**0.703441751**
1-Apr-09	8.9	0.21*V88	GTO6b2 1	0.70570	8.94603	0.2538	43	0.00051	0.70370
			GTO6b2 2	0.70404	8.93775	0.2595	39	0.00049	0.70246
			GTO6b2 3	0.70969	9.03967	0.2512	42	0.00049	0.70268
			GTO6b2 4	0.71066	9.06530	0.2372	43	0.00045	0.70274
			GTO6b2 5	0.70593	8.95088	0.2468	43	0.00049	0.70372
			GTO6b2 7	0.70571	8.97155	0.1932	33	0.00057	0.70313
			GTO6b2 8	0.70563	8.94699	0.1924	34	0.00056	0.70407
			GTO6b2 9	0.70571	8.94190	0.2152	35	0.00044	0.70420
			GTO6b2 10	0.70535	8.93770	0.2206	36	0.00045	0.70401
			GTO6b2 11	0.70877	9.02093	0.2363	32	0.00100	0.70313
			GTO6b2 12	0.71172	9.09561	0.1765	36	0.00077	0.70468
			GTO6b2 15	0.70535	8.96045	0.2026	36	0.00102	0.70313
			GTO6b2 16	0.70992	9.05489	0.2182	39	0.00085	0.70312
			GTO6b2 17	0.70455	8.96362	0.2196	42	0.00053	0.70199
			GTO6b2 18	0.70467	8.96595	0.2089	42	0.00065	0.70213
			GTO6b2 19	0.70616	8.95170	0.2160	39	0.00060	0.70420
			GTO6b2 20	0.70600	8.95693	0.2169	41	0.00061	0.70379
			GTO6b2 22	0.70535	8.95906	0.1340	37	0.00088	0.70392
			GTO6b2 23	0.70460	8.96045	0.1476	42	0.00091	0.70298
			GTO6b2 24	0.70801	9.01381	0.1625	44	0.00070	0.70437
			GTO6b2 25	0.70954	9.04126	0.1642	41	0.00053	0.70490
			GTO6b2 26	0.70836	9.04194	0.1648	42	0.00073	0.70368
			GTO6b2 27	0.70910	9.04812	0.1623	43	0.00062	0.70428
			GTO6b2 28	0.71023	9.05582	0.1600	40	0.00055	0.70521
		Average		**0.70711**					**0.703592651**
2-Apr-09	8.85	0.09*V88	GTO6b2 1	0.70554	8.94821	0.1700	34	0.00084	0.70415
			GTO6b2 2	0.70540	8.93194	0.2729	36	0.00038	0.70356
			GTO6b2 3	0.70526	8.92971	0.3361	41	0.00037	0.70307
			GTO6b2 4	0.70506	8.93016	0.2879	40	0.00049	0.70317
			GTO6b2 5	0.70548	8.93993	0.2761	39	0.00036	0.70343
			GTO6b2 6	0.70484	8.92823	0.2792	34	0.00066	0.70305
			GTO6b2 7	0.70493	8.94068	0.2803	38	0.00045	0.70283
			GTO6b2 8	0.70510	8.93575	0.2703	39	0.00057	0.70319
			GTO6b2 9	0.70527	8.93783	0.2524	42	0.00048	0.70344
			GTO6b2 10	0.70584	8.94643	0.2493	42	0.00052	0.70384
			GTO6b2 11	0.70569	8.95074	0.2325	42	0.00062	0.70374
			GTO6b2 12	0.70483	8.94440	0.2374	42	0.00061	0.70297
		Average		**0.70527**					**0.703371061**

Unit: El Chichon A
Thin Section: 05-PL01
Crystal: A

85 μm diameter spot
"pos." indicates center

Microprobe analyses

Pos. (μm)	Na2O	Al2O3	SiO2	K2O	CaO	FeO	SrO	Total
0.0	8.47	41.54	40.90	0.74	7.59	0.07	0.21	99.52
9.8	10.08	39.39	42.76	0.63	6.27	0.20	0.18	99.51
19.6	8.56	41.42	41.00	0.62	7.52	0.08	0.18	99.38
29.4	8.25	41.83	40.65	0.71	7.77	0.21	0.21	99.64
39.2	7.90	42.30	40.24	0.55	8.06	0.37	0.16	99.58
49.0	8.92	40.94	41.41	0.36	7.23	0.41	0.27	99.54
58.8	9.50	40.17	42.08	0.41	6.75	0.16	0.20	99.27
68.6	10.89	38.30	43.70	0.31	5.61	0.45	0.20	99.46
78.4	10.22	39.21	42.91	0.70	6.16	0.15	0.29	99.65
88.1	11.30	37.76	44.17	0.36	5.27	0.14	0.18	99.18
97.9	9.63	39.99	42.24	0.54	6.64	0.48	0.30	99.82
107.7	9.81	39.75	42.45	0.76	6.49	0.13	0.28	99.66
117.5	11.12	38.00	43.96	0.54	5.42	0.47	0.17	99.69
127.3	8.47	41.54	40.90	0.62	7.59	0.38	0.20	99.70
137.1	11.85	37.02	44.80	0.36	4.82	0.13	0.27	99.26
146.9	11.95	36.90	44.91	0.43	4.74	0.47	0.28	99.68
156.7	11.81	37.09	44.75	0.22	4.86	0.05	0.18	98.94
166.5	12.04	36.78	45.01	0.37	4.67	0.21	0.27	99.35
176.3	9.68	39.93	42.29	0.71	6.60	0.01	0.28	99.50
186.1	9.85	39.69	42.50	0.42	6.46	0.09	0.16	99.17
195.9	9.27	40.47	41.83	0.72	6.93	0.48	0.23	99.92
205.7	12.78	35.79	45.87	0.46	4.06	0.12	0.29	99.36
215.5	10.26	39.15	42.96	0.48	6.12	0.27	0.30	99.55
225.3	12.13	36.66	45.12	0.75	4.59	0.49	0.17	99.92
235.1	10.12	39.33	42.81	0.77	6.24	0.27	0.17	99.71
244.9	10.53	38.79	43.28	0.77	5.90	0.14	0.16	99.56
254.7	9.76	39.81	42.39	0.71	6.53	0.25	0.19	99.65
264.4	10.71	38.55	43.49	0.49	5.75	0.28	0.27	99.53
274.2	9.41	40.29	41.98	0.29	6.82	0.12	0.19	99.09
284.0	9.63	39.99	42.24	0.55	6.64	0.09	0.23	99.37
293.8	11.76	37.15	44.70	0.30	4.89	0.01	0.17	98.98
303.6	10.26	39.15	42.96	0.79	6.12	0.19	0.20	99.68
313.4	10.89	38.30	43.70	0.38	5.61	0.04	0.27	99.19
323.2	8.69	41.24	41.16	0.76	7.41	0.37	0.28	99.91
333.0	9.63	39.99	42.24	0.30	6.64	0.29	0.27	99.35
342.8	11.17	37.94	44.01	0.57	5.38	0.35	0.20	99.62
352.6	10.80	38.43	43.59	0.23	5.68	0.11	0.20	99.04
362.4	11.49	37.51	44.38	0.41	5.12	0.22	0.24	99.38
372.2	8.25	41.83	40.65	0.51	7.77	0.14	0.20	99.34
382.0	11.72	37.21	44.64	0.40	4.93	0.02	0.21	99.13
391.8	10.94	38.24	43.75	0.39	5.57	0.23	0.25	99.37
401.6	11.76	37.15	44.70	0.43	4.89	0.26	0.15	99.35
411.4	12.18	36.59	45.17	0.43	4.55	0.10	0.20	99.23
421.2	11.35	37.70	44.22	0.71	5.23	0.33	0.28	99.81
430.9	12.08	36.72	45.07	0.49	4.63	0.22	0.28	99.48
440.7	10.94	38.24	43.75	0.61	5.57	0.47	0.21	99.79
450.5	11.30	37.76	44.17	0.67	5.27	0.46	0.29	99.92
460.3	11.76	37.15	44.70	0.34	4.89	0.18	0.28	99.30
470.1	9.68	39.93	42.29	0.72	6.60	0.50	0.29	100.00

ICP-MS

Pos. (μm)	87/86	2 s.e.
70	0.70351	0.00053
215	0.70413	0.00032
354	0.70522	0.00046
414	0.70556	0.00046
528	0.70507	0.00061

Pos. (μm)	Na2O	Al2O3	SiO2	K2O	CaO	FeO	SrO	Total
479.9	11.26	37.82	44.12	0.47	5.31	0.27	0.22	99.47
489.7	11.44	37.58	44.33	0.22	5.16	0.49	0.18	99.38
499.5	11.17	37.94	44.01	0.60	5.38	0.22	0.16	99.48
509.3	11.03	38.12	43.85	0.70	5.49	0.16	0.29	99.65
519.1	11.62	37.33	44.54	0.53	5.01	0.47	0.28	99.78
528.9	9.81	39.75	42.45	0.62	6.49	0.22	0.16	99.50
538.7	10.03	39.45	42.70	0.41	6.31	0.49	0.18	99.58
548.5	11.08	38.06	43.91	0.68	5.46	0.46	0.24	99.88
558.3	8.30	41.77	40.70	0.60	7.73	0.22	0.24	99.56
568.1	10.62	38.67	43.38	0.56	5.83	0.28	0.22	99.55
577.9	8.52	41.48	40.95	0.72	7.55	0.04	0.26	99.51
587.7	11.12	38.00	43.96	0.74	5.42	0.29	0.24	99.76
597.5	12.04	36.78	45.01	0.79	4.67	0.35	0.23	99.86
607.2	10.76	38.49	43.54	0.80	5.72	0.08	0.28	99.66
617.0	10.58	38.73	43.33	0.22	5.87	0.40	0.29	99.40
626.8								
636.6								
646.4	9.81	39.75	42.45	0.67	6.49	0.13	0.20	99.49
656.2	11.40	37.64	44.27	0.54	5.19	0.34	0.18	99.56
666.0	10.80	38.43	43.59	0.50	5.68	0.38	0.24	99.62
675.8	10.58	38.73	43.33	0.74	5.87	0.38	0.25	99.86
685.6	10.35	39.03	43.07	0.58	6.05	0.23	0.29	99.60
695.4	7.55	42.77	39.84	0.21	8.35	0.01	0.21	98.93
705.2	8.43	41.59	40.85	0.33	7.63	0.07	0.18	99.08
715.0	6.76	43.82	38.93	0.25	8.99	0.30	0.22	99.27
724.8	9.90	39.63	42.55	0.35	6.42	0.05	0.15	99.05
734.6	10.67	38.61	43.43	0.31	5.79	0.06	0.26	99.13
744.4	10.35	39.03	43.07	0.35	6.05	0.33	0.16	99.34
754.2	10.67	38.61	43.43	0.32	5.79	0.46	0.19	99.48
764.0	9.36	40.35	41.93	0.73	6.86	0.37	0.24	99.85
773.8	8.69	41.24	41.16	0.79	7.41	0.32	0.25	99.86

Unit: El Chichon A
Thin Section: 05-PL01
Crystal: B

85 μm diameter spot
"pos." indicates center

Microprobe analyses

Pos. (μm)	Na2O	Al2O3	SiO2	K2O	CaO	FeO	SrO	Total
0.0	7.11	43.35	39.33	0.67	8.70	0.16	0.26	99.59
5.2	8.56	41.42	41.00	0.77	7.52	0.12	0.19	99.58
10.4	7.07	43.41	39.28	0.49	8.74	0.46	0.19	99.64
15.6	7.90	42.30	40.24	0.31	8.06	0.07	0.15	99.03
20.8	7.24	43.18	39.48	0.29	8.60	0.06	0.23	99.08
26.0	7.42	42.94	39.69	0.42	8.45	0.07	0.15	99.15
31.2	8.43	41.59	40.85	0.31	7.63	0.24	0.24	99.29
36.4	7.94	42.24	40.29	0.63	8.02	0.36	0.24	99.74
41.6	7.24	43.18	39.48	0.23	8.60	0.24	0.19	99.16
46.8	7.94	42.24	40.29	0.67	8.02	0.32	0.16	99.65
52.0	8.30	41.77	40.70	0.58	7.73	0.18	0.25	99.51
57.2	8.30	41.77	40.70	0.28	7.73	0.18	0.17	99.13
62.4	9.54	40.11	42.13	0.79	6.71	0.10	0.27	99.65
67.6	7.37	43.00	39.64	0.27	8.49	0.42	0.19	99.38
72.8	6.89	43.64	39.08	0.74	8.88	0.16	0.20	99.60
78.0	6.07	44.74	38.13	0.21	9.56	0.07	0.22	99.01
83.2	8.52	41.48	40.95	0.70	7.55	0.48	0.18	99.86
88.4	8.47	41.54	40.90	0.56	7.59	0.45	0.24	99.74
93.6	7.59	42.71	39.89	0.29	8.31	0.18	0.25	99.22
98.9	8.56	41.42	41.00	0.38	7.52	0.48	0.26	99.62
104.1	7.50	42.83	39.79	0.26	8.38	0.47	0.27	99.51
109.3	7.90	42.30	40.24	0.73	8.06	0.32	0.27	99.81
114.5	8.34	41.71	40.75	0.28	7.70	0.42	0.19	99.38
119.7	10.31	39.09	43.02	0.77	6.09	0.33	0.22	99.82
124.9	9.27	40.47	41.83	0.77	6.93	0.17	0.20	99.64
130.1								
135.3	7.99	42.18	40.34	0.24	7.99	0.45	0.24	99.43
140.5	7.42	42.94	39.69	0.44	8.45	0.32	0.30	99.55
145.7	6.55	44.10	38.68	0.62	9.17	0.45	0.20	99.76
150.9	6.42	44.28	38.53	0.62	9.27	0.18	0.25	99.55
156.1	6.81	43.76	38.98	0.68	8.95	0.39	0.16	99.73
161.3	5.17	45.94	37.10	0.76	10.29	0.04	0.23	99.54
166.5	8.25	41.83	40.65	0.65	7.77	0.19	0.18	99.52
171.7	7.02	43.47	39.23	0.28	8.78	0.02	0.23	99.03
176.9	6.55	44.10	38.68	0.59	9.17	0.35	0.28	99.72
182.1	8.07	42.07	40.44	0.24	7.91	0.16	0.21	99.10
187.3	6.20	44.57	38.28	0.59	9.45	0.19	0.29	99.57
192.5	6.50	44.16	38.63	0.21	9.20	0.00	0.23	98.94
197.7	7.55	42.77	39.84	0.40	8.35	0.08	0.23	99.21
202.9	7.37	43.00	39.64	0.51	8.49	0.18	0.18	99.36
208.1	6.94	43.58	39.13	0.32	8.85	0.41	0.28	99.52
213.3	8.25	41.83	40.65	0.28	7.77	0.29	0.17	99.25
218.5	8.38	41.65	40.80	0.58	7.66	0.47	0.22	99.77
223.7	8.69	41.24	41.16	0.35	7.41	0.09	0.20	99.15
228.9	9.32	40.41	41.88	0.35	6.90	0.36	0.30	99.50
234.1	10.03	39.45	42.70	0.37	6.31	0.34	0.17	99.37
239.3	10.49	38.85	43.22	0.50	5.94	0.31	0.23	99.54
244.5	9.99	39.51	42.65	0.46	6.35	0.06	0.26	99.27
249.7	8.96	40.88	41.47	0.62	7.19	0.15	0.27	99.53

ICP-MS

Pos. (μm)	87/86	2 s.e.
45	0.70395	0.00088
205	0.70484	0.00056
295	0.70597	0.00077
437	0.70370	0.00082
560	0.70434	0.00115

Pos. (μm)	Na2O	Al2O3	SiO2	K2O	CaO	FeO	SrO	Total
254.9	10.62	38.67	43.38	0.58	5.83	0.33	0.25	99.67
260.1	9.59	40.05	42.19	0.37	6.68	0.08	0.20	99.15
265.3	15.75	31.83	49.29	0.56	1.63	0.43	0.27	99.75
270.5								
275.7	12.18	36.59	45.17	0.75	4.55	0.47	0.28	100.00
280.9	11.99	36.84	44.96	0.57	4.71	0.29	0.20	99.56
286.2	10.99	38.18	43.80	0.73	5.53	0.26	0.18	99.66
291.4	10.31	39.09	43.02	0.72	6.09	0.01	0.25	99.48
296.6	12.45	36.23	45.49	0.29	4.33	0.28	0.22	99.29
301.8	12.73	35.85	45.81	0.45	4.10	0.08	0.20	99.23
307.0	12.22	36.53	45.23	0.22	4.52	0.27	0.23	99.21
312.2	12.64	35.98	45.71	0.45	4.18	0.30	0.23	99.48
317.4	10.26	39.15	42.96	0.40	6.12	0.47	0.23	99.61
322.6	11.72	37.21	44.64	0.70	4.93	0.34	0.19	99.73
327.8	10.49	38.85	43.22	0.73	5.94	0.15	0.15	99.53
333.0	13.06	35.42	46.19	0.21	3.83	0.46	0.19	99.36
338.2	11.35	37.70	44.22	0.71	5.23	0.46	0.16	99.83
343.4	10.62	38.67	43.38	0.71	5.83	0.28	0.20	99.68
348.6	11.03	38.12	43.85	0.60	5.49	0.20	0.17	99.46
353.8	10.71	38.55	43.49	0.26	5.75	0.32	0.25	99.33
359.0	11.81	37.09	44.75	0.67	4.86	0.02	0.19	99.38
364.2	12.13	36.66	45.12	0.32	4.59	0.37	0.26	99.44
369.4	11.30	37.76	44.17	0.67	5.27	0.23	0.22	99.61
374.6	11.53	37.45	44.43	0.35	5.08	0.50	0.25	99.59
379.8	12.50	36.16	45.55	0.35	4.29	0.28	0.29	99.43
385.0	11.49	37.51	44.38	0.31	5.12	0.06	0.29	99.15
390.2	10.80	38.43	43.59	0.25	5.68	0.06	0.22	99.03
395.4	9.90	39.63	42.55	0.30	6.42	0.12	0.30	99.21
400.6	10.80	38.43	43.59	0.72	5.68	0.41	0.21	99.85
405.8	10.35	39.03	43.07	0.64	6.05	0.10	0.28	99.52
411.0	11.58	37.39	44.48	0.46	5.04	0.20	0.16	99.32
416.2	10.35	39.03	43.07	0.42	6.05	0.46	0.22	99.60
421.4								
426.6	10.17	39.27	42.86	0.23	6.20	0.32	0.24	99.28
431.8	10.08	39.39	42.76	0.72	6.27	0.47	0.17	99.86
437.0	9.27	40.47	41.83	0.35	6.93	0.21	0.18	99.25
442.2	6.81	43.76	38.98	0.28	8.95	0.30	0.28	99.36
447.4	7.33	43.06	39.58	0.65	8.53	0.22	0.23	99.61
452.6	9.99	39.51	42.65	0.57	6.35	0.24	0.21	99.52
457.8	8.21	41.89	40.60	0.45	7.81	0.40	0.28	99.63
463.0	9.32	40.41	41.88	0.48	6.90	0.04	0.23	99.25
468.2	10.26	39.15	42.96	0.55	6.12	0.35	0.24	99.64
473.5	10.62	38.67	43.38	0.59	5.83	0.20	0.22	99.51
478.7	8.65	41.30	41.11	0.75	7.44	0.13	0.28	99.65
483.9	9.94	39.57	42.60	0.34	6.38	0.46	0.18	99.48
489.1	11.17	37.94	44.01	0.43	5.38	0.16	0.28	99.37
494.3	11.49	37.51	44.38	0.60	5.12	0.42	0.24	99.76
499.5	11.35	37.70	44.22	0.55	5.23	0.25	0.17	99.46
504.7	13.34	35.05	46.51	0.24	3.60	0.36	0.18	99.28
509.9	11.85	37.02	44.80	0.43	4.82	0.38	0.18	99.49
515.1	10.94	38.24	43.75	0.66	5.57	0.15	0.23	99.53
520.3	9.94	39.57	42.60	0.78	6.38	0.26	0.22	99.77
525.5	11.08	38.06	43.91	0.22	5.46	0.31	0.20	99.23
530.7	11.95	36.90	44.91	0.79	4.74	0.22	0.21	99.72

Pos. (μm)	Na2O	Al2O3	SiO2	K2O	CaO	FeO	SrO	Total
535.9	11.35	37.70	44.22	0.63	5.23	0.28	0.27	99.69
541.1	10.17	39.27	42.86	0.60	6.20	0.23	0.15	99.49
546.3	12.87	35.67	45.97	0.51	3.99	0.07	0.29	99.37
551.5	11.35	37.70	44.22	0.29	5.23	0.31	0.20	99.31
556.7	14.04	34.11	47.32	0.39	3.03	0.47	0.24	99.59
561.9	12.13	36.66	45.12	0.38	4.59	0.01	0.25	99.14
567.1	10.40	38.97	43.12	0.48	6.01	0.44	0.26	99.68
572.3	11.21	37.88	44.06	0.77	5.34	0.31	0.21	99.79
577.5	11.49	37.51	44.38	0.67	5.12	0.42	0.27	99.86
582.7	9.81	39.75	42.45	0.28	6.49	0.08	0.24	99.10
587.9	10.44	38.91	43.17	0.46	5.98	0.37	0.26	99.59
593.1	9.63	39.99	42.24	0.67	6.64	0.45	0.20	99.82
598.3	9.90	39.63	42.55	0.35	6.42	0.43	0.27	99.55
603.5	10.53	38.79	43.28	0.79	5.90	0.44	0.28	100.01
608.7	8.07	42.07	40.44	0.67	7.91	0.32	0.25	99.74
613.9	10.58	38.73	43.33	0.79	5.87	0.01	0.29	99.59
619.1	9.68	39.93	42.29	0.77	6.60	0.00	0.22	99.49
624.3	12.32	36.41	45.33	0.49	4.44	0.04	0.25	99.28
629.5	12.13	36.66	45.12	0.54	4.59	0.34	0.28	99.65

Unit: El Chichon A
Thin Section: 05-PL01
Crystal: D

85 μm diameter spot
"pos." indicates center

Microprobe analyses

Pos. (μm)	Na2O	Al2O3	SiO2	K2O	CaO	FeO	SrO	Total
0.0	9.54	40.11	42.13	0.53	6.71	0.33	0.19	99.54
6.8	10.67	38.61	43.43	0.28	5.79	0.39	0.16	99.33
13.5	10.03	39.45	42.70	0.73	6.31	0.39	0.18	99.79
20.3	10.62	38.67	43.38	0.51	5.83	0.35	0.22	99.59
27.1	10.85	38.37	43.64	0.45	5.64	0.22	0.22	99.39
33.8	10.17	39.27	42.86	0.37	6.20	0.47	0.28	99.63
40.6	9.94	39.57	42.60	0.34	6.38	0.10	0.16	99.10
47.4	12.27	36.47	45.28	0.27	4.48	0.03	0.19	98.98
54.1	11.72	37.21	44.64	0.78	4.93	0.37	0.18	99.82
60.9	10.53	38.79	43.28	0.29	5.90	0.13	0.30	99.23
67.7	10.12	39.33	42.81	0.41	6.24	0.16	0.29	99.36
74.4	10.89	38.30	43.70	0.47	5.61	0.21	0.25	99.42
81.2	11.35	37.70	44.22	0.41	5.23	0.34	0.30	99.54
88.0	9.32	40.41	41.88	0.54	6.90	0.34	0.24	99.62
94.7	10.58	38.73	43.33	0.35	5.87	0.16	0.19	99.21
101.5	11.76	37.15	44.70	0.56	4.89	0.30	0.22	99.58
108.3	11.40	37.64	44.27	0.61	5.19	0.36	0.27	99.73
115.0	10.89	38.30	43.70	0.60	5.61	0.15	0.23	99.48
121.8	11.03	38.12	43.85	0.40	5.49	0.02	0.26	99.18
128.6	9.94	39.57	42.60	0.73	6.38	0.49	0.25	99.97
135.3	10.31	39.09	43.02	0.46	6.09	0.33	0.16	99.45
142.1	10.62	38.67	43.38	0.31	5.83	0.01	0.17	98.99
148.9	10.80	38.43	43.59	0.72	5.68	0.50	0.21	99.93
155.7	11.40	37.64	44.27	0.47	5.19	0.39	0.28	99.65
162.4	11.21	37.88	44.06	0.64	5.34	0.05	0.28	99.48
169.2	10.80	38.43	43.59	0.44	5.68	0.48	0.16	99.58
176.0	12.18	36.59	45.17	0.45	4.55	0.30	0.22	99.46
182.7	12.18	36.59	45.17	0.27	4.55	0.23	0.18	99.18
189.5	12.45	36.23	45.49	0.65	4.33	0.24	0.23	99.62
196.3	11.76	37.15	44.70	0.51	4.89	0.43	0.22	99.66
203.0	12.18	36.59	45.17	0.44	4.55	0.41	0.21	99.56
209.8	11.49	37.51	44.38	0.63	5.12	0.44	0.24	99.81
216.6	11.81	37.09	44.75	0.72	4.86	0.13	0.28	99.62
223.3	10.58	38.73	43.33	0.66	5.87	0.42	0.17	99.75
230.1	11.17	37.94	44.01	0.35	5.38	0.06	0.29	99.21
236.9	11.90	36.96	44.86	0.43	4.78	0.48	0.29	99.70
243.6	11.03	38.12	43.85	0.35	5.49	0.18	0.29	99.31
250.4	12.22	36.53	45.23	0.40	4.52	0.22	0.30	99.42
257.2	11.26	37.82	44.12	0.39	5.31	0.06	0.15	99.10
263.9	10.58	38.73	43.33	0.59	5.87	0.07	0.25	99.41
270.7	12.55	36.10	45.60	0.62	4.25	0.25	0.19	99.56
277.5	11.40	37.64	44.27	0.26	5.19	0.49	0.17	99.41
284.2	12.18	36.59	45.17	0.72	4.55	0.15	0.18	99.56
291.0	11.30	37.76	44.17	0.64	5.27	0.07	0.30	99.50
297.8	9.50	40.17	42.08	0.67	6.75	0.06	0.20	99.42
304.5	16.38	30.99	50.01	0.67	1.12	0.31	0.26	99.74
311.3	10.85	38.37	43.64	0.41	5.64	0.05	0.24	99.20
318.1	11.17	37.94	44.01	0.73	5.38	0.09	0.23	99.55
324.8	10.12	39.33	42.81	0.46	6.24	0.08	0.24	99.28

ICP-MS

Pos. (μm)	87/86	2 s.e.
43	0.70399	0.00111
161	0.70655	0.00060
226	0.70433	0.00063
385	0.70495	0.00096

Pos. (µm)	Na2O	Al2O3	SiO2	K2O	CaO	FeO	SrO	Total
331.6	10.03	39.45	42.70	0.79	6.31	0.12	0.23	99.65
338.4	11.58	37.39	44.48	0.80	5.04	0.43	0.30	100.02
345.1	8.83	41.06	41.31	0.35	7.30	0.16	0.19	99.20
351.9	9.99	39.51	42.65	0.62	6.35	0.34	0.28	99.73
358.7	10.35	39.03	43.07	0.35	6.05	0.46	0.25	99.56
365.4	10.26	39.15	42.96	0.40	6.12	0.25	0.24	99.39
372.2	9.23	40.53	41.77	0.59	6.97	0.48	0.16	99.73
379.0	10.58	38.73	43.33	0.35	5.87	0.33	0.27	99.45
385.7	10.08	39.39	42.76	0.78	6.27	0.05	0.23	99.57
392.5	9.32	40.41	41.88	0.73	6.90	0.46	0.25	99.94
399.3	9.45	40.23	42.03	0.72	6.79	0.32	0.19	99.73
406.0	11.12	38.00	43.96	0.46	5.42	0.29	0.15	99.41
412.8	9.85	39.69	42.50	0.74	6.46	0.36	0.20	99.81
419.6	11.44	37.58	44.33	0.22	5.16	0.08	0.24	99.04
426.4	10.85	38.37	43.64	0.30	5.64	0.39	0.23	99.42
433.1	9.90	39.63	42.55	0.67	6.42	0.46	0.27	99.91
439.9	10.76	38.49	43.54	0.31	5.72	0.12	0.19	99.13
446.7	11.17	37.94	44.01	0.23	5.38	0.48	0.24	99.45
453.4	10.40	38.97	43.12	0.66	6.01	0.16	0.18	99.51
460.2	11.58	37.39	44.48	0.27	5.04	0.16	0.29	99.22
467.0	10.85	38.37	43.64	0.68	5.64	0.25	0.30	99.72
473.7	10.58	38.73	43.33	0.27	5.87	0.01	0.22	99.00
480.5	12.32	36.41	45.33	0.73	4.44	0.29	0.21	99.73
487.3	11.40	37.64	44.27	0.26	5.19	0.24	0.17	99.18
494.0	11.85	37.02	44.80	0.51	4.82	0.11	0.15	99.27
500.8	11.90	36.96	44.86	0.26	4.78	0.40	0.29	99.45
507.6	10.76	38.49	43.54	0.24	5.72	0.33	0.27	99.35
514.3	10.53	38.79	43.28	0.26	5.90	0.12	0.26	99.14
521.1	9.90	39.63	42.55	0.34	6.42	0.18	0.23	99.25
527.9	10.08	39.39	42.76	0.26	6.27	0.39	0.29	99.43
534.6	11.35	37.70	44.22	0.70	5.23	0.33	0.25	99.78
541.4	10.49	38.85	43.22	0.33	5.94	0.05	0.28	99.15
548.2	11.95	36.90	44.91	0.49	4.74	0.32	0.23	99.54
554.9	11.08	38.06	43.91	0.67	5.46	0.48	0.29	99.93
561.7	11.49	37.51	44.38	0.45	5.12	0.32	0.24	99.51
568.5	10.67	38.61	43.43	0.79	5.79	0.41	0.26	99.96
575.2	10.12	39.33	42.81	0.40	6.24	0.40	0.18	99.48
582.0	10.31	39.09	43.02	0.45	6.09	0.25	0.27	99.46
588.8	10.62	38.67	43.38	0.23	5.83	0.41	0.30	99.44
595.5	10.67	38.61	43.43	0.24	5.79	0.30	0.23	99.27
602.3	10.62	38.67	43.38	0.56	5.83	0.44	0.29	99.79
609.1	10.12	39.33	42.81	0.26	6.24	0.02	0.21	98.99
615.8	10.53	38.79	43.28	0.67	5.90	0.21	0.16	99.54
622.6	10.35	39.03	43.07	0.67	6.05	0.45	0.25	99.87
629.4	12.55	36.10	45.60	0.68	4.25	0.09	0.28	99.55
636.1	10.58	38.73	43.33	0.32	5.87	0.09	0.28	99.19
642.9	7.85	42.36	40.19	0.76	8.10	0.17	0.17	99.60
649.7	9.90	39.63	42.55	0.34	6.42	0.48	0.22	99.54
656.4	10.08	39.39	42.76	0.48	6.27	0.12	0.17	99.26
663.2	9.72	39.87	42.34	0.28	6.57	0.36	0.29	99.43
670.0	9.76	39.81	42.39	0.25	6.53	0.31	0.23	99.29
676.7	10.12	39.33	42.81	0.58	6.24	0.10	0.28	99.46
683.5	11.49	37.51	44.38	0.43	5.12	0.34	0.16	99.43
690.3	10.62	38.67	43.38	0.61	5.83	0.48	0.30	99.88

Pos. (μm)	Na2O	Al2O3	SiO2	K2O	CaO	FeO	SrO	Total
697.0	9.14	40.65	41.67	0.31	7.04	0.00	0.19	99.01
703.8	9.72	39.87	42.34	0.38	6.57	0.29	0.16	99.32
710.6	8.38	41.65	40.80	0.22	7.66	0.05	0.18	98.95
717.4	10.03	39.45	42.70	0.72	6.31	0.36	0.18	99.76
724.1	11.03	38.12	43.85	0.74	5.49	0.41	0.26	99.91
730.9	11.35	37.70	44.22	0.30	5.23	0.01	0.27	99.08
737.7	11.21	37.88	44.06	0.20	5.34	0.26	0.27	99.23
744.4	11.67	37.27	44.59	0.34	4.97	0.29	0.24	99.37
751.2	10.03	39.45	42.70	0.27	6.31	0.23	0.25	99.26
758.0	10.71	38.55	43.49	0.21	5.75	0.06	0.18	98.96
764.7	10.58	38.73	43.33	0.45	5.87	0.16	0.29	99.39
771.5	11.03	38.12	43.85	0.31	5.49	0.14	0.28	99.24
778.3	11.76	37.15	44.70	0.36	4.89	0.41	0.30	99.57
785.0	11.26	37.82	44.12	0.56	5.31	0.16	0.23	99.45
791.8	12.96	35.54	46.08	0.26	3.91	0.05	0.26	99.07
798.6	8.78	41.12	41.26	0.46	7.34	0.29	0.16	99.42
805.3	10.71	38.55	43.49	0.49	5.75	0.09	0.28	99.36
812.1	10.99	38.18	43.80	0.49	5.53	0.22	0.24	99.45
818.9	11.08	38.06	43.91	0.39	5.46	0.19	0.22	99.29
825.6	10.89	38.30	43.70	0.42	5.61	0.31	0.24	99.47
832.4	11.81	37.09	44.75	0.75	4.86	0.33	0.30	99.89
839.2	10.03	39.45	42.70	0.47	6.31	0.24	0.27	99.49
845.9	10.35	39.03	43.07	0.24	6.05	0.08	0.23	99.04
852.7	10.03	39.45	42.70	0.72	6.31	0.35	0.25	99.82
859.5	11.72	37.21	44.64	0.72	4.93	0.37	0.27	99.86
866.2	9.63	39.99	42.24	0.45	6.64	0.08	0.19	99.22
873.0	10.03	39.45	42.70	0.45	6.31	0.22	0.27	99.44
879.8	10.89	38.30	43.70	0.64	5.61	0.02	0.28	99.44
886.5	10.76	38.49	43.54	0.48	5.72	0.27	0.17	99.42
893.3	12.22	36.53	45.23	0.47	4.52	0.27	0.19	99.44
900.1	8.96	40.88	41.47	0.78	7.19	0.36	0.25	99.90
906.8	10.08	39.39	42.76	0.67	6.27	0.47	0.27	99.91
913.6	11.30	37.76	44.17	0.39	5.27	0.47	0.25	99.60
920.4	10.31	39.09	43.02	0.31	6.09	0.16	0.16	99.13
927.1	9.85	39.69	42.50	0.60	6.46	0.17	0.15	99.42
933.9	13.24	35.17	46.40	0.35	3.68	0.03	0.20	99.07

Unit: El Chichon B
Thin Section: CHI-1B
Crystal: A

Microprobe analyses

Pos. (μm)	Na2O	Al2O3	SiO2	K2O	CaO	FeO	Total
4.2	6.73	24.59	58.15	0.70	7.71	0.17	98.04
10.3	6.78	24.58	58.39	0.69	7.73	0.21	98.38
13.3	6.08	21.85	54.78	0.79	6.80	0.36	90.65
16.3	7.08	23.97	58.80	0.79	6.99	0.25	97.87
19.2	7.22	23.91	59.02	0.81	6.97	0.15	98.08
22.1	6.79	24.30	58.81	0.79	6.94	0.32	97.94
25.0	7.16	24.24	58.78	0.77	6.89	0.34	98.18
27.9	6.22	24.13	59.64	0.79	6.73	0.25	97.76
30.9	6.25	25.63	57.68	0.59	8.57	0.36	99.07
33.8	5.91	26.11	57.71	0.54	9.05	0.28	99.59
36.7	2.81	17.19	67.14	4.39	2.37	0.93	94.82
39.7	1.76	14.74	64.01	5.19	1.31	1.28	88.29
42.6	2.15	13.57	61.57	4.71	1.66	0.86	84.52
45.5	5.03	20.09	61.92	2.46	4.92	0.61	95.03
48.4	6.50	25.35	60.50	0.73	7.53	0.30	100.90
51.4	6.25	25.48	57.98	0.63	8.53	0.24	99.11
54.2	6.22	25.58	57.48	0.58	8.80	0.26	98.92
57.2	6.01	25.58	57.06	0.56	8.88	0.32	98.39
60.2	6.25	25.77	57.39	0.55	8.70	0.28	98.94
63.1	6.15	26.52	58.58	0.57	8.76	0.33	100.92
66.0	6.07	26.49	58.70	0.56	8.67	0.18	100.68
69.0	6.39	26.34	59.62	0.57	8.79	0.20	101.91
71.9	6.43	26.33	60.23	0.57	8.58	0.28	102.41
75.0	6.51	26.78	59.36	0.56	8.73	0.30	102.23
77.9	6.33	26.26	58.23	0.55	8.90	0.25	100.51
80.8	6.12	25.82	58.20	0.57	8.82	0.21	99.73
83.9	6.19	25.51	58.09	0.65	8.50	0.33	99.28
86.8	6.02	26.13	56.33	0.51	9.47	0.25	98.71
89.7	5.54	26.85	56.04	0.48	9.84	0.25	99.00
92.8	5.87	26.55	55.98	0.51	9.33	0.30	98.53
95.7	5.87	25.96	55.04	0.51	9.12	0.36	96.86
101.5	5.74	26.14	54.67	0.49	9.45	0.36	96.84
107.5	5.25	26.97	54.51	0.40	10.69	0.26	98.07
113.3	4.99	27.36	53.77	0.36	11.02	0.26	97.76
119.1	4.73	26.16	52.08	0.37	10.53	0.30	94.17
124.9	4.43	27.92	53.13	0.31	11.98	0.28	98.05
130.9	4.37	28.47	52.65	0.27	12.35	0.35	98.45
136.6	3.70	28.43	51.10	0.24	12.90	0.32	96.68
142.4	4.41	28.10	52.70	0.29	11.81	0.27	97.57
148.1	4.05	23.24	50.57	0.40	9.50	0.31	88.05
154.0	4.10	28.41	52.34	0.28	12.45	0.27	97.84
159.7	3.98	28.65	51.83	0.24	12.87	0.23	97.80
165.5	4.33	28.01	52.64	0.29	12.21	0.19	97.68
171.2	4.86	27.56	53.68	0.36	11.14	0.23	97.83
176.9	5.39	26.51	55.10	0.43	10.22	0.27	97.91
182.6	4.08	28.63	51.83	0.24	12.89	0.37	98.05
188.4	4.85	27.52	53.81	0.33	11.29	0.22	98.02
194.2	3.09	29.57	49.86	0.18	14.08	0.20	96.98
200.1	3.67	29.24	50.72	0.19	13.66	0.29	97.78

ICP-MS

Pos. (μm)	87/86	87/86
14		0.70608
27		0.70362
41		0.70464
54		0.70695
68		0.70319
81		0.70533
95		0.70581
108		0.70348
122	0.70426	0.70633
135	0.70456	0.70216
149	0.70486	0.70497
162	0.70336	0.70530
176	0.70638	0.70301
189	0.70423	0.70567
203	0.70457	0.70432
216	0.70588	0.70523
230	0.70539	0.70475
243	0.70560	0.70481
257	0.70403	0.70617
270	0.70312	0.70345
284	0.70471	0.70497
297	0.70449	0.70539
311	0.70543	0.70484
324	0.70524	0.70287
338	0.70457	0.70527
351	0.70373	0.70425
365	0.70266	0.70435
378	0.70451	0.70495
392	0.70445	0.70412
405	0.70632	0.70476
419	0.70453	0.70724
432	0.70448	0.70327
446	0.70286	0.70406
459	0.70458	0.70428
473	0.70442	0.70415
486	0.70426	0.70709
500	0.70535	0.70624
513	0.70427	0.70363
527	0.70475	0.70343
540	0.70342	0.70400
554	0.70490	0.70352
567	0.70384	0.70505
581	0.70377	0.70482
594	0.70509	0.70485
608	0.70458	0.70638
621	0.70469	0.70610
635	0.70716	0.70521
648	0.70452	0.70405
662	0.70030	0.70407

Pos. (μm)	Na2O	Al2O3	SiO2	K2O	CaO	FeO	Total
205.9	2.94	29.87	49.17	0.15	14.65	0.27	97.05
211.7	3.12	30.29	49.44	0.18	14.61	0.20	97.84
217.5	3.58	29.28	50.34	0.21	13.87	0.22	97.50
223.2	3.48	29.32	50.76	0.25	13.30	0.31	97.42
229.0	4.78	27.60	53.25	0.34	11.24	0.24	97.45
235.0	5.64	26.23	55.85	0.48	9.79	0.21	98.21
241.0	4.50	27.22	53.10	0.37	11.36	0.24	96.79
246.7	5.16	27.29	54.68	0.41	10.85	0.24	98.63
252.5	4.90	26.86	53.83	0.42	10.65	0.23	96.89
258.2	6.10	25.79	56.81	0.55	8.95	0.23	98.43
264.0	5.94	26.00	56.25	0.54	9.32	0.25	98.30
269.8	5.17	26.74	54.69	0.42	10.62	0.21	97.84
275.6	5.27	26.34	54.74	0.43	10.32	0.33	97.42
281.4	5.41	26.47	54.83	0.42	10.30	0.28	97.70
287.2	6.09	25.61	56.25	0.54	9.33	0.24	98.06
293.2	6.13	25.18	57.62	0.64	8.38	0.28	98.23
299.1	5.89	25.50	56.73	0.57	8.85	0.31	97.84
304.9	5.74	25.37	56.18	0.51	9.11	0.26	97.16
310.9	5.84	26.20	56.21	0.49	9.43	0.21	98.37
316.7	5.07	27.38	54.19	0.41	10.97	0.19	98.19
322.5	3.29	29.33	49.09	0.22	13.46	0.23	95.62
328.6	4.49	21.22	58.91	2.80	6.24	0.62	94.28
334.4	4.44	22.43	51.24	0.71	9.20	0.25	88.27
340.4	5.42	26.50	55.26	0.44	10.15	0.26	98.02
346.3	3.78	29.14	51.36	0.25	13.52	0.26	98.30
352.2	5.19	26.40	54.55	0.45	10.50	0.21	97.29
358.1	5.45	26.47	54.99	0.43	10.16	0.26	97.75
364.0	5.54	26.29	55.77	0.47	9.76	0.30	98.14
369.9	4.28	28.29	52.06	0.27	12.19	0.39	97.48
375.9	4.05	28.49	51.75	0.30	12.42	0.23	97.25
381.7	5.47	26.42	55.30	0.45	9.99	0.31	97.93
387.5	2.81	10.66	37.76	2.05	3.61	0.77	57.65
393.4	2.95	29.03	49.42	0.45	14.05	0.32	96.21
399.3	3.48	19.38	44.32	0.72	8.60	0.74	77.24
405.0	4.47	27.70	53.42	0.37	11.58	0.28	97.82
410.7	3.39	29.22	50.51	0.21	13.59	0.26	97.17
416.5	3.21	30.02	50.03	0.19	14.10	0.22	97.77
422.4	3.03	29.96	49.82	0.19	14.33	0.23	97.55
428.2	3.11	30.26	49.23	0.16	14.53	0.22	97.51
434.1	3.95	28.76	52.03	0.25	12.89	0.21	98.10
439.9	5.73	26.50	55.71	0.47	9.59	0.27	98.27
445.7	6.05	25.79	56.60	0.56	9.11	0.24	98.35
451.4	6.12	25.73	56.53	0.55	8.95	0.33	98.21
457.2	5.59	26.60	55.79	0.44	9.88	0.23	98.54
462.8	6.08	25.68	56.71	0.53	9.10	0.26	98.36
468.5	5.96	25.69	55.83	0.52	9.15	0.28	97.43
474.3	5.95	25.82	56.49	0.52	9.37	0.26	98.40
480.2	5.98	25.82	57.00	0.59	8.87	0.28	98.53
486.2	6.25	25.22	57.08	0.58	8.78	0.29	98.21
492.1	5.80	26.07	56.45	0.53	9.26	0.18	98.28
497.9	5.33	27.54	54.05	0.40	10.85	0.29	98.47
503.9	6.36	25.46	57.18	0.62	8.40	0.19	98.21
510.0	6.10	25.38	57.03	0.58	8.60	0.21	97.88
515.8	5.48	26.51	54.85	0.49	9.78	0.32	97.43

Pos. (μm)	87/86	87/86
675	0.70378	0.70297
689	0.70395	0.70379
702	0.70433	0.70471
716	0.70528	0.70403
729	0.70420	0.70395
743	0.70378	0.70393
756	0.70403	0.70325
770	0.70507	0.70325
783	0.70505	
796	0.70449	
810	0.70755	
823	0.70382	
837	0.70326	
850		
864		

Pos. (µm)	Na2O	Al2O3	SiO2	K2O	CaO	FeO	Total
521.7	5.87	25.82	56.66	0.57	8.90	0.31	98.14
527.6	5.49	26.42	56.06	0.48	9.50	0.22	98.17
533.4	5.90	26.38	55.52	0.50	9.62	0.27	98.17
539.4	5.75	24.91	56.82	0.79	8.74	0.37	97.37
545.3	5.84	26.03	57.06	0.56	9.13	0.21	98.82
551.1	4.70	27.74	52.76	0.34	11.31	0.27	97.13
557.0	4.35	28.49	52.37	0.31	11.88	0.23	97.64
562.8	4.57	28.24	53.41	0.35	11.74	0.27	98.57
565.7	4.62	28.06	53.47	0.35	11.64	0.30	98.43
571.4	5.86	26.27	55.53	0.54	9.60	0.29	98.10
577.1	6.10	25.46	57.00	0.60	8.79	0.31	98.26
583.1	6.09	25.63	56.64	0.57	8.90	0.26	98.09
588.9	5.69	26.58	55.33	0.48	9.67	0.32	98.08
594.7	5.96	25.99	56.18	0.53	9.17	0.27	98.11
600.5	5.89	26.13	56.13	0.55	9.06	0.19	97.94
606.3	5.99	26.12	55.94	0.52	9.31	0.42	98.30
612.2	6.02	26.31	56.68	0.52	9.29	0.19	99.02
618.1	6.21	25.82	56.69	0.57	9.04	0.28	98.60
623.9	5.50	26.40	55.30	0.50	9.51	0.21	97.42
629.7	5.79	26.19	56.25	0.50	9.66	0.24	98.63
635.3	5.61	26.56	56.12	0.50	9.77	0.30	98.86
641.1	5.86	25.98	55.70	0.54	9.35	0.25	97.67
646.9	6.02	26.02	56.21	0.58	8.92	0.26	98.01
652.6	6.02	25.21	57.25	0.62	8.58	0.23	97.91
658.5	6.24	25.68	56.78	0.60	8.80	0.23	98.33
664.2	6.15	25.30	56.88	0.57	8.70	0.22	97.82
669.9	6.11	25.70	57.16	0.59	8.79	0.22	98.57
675.6	6.12	25.69	57.07	0.59	8.54	0.20	98.20
681.3	6.30	25.94	58.06	0.60	8.62	0.29	99.80
687.1	4.65	21.82	48.86	0.62	7.56	0.65	84.16
692.9	5.96	25.84	56.35	0.58	8.91	0.28	97.92
698.9	5.27	26.17	53.55	0.45	10.12	0.23	95.79
704.6	5.20	26.71	54.36	0.43	10.39	0.29	97.37
710.4	4.88	24.82	50.18	0.56	9.42	0.71	90.56
716.1	3.75	20.28	47.24	1.40	7.84	0.66	81.16
721.9	3.95	27.01	50.92	0.37	11.98	0.31	94.54
727.7	5.94	26.17	56.08	0.52	9.45	0.20	98.37
733.5	5.62	26.12	54.55	0.45	9.88	0.34	96.95
739.3	5.93	26.14	55.65	0.50	9.66	0.22	98.11
745.2	5.70	26.30	55.56	0.47	9.75	0.15	97.93
751.1	5.97	25.86	55.71	0.48	9.36	0.19	97.57
756.9	5.89	26.05	55.92	0.51	9.46	0.30	98.14
762.6	5.61	25.91	55.75	0.46	9.65	0.24	97.61
768.4	5.61	26.37	54.64	0.44	10.05	0.25	97.36
774.1	5.56	26.65	55.29	0.46	9.93	0.29	98.16
779.9	5.56	26.47	55.32	0.47	9.68	0.31	97.81
785.7	5.35	26.37	54.74	0.45	10.33	0.25	97.50
791.4	4.08	28.90	52.13	0.25	12.90	0.19	98.45
797.2	3.66	29.36	51.01	0.22	13.40	0.24	97.90
803.0	3.79	28.81	51.52	0.24	12.74	0.24	97.33
809.0	4.05	28.78	52.08	0.25	12.88	0.22	98.27
814.7	4.09	28.28	52.06	0.26	12.50	0.27	97.46
820.6	4.27	28.19	52.74	0.26	12.16	0.31	97.92
826.4	4.42	28.47	52.56	0.30	11.79	0.25	97.79

Pos. (µm)	87/86	87/86

Pos. (μm)	Na2O	Al2O3	SiO2	K2O	CaO	FeO	Total
832.2	3.93	29.10	51.38	0.23	13.06	0.26	97.96
838.0	4.10	29.11	51.72	0.24	12.84	0.32	98.32
843.8	4.18	27.99	51.86	0.27	12.23	0.22	96.76
849.6	5.44	26.72	54.78	0.39	10.20	0.33	97.86

Pos. (μm)	87/86	87/86

Unit: El Chichon B
Thin Section: CHI-1B
Crystal: C

Microprobe analyses

Pos. (μm)	Na2O	Al2O3	SiO2	K2O	CaO	FeO	Total
0.0	5.69	26.27	55.55	0.38	9.79	0.16	97.84
9.8	5.80	26.06	55.76	0.45	9.43	0.13	97.64
19.8	5.83	26.38	55.57	0.43	9.57	0.20	97.97
29.7	5.13	27.41	53.81	0.32	10.82	0.25	97.75
39.7	5.14	27.02	54.10	0.31	10.79	0.21	97.57
49.7	5.36	26.64	55.00	0.33	10.37	0.15	97.85
59.7	5.67	26.72	55.06	0.37	10.20	0.19	98.21
69.8	5.29	27.26	54.50	0.32	10.71	0.24	98.31
79.7	5.13	26.55	54.59	0.33	10.44	0.16	97.20
89.7	5.54	26.31	54.90	0.37	10.20	0.21	97.52
99.7	5.67	26.55	54.95	0.37	10.01	0.29	97.83
109.7	5.29	26.49	55.20	0.36	10.11	0.18	97.64
119.7	5.38	26.06	54.73	0.37	9.98	0.19	96.71
129.7	5.37	26.77	55.05	0.35	10.02	0.29	97.85
139.7	5.75	26.40	55.64	0.37	9.80	0.18	98.14
149.6	5.00	24.94	55.24	0.43	9.15	0.22	94.97
159.6	6.36	25.56	56.88	0.45	8.97	0.16	98.37
169.6	6.66	24.10	58.02	0.57	7.58	0.20	97.13
179.6	6.51	24.93	57.95	0.53	7.99	0.18	98.09
189.6	6.20	25.38	56.84	0.49	8.64	0.20	97.74
199.6	6.35	25.48	56.67	0.47	8.61	0.26	97.85
209.6	6.36	24.92	57.53	0.55	8.00	0.13	97.48
219.6	6.33	24.95	57.12	0.57	8.33	0.19	97.48
229.7	6.60	24.77	57.97	0.59	7.94	0.15	98.02
239.7	6.52	24.41	58.09	0.61	7.73	0.18	97.53
249.6	6.88	24.51	58.64	0.62	7.48	0.14	98.27
259.6	6.96	24.11	58.15	0.64	7.44	0.12	97.41
269.6	6.28	24.58	57.96	0.57	8.04	0.17	97.60
279.7	6.62	24.61	57.44	0.56	8.12	0.16	97.50
289.7	6.16	25.03	57.09	0.53	8.53	0.18	97.51
299.7	6.49	24.88	57.01	0.56	8.23	0.20	97.38
309.7	6.41	25.14	57.34	0.56	8.30	0.12	97.87
319.7	6.01	25.25	56.86	0.50	8.66	0.21	97.49
329.7	6.22	24.99	57.62	0.55	8.29	0.24	97.90
339.7	5.11	27.33	53.43	0.31	11.00	0.32	97.49
349.6	5.39	25.98	55.39	0.42	9.84	0.23	97.25
359.8	4.83	27.15	53.92	0.36	10.96	0.31	97.53
369.8	5.49	26.63	54.47	0.40	10.28	0.18	97.45
379.8	5.82	25.87	55.55	0.46	9.24	0.16	97.11
389.8	6.23	25.53	57.13	0.54	8.50	0.17	98.10
399.8	6.47	24.26	57.40	0.62	7.72	0.20	96.67
409.9	6.77	24.09	57.71	0.63	7.83	0.24	97.27
419.9	6.73	24.12	58.61	0.76	7.07	0.28	97.57
429.9	6.65	24.71	57.33	0.65	7.59	0.21	97.14
439.9	6.44	24.63	57.79	0.65	7.71	0.18	97.41
449.9	6.16	24.96	55.90	0.53	8.48	0.25	96.27
459.9	5.97	24.91	56.28	0.55	8.41	0.35	96.45
469.9	6.08	25.39	55.86	0.56	8.38	0.28	96.54
479.9	4.80	27.24	53.52	0.33	11.22	0.40	97.51

ICP-MS

Pos. (μm)	87/86	87/86
22	0.70371	0.70352
29	0.70385	0.70444
37	0.70382	0.70492
44	0.70466	0.70413
51	0.70389	0.70406
59	0.70544	0.70446
66	0.70465	0.70385
74	0.70483	0.70420
81	0.70321	0.70383
88	0.70492	0.70414
96	0.70518	0.70396
103	0.70501	0.70390
110	0.70446	0.70479
118	0.70401	0.70387
125	0.70363	0.70382
132	0.70431	0.70537
140	0.70438	0.70389
147	0.70404	0.70452
154	0.70348	0.70463
162	0.70358	0.70409
169	0.70405	0.70333
177	0.70385	0.70496
184	0.70422	0.70500
191	0.70476	0.70487
199	0.70495	0.70466
206	0.70386	0.70465
213	0.70440	0.70467
221	0.70442	0.70427
228	0.70377	0.70399
235	0.70481	0.70437
243	0.70344	0.70491
250	0.70427	0.70384
257	0.70426	0.70446
265	0.70400	0.70432
272	0.70325	0.70422
280	0.70587	0.70433
287	0.70370	0.70393
294	0.70383	0.70494
302	0.70368	0.70451
309	0.70476	0.70412
316	0.70436	0.70521
324	0.70395	0.70464
331	0.70547	0.70314
338	0.70322	0.70436
346	0.70447	0.70488
353	0.70424	0.70444
360	0.70471	0.70445

Pos. (μm)	Na2O	Al2O3	SiO2	K2O	CaO	FeO	Total
489.9	4.71	26.91	52.96	0.34	11.00	0.36	96.27
500.0	5.06	25.82	52.37	0.39	10.04	0.33	94.02
500.2	5.73	22.59	58.99	1.47	7.20	0.67	96.66

Pos. (μm)	87/86	87/86
368	0.70453	0.70319
375	0.70439	0.70436
383	0.70408	0.70433
390	0.70575	0.70426
397	0.70425	0.70353
405	0.70419	0.70359
412	0.70310	0.70441
419	0.70427	0.70375
427	0.70455	0.70405
434	0.70517	0.70425
441	0.70313	0.70394
449	0.70284	0.70410
456	0.70284	0.70451
463	0.70339	0.70351
471	0.70357	0.70351
478	0.70375	0.70420
485	0.70439	0.70461
493	0.70521	0.70420
500	0.70454	0.70380
508	0.70387	0.70402
515	0.70321	0.70321
522	0.70405	0.70498
530	0.70390	0.70327

Unit: El Chichon B
Thin Section: CHI-1B
Crystal: D

Microprobe analyses

Pos. (μm)	Na2O	Al2O3	SiO2	K2O	CaO	FeO	Total
0.0	6.01	24.03	54.86	0.58	8.13	0.30	93.90
3.0	6.46	24.84	57.56	0.65	7.98	0.21	97.70
4.2	6.73	24.59	58.15	0.70	7.71	0.17	98.04
10.3	6.78	24.58	58.39	0.69	7.73	0.21	98.38
13.3	6.08	21.85	54.78	0.79	6.80	0.36	90.65
16.3	7.08	23.97	58.80	0.79	6.99	0.25	97.87
19.2	7.22	23.91	59.02	0.81	6.97	0.15	98.08
22.1	6.79	24.30	58.81	0.79	6.94	0.32	97.94
25.0	7.16	24.24	58.78	0.77	6.89	0.34	98.18
27.9	6.22	24.13	59.64	0.79	6.73	0.25	97.76
30.9	6.25	25.63	57.68	0.59	8.57	0.36	99.07
33.8	5.91	26.11	57.71	0.54	9.05	0.28	99.59
36.7	2.81	17.19	67.14	4.39	2.37	0.93	94.82
39.7	1.76	14.74	64.01	5.19	1.31	1.28	88.29
42.6	2.15	13.57	61.57	4.71	1.66	0.86	84.52
45.5	5.03	20.09	61.92	2.46	4.92	0.61	95.03
48.4	6.50	25.35	60.50	0.73	7.53	0.30	100.90
51.4	6.25	25.48	57.98	0.63	8.53	0.24	99.11
54.2	6.22	25.58	57.48	0.58	8.80	0.26	98.92
57.2	6.01	25.58	57.06	0.56	8.88	0.32	98.39
60.2	6.25	25.77	57.39	0.55	8.70	0.28	98.94
63.1	6.15	26.52	58.58	0.57	8.76	0.33	100.92
66.0	6.07	26.49	58.70	0.56	8.67	0.18	100.68
69.0	6.39	26.34	59.62	0.57	8.79	0.20	101.91
71.9	6.43	26.33	60.23	0.57	8.58	0.28	102.41
75.0	6.51	26.78	59.36	0.56	8.73	0.30	102.23
77.9	6.33	26.26	58.23	0.55	8.90	0.25	100.51
80.8	6.12	25.82	58.20	0.57	8.82	0.21	99.73
83.9	6.19	25.51	58.09	0.65	8.50	0.33	99.28
86.8	6.02	26.13	56.33	0.51	9.47	0.25	98.71
89.7	5.54	26.85	56.04	0.48	9.84	0.25	99.00
92.8	5.87	26.55	55.98	0.51	9.33	0.30	98.53
95.7	5.87	25.96	55.04	0.51	9.12	0.36	96.86
101.5	5.74	26.14	54.67	0.49	9.45	0.36	96.84
107.5	5.25	26.97	54.51	0.40	10.69	0.26	98.07
113.3	4.99	27.36	53.77	0.36	11.02	0.26	97.76
119.1	4.73	26.16	52.08	0.37	10.53	0.30	94.17
124.9	4.43	27.92	53.13	0.31	11.98	0.28	98.05
130.9	4.37	28.47	52.65	0.27	12.35	0.35	98.45
136.6	3.70	28.43	51.10	0.24	12.90	0.32	96.68
142.4	4.41	28.10	52.70	0.29	11.81	0.27	97.57
148.1	4.05	23.24	50.57	0.40	9.50	0.31	88.05
154.0	4.10	28.41	52.34	0.28	12.45	0.27	97.84
159.7	3.98	28.65	51.83	0.24	12.87	0.23	97.80
165.5	4.33	28.01	52.64	0.29	12.21	0.19	97.68
171.2	4.86	27.56	53.68	0.36	11.14	0.23	97.83
176.9	5.39	26.51	55.10	0.43	10.22	0.27	97.91
182.6	4.08	28.63	51.83	0.24	12.89	0.37	98.05
188.4	4.85	27.52	53.81	0.33	11.29	0.22	98.02

ICP-MS

Pos. (μm)	87/86	Pos. (μm)	87/86
80		80	0.70456
85	0.70300	85	0.70282
90	0.70440	90	0.70291
95	0.70235	95	0.70292
100	0.70545	100	0.70395
105	0.70474	105	0.70271
110	0.70509	110	0.70438
115	0.70336	115	0.70356
120	0.70454	120	0.70401
125	0.70468	125	0.70473
130	0.70300	130	0.70465
135	0.70286	135	0.70283
140	0.70332	140	0.70397
145	0.70403	145	0.70396
150	0.70298	150	0.70471
155	0.70460	155	0.70390
160	0.70520	160	0.70455
165	0.70252	165	0.70391
170	0.70392	170	0.70495
175	0.70301	175	0.70835
180	0.70434	180	0.70497
185	0.70352	185	0.70605
190	0.70326	190	0.70430
195	0.70257	195	0.70697
200	0.70378	200	0.70690
205	0.70458	205	0.70686
210	0.70362	210	0.70546
215	0.70381	215	0.70490
220	0.70494	220	0.70618
225	0.70627	225	0.70733
230	0.70512	230	0.70445
235	0.70674	235	0.70676
240	0.70663	240	0.70736
245	0.70450	245	0.70842
250	0.70437	250	0.70580
255	0.70372	255	0.70741
260	0.70353	260	0.70682
265	0.70363	265	0.70546
270	0.70399	270	0.70563
275	0.70472	275	0.70449
280	0.70502	280	0.70656
285	0.70291	285	0.70429
290	0.70485	290	0.70588
295	0.70488	295	0.70439
300	0.70586	300	0.70224
305	0.70307	305	0.70250
310	0.70303	310	0.70302
315	0.70331	315	0.70435
320	0.70394	320	0.70436

Pos. (μm)	Na2O	Al2O3	SiO2	K2O	CaO	FeO	Total
194.2	3.09	29.57	49.86	0.18	14.08	0.20	96.98
200.1	3.67	29.24	50.72	0.19	13.66	0.29	97.78
205.9	2.94	29.87	49.17	0.15	14.65	0.27	97.05
211.7	3.12	30.29	49.44	0.18	14.61	0.20	97.84
217.5	3.58	29.28	50.34	0.21	13.87	0.22	97.50
223.2	3.48	29.32	50.76	0.25	13.30	0.31	97.42
229.0	4.78	27.60	53.25	0.34	11.24	0.24	97.45
235.0	5.64	26.23	55.85	0.48	9.79	0.21	98.21
241.0	4.50	27.22	53.10	0.37	11.36	0.24	96.79
246.7	5.16	27.29	54.68	0.41	10.85	0.24	98.63
252.5	4.90	26.86	53.83	0.42	10.65	0.23	96.89
258.2	6.10	25.79	56.81	0.55	8.95	0.23	98.43
264.0	5.94	26.00	56.25	0.54	9.32	0.25	98.30
269.8	5.17	26.74	54.69	0.42	10.62	0.21	97.84
275.6	5.27	26.34	54.74	0.43	10.32	0.33	97.42
281.4	5.41	26.47	54.83	0.42	10.30	0.28	97.70
287.2	6.09	25.61	56.25	0.54	9.33	0.24	98.06
293.2	6.13	25.18	57.62	0.64	8.38	0.28	98.23
299.1	5.89	25.50	56.73	0.57	8.85	0.31	97.84
304.9	5.74	25.37	56.18	0.51	9.11	0.26	97.16
310.9	5.84	26.20	56.21	0.49	9.43	0.21	98.37
316.7	5.07	27.38	54.19	0.41	10.97	0.19	98.19
322.5	3.29	29.33	49.09	0.22	13.46	0.23	95.62
328.6	4.49	21.22	58.91	2.80	6.24	0.62	94.28
334.4	4.44	22.43	51.24	0.71	9.20	0.25	88.27
340.4	5.42	26.50	55.26	0.44	10.15	0.26	98.02
346.3	3.78	29.14	51.36	0.25	13.52	0.26	98.30
352.2	5.19	26.40	54.55	0.45	10.50	0.21	97.29
358.1	5.45	26.47	54.99	0.43	10.16	0.26	97.75
364.0	5.54	26.29	55.77	0.47	9.76	0.30	98.14
369.9	4.28	28.29	52.06	0.27	12.19	0.39	97.48
375.9	4.05	28.49	51.75	0.30	12.42	0.23	97.25
381.7	5.47	26.42	55.30	0.45	9.99	0.31	97.93
387.5	2.81	10.66	37.76	2.05	3.61	0.77	57.65
393.4	2.95	29.03	49.42	0.45	14.05	0.32	96.21
399.3	3.48	19.38	44.32	0.72	8.60	0.74	77.24
405.0	4.47	27.70	53.42	0.37	11.58	0.28	97.82
410.7	3.39	29.22	50.51	0.21	13.59	0.26	97.17
416.5	3.21	30.02	50.03	0.19	14.10	0.22	97.77
422.4	3.03	29.96	49.82	0.19	14.33	0.23	97.55
428.2	3.11	30.26	49.23	0.16	14.53	0.22	97.51
434.1	3.95	28.76	52.03	0.25	12.89	0.21	98.10
439.9	5.73	26.50	55.71	0.47	9.59	0.27	98.27
445.7	6.05	25.79	56.60	0.56	9.11	0.24	98.35
451.4	6.12	25.73	56.53	0.55	8.95	0.33	98.21
457.2	5.59	26.60	55.79	0.44	9.88	0.23	98.54
462.8	6.08	25.68	56.71	0.53	9.10	0.26	98.36
468.5	5.96	25.69	55.83	0.52	9.15	0.28	97.43
474.3	5.95	25.82	56.49	0.52	9.37	0.26	98.40
480.2	5.98	25.82	57.00	0.59	8.87	0.28	98.53
486.2	6.25	25.22	57.08	0.58	8.78	0.29	98.21
492.1	5.80	26.07	56.45	0.53	9.26	0.18	98.28
497.9	5.33	27.54	54.05	0.40	10.85	0.29	98.47
503.9	6.36	25.46	57.18	0.62	8.40	0.19	98.21

Pos. (μm)	87/86	Pos. (μm)	87/86
325	0.70435	325	0.70293
330	0.70379	330	0.70358
335	0.70432	335	0.70383
340	0.70329	340	0.70396
345	0.70301	345	0.70294
350	0.70273	350	0.70451
355	0.70324	355	0.70567
360	0.70343	360	0.70482
365	0.70328	365	0.70422
370	0.70474	370	0.70375
375	0.70364	375	0.70510
380	0.70329	380	0.70383
385	0.70446	385	0.70505
390	0.70483	390	0.70232
395	0.70540	395	0.70444
400	0.70200	400	0.70320
405	0.70522	405	0.70318
410	0.70305	410	0.70472
415	0.70368	415	0.70558
420	0.70329	420	0.70379
425	0.70440	425	0.70441
430	0.70624	430	0.70466
435	0.70318	435	0.70478
440	0.70436	440	0.70452
445	0.70492	445	0.70499
450	0.70341	450	0.70455
455	0.70291	455	0.70613
460	0.70566	460	0.70332
465	0.70550	465	0.70418
470	0.70448	470	0.70428
475	0.70459	475	0.70511
480	0.70399	480	0.70267
485	0.70546	485	0.70467
490	0.70519	490	0.70286
495	0.70455	495	0.70475
500	0.70485	500	0.70401
505	0.70410	505	0.70464
510	0.70564	510	0.70377
515	0.70539	515	0.70383
520	0.70322	520	0.70542
525	0.70179	525	0.70504
530	0.70368	530	0.70581
535	0.70560	535	0.70345
540	0.70516	540	0.70446
545	0.70392	545	0.70378
550	0.70325	550	0.70437
555	0.70506	555	0.70476
560	0.70483	560	0.70427
565	0.70292	565	0.70307
570	0.70356	570	0.70524
575	0.70483	575	0.70444
580	0.70396	580	0.70526
585	0.70481	585	0.70605
590	0.70389	590	0.70238

Pos. (μm)	Na2O	Al2O3	SiO2	K2O	CaO	FeO	Total
510.0	6.10	25.38	57.03	0.58	8.60	0.21	97.88
515.8	5.48	26.51	54.85	0.49	9.78	0.32	97.43
521.7	5.87	25.82	56.66	0.57	8.90	0.31	98.14
527.6	5.49	26.42	56.06	0.48	9.50	0.22	98.17
533.4	5.90	26.38	55.52	0.50	9.62	0.27	98.17
539.4	5.75	24.91	56.82	0.79	8.74	0.37	97.37
545.3	5.84	26.03	57.06	0.56	9.13	0.21	98.82
551.1	4.70	27.74	52.76	0.34	11.31	0.27	97.13
557.0	4.35	28.49	52.37	0.31	11.88	0.23	97.64
562.8	4.57	28.24	53.41	0.35	11.74	0.27	98.57
565.7	4.62	28.06	53.47	0.35	11.64	0.30	98.43
571.4	5.86	26.27	55.53	0.54	9.60	0.29	98.10
577.1	6.10	25.46	57.00	0.60	8.79	0.31	98.26
583.1	6.09	25.63	56.64	0.57	8.90	0.26	98.09
588.9	5.69	26.58	55.33	0.48	9.67	0.32	98.08
594.7	5.96	25.99	56.18	0.53	9.17	0.27	98.11
600.5	5.89	26.13	56.13	0.55	9.06	0.19	97.94
606.3	5.99	26.12	55.94	0.52	9.31	0.42	98.30
612.2	6.02	26.31	56.68	0.52	9.29	0.19	99.02
618.1	6.21	25.82	56.69	0.57	9.04	0.28	98.60
623.9	5.50	26.40	55.30	0.50	9.51	0.21	97.42
629.7	5.79	26.19	56.25	0.50	9.66	0.24	98.63
635.3	5.61	26.56	56.12	0.50	9.77	0.30	98.86
641.1	5.86	25.98	55.70	0.54	9.35	0.25	97.67
646.9	6.02	26.02	56.21	0.58	8.92	0.26	98.01
652.6	6.02	25.21	57.25	0.62	8.58	0.23	97.91
658.5	6.24	25.68	56.78	0.60	8.80	0.23	98.33
664.2	6.15	25.30	56.88	0.57	8.70	0.22	97.82
669.9	6.11	25.70	57.16	0.59	8.79	0.22	98.57
675.6	6.12	25.69	57.07	0.59	8.54	0.20	98.20
681.3	6.30	25.94	58.06	0.60	8.62	0.29	99.80
687.1	4.65	21.82	48.86	0.62	7.56	0.65	84.16
692.9	5.96	25.84	56.35	0.58	8.91	0.28	97.92
698.9	5.27	26.17	53.55	0.45	10.12	0.23	95.79
704.6	5.20	26.71	54.36	0.43	10.39	0.29	97.37
710.4	4.88	24.82	50.18	0.56	9.42	0.71	90.56
716.1	3.75	20.28	47.24	1.40	7.84	0.66	81.16
721.9	3.95	27.01	50.92	0.37	11.98	0.31	94.54
727.7	5.94	26.17	56.08	0.52	9.45	0.20	98.37
733.5	5.62	26.12	54.55	0.45	9.88	0.34	96.95
739.3	5.93	26.14	55.65	0.50	9.66	0.22	98.11
745.2	5.70	26.30	55.56	0.47	9.75	0.15	97.93
751.1	5.97	25.86	55.71	0.48	9.36	0.19	97.57
756.9	5.89	26.05	55.92	0.51	9.46	0.30	98.14
762.6	5.61	25.91	55.75	0.46	9.65	0.24	97.61
768.4	5.61	26.37	54.64	0.44	10.05	0.25	97.36
774.1	5.56	26.65	55.29	0.46	9.93	0.29	98.16
779.9	5.56	26.47	55.32	0.47	9.68	0.31	97.81
785.7	5.35	26.37	54.74	0.45	10.33	0.25	97.50
791.4	4.08	28.90	52.13	0.25	12.90	0.19	98.45
797.2	3.66	29.36	51.01	0.22	13.40	0.24	97.90
803.0	3.79	28.81	51.52	0.24	12.74	0.24	97.33
809.0	4.05	28.78	52.08	0.25	12.88	0.22	98.27
814.7	4.09	28.28	52.06	0.26	12.50	0.27	97.46

Pos. (μm)	87/86	Pos. (μm)	87/86
595	0.70366	595	0.70437
600	0.70351	600	0.70417
605	0.70440	605	0.70468
610	0.70581	610	0.70353
615	0.70497	615	0.70384
620	0.70525	620	0.70421
625	0.70430	625	0.70533
630	0.70424	630	0.70622
635	0.70541	635	0.70536
640	0.70457	640	0.70333
645	0.70565	645	0.70418
650	0.70348	650	0.70370
655	0.70358	655	0.70423
660	0.70374	660	0.70348
665	0.70415	665	0.70547
670	0.70382	670	0.70367
675	0.70473	675	0.70362
680	0.70411	680	0.70526
687	0.70468	685	0.70297
697	0.70183	690	0.70363
707	0.70404	695	0.70322
717	0.70475	700	0.70562
727	0.70366	705	0.70457
737	0.70394	710	0.70405
747	0.70557	715	0.70333
757	0.70555	720	0.70523
767		725	0.70191
777		730	0.70370
787	0.70412	735	0.70393
797	0.70320	740	0.70556
807	0.70397	745	0.70391
817	0.70531	750	0.70358
827	0.70617	755	0.70604
837	0.70672	760	0.70368
		765	0.70261
		770	0.70458
		775	0.70464
		780	0.70486
		785	0.70418
		790	0.70481
		795	0.70339
		800	0.70392
		805	0.70441
		810	0.70479
		815	0.70479
		820	0.70469
		825	0.70405
		830	0.70525
		835	0.70467
		840	0.70540
		845	0.70475
		850	0.70502
		855	0.70291
		860	0.70473

Pos. (μm)	Na2O	Al2O3	SiO2	K2O	CaO	FeO	Total
820.6	4.27	28.19	52.74	0.26	12.16	0.31	97.92
826.4	4.42	28.47	52.56	0.30	11.79	0.25	97.79
832.2	3.93	29.10	51.38	0.23	13.06	0.26	97.96
838.0	4.10	29.11	51.72	0.24	12.84	0.32	98.32
843.8	4.18	27.99	51.86	0.27	12.23	0.22	96.76
849.6	5.44	26.72	54.78	0.39	10.20	0.33	97.86

Pos. (μm)	87/86	Pos. (μm)	87/86
		865	0.70438
		870	0.70410
		875	0.70391
		880	0.70510
		885	0.70428
		890	0.70537
		895	0.70546
		900	0.70502
		905	0.70351
		910	0.70584
		915	0.70480
		920	0.70572
		925	0.70519
		930	0.70765
		935	0.70724
		940	0.70379
		945	0.70476
		950	0.70507
		955	0.70473
		960	0.70516
		965	0.70622
		970	0.70450
		975	0.70634
		980	0.70601
		985	0.70459

Unit: El Chichon C
Thin Section: CHI-9510
Crystal: A

85 μm diameter spot
"pos." indicates center

Microprobe analyses

Pos. (μm)	Na2O	Al2O3	SiO2	K2O	CaO	FeO	SrO	Total
0.0	6.50	44.16	38.63	0.34	9.20	0.32	0.16	99.32
5.5	5.98	44.85	38.04	0.43	9.63	0.05	0.26	99.24
11.0	5.30	45.77	37.24	0.23	10.19	0.39	0.25	99.38
16.5	5.38	45.65	37.34	0.44	10.12	0.38	0.26	99.58
21.9	6.24	44.51	38.33	0.67	9.41	0.10	0.27	99.54
27.4	8.96	40.88	41.47	0.77	7.19	0.15	0.26	99.69
32.9	9.85	39.69	42.50	0.66	6.46	0.31	0.16	99.63
38.4	9.94	39.57	42.60	0.22	6.38	0.23	0.23	99.18
43.9	8.34	41.71	40.75	0.56	7.70	0.37	0.24	99.67
49.4	7.81	42.42	40.14	0.53	8.13	0.35	0.18	99.55
54.9	8.52	41.48	40.95	0.77	7.55	0.24	0.19	99.70
60.4	9.14	40.65	41.67	0.53	7.04	0.42	0.29	99.74
65.8	11.21	37.88	44.06	0.32	5.34	0.02	0.28	99.12
71.3	9.50	40.17	42.08	0.39	6.75	0.37	0.24	99.51
76.8	10.31	39.09	43.02	0.31	6.09	0.21	0.22	99.24
82.3	7.37	43.00	39.64	0.48	8.49	0.44	0.29	99.72
87.8	9.68	39.93	42.29	0.58	6.60	0.14	0.27	99.49
93.3	8.16	41.95	40.55	0.29	7.84	0.42	0.21	99.42
98.8	11.67	37.27	44.59	0.29	4.97	0.40	0.26	99.46
104.3	8.07	42.07	40.44	0.77	7.91	0.44	0.28	99.99
109.7	8.78	41.12	41.26	0.59	7.34	0.34	0.17	99.59
115.2	9.85	39.69	42.50	0.52	6.46	0.15	0.29	99.47
120.7	6.94	43.58	39.13	0.21	8.85	0.22	0.15	99.08
126.2	10.12	39.33	42.81	0.77	6.24	0.11	0.29	99.68
131.7	10.12	39.33	42.81	0.51	6.24	0.45	0.17	99.63
137.2	6.68	43.93	38.83	0.64	9.06	0.38	0.28	99.80
142.7	9.32	40.41	41.88	0.32	6.90	0.09	0.18	99.10
148.2	7.64	42.65	39.94	0.59	8.27	0.43	0.18	99.70
153.6	10.94	38.24	43.75	0.39	5.57	0.44	0.26	99.60
159.1	7.90	42.30	40.24	0.43	8.06	0.26	0.21	99.40
164.6	9.23	40.53	41.77	0.79	6.97	0.30	0.29	99.88
170.1	11.58	37.39	44.48	0.20	5.04	0.42	0.24	99.36
175.6	10.76	38.49	43.54	0.78	5.72	0.26	0.24	99.79
181.1	11.67	37.27	44.59	0.76	4.97	0.06	0.26	99.59
186.6	12.78	35.79	45.87	0.77	4.06	0.41	0.19	99.87
192.0								
197.5								
203.0	12.22	36.53	45.23	0.61	4.52	0.34	0.27	99.72
208.5	12.32	36.41	45.33	0.64	4.44	0.29	0.27	99.70
214.0	11.21	37.88	44.06	0.38	5.34	0.05	0.15	99.09
219.5	9.32	40.41	41.88	0.38	6.90	0.07	0.23	99.18
225.0	8.87	41.00	41.36	0.78	7.26	0.20	0.25	99.73
230.5	11.85	37.02	44.80	0.26	4.82	0.48	0.27	99.51
235.9	10.58	38.73	43.33	0.21	5.87	0.03	0.26	98.99
241.4	9.32	40.41	41.88	0.72	6.90	0.21	0.30	99.73
246.9	10.22	39.21	42.91	0.23	6.16	0.41	0.26	99.39
252.4	13.24	35.17	46.40	0.71	3.68	0.16	0.19	99.56
257.9	12.78	35.79	45.87	0.64	4.06	0.38	0.28	99.80
263.4	9.05	40.77	41.57	0.21	7.12	0.19	0.29	99.19

ICP-MS

Pos. (μm)	87/86	2 s.e.
75	0.70408	0.00070
280	0.70486	0.00062
500	0.70584	0.00061
590	0.70458	0.00075
680	0.70523	0.00053
720	0.70434	0.00071
800	0.70478	0.00059
1000	0.70521	0.00063
1130	0.70597	0.00061
1247	0.70517	0.00057
1290	0.70620	0.00090
1461	0.70505	0.00155
1555	0.70519	0.00061
1594	0.70426	0.00066

Pos. (μm)	Na2O	Al2O3	SiO2	K2O	CaO	FeO	SrO	Total
268.9	12.41	36.29	45.44	0.70	4.37	0.02	0.20	99.42
274.4	12.32	36.41	45.33	0.59	4.44	0.39	0.21	99.70
279.8	13.43	34.92	46.62	0.57	3.53	0.43	0.23	99.73
285.3	12.22	36.53	45.23	0.32	4.52	0.15	0.24	99.22
290.8	13.34	35.05	46.51	0.77	3.60	0.15	0.16	99.58
296.3	9.14	40.65	41.67	0.70	7.04	0.11	0.16	99.47
301.8	11.21	37.88	44.06	0.22	5.34	0.01	0.23	98.97
307.3	10.31	39.09	43.02	0.34	6.09	0.26	0.19	99.29
312.8	12.41	36.29	45.44	0.48	4.37	0.43	0.15	99.57
318.3	13.71	34.55	46.94	0.49	3.30	0.07	0.23	99.28
323.7	12.59	36.04	45.65	0.21	4.21	0.21	0.26	99.18
329.2	13.43	34.92	46.62	0.60	3.53	0.34	0.27	99.71
334.7	11.12	38.00	43.96	0.77	5.42	0.33	0.21	99.81
340.2	11.67	37.27	44.59	0.74	4.97	0.16	0.17	99.57
345.7	10.58	38.73	43.33	0.71	5.87	0.44	0.25	99.91
351.2	13.71	34.55	46.94	0.67	3.30	0.26	0.17	99.60
356.7	10.03	39.45	42.70	0.64	6.31	0.28	0.23	99.65
362.2	10.85	38.37	43.64	0.22	5.64	0.04	0.21	98.97
367.6	12.32	36.41	45.33	0.27	4.44	0.30	0.21	99.29
373.1	10.94	38.24	43.75	0.54	5.57	0.44	0.19	99.67
378.6	10.94	38.24	43.75	0.59	5.57	0.27	0.16	99.52
384.1	11.03	38.12	43.85	0.76	5.49	0.28	0.21	99.75
389.6	11.49	37.51	44.38	0.24	5.12	0.28	0.23	99.25
395.1	9.59	40.05	42.19	0.78	6.68	0.32	0.15	99.75
400.6	9.68	39.93	42.29	0.59	6.60	0.05	0.17	99.31
406.0	12.22	36.53	45.23	0.26	4.52	0.46	0.26	99.49
411.5	10.58	38.73	43.33	0.74	5.87	0.47	0.21	99.92
417.0	10.12	39.33	42.81	0.46	6.24	0.28	0.23	99.47
422.5	10.85	38.37	43.64	0.57	5.64	0.31	0.22	99.61
428.0	9.50	40.17	42.08	0.32	6.75	0.34	0.28	99.43
433.5	9.14	40.65	41.67	0.78	7.04	0.22	0.18	99.68
439.0	12.04	36.78	45.01	0.54	4.67	0.36	0.28	99.67
444.5	8.25	41.83	40.65	0.35	7.77	0.11	0.26	99.22
449.9	9.85	39.69	42.50	0.31	6.46	0.49	0.29	99.59
455.4	10.85	38.37	43.64	0.77	5.64	0.34	0.23	99.83
460.9	9.50	40.17	42.08	0.76	6.75	0.29	0.22	99.77
466.4	11.85	37.02	44.80	0.40	4.82	0.32	0.25	99.48
471.9	11.21	37.88	44.06	0.51	5.34	0.12	0.19	99.33
477.4	10.40	38.97	43.12	0.38	6.01	0.22	0.16	99.26
482.9	11.30	37.76	44.17	0.77	5.27	0.45	0.17	99.89
488.4	10.85	38.37	43.64	0.63	5.64	0.25	0.17	99.56
493.8	9.32	40.41	41.88	0.49	6.90	0.08	0.28	99.36
499.3	11.40	37.64	44.27	0.56	5.19	0.35	0.24	99.65
504.8	11.21	37.88	44.06	0.29	5.34	0.19	0.17	99.15
510.3	12.59	36.04	45.65	0.46	4.21	0.35	0.27	99.59
515.8	8.96	40.88	41.47	0.32	7.19	0.44	0.22	99.47
521.3	10.85	38.37	43.64	0.40	5.64	0.45	0.27	99.62
526.8	10.40	38.97	43.12	0.41	6.01	0.14	0.29	99.34
532.3	10.03	39.45	42.70	0.71	6.31	0.01	0.22	99.44
537.7	11.30	37.76	44.17	0.67	5.27	0.34	0.21	99.72
543.2	10.94	38.24	43.75	0.34	5.57	0.37	0.30	99.51
548.7	8.87	41.00	41.36	0.64	7.26	0.06	0.26	99.46
554.2	9.41	40.29	41.98	0.61	6.82	0.48	0.27	99.86
559.7	12.50	36.16	45.55	0.39	4.29	0.38	0.16	99.43

Pos. (µm)	Na2O	Al2O3	SiO2	K2O	CaO	FeO	SrO	Total
565.2	12.04	36.78	45.01	0.22	4.67	0.29	0.20	99.22
570.7	11.40	37.64	44.27	0.65	5.19	0.44	0.24	99.83
576.1	9.32	40.41	41.88	0.47	6.90	0.26	0.22	99.45
581.6								
587.1	11.49	37.51	44.38	0.47	5.12	0.17	0.17	99.32
592.6	10.76	38.49	43.54	0.28	5.72	0.22	0.18	99.17
598.1	9.41	40.29	41.98	0.76	6.82	0.27	0.16	99.70
603.6	12.87	35.67	45.97	0.43	3.99	0.10	0.20	99.23
609.1	9.50	40.17	42.08	0.45	6.75	0.38	0.23	99.57
614.6	9.94	39.57	42.60	0.56	6.38	0.06	0.29	99.40
620.0	11.30	37.76	44.17	0.46	5.27	0.01	0.30	99.26
625.5	8.61	41.36	41.06	0.49	7.48	0.49	0.27	99.75
631.0	10.76	38.49	43.54	0.56	5.72	0.23	0.15	99.44
636.5	7.81	42.42	40.14	0.73	8.13	0.30	0.16	99.69
642.0								
647.5								
653.0								
658.5								
663.9								
669.4								
674.9	7.20	43.24	39.43	0.44	8.63	0.35	0.28	99.57
680.4	10.40	38.97	43.12	0.38	6.01	0.44	0.29	99.62
685.9	10.40	38.97	43.12	0.49	6.01	0.22	0.18	99.39
691.4	10.31	39.09	43.02	0.58	6.09	0.45	0.16	99.69
696.9	10.40	38.97	43.12	0.79	6.01	0.04	0.24	99.56
702.4	11.03	38.12	43.85	0.49	5.49	0.39	0.21	99.60
707.8	9.85	39.69	42.50	0.33	6.46	0.49	0.27	99.59
713.3	9.85	39.69	42.50	0.64	6.46	0.31	0.19	99.64
718.8	10.58	38.73	43.33	0.63	5.87	0.45	0.17	99.76
724.3	9.59	40.05	42.19	0.48	6.68	0.45	0.22	99.65
729.8	10.31	39.09	43.02	0.59	6.09	0.28	0.26	99.63
735.3	8.96	40.88	41.47	0.24	7.19	0.45	0.30	99.48
740.8	8.25	41.83	40.65	0.40	7.77	0.27	0.28	99.45
746.2	11.40	37.64	44.27	0.29	5.19	0.28	0.26	99.33
751.7	9.23	40.53	41.77	0.62	6.97	0.05	0.29	99.47
757.2	9.50	40.17	42.08	0.59	6.75	0.41	0.23	99.72
762.7	7.46	42.89	39.74	0.69	8.42	0.42	0.26	99.88
768.2	9.85	39.69	42.50	0.73	6.46	0.43	0.25	99.91
773.7	9.76	39.81	42.39	0.20	6.53	0.42	0.21	99.32
779.2	12.13	36.66	45.12	0.40	4.59	0.16	0.29	99.35
784.7	11.58	37.39	44.48	0.28	5.04	0.38	0.22	99.38
790.1	7.90	42.30	40.24	0.65	8.06	0.08	0.28	99.52
795.6	9.76	39.81	42.39	0.74	6.53	0.17	0.17	99.59
801.1	10.03	39.45	42.70	0.78	6.31	0.14	0.22	99.64
806.6	10.76	38.49	43.54	0.25	5.72	0.24	0.17	99.17
812.1	12.22	36.53	45.23	0.25	4.52	0.08	0.28	99.11
817.6	11.85	37.02	44.80	0.38	4.82	0.46	0.30	99.63
823.1	8.96	40.88	41.47	0.33	7.19	0.09	0.25	99.17
828.6	9.94	39.57	42.60	0.61	6.38	0.21	0.25	99.57
834.0	17.74	29.18	51.58	0.31	0.00	0.47	0.17	99.45
839.5	17.74	29.18	51.58	0.74	0.00	0.20	0.22	99.66
845.0	7.90	42.30	40.24	0.41	8.06	0.32	0.22	99.45
850.5	7.90	42.30	40.24	0.23	8.06	0.43	0.20	99.36
856.0	8.34	41.71	40.75	0.68	7.70	0.43	0.20	99.82

Pos. (μm)	Na2O	Al2O3	SiO2	K2O	CaO	FeO	SrO	Total
861.5	11.21	37.88	44.06	0.46	5.34	0.05	0.22	99.23
867.0	10.76	38.49	43.54	0.33	5.72	0.15	0.23	99.21
872.5	9.50	40.17	42.08	0.77	6.75	0.46	0.26	99.99
877.9	9.23	40.53	41.77	0.37	6.97	0.34	0.19	99.40
883.4	8.96	40.88	41.47	0.42	7.19	0.19	0.25	99.37
888.9	11.12	38.00	43.96	0.57	5.42	0.48	0.21	99.75
894.4	10.76	38.49	43.54	0.71	5.72	0.09	0.26	99.56
899.9	11.76	37.15	44.70	0.29	4.89	0.14	0.28	99.21
905.4	12.96	35.54	46.08	0.61	3.91	0.46	0.19	99.76
910.9	10.22	39.21	42.91	0.69	6.16	0.11	0.27	99.57
916.3	11.49	37.51	44.38	0.32	5.12	0.35	0.25	99.41
921.8	9.41	40.29	41.98	0.48	6.82	0.35	0.16	99.49
927.3	9.85	39.69	42.50	0.69	6.46	0.38	0.20	99.77
932.8	9.32	40.41	41.88	0.75	6.90	0.08	0.21	99.54
938.3	11.85	37.02	44.80	0.62	4.82	0.38	0.25	99.75
943.8	9.68	39.93	42.29	0.65	6.60	0.10	0.23	99.48
949.3	12.41	36.29	45.44	0.58	4.37	0.20	0.27	99.56
954.8	12.78	35.79	45.87	0.63	4.06	0.14	0.18	99.46
960.2	10.12	39.33	42.81	0.30	6.24	0.04	0.18	99.03
965.7	7.02	43.47	39.23	0.54	8.78	0.27	0.17	99.48
971.2	11.30	37.76	44.17	0.77	5.27	0.32	0.27	99.86
976.7	9.41	40.29	41.98	0.53	6.82	0.11	0.15	99.29
982.2	10.67	38.61	43.43	0.35	5.79	0.22	0.28	99.34
987.7	11.30	37.76	44.17	0.57	5.27	0.15	0.29	99.51
993.2	10.67	38.61	43.43	0.33	5.79	0.29	0.19	99.30
998.7	10.94	38.24	43.75	0.23	5.57	0.17	0.27	99.18
1004.1	10.76	38.49	43.54	0.73	5.72	0.28	0.30	99.81
1009.6	12.13	36.66	45.12	0.64	4.59	0.31	0.25	99.71
1015.1	11.21	37.88	44.06	0.21	5.34	0.43	0.18	99.33
1020.6	12.32	36.41	45.33	0.38	4.44	0.45	0.28	99.61
1026.1	8.96	40.88	41.47	0.61	7.19	0.20	0.27	99.59
1031.6	10.03	39.45	42.70	0.62	6.31	0.07	0.23	99.42
1037.1	10.03	39.45	42.70	0.58	6.31	0.39	0.29	99.75
1042.6	8.87	41.00	41.36	0.36	7.26	0.11	0.28	99.25
1048.0	9.32	40.41	41.88	0.23	6.90	0.32	0.26	99.31
1053.5	11.21	37.88	44.06	0.74	5.34	0.18	0.25	99.67
1059.0	9.59	40.05	42.19	0.54	6.68	0.26	0.29	99.60
1064.5	8.96	40.88	41.47	0.58	7.19	0.36	0.20	99.65
1070.0	10.40	38.97	43.12	0.22	6.01	0.33	0.26	99.30
1075.5	7.81	42.42	40.14	0.31	8.13	0.15	0.23	99.20
1081.0	10.76	38.49	43.54	0.29	5.72	0.19	0.15	99.13
1086.5	8.96	40.88	41.47	0.28	7.19	0.38	0.20	99.36
1091.9	9.05	40.77	41.57	0.51	7.12	0.35	0.26	99.62
1097.4	10.67	38.61	43.43	0.62	5.79	0.36	0.16	99.64
1102.9	9.32	40.41	41.88	0.41	6.90	0.04	0.17	99.12
1108.4	9.05	40.77	41.57	0.38	7.12	0.03	0.20	99.11
1113.9	9.68	39.93	42.29	0.55	6.60	0.44	0.16	99.65
1119.4	9.50	40.17	42.08	0.71	6.75	0.01	0.30	99.52
1124.9	10.94	38.24	43.75	0.30	5.57	0.22	0.18	99.21
1130.3	10.40	38.97	43.12	0.50	6.01	0.06	0.20	99.26
1135.8	8.61	41.36	41.06	0.28	7.48	0.25	0.19	99.22
1141.3	11.12	38.00	43.96	0.56	5.42	0.40	0.25	99.71
1146.8	9.32	40.41	41.88	0.74	6.90	0.18	0.27	99.69
1152.3	10.76	38.49	43.54	0.52	5.72	0.43	0.25	99.69

Pos. (µm)	Na2O	Al2O3	SiO2	K2O	CaO	FeO	SrO	Total
1157.8	10.22	39.21	42.91	0.65	6.16	0.25	0.15	99.56
1163.3	11.58	37.39	44.48	0.46	5.04	0.02	0.16	99.14
1168.8	8.43	41.59	40.85	0.43	7.63	0.42	0.19	99.54
1174.2	9.68	39.93	42.29	0.53	6.60	0.37	0.27	99.68
1179.7	10.12	39.33	42.81	0.48	6.24	0.36	0.19	99.54
1185.2	11.40	37.64	44.27	0.56	5.19	0.22	0.19	99.46
1190.7	9.05	40.77	41.57	0.55	7.12	0.25	0.22	99.52
1196.2	8.96	40.88	41.47	0.51	7.19	0.23	0.29	99.54
1201.7	11.21	37.88	44.06	0.66	5.34	0.42	0.25	99.83
1207.2	11.12	38.00	43.96	0.61	5.42	0.22	0.24	99.57
1212.7	10.12	39.33	42.81	0.40	6.24	0.10	0.17	99.17
1218.1	10.12	39.33	42.81	0.33	6.24	0.38	0.16	99.37
1223.6	8.96	40.88	41.47	0.79	7.19	0.11	0.24	99.64
1229.1	10.49	38.85	43.22	0.71	5.94	0.01	0.26	99.49
1234.6	9.41	40.29	41.98	0.62	6.82	0.45	0.17	99.74
1240.1	10.85	38.37	43.64	0.23	5.64	0.42	0.23	99.39
1245.6	12.04	36.78	45.01	0.43	4.67	0.32	0.25	99.50
1251.1	7.99	42.18	40.34	0.33	7.99	0.48	0.23	99.54
1256.6	8.25	41.83	40.65	0.77	7.77	0.18	0.17	99.62
1262.0	6.94	43.58	39.13	0.45	8.85	0.12	0.22	99.30
1267.5	5.47	45.54	37.44	0.37	10.05	0.49	0.21	99.56
1273.0	9.59	40.05	42.19	0.39	6.68	0.02	0.23	99.15
1278.5	9.85	39.69	42.50	0.25	6.46	0.18	0.23	99.17
1284.0	6.85	43.70	39.03	0.77	8.92	0.40	0.20	99.88
1289.5	9.85	39.69	42.50	0.57	6.46	0.48	0.24	99.79
1295.0	10.49	38.85	43.22	0.74	5.94	0.18	0.16	99.59
1300.4	10.58	38.73	43.33	0.63	5.87	0.34	0.22	99.70
1305.9	12.59	36.04	45.65	0.63	4.21	0.17	0.26	99.57
1311.4	12.87	35.67	45.97	0.20	3.99	0.05	0.16	98.91
1316.9	11.76	37.15	44.70	0.53	4.89	0.20	0.18	99.41
1322.4	11.95	36.90	44.91	0.36	4.74	0.14	0.20	99.20
1327.9	12.96	35.54	46.08	0.49	3.91	0.18	0.29	99.46
1333.4	12.04	36.78	45.01	0.75	4.67	0.31	0.23	99.79
1338.9	10.03	39.45	42.70	0.60	6.31	0.37	0.23	99.71
1344.3	12.69	35.92	45.76	0.62	4.14	0.22	0.16	99.50
1349.8	11.76	37.15	44.70	0.61	4.89	0.37	0.25	99.73
1355.3	10.85	38.37	43.64	0.29	5.64	0.09	0.26	99.14
1360.8	10.94	38.24	43.75	0.70	5.57	0.16	0.16	99.51
1366.3	11.12	38.00	43.96	0.21	5.42	0.16	0.20	99.08
1371.8	11.58	37.39	44.48	0.67	5.04	0.15	0.18	99.50
1377.3	12.22	36.53	45.23	0.71	4.52	0.09	0.28	99.59
1382.8	13.52	34.80	46.73	0.54	3.45	0.29	0.26	99.59
1388.2	10.58	38.73	43.33	0.36	5.87	0.37	0.25	99.48
1393.7	10.85	38.37	43.64	0.75	5.64	0.29	0.18	99.73
1399.2	10.58	38.73	43.33	0.40	5.87	0.32	0.18	99.40
1404.7	12.50	36.16	45.55	0.36	4.29	0.38	0.30	99.54
1410.2	11.67	37.27	44.59	0.71	4.97	0.42	0.21	99.84
1415.7	9.94	39.57	42.60	0.70	6.38	0.36	0.24	99.81
1421.2	13.43	34.92	46.62	0.71	3.53	0.31	0.16	99.68
1426.7	17.74	29.18	51.58	0.32	0.00	0.06	0.16	99.03
1432.1	9.41	40.29	41.98	0.79	6.82	0.15	0.20	99.64
1437.6	9.94	39.57	42.60	0.57	6.38	0.39	0.24	99.70
1443.1	11.21	37.88	44.06	0.64	5.34	0.42	0.28	99.85
1448.6	9.41	40.29	41.98	0.23	6.82	0.30	0.29	99.33

Pos. (μm)	Na2O	Al2O3	SiO2	K2O	CaO	FeO	SrO	Total
1454.1	11.49	37.51	44.38	0.73	5.12	0.31	0.20	99.73
1459.6	11.21	37.88	44.06	0.23	5.34	0.20	0.15	99.08
1465.1	9.76	39.81	42.39	0.42	6.53	0.40	0.28	99.60
1470.5	10.12	39.33	42.81	0.63	6.24	0.42	0.17	99.73
1476.0	11.58	37.39	44.48	0.37	5.04	0.01	0.23	99.11
1481.5	10.85	38.37	43.64	0.69	5.64	0.30	0.29	99.78
1487.0	11.95	36.90	44.91	0.31	4.74	0.02	0.24	99.08
1492.5	9.05	40.77	41.57	0.34	7.12	0.36	0.16	99.36
1498.0	8.43	41.59	40.85	0.26	7.63	0.04	0.25	99.05
1503.5	10.58	38.73	43.33	0.38	5.87	0.18	0.16	99.22
1509.0	9.68	39.93	42.29	0.71	6.60	0.16	0.20	99.56
1514.4	12.32	36.41	45.33	0.35	4.44	0.45	0.17	99.48
1519.9	9.76	39.81	42.39	0.39	6.53	0.20	0.20	99.29
1525.4	9.14	40.65	41.67	0.48	7.04	0.46	0.20	99.65
1530.9	9.76	39.81	42.39	0.71	6.53	0.48	0.16	99.85
1536.4	9.94	39.57	42.60	0.23	6.38	0.07	0.29	99.09
1541.9	10.31	39.09	43.02	0.39	6.09	0.42	0.23	99.54
1547.4	12.04	36.78	45.01	0.36	4.67	0.13	0.29	99.28
1552.9	12.59	36.04	45.65	0.80	4.21	0.14	0.25	99.69
1558.3	11.21	37.88	44.06	0.58	5.34	0.45	0.16	99.69
1563.8	11.30	37.76	44.17	0.26	5.27	0.37	0.22	99.34
1569.3	9.94	39.57	42.60	0.35	6.38	0.43	0.21	99.50
1574.8	11.40	37.64	44.27	0.55	5.19	0.10	0.22	99.37
1580.3	10.94	38.24	43.75	0.73	5.57	0.15	0.30	99.68
1585.8	12.22	36.53	45.23	0.39	4.52	0.46	0.26	99.61
1591.3	10.76	38.49	43.54	0.57	5.72	0.20	0.27	99.53
1596.8	9.14	40.65	41.67	0.66	7.04	0.17	0.23	99.56
1602.2	11.40	37.64	44.27	0.60	5.19	0.21	0.21	99.52
1607.7	9.41	40.29	41.98	0.29	6.82	0.17	0.27	99.23
1613.2	12.50	36.16	45.55	0.78	4.29	0.31	0.26	99.85
1618.7	8.25	41.83	40.65	0.55	7.77	0.29	0.22	99.56
1624.2	9.50	40.17	42.08	0.71	6.75	0.33	0.19	99.73
1629.7	10.31	39.09	43.02	0.45	6.09	0.12	0.21	99.28
1635.2	10.03	39.45	42.70	0.60	6.31	0.48	0.20	99.78
1640.6	9.68	39.93	42.29	0.29	6.60	0.49	0.18	99.46
1646.1	8.34	41.71	40.75	0.40	7.70	0.46	0.17	99.52
1651.6	7.90	42.30	40.24	0.51	8.06	0.27	0.20	99.48
1657.1	10.31	39.09	43.02	0.43	6.09	0.30	0.24	99.47
1662.6	7.20	43.24	39.43	0.47	8.63	0.29	0.20	99.46

Unit: El Chichon D
Thin Section: CHI-9615
Crystal: A

Microprobe analyses

Pos. (μm)	Na2O	Al2O3	SiO2	K2O	CaO	FeO	SrO	Total
0.0	9.66	39.95	42.28	0.88	6.61	0.31	0.20	99.23
4.9	8.95	40.90	41.45	0.80	7.20	0.09	0.25	99.24
9.9	9.09	40.71	41.62	0.88	7.08	0.37	0.26	99.78
14.8	9.71	39.88	42.33	0.92	6.57	0.18	0.22	99.16
19.7	11.06	38.08	43.89	1.06	5.47	0.05	0.16	99.39
24.7	10.19	39.24	42.89	0.95	6.18	0.36	0.19	99.26
29.6	10.63	38.66	43.39	1.07	5.82	0.28	0.20	99.39
34.5	10.38	38.98	43.11	1.00	6.02	0.31	0.26	99.87
39.4	10.68	38.60	43.44	1.04	5.78	0.31	0.20	99.59
44.4	10.38	38.98	43.11	1.06	6.02	0.30	0.22	99.77
49.3	9.09	40.71	41.62	0.76	7.08	0.16	0.24	99.57
54.2	9.42	40.27	42.00	0.85	6.81	0.01	0.19	99.01
59.2	11.70	37.23	44.62	1.29	4.95	0.22	0.20	99.47
64.1	10.72	38.53	43.50	1.08	5.75	0.23	0.17	99.25
69.0	10.34	39.05	43.05	1.07	6.06	0.27	0.29	99.82
74.0	10.14	39.31	42.83	0.96	6.22	0.46	0.18	99.37
78.9	11.26	37.82	44.11	1.14	5.31	0.33	0.22	99.69
83.8	11.84	37.04	44.79	1.31	4.83	0.34	0.29	99.53
88.8	9.86	39.69	42.50	0.96	6.46	0.23	0.24	99.77
93.7	9.52	40.14	42.11	0.85	6.73	0.14	0.19	99.37
98.6	9.52	40.14	42.11	0.83	6.73	0.38	0.21	99.55
103.6	11.26	37.82	44.11	1.13	5.31	0.41	0.19	99.60
108.5	9.66	39.95	42.28	0.91	6.61	0.31	0.15	99.20
113.4	10.92	38.27	43.72	1.11	5.59	0.17	0.23	99.29
118.3	10.82	38.40	43.61	1.07	5.67	0.43	0.23	99.56
123.3	9.23	40.52	41.78	0.79	6.97	0.14	0.21	99.13
128.2	8.52	41.47	40.96	0.79	7.55	0.12	0.20	99.45
133.1	9.14	40.65	41.67	0.75	7.04	0.12	0.19	99.33
138.1	9.38	40.33	41.95	0.86	6.85	0.44	0.26	99.96
143.0	10.14	39.31	42.83	1.04	6.22	0.31	0.22	99.45
147.9	10.68	38.60	43.44	1.12	5.78	0.00	0.24	99.36
152.9	9.66	39.95	42.28	0.98	6.61	0.25	0.22	99.55
157.8	10.77	38.47	43.55	1.02	5.71	0.47	0.19	99.54
162.7	11.06	38.08	43.89	1.03	5.47	0.13	0.27	99.31
167.7	9.81	39.75	42.44	0.90	6.50	0.34	0.17	99.30
172.6	9.71	39.88	42.33	0.85	6.57	0.01	0.18	98.97
177.5	10.14	39.31	42.83	0.98	6.22	0.25	0.21	99.27
182.4	9.52	40.14	42.11	0.88	6.73	0.19	0.24	99.63
187.4	9.57	40.07	42.17	0.82	6.69	0.01	0.16	99.24
192.3	8.66	41.28	41.12	0.68	7.43	0.48	0.19	99.77
197.2	9.33	40.39	41.89	0.93	6.89	0.20	0.28	99.56
202.2	9.76	39.82	42.39	0.93	6.53	0.04	0.21	99.50
207.1	9.86	39.69	42.50	1.01	6.46	0.17	0.23	99.62
212.0	9.66	39.95	42.28	0.86	6.61	0.03	0.26	99.08
217.0	9.52	40.14	42.11	0.91	6.73	0.24	0.23	99.49
221.9	9.81	39.75	42.44	0.99	6.50	0.46	0.16	99.60
226.8	8.66	41.28	41.12	0.80	7.43	0.47	0.28	99.71
231.8	10.19	39.24	42.89	0.89	6.18	0.01	0.28	99.01
236.7	9.76	39.82	42.39	0.97	6.53	0.11	0.18	99.10

ICP-MS

Pos. (μm)	87/86	87/86
6	0.70058	0.70456
11	0.70300	0.70282
17	0.70440	0.70291
22	0.70235	0.70292
28	0.70545	0.70395
33	0.70474	0.70271
39	0.70509	0.70438
44	0.70336	0.70356
50	0.70454	0.70401
55	0.70468	0.70473
61	0.70300	0.70465
66	0.70286	0.70283
72	0.70332	0.70397
77	0.70403	0.70396
83	0.70298	0.70471
88	0.70460	0.70390
94	0.70520	0.70455
99	0.70252	0.70391
105	0.70392	0.70495
110	0.70301	0.70835
116	0.70434	0.70497
121	0.70352	0.70605
127	0.70326	0.70430
132	0.70257	0.70697
138	0.70378	0.70690
143	0.70458	0.70686
149	0.70362	0.70546
154	0.70381	0.70490
160	0.70494	0.70618
165	0.70627	0.70733
171	0.70512	0.70445
176	0.70674	0.70676
182	0.70663	0.70736
187	0.70450	0.70842
193	0.70437	0.70580
198	0.70372	0.70741
204	0.70353	0.70682
209	0.70363	0.70546
215	0.70399	0.70563
220	0.70472	0.70449
226	0.70502	0.70656
231	0.70291	0.70429
237	0.70485	0.70588
242	0.70488	0.70439
248	0.70586	0.70224
253	0.70307	0.70250
259	0.70303	0.70302
264	0.70331	0.70435
270	0.70394	0.70436

Pos. (μm)	Na2O	Al2O3	SiO2	K2O	CaO	FeO	SrO	Total
241.6	8.90	40.96	41.40	0.84	7.24	0.38	0.29	99.66
246.5	9.28	40.46	41.84	0.94	6.93	0.47	0.17	99.85
251.5	9.33	40.39	41.89	0.82	6.89	0.46	0.22	99.96
256.4	8.47	41.53	40.91	0.74	7.59	0.36	0.28	99.51
261.3	8.76	41.15	41.23	0.73	7.35	0.06	0.18	99.29
266.3	8.43	41.60	40.85	0.77	7.63	0.46	0.17	99.37
271.2	8.43	41.60	40.85	0.76	7.63	0.37	0.16	99.70
276.1	9.42	40.27	42.00	0.81	6.81	0.30	0.21	99.31
281.1	9.76	39.82	42.39	0.99	6.53	0.17	0.26	99.54
286.0	9.81	39.75	42.44	0.97	6.50	0.48	0.17	99.78
290.9	9.04	40.77	41.56	0.86	7.12	0.39	0.15	99.78
295.9	8.90	40.96	41.40	0.80	7.24	0.00	0.28	99.48
300.8	9.95	39.56	42.61	1.00	6.38	0.16	0.23	99.11
305.7	9.95	39.56	42.61	1.03	6.38	0.27	0.20	99.74
310.7	9.86	39.69	42.50	0.92	6.46	0.03	0.23	99.41
315.6	9.71	39.88	42.33	0.86	6.57	0.18	0.16	99.51
320.5	9.19	40.58	41.73	0.85	7.00	0.21	0.20	99.58
325.4	9.71	39.88	42.33	0.95	6.57	0.14	0.28	99.12
330.4	9.71	39.88	42.33	0.83	6.57	0.16	0.21	99.25
335.3	10.10	39.37	42.77	0.92	6.26	0.23	0.29	99.41
340.2	11.11	38.01	43.95	1.18	5.43	0.13	0.23	99.58
345.2	11.70	37.23	44.62	1.28	4.95	0.26	0.17	99.55
350.1	9.76	39.82	42.39	1.02	6.53	0.17	0.28	99.25
355.0	10.97	38.21	43.78	1.15	5.55	0.22	0.15	99.62
360.0	9.66	39.95	42.28	1.00	6.61	0.23	0.25	99.63
364.9	9.66	39.95	42.28	0.88	6.61	0.40	0.22	99.33
369.8	10.92	38.27	43.72	1.11	5.59	0.30	0.24	99.29
374.8	10.72	38.53	43.50	1.02	5.75	0.23	0.21	99.49
379.7	10.14	39.31	42.83	1.01	6.22	0.09	0.22	99.18
384.6	10.53	38.79	43.28	1.07	5.90	0.33	0.23	99.26
389.5	11.45	37.56	44.34	1.25	5.15	0.12	0.27	99.38
394.5	10.05	39.43	42.72	0.99	6.30	0.22	0.25	99.30
399.4	8.95	40.90	41.45	0.86	7.20	0.08	0.29	99.30
404.3	9.28	40.46	41.84	0.80	6.93	0.46	0.28	99.94
409.3	9.81	39.75	42.44	0.85	6.50	0.49	0.17	99.64
414.2	8.90	40.96	41.40	0.73	7.24	0.07	0.17	99.27
419.1	9.14	40.65	41.67	0.83	7.04	0.36	0.21	99.56
424.1	8.66	41.28	41.12	0.84	7.43	0.30	0.23	99.75
429.0	8.29	41.78	40.69	0.74	7.74	0.42	0.17	99.52
433.9	9.04	40.77	41.56	0.84	7.12	0.45	0.18	99.59
438.9	8.38	41.66	40.80	0.66	7.66	0.07	0.19	99.00
443.8	9.71	39.88	42.33	0.83	6.57	0.17	0.27	99.43
448.7	11.36	37.69	44.23	1.17	5.23	0.08	0.25	99.17
453.6	9.81	39.75	42.44	1.01	6.50	0.15	0.18	99.32
458.6	8.81	41.09	41.29	0.77	7.32	0.48	0.28	99.60
463.5	9.09	40.71	41.62	0.83	7.08	0.32	0.16	99.46
468.4	8.47	41.53	40.91	0.76	7.59	0.49	0.22	99.60
473.4	9.66	39.95	42.28	0.97	6.61	0.31	0.20	99.46
478.3	8.85	41.03	41.34	0.86	7.28	0.36	0.22	99.76
483.2	9.57	40.07	42.17	0.85	6.69	0.44	0.23	99.53
488.2	9.04	40.77	41.56	0.82	7.12	0.25	0.21	99.42
493.1	8.81	41.09	41.29	0.74	7.32	0.30	0.24	99.78
498.0	9.71	39.88	42.33	0.94	6.57	0.16	0.29	99.16
503.0	8.19	41.91	40.58	0.66	7.82	0.15	0.27	99.34

Pos. (μm)	87/86	87/86
275	0.70435	0.70293
281	0.70379	0.70358
286	0.70432	0.70383
292	0.70329	0.70396
297	0.70301	0.70294
303	0.70273	0.70451
308	0.70324	0.70567
314	0.70343	0.70482
319	0.70328	0.70422
325	0.70474	0.70375
330	0.70364	0.70510
336	0.70329	0.70383
341	0.70446	0.70505
347	0.70483	0.70232
352	0.70540	0.70444
358	0.70200	0.70320
363	0.70522	0.70318
369	0.70305	0.70472
374	0.70368	0.70558
380	0.70329	0.70379
385	0.70440	0.70441
391	0.70624	0.70466
396	0.70318	0.70478
402	0.70436	0.70452
407	0.70492	0.70499
413	0.70341	0.70455
418	0.70291	0.70613
424	0.70566	0.70332
429	0.70550	0.70418
435	0.70448	0.70428
440	0.70459	0.70511
446	0.70399	0.70267
451	0.70546	0.70467
457	0.70519	0.70286
462	0.70455	0.70475
468	0.70485	0.70401
473	0.70410	0.70464
479	0.70564	0.70377
484	0.70539	0.70383
490	0.70322	0.70542
495	0.70179	0.70504
501	0.70368	0.70581
506	0.70560	0.70345
512	0.70516	0.70446
517	0.70392	0.70378
523	0.70325	0.70437
528	0.70506	0.70476
534	0.70483	0.70427
539	0.70292	0.70307
545	0.70356	0.70524
550	0.70483	0.70444
556	0.70396	0.70526
561	0.70481	0.70605
567	0.70389	0.70238

Pos. (μm)	Na2O	Al2O3	SiO2	K2O	CaO	FeO	SrO	Total
507.9	10.00	39.50	42.66	0.90	6.34	0.31	0.29	99.64
512.8	8.38	41.66	40.80	0.70	7.66	0.35	0.26	99.38
517.8	9.95	39.56	42.61	0.99	6.38	0.26	0.16	99.69
522.7	10.14	39.31	42.83	1.08	6.22	0.00	0.27	99.53
527.6	10.10	39.37	42.77	0.93	6.26	0.45	0.21	99.75
532.5	8.81	41.09	41.29	0.82	7.32	0.13	0.22	99.37
537.5	10.19	39.24	42.89	0.98	6.18	0.42	0.22	99.38
542.4	10.68	38.60	43.44	1.02	5.78	0.49	0.30	99.71
547.3	10.43	38.92	43.16	0.97	5.98	0.31	0.23	99.57
552.3	9.42	40.27	42.00	0.88	6.81	0.07	0.28	99.14
557.2	10.19	39.24	42.89	0.93	6.18	0.46	0.25	99.42
562.1	9.47	40.20	42.06	0.82	6.77	0.45	0.25	99.73
567.1	10.14	39.31	42.83	1.04	6.22	0.29	0.16	99.15
572.0	9.47	40.20	42.06	0.79	6.77	0.16	0.19	99.24
576.9	9.00	40.84	41.51	0.77	7.16	0.40	0.20	99.41
581.9	10.10	39.37	42.77	0.92	6.26	0.32	0.30	99.80
586.8	8.57	41.41	41.01	0.83	7.51	0.43	0.17	99.80
591.7	8.81	41.09	41.29	0.68	7.32	0.42	0.27	99.64
596.6	9.95	39.56	42.61	0.93	6.38	0.04	0.26	99.41
601.6	9.09	40.71	41.62	0.85	7.08	0.10	0.26	99.62
606.5	9.00	40.84	41.51	0.76	7.16	0.34	0.30	99.77
611.4	9.42	40.27	42.00	0.83	6.81	0.25	0.24	99.58
616.4	9.19	40.58	41.73	0.86	7.00	0.09	0.26	99.62
621.3	9.14	40.65	41.67	0.80	7.04	0.05	0.17	99.23
626.2	9.66	39.95	42.28	0.99	6.61	0.11	0.30	99.39
631.2	8.00	42.16	40.36	0.69	7.97	0.14	0.27	99.28
636.1	8.10	42.04	40.47	0.61	7.90	0.39	0.21	99.59
641.0	8.85	41.03	41.34	0.83	7.28	0.34	0.22	99.67
646.0	9.90	39.63	42.55	1.02	6.42	0.24	0.22	99.22
650.9	8.52	41.47	40.96	0.78	7.55	0.24	0.18	99.33
655.8	8.43	41.60	40.85	0.81	7.63	0.34	0.17	99.71
660.7	7.49	42.85	39.77	0.69	8.40	0.17	0.19	99.66
665.7	10.82	38.40	43.61	1.00	5.67	0.10	0.21	99.32
670.6	11.80	37.10	44.73	1.33	4.87	0.16	0.17	99.32
675.5	10.53	38.79	43.28	1.01	5.90	0.01	0.29	99.31
680.5	9.23	40.52	41.78	0.88	6.97	0.20	0.18	99.59
685.4	8.33	41.72	40.74	0.67	7.70	0.36	0.27	99.89
690.3	11.55	37.43	44.45	1.11	5.07	0.30	0.29	99.74
695.3	10.92	38.27	43.72	1.10	5.59	0.07	0.17	99.39
700.2	11.50	37.49	44.40	1.18	5.11	0.06	0.22	99.52
705.1	10.29	39.11	43.00	0.95	6.10	0.33	0.21	99.27
710.1	9.76	39.82	42.39	0.94	6.53	0.34	0.28	99.82
715.0	12.19	36.58	45.19	1.19	4.54	0.07	0.21	99.15
719.9	10.14	39.31	42.83	0.97	6.22	0.07	0.22	99.11
724.9	9.66	39.95	42.28	0.82	6.61	0.50	0.15	99.92
729.8	12.29	36.45	45.30	1.34	4.46	0.43	0.16	99.72
734.7	11.40	37.62	44.28	1.26	5.19	0.10	0.20	99.25
739.6	11.01	38.14	43.83	1.06	5.51	0.44	0.15	99.47
749.5	9.57	40.07	42.17	0.87	6.69	0.46	0.23	99.97
754.4	10.43	38.92	43.16	1.13	5.98	0.21	0.16	99.38
759.4	10.87	38.34	43.67	1.07	5.63	0.46	0.24	99.66
764.3	10.68	38.60	43.44	1.14	5.78	0.15	0.19	99.59
769.2	11.99	36.84	44.96	1.26	4.71	0.32	0.17	99.38

Pos. (μm)	87/86	87/86
572	0.70366	0.70437
578	0.70351	0.70417
583	0.70440	0.70468
589	0.70581	0.70353
594	0.70497	0.70384
600	0.70525	0.70421
605	0.70430	0.70533
611	0.70424	0.70622
616	0.70541	0.70536
622	0.70457	0.70333
627	0.70565	0.70418
633	0.70348	0.70370
638	0.70358	0.70423
644	0.70374	0.70348
649	0.70415	0.70547
655	0.70382	0.70367
660	0.70473	0.70362
666	0.70411	0.70526
671	0.70468	0.70297
677	0.70183	0.70363
682	0.70404	0.70322
688	0.70475	0.70562
693	0.70366	0.70457
699	0.70394	0.70405
704	0.70557	0.70333
710	0.70555	0.70523
715	0.70005	0.70191
721	0.70074	0.70370
726	0.70412	0.70393
732	0.70320	0.70556
737	0.70397	0.70391
743	0.70531	0.70358
748	0.70617	0.70604
754	0.70672	0.70368
759	0.70424	0.70261
765	0.70518	0.70458
770	0.70484	0.70464
776	0.70476	0.70486
781	0.70380	0.70418
787	0.70683	0.70481
792	0.70423	0.70339
798	0.70880	0.70392
803	0.70773	0.70441
809	0.70649	0.70479
814	0.70823	0.70479
820	0.70469	0.70469
825	0.70570	0.70405
831	0.70674	0.70525
836	0.70650	0.70467
842		0.70540
847		0.70475
853		0.70502
858		0.70291
864		0.70473

Pos. (µm)	Na2O	Al2O3	SiO2	K2O	CaO	FeO	SrO	Total
774.2	10.24	39.18	42.94	1.00	6.14	0.17	0.17	99.25
779.1	9.42	40.27	42.00	0.92	6.81	0.09	0.23	99.31
784.0	9.81	39.75	42.44	0.89	6.50	0.15	0.18	99.29
789.0	9.62	40.01	42.22	0.83	6.65	0.36	0.18	99.60
793.9	11.01	38.14	43.83	1.13	5.51	0.17	0.26	99.65
798.8	11.26	37.82	44.11	1.11	5.31	0.47	0.28	100.01
803.7	11.26	37.82	44.11	1.07	5.31	0.28	0.21	99.34
808.7	10.43	38.92	43.16	0.97	5.98	0.05	0.17	98.98
813.6	8.85	41.03	41.34	0.78	7.28	0.36	0.25	99.91
818.5	10.87	38.34	43.67	1.18	5.63	0.13	0.26	99.34
823.5	9.28	40.46	41.84	0.76	6.93	0.40	0.18	99.48
828.4	10.34	39.05	43.05	0.92	6.06	0.31	0.26	99.35
833.3	10.19	39.24	42.89	0.98	6.18	0.23	0.15	99.56
838.3	9.86	39.69	42.50	0.96	6.46	0.08	0.24	99.55
843.2	11.99	36.84	44.96	1.32	4.71	0.26	0.18	99.20
848.1	9.90	39.63	42.55	1.00	6.42	0.38	0.24	99.57
853.1	9.14	40.65	41.67	0.77	7.04	0.19	0.20	99.42
858.0	10.68	38.60	43.44	1.04	5.78	0.37	0.19	99.69
862.9	10.14	39.31	42.83	0.95	6.22	0.45	0.28	99.84
867.9	11.21	37.89	44.06	1.08	5.35	0.49	0.18	99.84
872.8	9.04	40.77	41.56	0.83	7.12	0.13	0.30	99.46
877.7	11.84	37.04	44.79	1.22	4.83	0.50	0.27	99.93
882.6	9.52	40.14	42.11	0.96	6.73	0.42	0.25	99.79
887.6	9.90	39.63	42.55	0.90	6.42	0.48	0.17	99.93
892.5	9.42	40.27	42.00	0.91	6.81	0.49	0.15	99.71
897.4	10.48	38.86	43.22	1.05	5.94	0.03	0.23	99.26
902.4	9.71	39.88	42.33	1.01	6.57	0.19	0.23	99.40
907.3	10.58	38.73	43.33	0.99	5.86	0.07	0.28	99.26
912.2	11.26	37.82	44.11	1.08	5.31	0.42	0.18	99.70
917.2	10.77	38.47	43.55	0.99	5.71	0.45	0.28	99.59
922.1	10.72	38.53	43.50	1.12	5.75	0.25	0.17	99.31
927.0	9.33	40.39	41.89	0.93	6.89	0.18	0.17	99.57
932.0	9.95	39.56	42.61	0.98	6.38	0.36	0.21	99.86
936.9	9.57	40.07	42.17	0.88	6.69	0.48	0.22	99.78
941.8	9.62	40.01	42.22	0.88	6.65	0.48	0.23	99.93
946.7	10.29	39.11	43.00	0.98	6.10	0.36	0.23	99.57
951.7	10.10	39.37	42.77	1.05	6.26	0.19	0.19	99.36
956.6	10.38	38.98	43.11	0.95	6.02	0.07	0.18	99.54
961.5	10.72	38.53	43.50	1.01	5.75	0.32	0.22	99.83
966.5	10.38	38.98	43.11	1.00	6.02	0.04	0.19	98.98
971.4	11.21	37.89	44.06	1.08	5.35	0.06	0.23	99.42
976.3	9.33	40.39	41.89	0.86	6.89	0.05	0.19	99.20
981.3	11.26	37.82	44.11	1.14	5.31	0.20	0.24	99.68
986.2	10.24	39.18	42.94	1.00	6.14	0.18	0.22	99.69
991.1	10.43	38.92	43.16	1.09	5.98	0.04	0.20	99.40
996.1	9.95	39.56	42.61	0.96	6.38	0.44	0.22	99.51

Pos. (µm)	87/86	87/86
869		0.70438
875		0.70410
880		0.70391
886		0.70510
891		0.70428
897		0.70537
902		0.70546
908		0.70502
913		0.70351
919		0.70584
924		0.70480
930		0.70572
935		0.70519
941		0.70765
946		0.70724
952		0.70379
957		0.70476
963		0.70507
968		0.70473
974		0.70516
979		0.70622
985		0.70450
990		0.70634
996		0.70601
1001		0.70459

Unit: El Chichon D
Thin Section: CHI-9615
Crystal: B

Microprobe analyses

Pos. (μm)	Na2O	Al2O3	SiO2	K2O	CaO	FeO	SrO	Total
0.0	10.68	38.60	43.44	0.92	5.78	0.28	0.24	99.71
5.6	9.42	40.27	42.00	0.59	6.81	0.18	0.19	99.19
11.2	10.82	38.40	43.61	0.92	5.67	0.02	0.17	98.98
16.8	9.14	40.65	41.67	0.68	7.04	0.05	0.27	99.57
22.4	9.81	39.75	42.44	0.82	6.50	0.02	0.25	99.14
27.9	10.92	38.27	43.72	0.82	5.59	0.11	0.25	99.24
33.5	11.31	37.76	44.17	0.87	5.27	0.47	0.24	99.89
39.1	9.47	40.20	42.06	0.70	6.77	0.43	0.17	99.35
44.7	9.14	40.65	41.67	0.67	7.04	0.45	0.21	99.62
50.3	10.68	38.60	43.44	0.82	5.78	0.50	0.17	99.71
55.9	12.58	36.05	45.64	1.18	4.22	0.38	0.17	99.47
61.5	9.71	39.88	42.33	0.64	6.57	0.44	0.21	99.38
67.1	9.81	39.75	42.44	0.66	6.50	0.01	0.20	99.22
72.6	10.34	39.05	43.05	0.76	6.06	0.45	0.23	99.68
83.8	11.01	38.14	43.83	0.97	5.51	0.26	0.17	99.72
89.4	9.71	39.88	42.33	0.71	6.57	0.12	0.16	99.27
95.0	9.28	40.46	41.84	0.61	6.93	0.11	0.26	99.66
100.6	9.81	39.75	42.44	0.64	6.50	0.32	0.27	99.62
106.2	9.14	40.65	41.67	0.61	7.04	0.12	0.26	99.60
111.8	8.29	41.78	40.69	0.53	7.74	0.44	0.16	99.33
117.3	9.76	39.82	42.39	0.74	6.53	0.14	0.15	99.17
122.9	9.57	40.07	42.17	0.67	6.69	0.19	0.20	99.39
128.5	9.76	39.82	42.39	0.70	6.53	0.47	0.18	99.75
134.1	10.87	38.34	43.67	0.96	5.63	0.18	0.30	99.64
139.7	9.71	39.88	42.33	0.78	6.57	0.45	0.22	99.83
145.3	11.01	38.14	43.83	0.85	5.51	0.22	0.20	99.41
150.9	9.76	39.82	42.39	0.69	6.53	0.06	0.20	99.06
156.5	8.95	40.90	41.45	0.68	7.20	0.37	0.22	99.59
162.0	11.16	37.95	44.00	1.00	5.39	0.27	0.20	99.50
167.6	10.38	38.98	43.11	0.86	6.02	0.29	0.17	99.56
173.2	10.10	39.37	42.77	0.71	6.26	0.12	0.22	99.35
178.8	10.19	39.24	42.89	0.83	6.18	0.21	0.30	99.66
184.4	10.29	39.11	43.00	0.74	6.10	0.48	0.15	99.33
190.0	9.66	39.95	42.28	0.69	6.61	0.06	0.22	99.15
195.6	10.87	38.34	43.67	0.93	5.63	0.26	0.26	99.32
201.2	11.11	38.01	43.95	0.84	5.43	0.26	0.24	99.43
206.7	9.62	40.01	42.22	0.71	6.65	0.02	0.27	99.08
212.3	10.24	39.18	42.94	0.75	6.14	0.19	0.30	99.32
217.9	10.38	38.98	43.11	0.82	6.02	0.24	0.29	99.81
223.5	9.95	39.56	42.61	0.85	6.38	0.34	0.17	99.63
229.1	9.23	40.52	41.78	0.72	6.97	0.17	0.29	99.53
234.7	10.10	39.37	42.77	0.87	6.26	0.31	0.27	99.74
240.3	10.72	38.53	43.50	0.81	5.75	0.33	0.17	99.65
245.9	9.47	40.20	42.06	0.62	6.77	0.05	0.22	99.32
251.5	9.90	39.63	42.55	0.77	6.42	0.28	0.18	99.75
257.0	10.48	38.86	43.22	0.86	5.94	0.18	0.24	99.67
262.6	10.63	38.66	43.39	0.77	5.82	0.38	0.19	99.71
268.2	9.57	40.07	42.17	0.74	6.69	0.30	0.29	99.83

ICP-MS

Pos. (μm)	87/86
6	0.70338
11	0.70316
17	0.70504
22	
28	0.70715
33	0.70396
39	0.70611
44	0.70492
50	0.70372
55	0.70824
61	0.70772
66	0.70418
72	0.70415
77	0.70433
6	0.70297
11	0.70285
17	0.70198
22	0.70384
28	0.70475
33	0.70420
39	0.70519
44	0.70441
50	0.70484
55	0.70392
61	0.70423
66	0.70267
72	0.70432
77	0.70381
83	0.70457
88	0.70509
94	0.70342
99	0.70414
105	0.70516
110	0.70344
116	0.70555
121	0.70646
127	0.70561
132	0.70464
138	0.70484
143	0.70411
149	0.70650
154	0.70527
160	0.70602
165	0.70470
171	0.70458
176	0.70628
182	0.70432
187	0.70521

Pos. (μm)	Na2O	Al2O3	SiO2	K2O	CaO	FeO	SrO	Total
273.8	9.52	40.14	42.11	0.76	6.73	0.06	0.21	99.05
279.4	10.48	38.86	43.22	0.82	5.94	0.16	0.29	99.20
285.0	9.86	39.69	42.50	0.83	6.46	0.25	0.24	99.63
290.6	10.48	38.86	43.22	0.90	5.94	0.28	0.18	99.34
296.2	11.01	38.14	43.83	0.92	5.51	0.36	0.30	99.58
301.7	11.70	37.23	44.62	1.04	4.95	0.48	0.26	99.95
307.3	9.38	40.33	41.95	0.70	6.85	0.09	0.26	99.49
312.9	9.28	40.46	41.84	0.61	6.93	0.36	0.24	99.47
318.5	10.63	38.66	43.39	0.92	5.82	0.13	0.19	99.52
324.1	10.24	39.18	42.94	0.84	6.14	0.28	0.19	99.21
329.7	9.81	39.75	42.44	0.68	6.50	0.13	0.23	99.38
335.3	10.38	38.98	43.11	0.90	6.02	0.48	0.15	99.48
340.9	8.81	41.09	41.29	0.57	7.32	0.49	0.29	100.07
346.4	9.86	39.69	42.50	0.84	6.46	0.34	0.29	99.57
352.0	9.95	39.56	42.61	0.68	6.38	0.33	0.20	99.35
357.6	11.01	38.14	43.83	0.88	5.51	0.21	0.21	99.57
363.2	10.05	39.43	42.72	0.79	6.30	0.32	0.20	99.81
368.8	11.11	38.01	43.95	0.95	5.43	0.15	0.28	99.21
374.4	9.00	40.84	41.51	0.60	7.16	0.19	0.21	99.56
380.0	9.38	40.33	41.95	0.58	6.85	0.04	0.21	99.29
385.6	11.36	37.69	44.23	0.89	5.23	0.38	0.27	99.89
391.1	10.72	38.53	43.50	0.90	5.75	0.36	0.29	99.83
396.7	8.90	40.96	41.40	0.52	7.24	0.19	0.26	99.45
402.3	10.00	39.50	42.66	0.86	6.34	0.27	0.16	99.72
407.9	9.86	39.69	42.50	0.69	6.46	0.14	0.27	99.58
413.5	10.72	38.53	43.50	0.93	5.75	0.04	0.20	99.28
419.1	11.75	37.17	44.68	0.94	4.91	0.01	0.20	99.37
424.7	9.42	40.27	42.00	0.59	6.81	0.45	0.17	99.48
430.3	8.81	41.09	41.29	0.61	7.32	0.42	0.19	99.79
435.8	9.76	39.82	42.39	0.68	6.53	0.00	0.17	98.94
441.4	8.71	41.22	41.18	0.50	7.39	0.13	0.26	99.68
447.0	9.47	40.20	42.06	0.64	6.77	0.23	0.26	99.28
452.6	10.53	38.79	43.28	0.93	5.90	0.37	0.28	99.41
458.2	11.06	38.08	43.89	0.83	5.47	0.42	0.20	99.46
463.8	9.86	39.69	42.50	0.83	6.46	0.33	0.23	99.46
469.4	9.57	40.07	42.17	0.69	6.69	0.10	0.26	99.27
475.0	9.57	40.07	42.17	0.66	6.69	0.39	0.21	99.73
480.5	10.97	38.21	43.78	0.84	5.55	0.30	0.21	99.58
486.1	10.24	39.18	42.94	0.84	6.14	0.41	0.17	99.53
491.7	8.90	40.96	41.40	0.64	7.24	0.26	0.21	99.18
497.3	10.82	38.40	43.61	0.92	5.67	0.33	0.16	99.58
502.9	9.71	39.88	42.33	0.71	6.57	0.08	0.22	99.32
508.5	10.72	38.53	43.50	0.80	5.75	0.20	0.27	99.77
514.1	9.04	40.77	41.56	0.61	7.12	0.31	0.20	99.30
519.7	10.92	38.27	43.72	0.99	5.59	0.21	0.28	99.55
525.3	10.24	39.18	42.94	0.83	6.14	0.49	0.19	99.98
530.8	9.47	40.20	42.06	0.71	6.77	0.27	0.23	99.63
536.4	10.53	38.79	43.28	0.85	5.90	0.42	0.24	99.87
542.0	10.05	39.43	42.72	0.78	6.30	0.09	0.23	99.12
547.6	10.68	38.60	43.44	0.84	5.78	0.12	0.16	99.42
553.2	10.68	38.60	43.44	0.79	5.78	0.04	0.27	99.57
558.8	10.34	39.05	43.05	0.82	6.06	0.48	0.25	99.62
564.4	11.31	37.76	44.17	0.91	5.27	0.41	0.26	99.84
570.0	10.05	39.43	42.72	0.73	6.30	0.12	0.30	99.51

Pos. (μm)	87/86
193	0.70604
198	0.70683
204	0.70420
209	0.70416
215	0.70405
220	0.70241
226	0.70625
231	0.70410
237	0.70427
242	0.70583
248	0.70466
253	0.70426
259	0.70524
264	0.70625
270	0.70564
275	0.70567
281	0.70669
286	0.70579
292	0.70591
297	0.70537
303	0.70669
308	0.70509
314	0.70385
319	0.70426
325	0.70408
330	0.70427
336	0.70401
341	0.70405
347	0.70220
352	0.70299
358	0.70450
363	0.70563
369	0.70648
374	0.70488
380	0.70557
385	0.70485
391	0.70481
396	0.70451
402	0.70409
407	0.70442
413	0.70343
418	0.70261
424	0.70380
429	0.70281
435	0.70575
440	0.70517
446	0.70292
451	0.70285
457	0.70528
462	0.70280
468	0.70456
473	0.70349
479	0.70378
484	0.70334

Pos. (µm)	Na2O	Al2O3	SiO2	K2O	CaO	FeO	SrO	Total
575.5	8.19	41.91	40.58	0.54	7.82	0.43	0.27	99.56
581.1	8.85	41.03	41.34	0.54	7.28	0.21	0.21	99.19
586.7	10.14	39.31	42.83	0.76	6.22	0.10	0.22	99.23
592.3	9.14	40.65	41.67	0.65	7.04	0.43	0.16	99.76
597.9	10.29	39.11	43.00	0.88	6.10	0.46	0.28	99.81
603.5	8.62	41.34	41.07	0.63	7.47	0.27	0.20	99.28
609.1	10.14	39.31	42.83	0.86	6.22	0.14	0.22	99.46
614.7	10.19	39.24	42.89	0.79	6.18	0.49	0.20	99.75
620.2	10.48	38.86	43.22	0.90	5.94	0.11	0.20	99.07
625.8	10.68	38.60	43.44	0.77	5.78	0.25	0.28	99.45
631.4	9.95	39.56	42.61	0.79	6.38	0.24	0.24	99.77
637.0	9.47	40.20	42.06	0.66	6.77	0.42	0.21	99.37
642.6	10.77	38.47	43.55	0.96	5.71	0.19	0.20	99.47
648.2	10.48	38.86	43.22	0.89	5.94	0.37	0.23	99.59
653.8	10.82	38.40	43.61	0.82	5.67	0.01	0.22	99.47
659.4	9.95	39.56	42.61	0.78	6.38	0.05	0.20	99.46
664.9	9.66	39.95	42.28	0.64	6.61	0.32	0.21	99.34
670.5	9.86	39.69	42.50	0.78	6.46	0.12	0.29	99.32
676.1	10.68	38.60	43.44	0.91	5.78	0.04	0.16	98.94
681.7	9.86	39.69	42.50	0.82	6.46	0.40	0.19	99.79
687.3	9.52	40.14	42.11	0.73	6.73	0.01	0.16	99.00
692.9	10.38	38.98	43.11	0.81	6.02	0.06	0.23	99.35
698.5	11.11	38.01	43.95	0.97	5.43	0.07	0.22	99.11
704.1	9.42	40.27	42.00	0.65	6.81	0.32	0.21	99.38
709.6	10.48	38.86	43.22	0.86	5.94	0.49	0.23	99.77
715.2	10.72	38.53	43.50	0.85	5.75	0.46	0.28	99.79
720.8	11.06	38.08	43.89	0.88	5.47	0.40	0.16	99.55
726.4	9.47	40.20	42.06	0.78	6.77	0.38	0.24	99.53

Pos. (µm)	87/86
490	0.70204
495	0.70280
501	0.70346
506	0.70444
512	0.70295
517	0.70456
523	0.70273
528	0.70402
534	0.70435
539	0.70276
545	0.70308
550	0.70448
556	0.70371
561	0.70523
567	0.70362
572	0.70369
578	0.70338
583	0.70254
589	0.70418
594	0.70481
600	0.70313
605	0.70371
611	0.70351
616	0.70489
622	0.70409
627	0.70276
633	0.70420
638	0.70275
644	0.70265
649	0.70453
655	0.70456
660	0.70456

Unit: El Chichon D
Thin Section: CHI-9615
Crystal: C

Microprobe analyses

Pos. (μm)	Na2O	Al2O3	SiO2	K2O	CaO	FeO	SrO	Total
0.0	9.03	40.79	41.54	0.82	7.13	0.29	0.23	99.82
5.4	9.41	40.29	41.98	0.79	6.82	0.48	0.16	99.37
10.9	8.93	40.92	41.43	0.89	7.21	0.26	0.29	99.60
16.3	8.68	41.26	41.14	0.70	7.42	0.10	0.20	99.41
21.8	9.09	40.71	41.62	0.81	7.08	0.48	0.28	99.95
27.2	8.27	41.80	40.67	0.73	7.75	0.38	0.22	99.39
32.6	9.00	40.84	41.51	0.91	7.16	0.49	0.28	99.76
38.1	7.55	42.77	39.84	0.52	8.34	0.50	0.17	99.44
43.5	8.49	41.51	40.92	0.71	7.57	0.50	0.26	99.73
48.9	9.38	40.33	41.95	0.93	6.85	0.10	0.17	99.17
54.4	8.81	41.09	41.29	0.76	7.32	0.44	0.22	99.69
59.8	11.01	38.14	43.83	1.12	5.51	0.20	0.22	99.62
65.3	7.83	42.39	40.16	0.55	8.11	0.25	0.26	99.69
70.7	9.03	40.79	41.54	0.89	7.13	0.10	0.29	99.59
76.1	7.86	42.35	40.20	0.69	8.09	0.19	0.28	99.56
81.6	7.21	43.22	39.45	0.61	8.62	0.01	0.28	99.28
87.0	7.30	43.10	39.55	0.65	8.55	0.38	0.16	99.59
92.4	7.52	42.81	39.80	0.56	8.37	0.33	0.18	99.40
97.9	7.55	42.77	39.84	0.55	8.34	0.02	0.23	99.13
103.3	7.33	43.06	39.59	0.61	8.52	0.32	0.25	99.83
108.8	8.02	42.14	40.38	0.57	7.96	0.22	0.29	99.27
114.2	7.46	42.89	39.73	0.55	8.42	0.34	0.18	99.79
119.6	7.83	42.39	40.16	0.69	8.11	0.42	0.26	99.91
125.1	8.24	41.85	40.63	0.72	7.78	0.46	0.27	99.99
130.5	8.62	41.34	41.07	0.78	7.47	0.02	0.28	99.54
135.9	9.38	40.33	41.95	0.89	6.85	0.02	0.25	99.41
141.4	10.02	39.48	42.68	0.88	6.32	0.16	0.24	99.12
146.8	9.47	40.20	42.06	0.79	6.77	0.23	0.24	99.40
152.3	9.86	39.69	42.50	0.97	6.46	0.32	0.22	99.34
157.7	8.81	41.09	41.29	0.69	7.32	0.23	0.22	99.36
163.1	10.02	39.48	42.68	0.88	6.32	0.15	0.19	99.28
168.6	9.35	40.37	41.91	0.77	6.87	0.39	0.26	99.78
174.0	7.27	43.14	39.52	0.46	8.57	0.04	0.18	99.41
179.4	7.64	42.64	39.95	0.52	8.27	0.45	0.29	99.76
184.9	7.83	42.39	40.16	0.73	8.11	0.22	0.23	99.25
190.3	9.70	39.90	42.31	1.00	6.59	0.50	0.29	99.87
195.8	8.71	41.22	41.18	0.72	7.39	0.07	0.17	99.40
201.2	9.70	39.90	42.31	0.94	6.59	0.04	0.29	99.44
206.6	8.74	41.17	41.21	0.71	7.37	0.17	0.26	99.38
212.1	9.98	39.52	42.65	0.98	6.35	0.36	0.18	99.81
217.5	9.35	40.37	41.91	0.81	6.87	0.06	0.24	99.22
223.0	10.18	39.26	42.87	1.03	6.19	0.07	0.23	99.02
228.4	8.30	41.76	40.71	0.67	7.73	0.08	0.21	99.39
233.8	9.19	40.58	41.73	0.87	7.00	0.43	0.25	99.83
239.3	9.82	39.73	42.46	0.90	6.48	0.09	0.16	99.06
244.7	9.44	40.24	42.02	0.96	6.80	0.42	0.29	99.79
250.1	10.59	38.71	43.35	1.11	5.85	0.23	0.15	99.29
255.6	9.31	40.41	41.87	0.76	6.90	0.26	0.26	99.33
261.0	9.50	40.16	42.09	0.92	6.74	0.42	0.27	99.73

ICP-MS

Pos. (μm)	87/86	87/86
5	0.70504	0.70420
11	0.70300	0.70372
16		0.70408
21	0.70374	
27		
32	0.70317	
37	0.70398	0.70481
43	0.70404	
48		0.70106
53	0.70348	0.70317
59		0.70399
64	0.70296	0.70430
69	0.70301	
75		0.70300
80		0.70567
85		0.70350
91	0.70280	0.70290
96	0.70305	0.70482
102		0.70343
107	0.70523	0.70166
112	0.70525	0.70383
118	0.70496	0.70059
123	0.70512	
128	0.70336	0.70590
134	0.70371	0.70365
139	0.70267	0.70259
144	0.70293	0.70393
150	0.70302	
155	0.70438	0.70126
160	0.70355	0.70368
166	0.70424	0.70442
171	0.70417	0.70346
176	0.70370	0.70286
182	0.70340	0.70265
187	0.70404	0.70393
192	0.70314	0.70391
198	0.70323	0.70444
203	0.70415	0.70397
208	0.70291	0.70411
214	0.70417	0.70406
219	0.70420	0.70362
224	0.70489	0.70283
230	0.70416	0.70341
235	0.70413	0.70344
241	0.70422	0.70397
246	0.70372	0.70325
251	0.70446	0.70535
257	0.70241	0.70553
262	0.70437	0.70402

Pos. (µm)	Na2O	Al2O3	SiO2	K2O	CaO	FeO	SrO	Total
266.5	10.02	39.48	42.68	1.06	6.32	0.00	0.19	99.21
271.9	9.19	40.58	41.73	0.81	7.00	0.03	0.18	99.45
277.3	9.60	40.03	42.20	0.93	6.67	0.08	0.18	99.07
282.8	9.03	40.79	41.54	0.85	7.13	0.07	0.18	99.01
288.2	9.41	40.29	41.98	0.81	6.82	0.39	0.26	99.41
293.6	9.35	40.37	41.91	0.95	6.87	0.30	0.26	99.84
299.1	9.47	40.20	42.06	0.81	6.77	0.12	0.30	99.22
304.5	9.95	39.56	42.61	1.00	6.38	0.26	0.18	99.44
310.0	9.00	40.84	41.51	0.82	7.16	0.05	0.17	99.38
315.4	9.92	39.61	42.57	0.90	6.40	0.45	0.21	99.55
320.8	9.35	40.37	41.91	0.95	6.87	0.27	0.19	99.26
326.3	9.35	40.37	41.91	0.84	6.87	0.02	0.26	99.19
331.7	10.53	38.79	43.28	1.08	5.90	0.39	0.15	99.82
337.1	8.33	41.72	40.74	0.80	7.70	0.36	0.30	99.63
342.6	9.44	40.24	42.02	0.88	6.80	0.20	0.26	99.76
348.0	9.73	39.86	42.35	0.85	6.56	0.29	0.16	99.33
353.5	9.76	39.82	42.39	0.98	6.53	0.30	0.17	99.46
358.9	9.66	39.95	42.28	0.91	6.61	0.49	0.28	99.89
364.3	8.77	41.13	41.25	0.70	7.34	0.03	0.18	99.17
369.8	9.66	39.95	42.28	0.94	6.61	0.50	0.25	99.60
375.2	9.54	40.12	42.13	0.85	6.72	0.13	0.19	99.12
380.7	9.28	40.46	41.84	0.84	6.93	0.08	0.27	99.33
386.1	9.50	40.16	42.09	0.97	6.74	0.25	0.17	99.43
391.5	9.15	40.63	41.69	0.84	7.03	0.30	0.23	99.41
397.0	9.15	40.63	41.69	0.82	7.03	0.03	0.17	98.97
402.4	8.96	40.88	41.47	0.88	7.19	0.24	0.20	99.55
407.8	8.40	41.64	40.82	0.64	7.65	0.39	0.21	99.57
413.3	7.36	43.01	39.62	0.57	8.50	0.26	0.18	99.45
418.7	9.47	40.20	42.06	0.92	6.77	0.13	0.23	99.59
424.2	8.77	41.13	41.25	0.87	7.34	0.33	0.26	99.33
429.6	10.66	38.62	43.42	1.14	5.80	0.22	0.29	99.76
435.0	9.31	40.41	41.87	0.82	6.90	0.38	0.24	99.40
440.5	9.28	40.46	41.84	0.85	6.93	0.17	0.27	99.58
445.9	9.79	39.78	42.42	0.89	6.51	0.43	0.28	99.96
451.3	8.77	41.13	41.25	0.85	7.34	0.40	0.17	99.71
456.8	8.30	41.76	40.71	0.73	7.73	0.22	0.27	99.74
462.2	8.33	41.72	40.74	0.75	7.70	0.46	0.21	99.77
467.7	8.27	41.80	40.67	0.66	7.75	0.11	0.24	99.16
473.1	8.68	41.26	41.14	0.69	7.42	0.35	0.25	99.52
478.5	9.00	40.84	41.51	0.87	7.16	0.08	0.29	99.60
484.0	9.92	39.61	42.57	1.02	6.40	0.33	0.16	99.26
489.4	9.47	40.20	42.06	0.93	6.77	0.45	0.22	99.90
494.8	9.47	40.20	42.06	0.88	6.77	0.18	0.28	99.73
500.3	8.93	40.92	41.43	0.75	7.21	0.27	0.29	99.39
505.7	9.41	40.29	41.98	0.79	6.82	0.16	0.15	99.40
511.2	9.50	40.16	42.09	0.83	6.74	0.50	0.18	99.73
516.6	9.54	40.12	42.13	0.92	6.72	0.14	0.16	99.57
522.0	9.15	40.63	41.69	0.79	7.03	0.12	0.24	99.24
527.5	9.19	40.58	41.73	0.80	7.00	0.39	0.27	99.85
532.9	9.60	40.03	42.20	0.86	6.67	0.21	0.27	99.33
538.3	9.28	40.46	41.84	0.92	6.93	0.09	0.26	99.40
543.8	10.02	39.48	42.68	0.95	6.32	0.50	0.16	99.70
549.2	10.63	38.66	43.39	1.13	5.82	0.16	0.18	99.51
554.7	9.19	40.58	41.73	0.93	7.00	0.33	0.25	99.65

Pos. (µm)	87/86	87/86
267	0.70368	0.70290
273	0.70291	0.70422
278	0.70358	0.70441
283	0.70375	0.70354
289	0.70325	0.70223
294	0.70452	0.70308
299	0.70403	0.70370
305	0.70412	0.70501
310	0.70399	0.70321
315	0.70370	0.70363
321	0.70375	0.70374
326	0.70225	0.70262
331	0.70256	0.70460
337	0.70334	0.70227
342	0.70405	0.70376
347	0.70490	0.70426
353	0.70488	0.70451
358	0.70390	0.70339
363	0.70490	0.70383
369	0.70351	0.70408
374	0.70413	0.70330
380	0.70437	0.70304
385	0.70521	0.70472
390	0.70469	0.70292
396	0.70439	0.70492
401	0.70499	0.70407
406	0.70405	0.70374
412	0.70394	0.70386
417	0.70375	0.70350
422	0.70248	0.70459
428	0.70348	0.70369
433	0.70277	0.70410
438	0.70368	0.70397
444	0.70346	0.70355
449		0.70395
454	0.70386	0.70402
460	0.70377	0.70461
465	0.70400	0.70289
470	0.70368	0.70517
476	0.70417	0.70171
481	0.70333	0.70425
486	0.70376	0.70388
492	0.70517	0.70370
497	0.70501	0.70354
502	0.70340	0.70416
508	0.70312	0.70379
513	0.70392	0.70417
519	0.70343	0.70353
524	0.70321	0.70299
529	0.70341	0.70314
535	0.70448	0.70366
540	0.70413	0.70297
545	0.70492	0.70459
551	0.70428	0.70398

Pos. (μm)	Na2O	Al2O3	SiO2	K2O	CaO	FeO	SrO	Total
560.1	7.96	42.22	40.31	0.70	8.01	0.48	0.21	99.40
565.5	9.54	40.12	42.13	0.98	6.72	0.39	0.22	99.32
571.0	9.15	40.63	41.69	0.74	7.03	0.04	0.26	99.24
576.4	8.52	41.47	40.96	0.68	7.55	0.19	0.16	99.42
581.9	8.84	41.05	41.32	0.86	7.29	0.22	0.23	99.32
587.3	9.95	39.56	42.61	1.01	6.38	0.14	0.27	99.16
592.7	10.58	38.73	43.33	1.05	5.86	0.03	0.28	99.34
603.6	8.33	41.72	40.74	0.81	7.70	0.26	0.25	99.29
609.0	8.81	41.09	41.29	0.74	7.32	0.17	0.29	99.66
614.5	7.86	42.35	40.20	0.72	8.09	0.18	0.25	99.21
619.9	6.99	43.51	39.20	0.50	8.80	0.37	0.27	99.86
625.4	9.44	40.24	42.02	0.82	6.80	0.48	0.18	99.49
630.8	9.76	39.82	42.39	0.86	6.53	0.16	0.19	99.30
636.2	8.49	41.51	40.92	0.73	7.57	0.10	0.18	99.16
641.7	7.33	43.06	39.59	0.59	8.52	0.42	0.16	99.64
647.1	7.83	42.39	40.16	0.65	8.11	0.04	0.20	99.04
652.5	9.19	40.58	41.73	0.82	7.00	0.39	0.21	99.58
658.0	8.36	41.68	40.78	0.63	7.68	0.34	0.19	99.23
663.4	8.93	40.92	41.43	0.73	7.21	0.47	0.17	99.84
668.9	9.41	40.29	41.98	0.83	6.82	0.43	0.27	99.54
674.3	9.98	39.52	42.65	0.98	6.35	0.03	0.28	99.51
679.7	10.18	39.26	42.87	0.95	6.19	0.33	0.26	99.89
685.2	7.99	42.18	40.34	0.63	7.99	0.26	0.27	99.54
690.6	9.28	40.46	41.84	0.80	6.93	0.27	0.29	99.52
696.0	9.25	40.50	41.80	0.87	6.95	0.25	0.15	99.45
701.5	10.08	39.39	42.76	1.02	6.27	0.18	0.27	99.33
706.9	9.35	40.37	41.91	0.96	6.87	0.12	0.16	99.04
712.4	9.15	40.63	41.69	0.85	7.03	0.50	0.30	99.93
717.8	9.73	39.86	42.35	0.91	6.56	0.23	0.19	99.65
723.2	9.63	39.99	42.24	1.00	6.64	0.12	0.26	99.28
728.7	10.27	39.13	42.98	1.08	6.11	0.36	0.26	99.86
734.1	11.47	37.54	44.36	1.13	5.13	0.29	0.25	99.30
739.6	10.05	39.43	42.72	0.99	6.30	0.12	0.19	99.37
745.0	9.28	40.46	41.84	0.89	6.93	0.18	0.23	99.26
750.4	11.24	37.84	44.10	1.06	5.32	0.28	0.25	99.72
755.9	10.82	38.40	43.61	1.11	5.67	0.37	0.15	99.63
761.3	10.24	39.18	42.94	1.06	6.14	0.31	0.18	99.48
766.7	11.53	37.45	44.43	1.19	5.08	0.05	0.18	99.13
772.2	10.50	38.83	43.24	1.12	5.93	0.45	0.19	99.63
777.6	10.40	38.96	43.13	1.05	6.01	0.04	0.23	99.40
783.1	10.79	38.45	43.57	1.09	5.69	0.15	0.17	99.59
788.5	9.76	39.82	42.39	0.89	6.53	0.43	0.16	99.77
793.9	10.05	39.43	42.72	0.92	6.30	0.44	0.18	99.85
799.4	9.54	40.12	42.13	0.91	6.72	0.39	0.21	99.55
804.8	9.06	40.75	41.58	0.87	7.11	0.48	0.24	99.63
810.2	10.34	39.05	43.05	1.09	6.06	0.10	0.28	99.51
815.7	9.31	40.41	41.87	0.77	6.90	0.20	0.15	99.60
821.1	8.33	41.72	40.74	0.65	7.70	0.22	0.25	99.37
826.6	8.11	42.01	40.49	0.62	7.88	0.04	0.18	99.02
832.0	8.02	42.14	40.38	0.69	7.96	0.06	0.28	99.15
837.4	9.19	40.58	41.73	0.77	7.00	0.44	0.26	99.43
842.9	8.52	41.47	40.96	0.73	7.55	0.04	0.18	99.37
848.3	8.90	40.96	41.40	0.75	7.24	0.41	0.24	99.60

Pos. (μm)	87/86	87/86
556	0.70383	0.70333
561	0.70464	0.70336
567	0.70451	0.70413
572	0.70457	0.70373
577	0.70505	0.70484
583	0.70333	0.70201
588	0.70448	0.70496
593	0.70329	0.70357
599	0.70391	0.70401
604	0.70461	0.70209
609	0.70456	0.70250
615	0.70272	0.70374
620	0.70358	0.70357
625	0.70421	0.70475
631	0.70476	0.70453
636	0.70373	0.70270
641	0.70315	0.70212
647	0.70428	0.70284
652	0.70326	0.70377
657	0.70383	0.70339
663	0.70359	0.70311
668	0.70307	0.70297
674	0.70275	0.70343
679	0.70419	0.70468
684	0.70409	0.70343
690	0.70338	0.70481
695	0.70509	0.70276
700	0.70354	0.70374
706	0.70321	0.70362
711	0.70277	0.70289
716	0.70335	0.70334
722	0.70273	0.70310
727	0.70396	0.70445
732	0.70420	0.70334
738	0.70428	0.70330
743	0.70347	0.70342
748	0.70230	0.70410
754	0.70343	0.70183
759	0.70381	0.70297
764	0.70204	0.70287
770	0.70276	0.70288
775	0.70355	0.70361
780	0.70210	0.70279
786	0.70297	0.70344
791	0.70281	0.70285
797	0.70357	0.70283
802	0.70302	0.70456
807	0.70412	0.70221
813	0.70262	0.70372
818	0.70428	0.70387
823	0.70313	0.70284
829	0.70347	0.70302
834	0.70465	0.70512
839	0.70320	0.70325

Pos. (μm)	Na2O	Al2O3	SiO2	K2O	CaO	FeO	SrO	Total
853.7	8.43	41.60	40.85	0.79	7.63	0.04	0.18	99.38
859.2	9.73	39.86	42.35	0.95	6.56	0.05	0.20	99.32
864.6	8.65	41.30	41.11	0.85	7.45	0.23	0.26	99.43
870.1	7.86	42.35	40.20	0.64	8.09	0.25	0.29	99.72
875.5	7.36	43.01	39.62	0.59	8.50	0.41	0.16	99.65
880.9	8.02	42.14	40.38	0.69	7.96	0.17	0.23	99.28
886.4	8.87	41.01	41.36	0.83	7.26	0.13	0.29	99.28
891.8	9.44	40.24	42.02	0.95	6.80	0.26	0.27	99.79
897.2	9.63	39.99	42.24	0.83	6.64	0.31	0.18	99.29
902.7	9.03	40.79	41.54	0.83	7.13	0.40	0.28	99.75
908.1	11.01	38.14	43.83	1.08	5.51	0.01	0.16	98.98
913.6	8.55	41.43	41.00	0.67	7.52	0.28	0.21	99.48

Pos. (μm)	87/86	87/86
845	0.70359	0.70254
850	0.70277	0.70268
855		0.70517
861	0.70297	0.70224
866	0.70340	0.70357
871	0.70312	0.70300
877	0.70364	
882	0.70347	0.70445
887	0.70279	0.70349
893	0.70391	
898	0.70483	
903	0.70371	
909	0.70748	
914	0.70930	0.70408
919	0.70765	0.70356

Unit: El Chichon D
Thin Section: CHI-9615
Crystal: D

Microprobe analyses

Pos. (μm)	Na2O	Al2O3	SiO2	K2O	CaO	FeO	SrO	Total
0.0	6.90	43.63	39.09	0.54	8.88	0.33	0.25	99.34
4.5	7.36	43.01	39.62	0.61	8.50	0.13	0.27	99.30
9.1	7.21	43.22	39.45	0.61	8.62	0.43	0.23	99.80
13.6	8.02	42.14	40.38	0.68	7.96	0.37	0.25	99.76
18.2	7.55	42.77	39.84	0.65	8.34	0.27	0.29	99.36
22.7	7.89	42.31	40.24	0.73	8.06	0.11	0.24	99.61
27.3	8.33	41.72	40.74	0.89	7.70	0.31	0.22	99.37
31.8	6.96	43.55	39.16	0.68	8.83	0.47	0.29	99.69
36.3	6.99	43.51	39.20	0.69	8.80	0.23	0.24	99.33
40.9	7.46	42.89	39.73	0.64	8.42	0.26	0.19	99.57
45.4	9.70	39.90	42.31	1.08	6.59	0.47	0.19	99.51
50.0	9.70	39.90	42.31	1.05	6.59	0.41	0.18	99.65
54.5	7.52	42.81	39.80	0.61	8.37	0.16	0.15	99.49
59.1	8.05	42.10	40.42	0.84	7.93	0.04	0.16	99.15
63.6	8.74	41.17	41.21	0.80	7.37	0.19	0.20	99.22
68.1	6.96	43.55	39.16	0.62	8.83	0.26	0.21	99.60
72.7	6.44	44.25	38.55	0.47	9.26	0.49	0.25	99.60
77.2	5.70	45.23	37.71	0.35	9.86	0.17	0.27	99.57
81.8	6.22	44.54	38.31	0.52	9.43	0.14	0.22	99.15
86.3	6.53	44.13	38.66	0.48	9.18	0.01	0.27	99.02
90.9	6.04	44.78	38.09	0.40	9.58	0.10	0.20	99.24
95.4	6.13	44.66	38.20	0.39	9.51	0.20	0.30	99.64
99.9	6.65	43.96	38.80	0.49	9.08	0.24	0.20	99.48
104.5	7.36	43.01	39.62	0.62	8.50	0.04	0.20	99.02
109.0	8.24	41.85	40.63	0.79	7.78	0.37	0.18	99.73
113.6	8.08	42.06	40.45	0.83	7.91	0.47	0.25	100.01
118.1	7.63	42.66	39.93	0.73	8.28	0.45	0.28	99.52
122.7	7.21	43.22	39.45	0.65	8.62	0.41	0.16	99.84
127.2	7.77	42.47	40.09	0.69	8.17	0.20	0.22	99.14
131.7	6.74	43.84	38.91	0.56	9.01	0.21	0.25	99.54
136.3	7.80	42.43	40.13	0.66	8.14	0.16	0.18	99.37
140.8	8.81	41.09	41.29	0.94	7.32	0.25	0.19	99.72
145.4	6.37	44.33	38.48	0.53	9.31	0.14	0.25	99.10
149.9	7.46	42.89	39.73	0.75	8.42	0.34	0.28	99.63
154.5	8.62	41.34	41.07	0.88	7.47	0.07	0.28	99.20
159.0	8.84	41.05	41.32	0.92	7.29	0.36	0.21	99.74
163.5	9.86	39.69	42.50	1.13	6.46	0.15	0.25	99.56
168.1	10.24	39.18	42.94	1.18	6.14	0.50	0.22	99.48
172.6	10.72	38.53	43.50	1.19	5.75	0.42	0.29	99.48
177.2	9.60	40.03	42.20	1.00	6.67	0.36	0.21	99.63
181.7	10.05	39.43	42.72	1.09	6.30	0.26	0.17	99.32
186.3	9.66	39.95	42.28	1.02	6.61	0.42	0.27	99.87
190.8	10.05	39.43	42.72	1.16	6.30	0.20	0.20	99.70
195.3	9.00	40.84	41.51	0.99	7.16	0.22	0.27	99.27
199.9	9.57	40.07	42.17	0.94	6.69	0.40	0.26	99.44
204.4	9.76	39.82	42.39	1.08	6.53	0.02	0.24	99.42
209.0	9.66	39.95	42.28	0.96	6.61	0.44	0.22	99.46
213.5	8.84	41.05	41.32	0.96	7.29	0.35	0.27	99.33
218.1	9.54	40.12	42.13	1.05	6.72	0.09	0.28	99.32

ICP-MS

Pos. (μm)	87/86	87/86
5	0.70271	0.70374
11	0.70183	0.70411
16	0.70206	0.70416
21	0.70304	0.70350
27	0.70260	0.70416
32	0.70309	0.70300
37	0.70285	0.70467
43	0.70238	0.70385
48		0.70460
53	0.70261	0.70392
59	0.70412	0.70359
64	0.70291	0.70419
69	0.70362	0.70390
75	0.70285	0.70323
80	0.70332	0.70374
85	0.70196	0.70387
91	0.70313	0.70336
96	0.70366	0.70397
102	0.70312	0.70381
107	0.70306	0.70383
112	0.70290	0.70430
118	0.70298	0.70334
123	0.70328	0.70466
128	0.70232	0.70430
134	0.70272	0.70316
139	0.70302	0.70521
144	0.70223	0.70473
150	0.70388	0.70347
155	0.70314	0.70386
160	0.70376	0.70460
166	0.70310	0.70453
171	0.70340	0.70428
176	0.70244	0.70379
182	0.70253	0.70413
187	0.70197	0.70391
192	0.70288	0.70347
198	0.70309	0.70453
203	0.70272	0.70343
208	0.70212	0.70383
214	0.70397	0.70472
219	0.70201	0.70384
224	0.70422	0.70515
230	0.70318	0.70367
235	0.70341	0.70478
241	0.70374	0.70410
246	0.70347	0.70365
251	0.70297	0.70428
257		0.70482
262	0.70283	0.70422

Pos. (μm)	Na2O	Al2O3	SiO2	K2O	CaO	FeO	SrO	Total
222.6	9.70	39.90	42.31	1.12	6.59	0.37	0.30	99.79
227.1	8.84	41.05	41.32	0.85	7.29	0.42	0.24	99.88
231.7	8.84	41.05	41.32	0.82	7.29	0.28	0.20	99.75
236.2	8.62	41.34	41.07	0.81	7.47	0.08	0.20	99.17
240.8	9.60	40.03	42.20	1.01	6.67	0.32	0.16	99.69
245.3	10.34	39.05	43.05	1.07	6.06	0.22	0.21	99.26
249.9	10.85	38.36	43.65	1.10	5.64	0.29	0.19	99.57
254.4	10.05	39.43	42.72	1.16	6.30	0.15	0.22	99.63
258.9	9.63	39.99	42.24	0.96	6.64	0.10	0.26	99.24
263.5	8.18	41.93	40.56	0.78	7.83	0.01	0.17	99.37
268.0	10.21	39.22	42.90	1.03	6.17	0.44	0.17	99.67
272.6	9.92	39.61	42.57	1.12	6.40	0.11	0.24	99.46
277.1	10.05	39.43	42.72	1.08	6.30	0.18	0.25	99.72
281.7	9.03	40.79	41.54	0.96	7.13	0.13	0.29	99.27
286.2	9.47	40.20	42.06	0.95	6.77	0.45	0.26	99.65
290.7	9.22	40.54	41.76	0.92	6.98	0.13	0.23	99.45
295.3	8.65	41.30	41.11	0.93	7.45	0.29	0.15	99.37
299.8	10.34	39.05	43.05	1.15	6.06	0.16	0.27	99.43
304.4	9.76	39.82	42.39	0.97	6.53	0.13	0.18	99.26
308.9	8.74	41.17	41.21	0.79	7.37	0.01	0.25	99.37
313.5	8.21	41.89	40.60	0.87	7.81	0.48	0.26	99.59
318.0	9.03	40.79	41.54	0.94	7.13	0.48	0.19	99.47
322.5	7.77	42.47	40.09	0.82	8.17	0.41	0.23	99.37
327.1	8.93	40.92	41.43	0.97	7.21	0.17	0.22	99.18
331.6	8.33	41.72	40.74	0.82	7.70	0.22	0.17	99.15
336.2	8.43	41.60	40.85	0.81	7.63	0.03	0.18	99.03
340.7	8.36	41.68	40.78	0.74	7.68	0.49	0.23	99.49
345.3	9.35	40.37	41.91	0.90	6.87	0.21	0.18	99.68
349.8	10.05	39.43	42.72	0.99	6.30	0.09	0.26	99.57
354.3	9.70	39.90	42.31	0.98	6.59	0.23	0.19	99.44
358.9	9.76	39.82	42.39	0.95	6.53	0.13	0.15	99.17
363.4	8.68	41.26	41.14	0.82	7.42	0.10	0.25	99.44
368.0	7.55	42.77	39.84	0.61	8.34	0.32	0.29	99.78
372.5	7.61	42.68	39.91	0.71	8.29	0.04	0.27	99.46
377.1	8.05	42.10	40.42	0.80	7.93	0.06	0.24	99.17
381.6	9.12	40.67	41.65	0.97	7.06	0.09	0.17	99.22
386.1	7.08	43.39	39.30	0.54	8.73	0.48	0.28	99.87
390.7	8.11	42.01	40.49	0.75	7.88	0.47	0.27	99.85
395.2	8.24	41.85	40.63	0.71	7.78	0.14	0.17	99.44
399.8	7.68	42.60	39.98	0.78	8.24	0.03	0.28	99.50
404.3	7.83	42.39	40.16	0.67	8.11	0.09	0.22	99.31
408.9	8.87	41.01	41.36	0.79	7.26	0.37	0.16	99.44
413.4	7.52	42.81	39.80	0.68	8.37	0.33	0.20	99.48
417.9	7.71	42.56	40.02	0.70	8.22	0.47	0.23	99.63
422.5	7.68	42.60	39.98	0.66	8.24	0.30	0.28	99.75
427.0	8.43	41.60	40.85	0.93	7.63	0.39	0.18	99.64
431.6	8.46	41.55	40.89	0.87	7.60	0.24	0.28	99.79
436.1	8.68	41.26	41.14	0.91	7.42	0.40	0.22	99.52
440.7	7.55	42.77	39.84	0.75	8.34	0.24	0.15	99.23
445.2	8.18	41.93	40.56	0.70	7.83	0.09	0.27	99.17
449.7	7.49	42.85	39.77	0.68	8.40	0.48	0.28	99.94
454.3	7.77	42.47	40.09	0.64	8.17	0.12	0.19	99.46
458.8	7.61	42.68	39.91	0.74	8.29	0.35	0.22	99.87
463.4	8.59	41.39	41.03	0.82	7.50	0.08	0.16	99.32

Pos. (μm)	87/86	87/86
267	0.70312	0.70442
273	0.70368	0.70485
278	0.70347	0.70395
283	0.70310	0.70397
289	0.70353	0.70449
294	0.70381	0.70427
299	0.70367	0.70477
305	0.70309	0.70420
310	0.70248	0.70472
315	0.70295	0.70357
321	0.70311	0.70515
326	0.70382	0.70569
331	0.70262	0.70421
337	0.70361	0.70481
342	0.70324	0.70461
347	0.70464	0.70437
353	0.70356	0.70429
358	0.70319	0.70457
363	0.70413	0.70454
369	0.70378	0.70442
374	0.70402	0.70369
380	0.70387	0.70409
385	0.70340	0.70459
390	0.70370	0.70419
396	0.70339	0.70409
401	0.70406	0.70430
406	0.70273	0.70428
412	0.70323	0.70484
417	0.70441	0.70524
422	0.70442	0.70461
428	0.70325	0.70363
433	0.70370	0.70471
438	0.70329	0.70364
444	0.70371	0.70445
449	0.70423	0.70425
454	0.70372	0.70453
460	0.70320	0.70547
465	0.70421	0.70349
470	0.70404	0.70419
476	0.70346	0.70377
481	0.70398	0.70368
486	0.70282	0.70456
492		0.70334
497	0.70252	0.70442
503	0.70378	
508	0.70383	0.70496
513	0.70420	0.70403
519	0.70375	0.70429
524	0.70353	0.70206
529	0.70390	0.70377
535	0.70367	0.70440
540	0.70302	0.70373
545	0.70401	0.70464
551	0.70302	0.70389

Pos. (μm)	Na2O	Al2O3	SiO2	K2O	CaO	FeO	SrO	Total
467.9	7.30	43.10	39.55	0.56	8.55	0.36	0.24	99.45
472.5	8.08	42.06	40.45	0.83	7.91	0.03	0.29	99.29
477.0	8.08	42.06	40.45	0.80	7.91	0.19	0.17	99.15
481.5	7.64	42.64	39.95	0.63	8.27	0.26	0.16	99.67
486.1	7.99	42.18	40.34	0.85	7.99	0.46	0.20	99.54
490.6	8.84	41.05	41.32	0.89	7.29	0.02	0.17	98.98
495.2	10.18	39.26	42.87	1.07	6.19	0.08	0.29	99.51
499.7	9.70	39.90	42.31	0.93	6.59	0.37	0.22	99.66
504.3	9.98	39.52	42.65	1.02	6.35	0.25	0.29	99.48
508.8	8.96	40.88	41.47	0.83	7.19	0.26	0.28	99.45
513.3	8.65	41.30	41.11	0.88	7.45	0.09	0.23	99.31
517.9	8.14	41.97	40.53	0.81	7.86	0.22	0.25	99.26
522.4	9.98	39.52	42.65	0.96	6.35	0.27	0.27	99.70
527.0	8.84	41.05	41.32	0.96	7.29	0.09	0.28	99.67
531.5	10.18	39.26	42.87	1.05	6.19	0.47	0.20	99.70
536.1	10.43	38.92	43.16	1.11	5.98	0.39	0.25	99.50
540.6	9.31	40.41	41.87	0.91	6.90	0.13	0.16	99.49
545.1	7.33	43.06	39.59	0.61	8.52	0.23	0.27	99.22
549.7	8.74	41.17	41.21	0.87	7.37	0.47	0.21	99.72
554.2	9.57	40.07	42.17	1.08	6.69	0.45	0.19	99.54
558.8	7.80	42.43	40.13	0.75	8.14	0.12	0.30	99.32
563.3	8.18	41.93	40.56	0.89	7.83	0.34	0.15	99.21
567.9	6.81	43.76	38.98	0.49	8.95	0.03	0.17	99.08
572.4	8.81	41.09	41.29	0.88	7.32	0.15	0.17	99.19
576.9	7.64	42.64	39.95	0.72	8.27	0.49	0.16	99.51
581.5	9.35	40.37	41.91	0.98	6.87	0.41	0.26	99.45
586.0	9.28	40.46	41.84	0.99	6.93	0.48	0.24	99.80
590.6	10.34	39.05	43.05	1.09	6.06	0.22	0.24	99.41
595.1	9.98	39.52	42.65	1.04	6.35	0.07	0.25	99.37
599.7	10.38	38.98	43.11	1.12	6.02	0.03	0.18	99.10
604.2	8.30	41.76	40.71	0.79	7.73	0.48	0.23	99.74
608.7	8.55	41.43	41.00	0.91	7.52	0.48	0.21	99.58
613.3	9.38	40.33	41.95	0.96	6.85	0.50	0.16	99.83
617.8	9.50	40.16	42.09	1.04	6.74	0.27	0.21	99.57
622.4	9.06	40.75	41.58	0.88	7.11	0.07	0.28	99.41
626.9	9.66	39.95	42.28	0.92	6.61	0.07	0.18	99.18
631.5	9.41	40.29	41.98	0.89	6.82	0.48	0.18	99.50
636.0	9.50	40.16	42.09	0.92	6.74	0.34	0.27	99.42
640.5	8.65	41.30	41.11	0.93	7.45	0.21	0.29	99.21
645.1	9.44	40.24	42.02	0.91	6.80	0.18	0.25	99.58
649.6	9.73	39.86	42.35	1.00	6.56	0.26	0.18	99.51
654.2	10.05	39.43	42.72	1.17	6.30	0.32	0.19	99.44
658.7	9.57	40.07	42.17	1.06	6.69	0.11	0.19	99.09
663.3	10.85	38.36	43.65	1.23	5.64	0.09	0.22	99.30
667.8	9.15	40.63	41.69	1.01	7.03	0.21	0.23	99.30
672.3	9.70	39.90	42.31	1.11	6.59	0.32	0.19	99.27
676.9	10.18	39.26	42.87	1.09	6.19	0.16	0.19	99.25
681.4	10.19	39.24	42.89	1.09	6.18	0.04	0.25	99.12
686.0	9.63	39.99	42.24	1.07	6.64	0.48	0.18	99.57
690.5	9.86	39.69	42.50	0.94	6.46	0.27	0.19	99.71
695.1	9.09	40.71	41.62	0.96	7.08	0.48	0.20	99.64
699.6	9.76	39.82	42.39	0.98	6.53	0.35	0.19	99.49
704.1	10.08	39.39	42.76	1.14	6.27	0.44	0.19	99.45
708.7	9.57	40.07	42.17	0.98	6.69	0.39	0.28	99.51

Pos. (μm)	87/86	87/86
556	0.70386	0.70379
561	0.70452	0.70418
567	0.70358	0.70358
572	0.70342	0.70461
577	0.70336	0.70454
583	0.70304	0.70422
588	0.70383	0.70370
593	0.70274	0.70408
599	0.70328	0.70397
604	0.70297	0.70494
609	0.70344	0.70441
615	0.70397	0.70447
620	0.70300	0.70314
625	0.70252	0.70443
631	0.70376	0.70437
636	0.70310	0.70373
641	0.70301	0.70409
647	0.70294	
652	0.70275	
658	0.70369	0.70418
663	0.70248	0.70348
668	0.70282	0.70427
674	0.70217	0.70399
679	0.70271	0.70465
684	0.70372	
690	0.70442	0.70354
695		0.70308
700	0.70276	0.70347
706	0.70234	0.70419
711	0.70246	0.70365
716	0.70316	0.70402
722	0.70240	
727	0.70428	0.70246
732	0.70294	0.70446
738		0.70407
743	0.70274	0.70383
748	0.70374	0.70274
754	0.70339	0.70356
759	0.70399	0.70331
764	0.70230	0.70405
770	0.70296	0.70347
775	0.70356	
781	0.70315	0.70322
786	0.70316	
791	0.70320	0.70450
797	0.70315	0.70317
802		0.70465
807	0.70247	0.70414
813	0.70264	0.70364
818	0.70228	0.70486
823	0.70243	0.70462
829	0.70363	0.70291
834	0.70313	0.70450
839	0.70310	0.70491

Pos. (µm)	Na2O	Al2O3	SiO2	K2O	CaO	FeO	SrO	Total
713.2	10.82	38.40	43.61	1.18	5.67	0.09	0.27	99.43
717.8	9.73	39.86	42.35	1.00	6.56	0.45	0.26	99.61
722.3	10.37	39.01	43.09	1.11	6.04	0.06	0.27	99.03
726.9	10.30	39.09	43.02	1.11	6.09	0.31	0.17	99.55
731.4	9.31	40.41	41.87	0.97	6.90	0.11	0.21	99.48
735.9	10.24	39.18	42.94	1.05	6.14	0.49	0.17	99.92
740.5	9.47	40.20	42.06	0.93	6.77	0.43	0.21	99.66
745.0	10.79	38.45	43.57	1.10	5.69	0.49	0.23	99.76
749.6	8.62	41.34	41.07	0.83	7.47	0.39	0.22	99.41
754.1	9.47	40.20	42.06	1.06	6.77	0.49	0.23	99.87
758.7	10.24	39.18	42.94	1.13	6.14	0.18	0.27	99.62
763.2	9.60	40.03	42.20	1.01	6.67	0.48	0.17	99.54
767.7	9.54	40.12	42.13	0.96	6.72	0.24	0.30	99.41
772.3	9.22	40.54	41.76	0.86	6.98	0.36	0.24	99.41
776.8	8.77	41.13	41.25	0.90	7.34	0.45	0.21	99.91
781.4	7.89	42.31	40.24	0.76	8.06	0.43	0.19	99.63
785.9	9.35	40.37	41.91	0.93	6.87	0.07	0.27	99.54
790.5	10.08	39.39	42.76	1.05	6.27	0.44	0.21	99.39
795.0	10.30	39.09	43.02	1.11	6.09	0.40	0.29	99.58
799.5	10.18	39.26	42.87	1.13	6.19	0.48	0.20	99.51
804.1	9.95	39.56	42.61	1.15	6.38	0.03	0.27	99.19
808.6	12.12	36.67	45.11	1.47	4.60	0.20	0.30	99.75
813.2	10.24	39.18	42.94	1.01	6.14	0.40	0.23	99.38
817.7	10.37	39.01	43.09	1.15	6.04	0.16	0.26	99.65
822.3	9.89	39.65	42.53	1.08	6.43	0.17	0.26	99.51
826.8	11.14	37.97	43.98	1.33	5.40	0.15	0.28	99.68
831.3	9.95	39.56	42.61	0.97	6.38	0.08	0.22	99.11
835.9	9.28	40.46	41.84	0.88	6.93	0.03	0.17	99.44
840.4	9.22	40.54	41.76	1.01	6.98	0.14	0.27	99.14
845.0	10.05	39.43	42.72	1.01	6.30	0.00	0.26	99.22
849.5	9.06	40.75	41.58	0.83	7.11	0.09	0.28	99.63
854.1	9.06	40.75	41.58	0.94	7.11	0.34	0.15	99.64
858.6	9.35	40.37	41.91	1.05	6.87	0.20	0.19	99.36
863.1	9.31	40.41	41.87	0.96	6.90	0.14	0.16	99.13
867.7	9.09	40.71	41.62	0.89	7.08	0.00	0.26	99.37
872.2	8.55	41.43	41.00	0.86	7.52	0.32	0.16	99.51
876.8	9.70	39.90	42.31	1.04	6.59	0.23	0.28	99.71
881.3	9.63	39.99	42.24	0.95	6.64	0.21	0.27	99.64
885.9	9.63	39.99	42.24	0.92	6.64	0.21	0.29	99.58
890.4	10.66	38.62	43.42	1.21	5.80	0.23	0.20	99.32
894.9	10.50	38.83	43.24	1.08	5.93	0.22	0.22	99.72
899.5	9.95	39.56	42.61	1.00	6.38	0.05	0.30	99.18
904.0	9.15	40.63	41.69	0.84	7.03	0.32	0.16	99.68
908.6	8.11	42.01	40.49	0.78	7.88	0.46	0.23	99.91
913.1	8.33	41.72	40.74	0.86	7.70	0.37	0.18	99.84
917.7	8.84	41.05	41.32	0.82	7.29	0.40	0.22	99.60
922.2	8.74	41.17	41.21	0.83	7.37	0.01	0.19	99.32
926.7	8.24	41.85	40.63	0.81	7.78	0.04	0.16	99.13
931.3	8.02	42.14	40.38	0.76	7.96	0.12	0.21	99.32
935.8	7.21	43.22	39.45	0.63	8.62	0.38	0.16	99.57
940.4	7.39	42.97	39.66	0.67	8.47	0.37	0.23	99.54
944.9	5.97	44.87	38.02	0.48	9.64	0.07	0.19	99.06
949.5	6.50	44.17	38.63	0.60	9.21	0.50	0.19	99.86
954.0	7.80	42.43	40.13	0.75	8.14	0.09	0.27	99.33

Pos. (µm)	87/86	87/86
845	0.70276	0.70461
850	0.70259	0.70416
855	0.70367	0.70383
861	0.70329	0.70411
866	0.70277	0.70371
871	0.70244	0.70381
877	0.70131	0.70293
882	0.70176	0.70301
887	0.70326	0.70368
893	0.70349	0.70335
898	0.70310	0.70263
903	0.70345	0.70230
909	0.70371	0.70438
914	0.70291	0.70391
919	0.70210	0.70374
925	0.70336	0.70367
930	0.70367	0.70494
936	0.70359	0.70387
941	0.70390	0.70424
946	0.70319	
952		0.70391
957	0.70430	0.70451
962	0.70314	0.70294
968	0.70397	0.70439
973	0.70350	0.70467
978	0.70316	0.70384
984	0.70302	0.70330
989	0.70328	0.70416
994	0.70246	
1000	0.70268	0.70374
1005	0.70366	0.70513
1010	0.70366	0.70811
1016	0.70674	0.70625
1021	0.70667	0.70518

Pos. (µm)	Na2O	Al2O3	SiO2	K2O	CaO	FeO	SrO	Total
958.5	8.81	41.09	41.29	0.98	7.32	0.37	0.25	99.86
963.1	7.15	43.30	39.37	0.66	8.68	0.38	0.22	99.68
967.6	8.14	41.97	40.53	0.75	7.86	0.29	0.22	99.49
972.2	8.77	41.13	41.25	0.93	7.34	0.09	0.28	99.66
976.7	8.52	41.47	40.96	0.86	7.55	0.41	0.18	99.83
981.3	7.61	42.68	39.91	0.76	8.29	0.14	0.16	99.38
985.8	8.81	41.09	41.29	0.92	7.32	0.50	0.17	99.79
990.3	8.74	41.17	41.21	0.92	7.37	0.09	0.15	99.27
994.9	8.49	41.51	40.92	0.90	7.57	0.47	0.21	99.56
999.4	8.62	41.34	41.07	0.88	7.47	0.35	0.27	99.80
1004.0	8.36	41.68	40.78	0.88	7.68	0.27	0.16	99.36
1008.5	8.65	41.30	41.11	0.87	7.45	0.22	0.18	99.25
1013.1	9.35	40.37	41.91	1.01	6.87	0.29	0.27	99.47
1017.6	9.25	40.50	41.80	0.89	6.95	0.45	0.23	99.50

Pos. (µm)	87/86	87/86

Unit: El Chichon D
Thin Section: CHI-9615
Crystal: E

Microprobe analyses

Pos. (μm)	Na2O	Al2O3	SiO2	K2O	CaO	FeO	SrO	Total
0.0	8.66	41.28	41.12	0.86	7.43	0.20	0.22	99.43
6.9	9.33	40.39	41.89	0.86	6.89	0.05	0.23	99.00
13.7	8.57	41.41	41.01	0.66	7.51	0.16	0.25	99.19
20.6	9.28	40.46	41.84	0.78	6.93	0.09	0.15	99.31
27.5	8.47	41.53	40.91	0.72	7.59	0.07	0.29	99.12
34.3	7.77	42.47	40.09	0.60	8.17	0.01	0.16	99.05
41.2	8.95	40.90	41.45	0.86	7.20	0.00	0.16	99.24
48.1	8.71	41.22	41.18	0.70	7.39	0.18	0.16	99.20
54.9	7.91	42.29	40.25	0.60	8.05	0.39	0.15	99.48
61.8	7.16	43.28	39.39	0.44	8.66	0.12	0.25	99.46
68.7	8.85	41.03	41.34	0.82	7.28	0.28	0.25	99.78
75.5	9.23	40.52	41.78	0.79	6.97	0.45	0.25	99.42
82.4	8.43	41.60	40.85	0.66	7.63	0.32	0.28	99.81
89.3	8.62	41.34	41.07	0.76	7.47	0.35	0.26	99.61
96.1	8.71	41.22	41.18	0.75	7.39	0.41	0.26	99.75
103.0	7.25	43.16	39.50	0.61	8.59	0.01	0.24	99.01
109.9	9.28	40.46	41.84	0.89	6.93	0.02	0.22	98.98
116.7	8.33	41.72	40.74	0.67	7.70	0.34	0.21	99.67
123.6	11.16	37.95	44.00	1.04	5.39	0.37	0.29	99.61
130.5	10.05	39.43	42.72	1.05	6.30	0.48	0.27	99.47
137.3	6.47	44.21	38.59	0.36	9.23	0.25	0.20	99.65
144.2	10.58	38.73	43.33	1.05	5.86	0.49	0.28	99.77
151.1	10.10	39.37	42.77	0.90	6.26	0.22	0.24	99.65
157.9	7.12	43.35	39.34	0.44	8.70	0.45	0.28	99.93
164.8	6.93	43.59	39.12	0.51	8.85	0.44	0.19	99.34
171.7	8.76	41.15	41.23	0.82	7.35	0.20	0.22	99.44
178.6	9.00	40.84	41.51	0.77	7.16	0.10	0.27	99.25
185.4	9.52	40.14	42.11	0.96	6.73	0.30	0.15	99.33
192.3	8.85	41.03	41.34	0.86	7.28	0.07	0.28	99.49
199.2	8.19	41.91	40.58	0.70	7.82	0.37	0.30	99.83
206.0	6.51	44.15	38.64	0.51	9.19	0.19	0.19	99.14
212.9	6.47	44.21	38.59	0.46	9.23	0.38	0.17	99.57
219.8	6.10	44.70	38.16	0.28	9.53	0.17	0.22	99.60
226.6	7.30	43.10	39.55	0.66	8.55	0.34	0.21	99.28
233.5	6.24	44.52	38.32	0.35	9.42	0.17	0.16	99.42
240.4	8.10	42.04	40.47	0.75	7.90	0.43	0.21	99.91
247.2	7.21	43.22	39.45	0.64	8.62	0.37	0.18	99.75
254.1	6.88	43.66	39.07	0.50	8.89	0.46	0.29	99.90
261.0	7.82	42.41	40.15	0.54	8.13	0.41	0.15	99.52
267.8	8.05	42.10	40.42	0.60	7.93	0.09	0.24	99.33
274.7	8.14	41.97	40.53	0.70	7.86	0.49	0.29	100.04
281.6	8.52	41.47	40.96	0.80	7.55	0.19	0.21	99.32
288.4	9.57	40.07	42.17	0.88	6.69	0.41	0.21	99.82
295.3	8.38	41.66	40.80	0.72	7.66	0.21	0.25	99.22
302.2	9.76	39.82	42.39	0.95	6.53	0.46	0.23	99.74
309.0	9.09	40.71	41.62	0.86	7.08	0.15	0.19	99.36
315.9	10.05	39.43	42.72	1.04	6.30	0.19	0.30	99.74
322.8	8.43	41.60	40.85	0.64	7.63	0.28	0.19	99.41
329.6	9.71	39.88	42.33	0.95	6.57	0.26	0.28	99.48

ICP-MS

Pos. (μm)	87/86	87/86
5	0.70176	0.70384
11	0.70528	0.70440
16	0.70486	0.70477
21	0.70397	0.70390
27	0.70387	0.70447
32	0.70410	
37	0.70330	
43	0.70304	
48	0.70522	0.70515
53	0.70384	0.70580
59	0.70311	0.70401
64	0.70530	0.70480
69	0.70456	0.70559
75	0.70572	0.70447
80	0.70176	0.70464
85	0.70467	0.70407
91	0.70162	0.70330
96	0.70392	0.70436
102	0.70490	0.70527
107	0.70486	0.70367
112	0.70174	0.70470
118	0.70500	0.70471
123	0.70210	0.70539
128	0.70231	0.70311
134	0.69958	0.70356
139	0.70095	0.70402
144	0.70038	0.70435
150	0.70170	0.70473
155	0.70190	0.70429
160	0.70083	0.70481
166	0.70146	0.70601
171	0.69752	0.70406
176	0.69969	0.70625
182	0.70088	0.70530
187	0.70278	0.70483
192	0.70376	0.70336
198	0.70320	0.70432
203	0.69904	0.70457
208	0.69925	0.70448
214	0.70215	0.70456
219	0.70076	0.70361
224	0.70455	0.70282
230	0.70174	0.70396
235	0.70268	0.70380
241	0.70107	0.70378
246	0.70329	0.70500
251	0.70129	0.70565
257	0.70019	0.70525
262	0.70236	0.70454

Pos. (μm)	Na2O	Al2O3	SiO2	K2O	CaO	FeO	SrO	Total
336.5	10.10	39.37	42.77	0.99	6.26	0.18	0.19	99.58
343.4	8.66	41.28	41.12	0.70	7.43	0.04	0.19	99.41
350.2	9.38	40.33	41.95	0.80	6.85	0.04	0.28	99.33
357.1	9.66	39.95	42.28	0.88	6.61	0.14	0.22	99.61
364.0	8.52	41.47	40.96	0.73	7.55	0.12	0.15	99.02
370.8	9.28	40.46	41.84	0.91	6.93	0.31	0.18	99.65
377.7	8.90	40.96	41.40	0.89	7.24	0.36	0.22	99.79
384.6	9.38	40.33	41.95	0.97	6.85	0.20	0.16	99.62
391.4	8.38	41.66	40.80	0.75	7.66	0.31	0.29	99.80
398.3	8.95	40.90	41.45	0.73	7.20	0.19	0.25	99.16
405.2	8.71	41.22	41.18	0.72	7.39	0.46	0.20	99.52
412.0	8.90	40.96	41.40	0.90	7.24	0.30	0.16	99.39
418.9	9.19	40.58	41.73	0.88	7.00	0.29	0.20	99.72
425.8	9.09	40.71	41.62	0.76	7.08	0.41	0.21	99.77
432.6	8.52	41.47	40.96	0.77	7.55	0.37	0.22	99.68
439.5	9.47	40.20	42.06	0.87	6.77	0.23	0.19	99.67
446.4	8.00	42.16	40.36	0.59	7.97	0.29	0.16	99.24
453.2	9.38	40.33	41.95	0.92	6.85	0.35	0.26	99.61
467.0	9.04	40.77	41.56	0.73	7.12	0.35	0.16	99.35
473.8	8.71	41.22	41.18	0.78	7.39	0.14	0.17	99.21
480.7	9.71	39.88	42.33	0.89	6.57	0.38	0.18	99.48
487.6	8.47	41.53	40.91	0.72	7.59	0.00	0.28	99.10
494.4	8.62	41.34	41.07	0.73	7.47	0.48	0.28	99.49
501.3	8.95	40.90	41.45	0.77	7.20	0.24	0.16	99.64
508.2	9.76	39.82	42.39	0.90	6.53	0.49	0.24	99.91
515.1	8.38	41.66	40.80	0.75	7.66	0.02	0.21	99.19
521.9	4.19	47.25	35.96	0.10	11.10	0.33	0.20	99.43
528.8	10.19	39.24	42.89	0.92	6.18	0.44	0.22	99.89
535.7	13.38	34.99	46.56	1.49	3.57	0.44	0.21	99.56
542.5	11.21	37.89	44.06	1.08	5.35	0.37	0.27	99.82
549.4	10.72	38.53	43.50	1.04	5.75	0.12	0.27	99.17
556.3	10.77	38.47	43.55	1.03	5.71	0.06	0.20	99.37
563.1	9.52	40.14	42.11	0.96	6.73	0.43	0.27	99.75
576.9	9.52	40.14	42.11	0.99	6.73	0.20	0.22	99.70
583.7	10.05	39.43	42.72	0.89	6.30	0.08	0.27	99.28
590.6	10.19	39.24	42.89	0.92	6.18	0.15	0.17	99.40
597.5	10.68	38.60	43.44	1.03	5.78	0.27	0.24	99.61
604.3	9.47	40.20	42.06	0.94	6.77	0.15	0.24	99.58
611.2	9.09	40.71	41.62	0.84	7.08	0.01	0.17	98.95
618.1	9.57	40.07	42.17	0.90	6.69	0.31	0.20	99.31
624.9	10.97	38.21	43.78	1.10	5.55	0.21	0.15	99.22
631.8	8.62	41.34	41.07	0.71	7.47	0.48	0.19	99.70
638.7	9.28	40.46	41.84	0.81	6.93	0.32	0.28	99.80
645.5	9.09	40.71	41.62	0.74	7.08	0.42	0.19	99.59
652.4	8.52	41.47	40.96	0.80	7.55	0.34	0.18	99.41
659.3	9.71	39.88	42.33	0.87	6.57	0.27	0.15	99.24
666.1	8.24	41.85	40.63	0.61	7.78	0.05	0.24	99.51
673.0	9.47	40.20	42.06	0.90	6.77	0.11	0.19	99.04
679.9	10.58	38.73	43.33	1.08	5.86	0.06	0.22	99.09
686.7	10.77	38.47	43.55	1.07	5.71	0.21	0.26	99.32
693.6	10.14	39.31	42.83	0.95	6.22	0.19	0.19	99.66
700.5	9.62	40.01	42.22	1.00	6.65	0.28	0.21	99.67

Pos. (μm)	87/86	87/86
267	0.70331	0.70443
273	0.70461	0.70253
278	0.70413	0.70477
283	0.70485	0.70456
289	0.70340	0.70502
294	0.70428	0.70456
299	0.70542	0.70449
305	0.70328	0.70566
310	0.70450	0.70240
315	0.70559	0.70186
321	0.70545	0.70138
326	0.70425	0.70385
331	0.70332	0.70524
337	0.70627	0.70684
342	0.70311	0.70520
347	0.70383	0.70436
353	0.70347	0.70396
358	0.70394	0.70426
363	0.70297	0.70305
369	0.70426	0.70420
374	0.70510	0.70222
379	0.70421	0.70235
385	0.70342	
390	0.70315	
396	0.70391	0.70415
401	0.70388	0.70343
406	0.70528	0.70491
412	0.70300	0.70452
417	0.70168	0.70411
422	0.70237	0.70411
428		0.70330
433	0.70407	0.70383
438	0.70357	0.70435
444	0.70494	
449	0.70491	0.70509
454	0.70339	0.70529
460	0.70684	0.70525
465	0.70393	0.70487
470	0.70624	0.70456
476	0.70442	
481	0.70253	0.70408
486	0.70411	0.70385
492	0.70408	0.70445
497	0.70289	0.70339
502	0.70293	
508	0.70394	
513	0.70534	
518	0.70478	
524	0.70046	
529	0.70131	0.70228
535	0.70177	0.70274
540	0.70301	0.70395
545	0.70062	0.70295
551	0.70302	0.70559

Pos. (μm)	Na2O	Al2O3	SiO2	K2O	CaO	FeO	SrO	Total
707.3	10.68	38.60	43.44	1.16	5.78	0.07	0.17	99.44
714.2	11.26	37.82	44.11	1.10	5.31	0.37	0.21	99.79
721.1	9.52	40.14	42.11	0.86	6.73	0.10	0.25	99.39
727.9	11.31	37.76	44.17	1.08	5.27	0.47	0.26	99.73
734.8	9.62	40.01	42.22	0.98	6.65	0.44	0.27	99.50
741.7	9.62	40.01	42.22	0.96	6.65	0.24	0.18	99.27
748.5	10.53	38.79	43.28	1.05	5.90	0.27	0.27	99.61
755.4	9.66	39.95	42.28	0.86	6.61	0.01	0.18	99.49
762.3	9.71	39.88	42.33	0.99	6.57	0.21	0.22	99.40
769.1	9.38	40.33	41.95	0.80	6.85	0.09	0.19	99.47
776.0	10.34	39.05	43.05	1.11	6.06	0.21	0.29	99.69
782.9	10.38	38.98	43.11	1.08	6.02	0.28	0.20	99.39
789.7	11.55	37.43	44.45	1.27	5.07	0.04	0.29	99.38
796.6	9.90	39.63	42.55	1.00	6.42	0.25	0.28	99.67
803.5	10.53	38.79	43.28	1.05	5.90	0.41	0.15	99.38
810.3	10.10	39.37	42.77	1.01	6.26	0.42	0.20	99.56
824.1	12.48	36.18	45.53	1.43	4.30	0.18	0.18	99.61
837.8	8.05	42.10	40.42	0.74	7.93	0.03	0.27	99.55
844.7	9.95	39.56	42.61	0.94	6.38	0.17	0.30	99.21
851.5	8.85	41.03	41.34	0.89	7.28	0.19	0.21	99.70
858.4	10.68	38.60	43.44	1.00	5.78	0.49	0.16	99.69
865.3	12.58	36.05	45.64	1.40	4.22	0.01	0.23	99.40
872.2	10.97	38.21	43.78	1.09	5.55	0.34	0.28	99.91
879.0	10.00	39.50	42.66	0.92	6.34	0.40	0.22	99.69
885.9	10.00	39.50	42.66	0.89	6.34	0.07	0.23	99.19
892.8	10.43	38.92	43.16	0.97	5.98	0.33	0.20	99.80
899.6	9.62	40.01	42.22	0.88	6.65	0.29	0.17	99.44
906.5	9.47	40.20	42.06	0.84	6.77	0.46	0.29	99.74
913.4	10.19	39.24	42.89	1.07	6.18	0.38	0.30	99.45
920.2	10.82	38.40	43.61	1.01	5.67	0.39	0.19	99.63
927.1	10.29	39.11	43.00	1.02	6.10	0.20	0.28	99.53
934.0	8.81	41.09	41.29	0.86	7.32	0.17	0.21	99.14
940.8	9.90	39.63	42.55	0.87	6.42	0.14	0.28	99.43
947.7	9.90	39.63	42.55	0.89	6.42	0.02	0.25	99.25
954.6	9.33	40.39	41.89	0.89	6.89	0.20	0.16	99.07
961.4	9.28	40.46	41.84	0.86	6.93	0.21	0.18	99.27
968.3	10.58	38.73	43.33	1.02	5.86	0.06	0.29	99.10
975.2	8.62	41.34	41.07	0.75	7.47	0.12	0.25	99.55
982.0	9.57	40.07	42.17	0.85	6.69	0.29	0.16	99.42
988.9	8.57	41.41	41.01	0.78	7.51	0.30	0.15	99.38
995.8	10.05	39.43	42.72	1.03	6.30	0.48	0.26	99.45
1002.6	10.24	39.18	42.94	1.01	6.14	0.34	0.27	99.33
1009.5	9.04	40.77	41.56	0.92	7.12	0.24	0.16	99.38
1016.4	8.33	41.72	40.74	0.62	7.70	0.43	0.25	99.89
1023.2	9.90	39.63	42.55	0.93	6.42	0.33	0.26	99.36
1030.1	10.48	38.86	43.22	1.09	5.94	0.03	0.19	99.04
1037.0	8.71	41.22	41.18	0.86	7.39	0.16	0.20	99.20
1043.8	11.36	37.69	44.23	1.12	5.23	0.36	0.22	99.32
1050.7	10.05	39.43	42.72	0.90	6.30	0.33	0.23	99.40
1057.6	10.10	39.37	42.77	0.92	6.26	0.41	0.21	99.62
1064.4	9.66	39.95	42.28	0.96	6.61	0.48	0.18	99.59
1071.3	12.68	35.92	45.76	1.38	4.14	0.40	0.16	99.48

Pos. (μm)	87/86	87/86
556	0.70394	0.70335
561		0.70298
567		0.70438
572		0.70386
577	0.70399	0.70424
583	0.70533	0.70378
588	0.70185	0.70383
593	0.70514	0.70298
599	0.70290	0.70339
604	0.70146	0.70319
609	0.70431	0.70381
615	0.70498	0.70278
620	0.70310	0.70319
625	0.70462	0.70342
631	0.70487	0.70330
636	0.70402	0.70305
641	0.70455	0.70443
647	0.70351	0.70379
652	0.70465	0.70463
657	0.70418	0.70520
663	0.70551	0.70523
668	0.70705	0.70393
673		0.70529
679	0.70260	
684	0.70393	0.70601
690	0.70327	0.70490
695	0.70459	0.70547
700	0.70498	0.70381
706		0.70435
711	0.70255	0.70436
716	0.70305	0.70426
722	0.70412	0.70510
727	0.70388	0.70471
732	0.70375	0.70322
738	0.70497	0.70312
743		0.70445
748		0.70153
754	0.70354	0.70270
759	0.70246	0.70191
764	0.70434	
770	0.70148	0.70372
775	0.70469	0.70292
780		0.70507
786	0.70477	0.70576
791	0.70337	
796	0.70350	0.70440
802	0.70338	0.70361
807	0.70490	0.70411
812	0.70347	0.70276
818	0.70415	0.70537
823	0.70356	0.70532
829	0.70600	0.70302
834	0.70474	0.70486
839	0.70656	0.70448

Pos. (µm)	Na2O	Al2O3	SiO2	K2O	CaO	FeO	SrO	Total
1078.2	8.76	41.15	41.23	0.73	7.35	0.45	0.20	99.61
1085.0	10.29	39.11	43.00	1.03	6.10	0.04	0.20	99.16
1091.9	10.77	38.47	43.55	1.11	5.71	0.01	0.24	99.20
1098.8	9.52	40.14	42.11	0.84	6.73	0.14	0.18	99.29
1105.6	9.86	39.69	42.50	0.86	6.46	0.14	0.29	99.41
1112.5	9.19	40.58	41.73	0.79	7.00	0.22	0.19	99.23
1119.4	8.71	41.22	41.18	0.86	7.39	0.14	0.25	99.40
1126.2	10.14	39.31	42.83	0.91	6.22	0.29	0.29	99.78
1133.1	10.63	38.66	43.39	1.02	5.82	0.46	0.17	99.40
1140.0	10.38	38.98	43.11	0.99	6.02	0.08	0.17	99.24
1146.8	8.24	41.85	40.63	0.60	7.78	0.44	0.16	99.81
1153.7	9.23	40.52	41.78	0.90	6.97	0.08	0.16	99.23
1160.6	9.66	39.95	42.28	1.01	6.61	0.06	0.22	99.12
1167.4	10.00	39.50	42.66	0.92	6.34	0.21	0.19	99.19
1174.3	9.33	40.39	41.89	0.83	6.89	0.46	0.18	99.92
1181.2	9.62	40.01	42.22	0.97	6.65	0.43	0.29	99.96
1188.0	9.71	39.88	42.33	0.83	6.57	0.15	0.22	99.63
1194.9	7.86	42.35	40.20	0.71	8.09	0.17	0.17	99.42
1201.8	9.57	40.07	42.17	0.97	6.69	0.05	0.26	99.08
1208.7	10.14	39.31	42.83	1.03	6.22	0.50	0.29	99.91
1215.5	8.76	41.15	41.23	0.88	7.35	0.32	0.18	99.77
1222.4	9.42	40.27	42.00	0.92	6.81	0.15	0.18	99.57
1229.3	8.81	41.09	41.29	0.72	7.32	0.38	0.15	99.25
1236.1	9.28	40.46	41.84	0.86	6.93	0.45	0.24	99.40
1243.0	9.57	40.07	42.17	0.99	6.69	0.34	0.26	99.63
1249.9	10.34	39.05	43.05	0.92	6.06	0.41	0.15	99.36
1256.7	10.38	38.98	43.11	1.07	6.02	0.33	0.28	99.49
1263.6	8.85	41.03	41.34	0.70	7.28	0.20	0.22	99.42
1270.5	9.38	40.33	41.95	0.81	6.85	0.44	0.20	99.78
1277.3	10.05	39.43	42.72	0.90	6.30	0.24	0.15	99.10
1284.2	8.71	41.22	41.18	0.82	7.39	0.00	0.21	99.24
1291.1	10.68	38.60	43.44	1.01	5.78	0.25	0.19	99.16
1297.9	10.00	39.50	42.66	1.00	6.34	0.45	0.26	99.68
1304.8	9.33	40.39	41.89	0.92	6.89	0.35	0.16	99.79
1311.7	9.23	40.52	41.78	0.81	6.97	0.45	0.25	99.86
1318.5	10.14	39.31	42.83	1.05	6.22	0.41	0.23	99.54
1325.4	9.81	39.75	42.44	1.00	6.50	0.21	0.28	99.64
1332.3	8.76	41.15	41.23	0.86	7.35	0.49	0.25	99.62
1339.1	10.43	38.92	43.16	0.95	5.98	0.22	0.25	99.45
1346.0	10.72	38.53	43.50	1.13	5.75	0.15	0.21	99.44
1352.9	9.38	40.33	41.95	0.92	6.85	0.38	0.29	99.77
1359.7	10.24	39.18	42.94	1.08	6.14	0.07	0.29	99.10
1366.6	9.04	40.77	41.56	0.90	7.12	0.34	0.19	99.37
1373.5	10.53	38.79	43.28	0.96	5.90	0.42	0.16	99.29
1380.3	9.09	40.71	41.62	0.78	7.08	0.45	0.15	99.48
1387.2	10.24	39.18	42.94	0.92	6.14	0.05	0.23	99.45
1394.1	9.95	39.56	42.61	0.94	6.38	0.04	0.29	99.22
1400.9	10.24	39.18	42.94	1.02	6.14	0.33	0.16	99.79
1407.8	9.90	39.63	42.55	0.98	6.42	0.22	0.26	99.46
1414.7	8.43	41.60	40.85	0.76	7.63	0.28	0.24	99.66
1421.5	6.93	43.59	39.12	0.59	8.85	0.38	0.30	99.41
1428.4	6.65	43.96	38.80	0.45	9.08	0.11	0.27	99.11
1435.3	8.90	40.96	41.40	0.89	7.24	0.41	0.20	99.52
1442.1	9.42	40.27	42.00	0.89	6.81	0.45	0.17	99.43

Pos. (µm)	87/86	87/86
845	0.70498	0.70406
850	0.70446	0.70495
855	0.70549	
861	0.70646	0.70506
866		0.70641
871		0.70481
877	0.70727	
882	0.70542	
887	0.70526	
893	0.70478	
898	0.70464	
903	0.70458	
909	0.70500	
914	0.70040	
919	0.70164	0.70416
925	0.70396	0.70348
930	0.70391	0.70314
935	0.70367	0.70463
941	0.70327	0.70567
946	0.70390	0.70505
951	0.70484	0.70526
957	0.70282	0.70434
962	0.70322	0.70300
968	0.70561	0.70361
973	0.70405	0.70399
978	0.70544	0.70244
984	0.70472	0.70524
989	0.70317	0.70555
994	0.70677	0.70497
1000	0.70382	0.70373
1005	0.70550	0.70531
1010	0.70444	0.70253
1016	0.70339	0.70404
1021	0.70477	0.70451
1026		0.70488
1032	0.70448	0.70609
1037	0.70318	0.70410
1042	0.70228	0.70517
1048	0.70462	0.70560
1053	0.70317	0.70480
1058	0.70599	0.70462
1064	0.70445	0.70405
1069	0.70386	
1074	0.70476	0.70542
1080	0.70589	0.70527
1085	0.70504	0.70427
1091	0.70294	0.70347
1096	0.70386	0.70357
1101	0.70557	0.70316
1107	0.70282	0.70350
1112	0.70644	0.70515
1117	0.70494	0.70223
1123	0.70408	0.70318
1128	0.70342	0.70511

Pos. (µm)	Na2O	Al2O3	SiO2	K2O	CaO	FeO	SrO	Total
1449.0	10.43	38.92	43.16	0.98	5.98	0.12	0.24	99.23
1455.9	9.71	39.88	42.33	1.00	6.57	0.33	0.27	99.64
1462.7	9.52	40.14	42.11	0.97	6.73	0.04	0.23	99.34
1469.6	8.90	40.96	41.40	0.84	7.24	0.48	0.23	99.68
1476.5	7.86	42.35	40.20	0.57	8.09	0.08	0.18	99.22
1483.3	8.19	41.91	40.58	0.78	7.82	0.48	0.16	99.93
1490.2	10.19	39.24	42.89	0.98	6.18	0.14	0.20	99.19
1497.1	8.62	41.34	41.07	0.79	7.47	0.49	0.20	99.58
1503.9	8.57	41.41	41.01	0.70	7.51	0.27	0.17	99.47
1510.8	8.43	41.60	40.85	0.75	7.63	0.06	0.17	99.12
1517.7	8.43	41.60	40.85	0.77	7.63	0.05	0.27	99.12
1524.5	9.28	40.46	41.84	0.80	6.93	0.30	0.20	99.43
1531.4	9.47	40.20	42.06	0.88	6.77	0.45	0.28	99.94
1538.3	9.00	40.84	41.51	0.78	7.16	0.11	0.27	99.53

Pos. (µm)	87/86	87/86
1133	0.70429	0.70432
1139	0.70401	0.70453
1144	0.70372	0.70474
1149	0.70368	0.70559
1155	0.70402	0.70511
1160	0.70301	0.70540
1165	0.70304	0.70498
1171	0.70271	0.70391
1176	0.70370	
1181	0.70412	0.70493
1187	0.70328	0.70576
1192	0.70518	0.70459
1197	0.70592	0.70494
1203	0.70372	0.70404
1208	0.70388	0.70455
1213	0.70293	0.70529
1219	0.70604	0.70506
1224		0.70540
1229	0.70548	0.70521
1235	0.70567	0.70517
1240	0.70243	0.70491
1246	0.70503	0.70539
1251	0.70524	0.70525
1256	0.70558	0.70489
1262	0.70385	0.70484
1267	0.70567	0.70409
1272	0.70622	0.70416
1278	0.70379	
1283	0.70485	0.70515
1288	0.70665	0.70515
1294	0.70391	0.70450
1299		0.70499
1304		0.70351
1310	0.70439	0.70541
1315	0.70464	0.70465
1320	0.70395	0.70607
1326		0.70506
1331	0.70540	0.70377
1336	0.70397	0.70437
1342	0.70590	0.70526
1347	0.70492	
1352	0.70373	0.70467
1358	0.70647	0.70394
1363	0.70405	0.70388
1368	0.70335	0.70555
1374	0.70546	0.70352
1379	0.70452	0.70427
1385	0.70530	0.70468
1390	0.70468	0.70407
1395	0.70489	0.70319
1401	0.70364	0.70444
1406	0.70522	0.70414
1411	0.70544	0.70479
1417	0.70346	0.70465

Pos. (µm)	Na2O	Al2O3	SiO2	K2O	CaO	FeO	SrO	Total

Pos. (µm)	87/86	87/86
1422	0.70522	0.70513
1427	0.70473	0.70458
1433	0.70503	0.70415
1438		0.70320
1443	0.70471	0.70517
1449	0.70441	0.70456
1454	0.70278	0.70350
1459	0.70564	0.70342
1465	0.70428	0.70551
1470	0.70489	0.70451
1475	0.70375	0.70307
1481	0.70529	0.70264
1486	0.70372	0.70485
1491	0.70482	0.70512
1497	0.70367	0.70504
1502	0.70477	0.70402
1507	0.70419	
1513	0.70365	
1518	0.70543	
1524	0.70620	0.70459
1529	0.70454	0.70355
1534	0.70470	0.70446
1540	0.70496	0.70412

Unit: El Chichon E
Thin Section: CHI-9516
Crystal: A

Microprobe analyses

Pos. (μm)	Na2O	Al2O3	SiO2	K2O	CaO	FeO	SrO	Total
0.0	5.63	27.56	55.59	0.43	9.88	0.21	0.19	99.52
4.5	5.53	27.84	55.61	0.40	10.11	0.28	0.22	99.99
8.9	5.44	27.99	55.28	0.40	10.14	0.23	0.24	99.73
13.5	5.69	28.16	55.40	0.41	10.16	0.19	0.20	100.22
18.0	5.72	28.25	55.26	0.38	10.07	0.20	0.23	100.13
22.5	5.60	27.99	55.09	0.39	10.26	0.23	0.24	99.78
27.0	5.32	28.12	54.79	0.38	10.27	0.22	0.21	99.34
31.6	5.54	28.18	55.27	0.37	10.38	0.24	0.21	100.21
36.1	5.21	28.46	55.01	0.38	10.48	0.19	0.23	99.97
40.7	5.51	28.59	54.97	0.37	10.54	0.19	0.20	100.36
45.4	5.15	28.92	54.41	0.34	10.92	0.25	0.13	100.18
49.9	5.21	28.64	54.13	0.31	11.01	0.18	0.20	99.67
54.4	5.07	29.06	54.66	0.33	10.98	0.26	0.24	100.62
59.0	5.03	29.20	54.39	0.33	11.04	0.27	0.19	100.49
63.5	4.88	28.94	53.53	0.35	11.17	0.24	0.17	99.31
68.0	5.01	28.56	54.81	0.33	11.13	0.11	0.23	100.20
72.5	4.87	28.12	55.28	0.31	11.09	0.17	0.20	100.04
77.1	4.75	28.61	53.93	0.32	11.19	0.34	0.22	99.42
81.7	4.70	28.72	53.79	0.29	11.64	0.21	0.15	99.55
86.2	4.35	27.70	52.77	0.29	11.81	0.23	0.21	97.35
90.9	4.48	27.81	52.70	0.31	11.57	0.22	0.21	97.33
95.4	4.73	27.65	53.25	0.31	11.37	0.19	0.25	97.82
99.9	4.58	28.19	53.25	0.31	11.38	0.26	0.18	98.19
104.4	4.15	27.92	52.68	0.28	11.73	0.23	0.20	97.24
109.1	4.42	28.09	52.61	0.27	12.00	0.23	0.24	97.87
113.7	4.15	28.76	51.88	0.25	12.54	0.20	0.22	98.06
121.2	3.93	28.74	51.55	0.27	12.50	0.18	0.18	97.37
125.6	3.95	28.67	52.33	0.27	12.36	0.23	0.17	98.04
130.0	3.89	28.70	51.17	0.23	12.82	0.20	0.21	97.22
134.4	4.20	28.58	52.45	0.26	12.40	0.21	0.21	98.33
139.0	4.48	27.85	52.80	0.29	11.80	0.19	0.22	97.65
143.4	4.78	28.19	53.53	0.31	11.56	0.24	0.19	98.83
147.8	4.71	28.12	54.07	0.31	11.44	0.23	0.20	99.18
152.2	4.54	28.35	53.20	0.28	11.71	0.23	0.23	98.54
156.6	4.14	28.23	52.41	0.29	12.19	0.28	0.22	97.78
161.1	4.24	28.63	52.00	0.26	12.43	0.22	0.22	98.02
165.6	3.99	28.47	52.53	0.23	12.32	0.36	0.21	98.13
169.4	3.98	28.46	51.83	0.24	12.23	0.22	0.24	97.21
173.2	4.23	28.62	52.64	0.28	11.94	0.33	0.21	98.23
177.1	4.66	27.73	53.61	0.29	11.44	0.25	0.20	98.26
181.0	4.46	28.03	53.74	0.30	11.50	0.35	0.19	98.61
184.8	4.60	28.35	53.47	0.29	11.44	0.29	0.20	98.68
189.2	4.49	28.49	52.93	0.29	11.86	0.32	0.19	98.61
193.7	5.70	26.43	56.07	0.49	9.40	0.22	0.22	98.55
198.2	6.49	25.65	57.47	0.62	8.38	0.37	0.24	99.26
202.8	6.21	26.25	56.17	0.50	9.12	0.26	0.19	98.76
207.2	5.19	27.19	54.48	0.42	10.23	0.34	0.23	98.16
211.7	5.52	26.74	56.57	0.49	9.49	0.34	0.23	99.45
218.1	5.53	25.99	56.13	0.49	9.31	0.25	0.22	97.95
222.8	6.02	25.97	56.08	0.54	9.01	0.30	0.25	98.17
227.3	5.46	26.25	56.42	0.45	9.57	0.29	0.22	98.71
231.8	6.09	25.97	57.19	0.53	8.97	0.31	0.22	99.35

ICP-MS

Pos. (μm)	87/86	87/86	87/87
38			
45	0.70123		0.70838
53	0.70643	0.70959	0.70404
61	0.70623	0.70571	0.70397
68	0.70365	0.70263	0.70584
76	0.70064	0.70515	0.69884
83	0.70289	0.70364	0.69915
91	0.70696	0.70547	0.70602
98	0.70524	0.70400	0.70410
106	0.70652	0.70434	0.70258
114	0.70006	0.70576	0.70493
121	0.70511	0.70501	0.70545
129	0.70503	0.70451	0.70438
136	0.70538	0.70370	0.70550
144	0.70441	0.70585	0.70307
151	0.70293	0.70360	0.70323
159	0.70445	0.70472	0.70301
167	0.70548	0.70477	0.70537
174	0.70562	0.70442	0.70596
182	0.70432	0.70594	0.70474
189	0.70735	0.70605	0.70469
197	0.70521	0.70493	0.70488
204	0.70448	0.70595	0.70576
212	0.70637	0.70518	0.70455
220	0.70589	0.70615	0.70453
227	0.70541	0.70506	0.70441
235	0.70566	0.70528	0.70469
242	0.70539	0.70582	0.70566
250	0.70416	0.70355	0.70625
257	0.70574	0.70459	0.70382
265	0.70450	0.70539	0.70527
273	0.70582	0.70550	0.70476
280	0.70534	0.70533	0.70447
288	0.70457	0.70599	0.70592
295	0.70577	0.70521	0.70417
303	0.70495	0.70488	0.70484
310	0.70523	0.70572	0.70599
318	0.70549	0.70519	0.70535
326	0.70482	0.70548	0.70571
333	0.70546	0.70464	0.70530
341	0.70515	0.70600	0.70533
348	0.70482	0.70521	0.70606
356	0.70467	0.70463	0.70618
363	0.70527	0.70628	0.70577
371	0.70540	0.70421	0.70588
379	0.70542	0.70481	0.70661
386	0.70459	0.70525	0.70673
394	0.70560	0.70567	0.70636

Pos. (μm)	Na2O	Al2O3	SiO2	K2O	CaO	FeO	SrO	Total
236.1	5.98	26.02	56.63	0.52	9.05	0.32	0.23	98.79
240.7	5.23	27.18	54.70	0.36	10.50	0.26	0.18	98.47
245.3	4.05	28.51	53.41	0.27	12.21	0.32	0.24	99.05
249.9	5.48	26.50	55.89	0.43	10.00	0.31	0.23	98.90
254.3	6.19	25.80	57.41	0.58	8.49	0.27	0.20	99.03
258.8	6.11	25.80	57.28	0.53	8.79	0.21	0.21	98.93
263.3	6.15	26.13	57.06	0.50	8.95	0.21	0.17	99.18
267.8	5.94	26.08	56.99	0.56	8.67	0.26	0.26	98.81
272.2	5.93	24.58	57.16	0.59	8.55	0.18	0.23	97.21
276.9	6.00	24.85	55.52	0.55	28.16	0.24	0.26	96.17
281.5	5.80	5.72	55.30	0.57	8.41	0.28	0.18	94.93
285.9	5.90	24.63	55.91	0.56	8.54	0.27	0.23	96.10
290.5	6.11	24.11	56.35	0.60	8.12	0.29	0.24	95.89
295.1	6.01	24.38	56.78	0.62	8.25	0.27	0.25	96.58
299.6	6.02	24.39	56.36	0.59	8.23	0.20	0.26	96.04
304.1	6.21	24.79	56.24	0.57	8.29	0.18	0.23	96.58
308.5	6.12	24.58	56.37	0.58	8.21	0.25	0.25	96.38
313.0	5.30	26.21	54.44	0.41	10.18	0.33	0.25	97.11
317.6	5.40	25.93	54.34	0.46	9.59	0.22	0.27	96.24
320.3	5.50	25.77	54.34	0.48	9.47	0.21	0.23	96.00
324.8	5.78	25.34	54.85	0.46	9.10	0.25	0.19	96.06
329.4	5.92	24.44	55.75	0.56	8.41	0.28	0.22	95.64
333.9	5.89	24.59	56.39	0.57	8.40	0.24	0.25	96.38
338.4	5.90	24.22	55.93	0.59	8.39	0.33	0.22	95.57
342.9	6.49	24.46	56.41	0.64	7.97	0.23	0.19	96.42
347.5	6.35	24.21	56.71	0.68	7.59	0.19	0.26	96.09
352.0	6.27	24.51	56.69	0.62	7.96	0.15	0.27	96.53
356.5	6.38	23.49	57.29	0.73	7.10	0.14	0.25	95.46
361.1	6.56	23.58	58.12	0.79	7.04	0.23	0.23	96.63
365.5	6.56	23.89	57.45	0.76	7.12	0.26	0.21	96.30
370.0	6.46	23.88	57.49	0.77	7.28	0.23	0.22	96.42
374.5	6.62	23.09	58.33	0.76	6.99	0.32	0.23	96.37
379.0	5.77	24.67	55.57	0.55	8.50	0.22	0.25	95.64
383.6	6.01	24.18	56.24	0.68	7.74	0.32	0.27	95.47
388.2	6.24	24.28	56.49	0.70	7.64	0.22	0.22	95.84
392.8	6.28	24.41	55.86	0.61	8.05	0.26	0.29	95.74
397.3	6.50	24.10	56.80	0.71	7.47	0.23	0.23	96.08
401.8	6.45	23.57	57.51	0.73	7.43	0.23	0.29	96.27
406.3	6.38	24.49	56.65	0.66	7.98	0.30	0.24	96.77
410.9	5.97	24.30	56.85	0.64	8.18	0.24	0.31	96.56
415.4	5.96	24.15	55.81	0.63	8.13	0.34	0.30	95.31
419.9	6.31	24.25	56.92	0.64	7.75	0.23	0.21	96.34
424.5	6.40	24.09	57.00	0.70	7.46	0.26	0.28	96.28
429.3	6.11	24.06	56.77	0.62	8.01	0.26	0.25	96.17
431.9	6.40	23.38	56.69	0.80	7.16	0.27	0.27	95.05

Pos. (μm)	87/86	87/86	87/87
401	0.70452	0.70542	0.70659
409	0.70452	0.70542	0.70647
416			0.70647

Unit: El Chichon E
Thin Section: CHI-9516
Crystal: B

Microprobe analyses

Pos. (μm)	Na2O	Al2O3	SiO2	K2O	CaO	FeO	SrO	Total
0	4.54	28.55	56.01	0.30	9.93	0.00	0.24	99.56
4.2	4.59	28.89	56.16	0.29	9.87	0.00	0.27	100.07
8.3	4.64	29.33	55.32	0.27	10.31	0.00	0.27	100.13
12.3	4.74	28.53	56.22	0.34	9.51	0.00	0.26	99.60
16.5	4.86	29.27	55.41	0.28	10.21	0.00	0.27	100.29
20.5	4.54	29.85	55.62	0.27	10.40	0.00	0.23	100.90
24.6	4.31	29.41	55.85	0.28	10.36	0.00	0.29	100.50
28.7	4.60	29.41	56.26	0.27	10.37	0.00	0.30	101.20
32.8	4.64	28.96	56.08	0.29	9.99	0.00	0.31	100.27
36.9	4.90	28.84	55.87	0.28	9.92	0.00	0.29	100.11
40.9	5.04	28.50	56.55	0.31	9.82	0.00	0.28	100.50
45	4.18	28.13	54.00	0.30	9.91	0.00	0.27	96.79
49.2	4.93	29.04	55.62	0.29	9.84	0.00	0.27	99.98
53.3	4.83	28.95	55.64	0.28	9.84	0.00	0.28	99.82
57.3	5.15	28.90	56.53	0.31	9.62	0.00	0.24	100.75
61.4	5.00	28.58	56.32	0.32	9.23	0.00	0.22	99.66
65.8	5.25	28.20	56.00	0.32	9.27	0.00	0.27	99.31
70	5.02	28.69	55.43	0.31	9.31	0.00	0.26	99.03
74.4	5.14	29.24	55.85	0.31	9.40	0.00	0.26	100.20
78.5	5.41	28.21	55.90	0.31	9.10	0.00	0.27	99.21
82.7	5.43	28.19	57.03	0.33	8.82	0.00	0.24	100.04
87.1	5.43	28.14	57.67	0.36	8.68	0.00	0.24	100.52
91.3	5.46	28.26	57.58	0.38	8.53	0.00	0.24	100.44
95.5	5.39	28.35	58.18	0.37	8.54	0.00	0.27	101.10
99.7	5.57	28.07	57.36	0.37	9.01	0.00	0.26	100.63
103.9	5.53	27.90	57.64	0.37	8.96	0.00	0.29	100.69
108.1	5.53	27.71	57.70	0.39	8.85	0.00	0.24	100.42
112.3	5.76	28.01	58.54	0.39	8.73	0.00	0.28	101.71
116.6	5.84	28.01	57.45	0.37	8.89	0.00	0.25	100.83
120.8	5.74	28.00	59.59	0.37	8.68	0.00	0.26	102.62
125.2	5.72	27.33	58.25	0.38	8.77	0.00	0.24	100.69
129.4	5.63	27.27	57.90	0.39	8.76	0.00	0.31	100.26
133.5	6.08	27.99	59.21	0.41	8.41	0.00	0.24	102.32
137.7	5.49	26.01	56.71	0.43	8.52	0.00	0.23	97.38
142.1	5.92	26.85	58.58	0.41	8.29	0.00	0.28	100.33
146.4	5.91	26.77	58.03	0.45	8.13	0.00	0.28	99.57
150.6	6.09	27.07	58.57	0.44	8.22	0.00	0.27	100.66
154.9	5.96	27.09	58.15	0.42	8.24	0.00	0.27	100.13
159.2	6.07	26.96	58.38	0.43	8.22	0.00	0.26	100.31
163.4	5.99	27.04	58.49	0.43	7.98	0.00	0.25	100.17
167.8	5.70	27.14	58.36	0.44	8.06	0.00	0.25	99.95
172	5.32	25.59	55.28	0.43	8.06	0.00	0.26	94.94
176.2	5.75	26.48	56.52	0.43	8.17	0.00	0.29	97.64
180.4	6.10	26.81	57.25	0.41	8.08	0.00	0.27	98.93
184.6	6.07	26.60	57.09	0.45	8.12	0.00	0.25	98.58
188.9	6.02	26.94	58.26	0.44	7.93	0.00	0.28	99.87
193	6.08	26.52	58.31	0.45	7.86	0.00	0.30	99.53
197.3	6.10	26.59	58.39	0.49	7.83	0.00	0.28	99.67
201.4	6.30	27.14	59.24	0.49	7.65	0.00	0.25	101.07

ICP-MS

Pos. (μm)	87/86	87/86
9		0.70417
18	0.70449	0.70419
26	0.70374	0.70456
35	0.70548	0.70438
44	0.70324	0.70360
53	0.70366	0.70385
62	0.70388	0.70357
71	0.70418	0.70361
79	0.70444	0.70473
88	0.70405	0.70397
97	0.70356	0.70381
106	0.70344	0.70320
115	0.70413	0.70358
124	0.70474	0.70398
132	0.70330	0.70297
141	0.70398	0.70487
150	0.70432	0.70350
159	0.70453	0.70458
168	0.70410	0.70371
176	0.70421	0.70358
185	0.70536	0.70346
194	0.70462	0.70454
203	0.70387	0.70400
212	0.70370	0.70411
221	0.70490	0.70389
229	0.70506	0.70371
238	0.70452	0.70361
247	0.70470	0.70416
256	0.70415	0.70468
265	0.70423	0.70339
274	0.70419	0.70440
282	0.70511	0.70318
291	0.70393	0.70432
300	0.70408	0.70296
309	0.70428	0.70323
318	0.70330	0.70288
327	0.70463	0.70390
335	0.70455	0.70396
344	0.70425	0.70348
353	0.70451	0.70406
362	0.70435	0.70490
371	0.70448	0.70490
379	0.70488	
388	0.70479	
397	0.70358	
406	0.70358	

Pos. (µm)	Na2O	Al2O3	SiO2	K2O	CaO	FeO	SrO	Total
205.6	5.74	26.49	59.76	0.49	7.76	0.00	0.33	100.57
209.9	5.94	27.04	59.21	0.46	7.69	0.00	0.29	100.64
214.1	6.19	27.49	59.91	0.45	7.79	0.00	0.27	102.10
218.3	5.70	28.00	58.88	0.44	8.39	0.00	0.32	101.73
222.2	5.67	26.79	57.24	0.44	7.94	0.00	0.30	98.37
226.4	5.56	27.71	58.63	0.42	8.05	0.00	0.30	100.67
230.6	5.51	24.64	53.52	0.50	6.63	0.00	0.29	91.09
234.7	5.75	27.92	57.88	0.43	8.30	0.00	0.29	100.58
238.9	5.23	28.71	56.02	0.31	9.33	0.00	0.30	99.91
243.1	5.75	27.47	57.56	0.41	8.41	0.00	0.33	99.93
247.3	5.91	27.98	57.42	0.40	8.32	0.00	0.29	100.32
251.5	6.05	27.35	59.06	0.42	7.95	0.00	0.30	101.13
255.7	5.72	26.99	59.08	0.46	7.65	0.00	0.34	100.24
260	5.67	27.21	57.60	0.44	7.86	0.00	0.32	99.10
264.3	5.76	27.77	57.50	0.36	8.46	0.00	0.29	100.14
268.4	5.59	27.66	56.85	0.37	8.18	0.00	0.29	98.95
276.9	6.31	26.96	59.25	0.46	7.31	0.00	0.27	100.57
281	6.04	26.24	58.76	0.53	6.32	0.00	0.22	98.11
289.4	7.09	26.55	60.01	0.57	6.01	0.00	0.26	100.49
293.7	6.99	26.37	58.36	0.57	5.97	0.00	0.28	98.53
297.8	6.78	23.83	57.38	0.58	5.61	0.00	0.24	94.42
302	7.16	27.67	61.19	0.54	6.76	0.00	0.28	103.59
306.1	6.86	27.26	62.05	0.54	6.75	0.00	0.34	103.80
310.3	6.67	27.06	62.41	0.54	6.70	0.00	0.30	103.68
318.6	6.59	26.49	60.97	0.55	6.89	0.00	0.29	101.79
322.8	6.26	26.43	60.16	0.52	7.04	0.00	0.30	100.70
326.9	6.72	23.80	61.68	0.50	6.91	0.00	0.32	99.94
331	6.66	25.85	60.21	0.54	7.43	0.00	0.29	100.98
335.1	6.69	26.00	60.31	0.53	7.32	0.00	0.31	101.16
339.2	6.56	26.42	59.35	0.51	7.47	0.00	0.28	100.59
343.4	6.55	25.88	58.33	0.55	7.16	0.00	0.30	98.78
347.7	6.82	25.26	57.33	0.54	7.15	0.00	0.27	97.37
351.8	6.39	25.48	57.80	0.57	6.96	0.00	0.32	97.52
355.9	7.15	25.38	59.76	0.59	6.85	0.00	0.30	100.03
360	6.84	26.05	59.77	0.60	6.59	0.00	0.28	100.13
364.3	7.33	26.76	60.50	0.63	6.49	0.00	0.32	102.03
376.7	5.87	27.17	57.67	0.38	8.45	0.00	0.35	99.90
385.2	6.64	27.66	59.38	0.43	7.65	0.00	0.36	102.12
385.4789	5.67	28.06	57.90	0.39	8.58	0.00	0.33	100.92
389.5781	5.36	28.22	57.07	0.38	8.63	0.00	0.38	100.03
393.7773	6.37	26.93	58.80	0.47	7.58	0.00	0.31	100.46
397.9764	6.28	26.24	57.96	0.52	7.30	0.00	0.33	98.63
402.1756	6.86	25.62	60.16	0.61	6.63	0.00	0.26	100.14
406.3749	7.22	25.20	60.16	0.65	6.11	0.00	0.25	99.58
410.4741	6.95	25.36	60.16	0.66	6.16	0.00	0.26	99.55
414.7733	8.09	23.31	63.24	1.16	3.98	0.00	0.32	100.09

Pos. (µm)	87/86	87/86

Unit: El Chichon E
Thin Section: CHI-9516
Crystal: C

Microprobe analyses

Pos. (μm)	Na2O	Al2O3	SiO2	K2O	CaO	FeO	SrO	Total
5.1	6.92	28.12	58.40	0.67	7.57	0.00	0.31	101.98
10.2	7.24	27.18	57.48	0.74	7.53	0.00	0.32	100.48
15.3	6.88	24.21	61.25	3.05	4.38	0.00	0.13	99.91
20.3	5.04	23.15	54.78	3.59	5.33	0.00	0.20	92.09
25.4	6.59	28.17	57.88	0.61	7.64	0.00	0.29	101.19
30.5	6.85	28.15	58.08	0.65	7.62	0.00	0.32	101.67
35.6	7.04	27.69	57.29	0.64	7.49	0.00	0.37	100.52
40.7	6.78	28.22	58.32	0.56	7.71	0.00	0.35	101.94
45.8	6.58	28.62	58.90	0.58	7.93	0.00	0.34	102.94
50.8	6.61	29.29	57.28	0.51	8.31	0.00	0.37	102.37
55.9	6.15	29.27	57.04	0.46	8.67	0.00	0.29	101.88
61.0	5.79	30.06	55.93	0.43	9.02	0.00	0.34	101.58
66.1	6.07	29.54	56.63	0.46	8.58	0.00	0.30	101.58
71.2	4.92	30.75	54.01	0.33	10.15	0.00	0.36	100.52
76.3	5.81	28.71	57.10	0.48	8.48	0.00	0.34	100.93
81.3	5.90	28.48	57.85	0.47	8.46	0.00	0.32	101.48
86.4	6.23	29.28	56.82	0.46	8.43	0.00	0.31	101.53
91.5	6.29	29.09	58.11	0.49	8.40	0.00	0.35	102.71
96.6	6.08	29.11	56.03	0.47	8.35	0.00	0.29	100.32
101.7	6.20	28.26	55.90	0.45	8.36	0.00	0.27	99.44
106.8	6.11	28.04	56.20	0.47	8.17	0.00	0.37	99.36
111.8	6.04	28.66	56.32	0.50	8.16	0.00	0.29	99.97
116.9	6.35	29.01	56.20	0.49	8.14	0.00	0.35	100.54
122.0	6.37	29.28	56.46	0.51	7.99	0.00	0.34	100.96
127.1	6.51	29.26	57.03	0.56	7.58	0.00	0.35	101.29
132.2	6.14	28.56	56.43	0.49	7.90	0.00	0.32	99.84
137.3	6.18	29.50	56.33	0.49	7.90	0.00	0.31	100.70
142.3	6.05	28.66	54.43	0.48	7.95	0.00	0.30	97.87
147.4	6.39	28.22	53.63	0.54	7.86	0.00	0.29	96.92
152.5	6.15	28.12	54.04	0.51	7.69	0.00	0.35	96.85
157.6	6.61	27.36	55.13	0.56	7.61	0.00	0.30	97.57
162.7	6.25	28.30	55.92	0.50	7.72	0.00	0.25	98.93
167.8	6.32	28.69	55.55	0.48	7.58	0.00	0.30	98.92
172.8	6.03	28.12	54.01	0.50	7.74	0.00	0.32	96.71
177.9	6.19	29.26	54.61	0.47	7.80	0.00	0.34	98.67
183.0	6.24	28.35	54.80	0.51	7.67	0.00	0.29	97.86
188.1	6.54	28.19	55.52	0.48	7.50	0.00	0.28	98.51
193.2	6.00	27.93	57.61	0.50	7.65	0.00	0.29	99.98
198.3	6.55	27.03	61.28	0.54	7.05	0.00	0.32	102.76
203.3	6.69	26.99	60.65	0.58	6.86	0.00	0.32	102.09
208.4	6.38	26.90	60.90	0.55	6.97	0.00	0.30	102.01
213.5	6.57	26.95	59.62	0.56	6.88	0.00	0.28	100.86
218.6	6.08	27.59	59.88	0.51	7.38	0.00	0.29	101.73
223.7	3.97	23.45	48.79	0.40	13.15	0.00	0.31	90.06
228.8	5.45	6.43	57.55	0.40	7.87	0.00	0.28	77.99
233.8	6.16	27.87	58.68	0.45	7.66	0.00	0.33	101.15
238.9	5.22	28.55	57.98	1.05	7.89	0.00	0.31	101.01
244.0	5.26	27.85	54.45	0.71	8.33	0.00	0.23	96.84
249.1	5.46	28.16	57.31	0.39	8.11	0.00	0.29	99.71

ICP-MS

Pos. (μm)	87/86	87/86
0		0.70500
5		0.70529
10	0.70503	
15	0.70501	
20	0.70490	0.70535
25	0.70490	0.70508
30		0.70528
35	0.70501	0.70517
40	0.70382	0.70532
45	0.70495	0.70522
50	0.70455	0.70497
55	0.70536	0.70509
60	0.70452	0.70525
65	0.70500	0.70531
70	0.70444	0.70509
75	0.70547	0.70510
80	0.70435	
85	0.70490	0.70503
90	0.70559	0.70475
95	0.70591	0.70485
100	0.70578	0.70501
105	0.70542	0.70487
110	0.70625	0.70506
115	0.70503	0.70498
120	0.70531	0.70494
125	0.70531	0.70498
130	0.70480	0.70474
135	0.70436	0.70485
140	0.70454	0.70470
145	0.70456	0.70476
150	0.70475	0.70487
155	0.70412	0.70481
160	0.70513	0.70489
165	0.70542	0.70481
170	0.70517	0.70491
175	0.70535	0.70475
180	0.70416	0.70476
185	0.70434	0.70466
190	0.70496	0.70466
195	0.70613	0.70478
200	0.70521	0.70462
205	0.70520	0.70476
210	0.70511	0.70486
215	0.70487	0.70488
220	0.70469	0.70497
225	0.70464	0.70490
230	0.70497	0.70503
235	0.70504	0.70501
240	0.70441	0.70489

Pos. (μm)	Na2O	Al2O3	SiO2	K2O	CaO	FeO	SrO	Total
254.2	6.18	26.98	59.61	0.45	7.42	0.00	0.38	101.02
259.3	5.93	27.89	59.06	0.46	7.72	0.00	0.32	101.37
264.3	5.28	28.99	57.72	0.38	8.35	0.00	0.26	100.99
269.4	6.80	27.16	60.45	0.53	6.75	0.00	0.30	101.98
274.5	6.66	26.43	61.39	0.58	6.38	0.00	0.31	101.75
279.6	6.61	26.58	61.18	0.54	6.57	0.00	0.32	101.80
284.7	5.50	28.95	57.51	0.38	8.44	0.00	0.30	101.07
289.8	5.04	29.91	56.55	0.31	8.67	0.00	0.29	100.76
294.8	5.48	29.50	58.86	0.39	7.97	0.00	0.29	102.47
299.9	5.51	29.21	59.53	0.43	7.76	0.00	0.32	102.76
305.0	5.63	29.20	60.16	0.41	7.67	0.00	0.30	103.38
310.1	5.71	29.12	59.81	0.42	7.56	0.00	0.30	102.92
315.2	6.05	29.01	59.87	0.49	7.41	0.00	0.33	103.15
320.3	6.05	28.55	61.05	0.40	7.51	0.00	0.31	103.86
325.3	5.48	26.79	56.44	0.44	7.87	0.00	0.34	97.35
330.4	5.53	27.74	57.05	0.41	8.01	0.00	0.33	99.07
335.5	5.52	27.75	56.83	0.39	7.98	0.00	0.32	98.78
340.6	4.78	29.43	54.74	0.30	9.31	0.00	0.32	98.88
345.7	5.88	27.67	59.29	0.46	7.77	0.00	0.30	101.37
350.8	4.77	30.69	58.23	0.36	9.74	0.00	0.36	104.15
355.8	4.67	31.16	59.45	0.32	10.30	0.00	0.35	106.25
360.9	6.23	29.70	61.87	0.47	8.01	0.00	0.32	106.60
366.0	6.38	26.52	56.36	0.50	8.03	0.00	0.34	98.14
371.1	3.48	29.96	50.99	0.20	11.63	0.00	0.31	96.57
376.2	4.83	28.26	52.78	0.33	9.52	0.00	0.41	96.14
381.3	4.18	28.33	52.70	0.32	10.00	0.00	0.37	95.89
386.3	3.27	30.09	50.28	0.18	11.73	0.00	0.29	95.84
391.4	2.91	30.04	49.77	0.17	11.76	0.00	0.37	95.03
396.5	4.77	27.98	52.37	0.34	9.77	0.00	0.30	95.53
401.6	5.85	26.27	56.28	0.47	8.00	0.00	0.41	97.28
406.7	5.25	27.61	52.52	0.40	8.84	0.00	0.37	95.00
411.8	5.75	26.88	54.12	0.43	8.27	0.00	0.32	95.78
416.8	6.41	25.66	56.22	0.54	7.39	0.00	0.36	96.57
421.9	6.19	25.57	55.47	0.59	7.10	0.00	0.36	95.27
427.0	6.31	25.42	57.74	0.55	7.30	0.00	0.37	97.68
432.1	6.26	25.26	57.91	0.55	6.88	0.00	0.38	97.23
437.2	6.70	25.65	59.39	0.63	6.43	0.00	0.28	99.09
442.3	6.34	26.13	59.47	0.60	6.69	0.00	0.35	99.57
447.3	6.17	27.67	60.64	0.56	7.16	0.00	0.33	102.53
452.4	5.31	28.22	55.10	0.44	7.13	0.00	0.30	96.49
457.5	5.78	26.72	58.44	0.45	7.93	0.00	0.36	99.68
462.6	5.36	25.72	55.37	0.44	7.97	0.00	0.39	95.24
467.7	5.09	26.47	53.21	0.39	8.11	0.00	0.35	93.62
472.8	3.84	30.14	49.95	0.26	10.19	0.00	0.25	94.64
477.8	3.98	32.56	54.51	0.26	10.06	0.00	0.36	101.74
482.9	3.60	28.16	53.57	0.27	9.76	0.00	0.38	95.74
488.0	4.16	29.30	56.75	0.28	9.88	0.00	0.36	100.73
493.1	4.44	32.30	55.49	0.28	9.49	0.00	0.32	102.32
498.2	4.97	30.78	58.93	0.33	9.12	0.00	0.29	104.42
503.3	5.26	25.72	55.34	0.46	7.64	0.00	0.45	94.87
508.3	5.68	29.93	55.72	0.49	7.34	0.00	0.36	99.52
513.4	6.49	26.00	62.48	0.56	6.69	0.00	0.35	102.57
518.5	6.60	25.66	58.14	0.64	6.31	0.00	0.43	97.78
523.6	6.43	25.61	55.98	0.64	6.28	0.00	0.40	95.33

Pos. (μm)	87/86	87/86
245	0.70548	0.70488
250	0.70466	0.70477
255	0.70501	0.70484
260	0.70443	0.70485
265	0.70592	0.70490
270	0.70415	0.70490
275	0.70475	0.70486
280	0.70488	0.70466
285	0.70545	0.70437
290	0.70593	0.70421
295	0.70463	0.70421
300	0.70531	0.70420
305	0.70498	0.70428
310	0.70553	0.70447
315	0.70520	0.70459
320	0.70549	0.70470
325	0.70410	0.70462
330	0.70477	0.70479
335	0.70471	0.70477
340	0.70430	0.70484
345	0.70545	0.70486
350	0.70511	0.70478
355	0.70466	0.70487
360	0.70523	0.70475
365	0.70429	0.70469
370	0.70452	0.70454
375	0.70406	0.70450
380	0.70458	0.70442
385	0.70546	0.70444
390	0.70510	0.70432
395	0.70411	0.70433
400	0.70362	0.70439
405	0.70456	0.70455
410	0.70480	0.70471
415	0.70506	0.70460
420	0.70401	0.70456
425	0.70423	0.70453
430	0.70429	0.70436
435	0.70349	0.70419
440	0.70417	0.70408
445	0.70485	0.70401
450	0.70529	0.70398
455	0.70388	0.70391
460	0.70424	0.70404
465	0.70478	0.70402
470	0.70413	0.70404
475	0.70465	0.70422
480	0.70374	0.70418
485	0.70407	0.70411
490	0.70404	0.70412
495	0.70387	0.70421
500	0.70351	0.70412
505	0.70380	0.70399
510	0.70423	0.70408

Pos. (μm)	Na2O	Al2O3	SiO2	K2O	CaO	FeO	SrO	Total
528.7	6.31	27.79	58.58	0.63	6.37	0.00	0.40	100.08
533.8	6.70	25.87	61.41	0.63	6.22	0.00	0.40	101.23
538.8	6.54	26.88	59.10	0.60	6.34	0.00	0.39	99.86
543.9	6.31	28.75	60.90	0.61	6.20	0.00	0.43	103.21
549.0	6.45	26.62	63.35	0.59	6.34	0.00	0.38	103.74
554.1	6.37	26.92	60.77	0.61	6.30	0.00	0.41	101.39
559.2	6.46	29.71	59.15	0.59	6.29	0.00	0.38	102.58
564.3	6.87	28.11	63.78	0.64	6.11	0.00	0.36	105.87
569.3	6.63	27.23	62.42	0.64	6.01	0.00	0.45	103.38
574.4	6.57	26.40	61.21	0.62	5.90	0.00	0.41	101.11
579.5	6.98	25.59	59.64	0.65	5.79	0.00	0.41	99.05
584.6	6.42	26.87	59.21	0.61	6.22	0.00	0.44	99.77
589.7	7.06	25.51	61.36	0.61	6.07	0.00	0.37	100.98
594.8	6.19	29.77	59.31	0.61	6.12	0.00	0.40	102.41
599.8	6.82	26.38	65.22	0.61	6.25	0.00	0.40	105.67
604.9	6.54	28.40	60.84	0.60	6.21	0.00	0.43	103.02
610.0	6.80	26.14	62.86	0.58	6.27	0.00	0.42	103.07
615.1	6.45	26.72	58.01	0.57	6.30	0.00	0.48	98.53
620.2	5.82	25.97	58.23	0.55	6.26	0.00	0.44	97.27
625.3	6.09	30.11	58.90	0.55	6.52	0.00	0.40	102.57
630.3	6.46	30.88	63.99	0.49	6.76	0.00	0.47	109.04
635.4	7.10	26.08	67.30	0.63	5.91	0.00	0.39	107.40
640.5	6.54	27.47	59.89	0.62	5.60	0.00	0.51	100.61
645.6	7.10	24.95	65.44	0.72	5.29	0.00	0.42	103.92
650.7	6.84	28.11	59.75	0.69	5.33	0.00	0.37	101.10
655.8	6.84	26.47	65.06	0.61	5.78	0.00	0.36	105.12
660.8	6.27	29.29	59.11	0.57	5.83	0.00	0.40	101.46
665.9	6.94	25.02	66.03	0.68	5.65	0.00	0.40	104.72
671.0	6.26	24.78	58.63	0.62	5.72	0.00	0.43	96.44
676.1	6.43	25.05	58.48	0.62	5.77	0.00	0.50	96.85
681.2	6.45	30.31	60.02	0.56	6.03	0.00	0.45	103.81
686.3	6.84	27.22	63.17	0.55	5.93	0.00	0.44	104.15
691.3	6.27	26.53	57.74	0.57	5.87	0.00	0.50	97.47
696.4	6.32	26.48	57.92	0.62	5.81	0.00	0.57	97.73
701.5	6.62	26.13	59.31	0.62	5.86	0.00	0.42	98.96
706.6	6.66	29.44	60.30	0.68	5.44	0.00	0.49	103.02
711.7	6.89	26.06	64.80	0.63	5.66	0.00	0.45	104.49
716.8	6.19	28.20	56.87	0.64	5.59	0.00	0.50	97.99
721.8	6.88	26.21	63.36	0.68	5.34	0.00	0.43	102.90
726.9	6.49	27.15	60.62	0.65	5.41	0.00	0.45	100.76
732.0	6.54	26.80	63.63	0.65	5.42	0.00	0.55	103.60
737.1	6.69	26.27	62.93	0.66	5.49	0.00	0.44	102.49
742.2	6.74	29.08	61.73	0.67	5.36	0.00	0.41	103.99
747.3	7.38	27.65	66.74	0.69	5.23	0.00	0.46	108.15
752.3	7.20	25.58	63.80	0.65	5.33	0.00	0.50	103.07
757.4	6.64	24.55	59.09	0.65	5.24	0.00	0.54	96.72
762.5	5.96	30.03	58.25	0.59	5.77	0.00	0.46	101.06
767.6	7.29	28.50	63.57	0.59	5.62	0.00	0.45	106.02
772.7	6.68	26.22	62.24	0.66	5.19	0.00	0.50	101.51
777.8	7.10	28.88	60.84	0.73	5.05	0.00	0.39	102.98
782.8	6.72	25.55	64.73	0.64	5.33	0.00	0.49	103.46
787.9	6.18	25.38	57.61	0.74	4.89	0.00	0.44	95.24
793.0	6.65	27.16	58.48	0.65	5.12	0.00	0.49	98.54
798.1	6.87	29.04	61.61	0.68	5.10	0.00	0.43	103.74

Pos. (μm)	87/86	87/86
515	0.70365	0.70403
520	0.70380	0.70402
525		0.70387
530	0.70453	0.70393
535	0.70309	0.70399
540	0.70408	0.70384
545	0.70391	0.70381
550	0.70392	0.70362
555	0.70477	0.70360
560	0.70383	0.70355
565	0.70420	0.70354
570	0.70432	0.70360
575	0.70532	0.70370
580	0.70318	0.70362
585	0.70355	0.70372
590	0.70419	0.70380
595	0.70418	0.70373
600	0.70404	0.70384
605	0.70458	0.70378
610	0.70406	0.70397
615		0.70398
620		0.70367
625		0.70356
630		0.70353
635		0.70350
640		
645	0.70480	0.70368
650	0.70515	
655	0.70515	0.70411
660	0.70406	0.70404
665	0.70489	0.70429
670	0.70539	0.70427
675	0.70391	0.70429
680	0.70500	0.70420
685	0.70505	0.70409
690	0.70429	0.70425
695	0.70426	0.70408
700	0.70376	0.70407
705	0.70426	0.70417
710	0.70381	0.70424
715	0.70392	0.70421
720	0.70421	0.70420
725	0.70348	0.70435
730	0.70470	0.70428
735	0.70394	0.70409
740		0.70407
745		0.70419
750		0.70421
755		0.70393
760		0.70403
765		0.70424
770		0.70431
775		0.70443
780	0.70415	0.70425

Pos. (μm)	Na2O	Al2O3	SiO2	K2O	CaO	FeO	SrO	Total
803.2	6.80	25.83	64.46	0.62	5.23	0.00	0.45	103.39
808.3	6.15	26.57	58.54	0.56	5.64	0.00	0.52	97.98
813.3	6.50	28.40	61.33	0.73	4.71	0.00	0.46	102.12
818.4	7.11	25.24	66.63	0.78	4.59	0.00	0.43	104.76
823.5	7.09	23.57	62.75	0.85	4.26	0.00	0.47	98.98
828.6	6.88	24.20	61.02	0.77	4.69	0.00	0.45	98.01
833.7	6.38	24.23	59.49	0.71	4.83	0.00	0.45	96.09
838.8	6.17	27.45	60.52	0.67	5.05	0.00	0.59	100.44
843.8	6.62	28.86	61.75	0.61	5.36	0.00	0.47	103.67
848.9	6.74	25.04	61.26	0.59	5.27	0.00	0.43	99.34
854.0	5.75	24.96	56.11	0.58	5.59	0.00	0.49	93.48
859.1	6.06	25.75	56.31	0.58	5.49	0.00	0.47	94.66
864.2	6.50	27.02	59.92	0.58	5.44	0.00	0.50	99.96
869.3	5.87	24.55	57.13	0.58	5.28	0.00	0.59	93.99
874.3	6.17	25.85	57.95	0.58	5.18	0.00	0.50	96.23
879.4	6.19	26.28	57.75	0.56	5.41	0.00	0.44	96.62
884.5	5.40	26.64	58.13	0.47	5.77	0.00	0.53	96.94
889.6	5.81	26.64	57.03	0.49	5.75	0.00	0.59	96.31
894.7	5.42	26.54	56.17	0.46	5.73	0.00	0.48	94.80
899.8	5.47	28.74	55.04	0.46	6.07	0.00	0.58	96.36
904.8	5.73	27.66	55.96	0.45	5.82	0.00	0.50	96.12
909.9	5.89	26.38	57.42	0.57	5.23	0.00	0.55	96.03
915.0	6.83	26.10	59.28	0.68	4.38	0.00	0.47	97.73

Pos. (μm)	87/86	87/86
785	0.70408	0.70438
790	0.70471	0.70441
795	0.70536	0.70433
800	0.70416	0.70423
805	0.70455	0.70379
810		0.70390
815	0.70443	0.70399
820	0.70322	
825	0.70481	
830		0.70408
835	0.70371	0.70410
840	0.70409	0.70387
845	0.70404	0.70374
850	0.70365	
855	0.70396	
860	0.70350	0.70357
865	0.70358	0.70373
870	0.70476	0.70377
875	0.70330	0.70379
880	0.70397	0.70377
885	0.70418	0.70382
890	0.70465	0.70387
895		0.70331

Unit: El Chichon E
Thin Section: CHI-9516
Crystal: D

Microprobe analyses

Pos. (μm)	Na2O	Al2O3	SiO2	K2O	CaO	FeO	SrO	Total
0.0	7.98	42.19	40.33	0.25	7.99	0.28	0.23	99.27
4.1	7.50	42.84	39.78	0.22	8.39	0.36	0.21	99.29
8.1	8.23	41.86	40.63	0.51	7.79	0.00	0.15	99.17
12.2	8.35	41.69	40.77	0.66	7.69	0.04	0.26	99.45
16.3	7.85	42.36	40.19	0.78	8.10	0.39	0.24	99.91
20.4	7.92	42.27	40.27	0.44	8.04	0.32	0.27	99.52
24.6	7.48	42.85	39.76	0.60	8.40	0.01	0.26	99.37
28.7	6.01	44.82	38.06	0.49	9.61	0.33	0.25	99.57
32.8	7.28	43.12	39.53	0.72	8.56	0.02	0.28	99.52
37.2	7.78	42.46	40.10	0.52	8.16	0.01	0.17	99.20
41.4	7.70	42.57	40.01	0.35	8.22	0.22	0.24	99.32
45.6	7.85	42.36	40.19	0.70	8.10	0.47	0.26	99.94
49.8	8.34	41.71	40.75	0.76	7.70	0.18	0.24	99.68
53.9	7.06	43.43	39.27	0.44	8.75	0.16	0.24	99.35
58.1	5.65	45.29	37.65	0.38	9.90	0.45	0.25	99.58
62.2	6.40	44.30	38.52	0.30	9.29	0.32	0.28	99.40
66.4	7.31	43.09	39.56	0.71	8.54	0.20	0.26	99.67
70.5	6.95	43.56	39.15	0.46	8.83	0.31	0.27	99.54
74.6	7.56	42.75	39.85	0.35	8.34	0.27	0.19	99.31
78.7	8.58	41.39	41.03	0.32	7.50	0.02	0.22	99.06
82.8	8.57	41.41	41.01	0.55	7.51	0.22	0.22	99.49
87.0	8.53	41.45	40.97	0.34	7.54	0.17	0.20	99.21
91.1	8.98	40.86	41.48	0.69	7.18	0.14	0.28	99.61
95.1	8.80	41.10	41.28	0.26	7.32	0.38	0.25	99.38
99.3	9.08	40.72	41.61	0.39	7.09	0.28	0.19	99.35
103.4	8.99	40.85	41.50	0.71	7.17	0.32	0.16	99.69
107.5	8.83	41.06	41.32	0.29	7.29	0.35	0.22	99.36
111.6	8.96	40.88	41.47	0.71	7.19	0.37	0.25	99.83
115.7	9.13	40.66	41.66	0.36	7.05	0.42	0.20	99.48
119.8	8.99	40.85	41.50	0.65	7.17	0.32	0.17	99.64
123.9	9.01	40.82	41.52	0.76	7.15	0.12	0.19	99.57
127.9	9.07	40.74	41.59	0.46	7.10	0.17	0.24	99.37
132.0	8.77	41.14	41.25	0.69	7.34	0.31	0.22	99.71
136.1	9.08	40.73	41.60	0.55	7.09	0.38	0.23	99.65
140.2	9.09	40.72	41.61	0.27	7.09	0.25	0.22	99.23
144.4	9.18	40.60	41.71	0.34	7.01	0.48	0.16	99.48
148.4	9.18	40.60	41.71	0.68	7.01	0.22	0.25	99.65
152.4	9.24	40.51	41.79	0.48	6.96	0.19	0.20	99.38
156.6	9.00	40.83	41.51	0.54	7.15	0.10	0.18	99.33
160.7	9.25	40.49	41.80	0.29	6.95	0.41	0.29	99.48
164.7	9.18	40.59	41.72	0.36	7.01	0.10	0.17	99.13
168.8	9.22	40.54	41.76	0.76	6.98	0.10	0.26	99.62
172.8	9.08	40.73	41.60	0.25	7.09	0.41	0.23	99.39
176.9	9.18	40.59	41.72	0.46	7.01	0.22	0.30	99.48
181.0	9.29	40.45	41.84	0.78	6.92	0.37	0.22	99.87
185.2	9.27	40.47	41.82	0.38	6.94	0.46	0.25	99.59
189.3	8.67	41.27	41.13	0.40	7.43	0.07	0.20	99.16
193.4	9.02	40.80	41.54	0.42	7.14	0.17	0.17	99.26
197.6	9.03	40.79	41.55	0.33	7.13	0.13	0.15	99.11
193.7	8.38	41.66	40.80	0.38	7.66	0.12	0.25	99.24
201.8	8.96	40.89	41.46	0.62	7.19	0.36	0.20	99.67
205.8	8.75	41.17	41.22	0.72	7.37	0.02	0.17	99.41

ICP-MS

Pos. (μm)	87/86	Pos. (μm)	87/86
12	0.70351	12	0.70410
24	0.70378	24	0.70401
36	0.70497	36	0.70412
48	0.70432	48	
59	0.70482	59	
71	0.70503	71	
83	0.70507	83	
95	0.70478	95	
107	0.70452	107	
119	0.70488	119	
131	0.70410	131	
143	0.70523	143	
155	0.70445	155	
167	0.70498	167	
178	0.70400	178	
190	0.70393	190	
202	0.70445	202	
214	0.70343	214	
226	0.70487	226	
238	0.70450	238	
250	0.70378	250	
262	0.70436	262	
274	0.70352	274	0.70375
286	0.70488	286	0.70508
297	0.70473	297	0.70505
309		309	0.70438
321	0.70424	321	0.70385
333	0.70409	333	
345	0.70531	345	0.70389
357	0.70471	357	0.70408
369	0.70395	369	0.70433
381	0.70476	381	0.70460
393	0.70391	393	
405	0.70502	405	0.70415
416	0.70441	416	0.70402
428	0.70446	428	0.70373
440	0.70428	440	0.70451
452	0.70339	452	0.70443
464	0.70517	464	0.70314
476		476	0.70389
488	0.70420	488	0.70470
500	0.70404	500	0.70423
512	0.70492	512	0.70365
524	0.70447	524	0.70478
535	0.70401	535	0.70406
547	0.70420	547	0.70447
559	0.70446	559	
571	0.70481	571	0.70383
583	0.70406	583	0.70438
595	0.70437	595	
607	0.70441	607	0.70420
619		619	0.70476

Pos. (μm)	Na2O	Al2O3	SiO2	K2O	CaO	FeO	SrO	Total
210.0	8.87	41.01	41.36	0.64	7.26	0.36	0.17	99.66
214.1	9.23	40.52	41.78	0.69	6.97	0.11	0.21	99.51
218.3	9.11	40.69	41.63	0.74	7.07	0.49	0.19	99.92
222.4	8.85	41.03	41.34	0.79	7.28	0.12	0.16	99.56
226.6	9.99	39.51	42.65	0.61	6.35	0.18	0.28	99.57
230.7	9.18	40.59	41.72	0.79	7.01	0.43	0.24	99.95
234.7	8.92	40.94	41.42	0.45	7.22	0.37	0.27	99.59
238.9	7.57	42.74	39.86	0.44	8.33	0.02	0.22	99.18
243.0	8.33	41.73	40.74	0.57	7.71	0.08	0.16	99.31
247.0	9.05	40.77	41.57	0.54	7.12	0.02	0.29	99.35
251.1	8.65	41.29	41.11	0.29	7.44	0.25	0.22	99.25
255.3	8.30	41.76	40.70	0.61	7.73	0.46	0.19	99.76
259.3	8.20	41.90	40.59	0.47	7.82	0.07	0.24	99.28
263.5	8.55	41.43	41.00	0.70	7.52	0.02	0.22	99.44
267.6	7.99	42.17	40.35	0.33	7.98	0.17	0.16	99.16
271.7	8.19	41.92	40.57	0.40	7.82	0.22	0.26	99.39
275.8	8.13	41.99	40.51	0.20	7.87	0.12	0.17	99.00
279.9	8.25	41.84	40.64	0.64	7.77	0.36	0.21	99.71
284.1	8.12	42.00	40.50	0.51	7.87	0.19	0.20	99.40
288.3	7.40	42.97	39.67	0.28	8.47	0.17	0.23	99.18
292.4	8.03	42.12	40.40	0.21	7.95	0.29	0.26	99.26
296.4	7.46	42.88	39.74	0.28	8.42	0.43	0.19	99.40
300.6	6.52	44.14	38.65	0.59	9.19	0.49	0.18	99.76
304.8	6.06	44.75	38.12	0.50	9.56	0.20	0.17	99.36
308.8	6.42	44.28	38.53	0.73	9.27	0.33	0.22	99.78
312.8	6.45	44.24	38.57	0.42	9.25	0.05	0.28	99.25
316.9	6.51	44.15	38.64	0.24	9.20	0.14	0.20	99.08
321.1	6.41	44.29	38.52	0.59	9.28	0.34	0.18	99.60
325.2	6.25	44.50	38.34	0.80	9.41	0.49	0.29	100.08
329.2	6.64	43.98	38.79	0.74	9.09	0.27	0.18	99.70
333.5	6.61	44.02	38.76	0.72	9.11	0.24	0.16	99.61
337.5	6.40	44.30	38.52	0.37	9.28	0.32	0.20	99.39
341.6	6.75	43.83	38.92	0.53	9.00	0.32	0.17	99.52
345.8	6.81	43.75	38.99	0.76	8.95	0.33	0.20	99.79
349.8	6.94	43.58	39.13	0.71	8.85	0.21	0.24	99.66
354.1	6.74	43.84	38.91	0.58	9.01	0.12	0.26	99.46
358.2	6.51	44.16	38.63	0.28	9.20	0.06	0.25	99.09
362.4	7.17	43.28	39.40	0.54	8.66	0.34	0.21	99.59
366.5	6.90	43.64	39.08	0.64	8.88	0.42	0.27	99.83
370.7	6.34	44.39	38.44	0.27	9.34	0.06	0.16	99.00
374.8	6.46	44.22	38.58	0.60	9.24	0.24	0.19	99.53
379.1	5.57	45.41	37.55	0.26	9.97	0.49	0.26	99.50
383.3	5.23	45.87	37.16	0.38	10.25	0.10	0.24	99.22
387.3	4.34	47.04	36.14	0.38	10.97	0.07	0.25	99.19
391.5	6.11	44.69	38.18	0.73	9.52	0.08	0.20	99.52
395.7	6.39	44.32	38.50	0.59	9.30	0.02	0.28	99.39
399.9	5.74	45.18	37.75	0.80	9.83	0.12	0.30	99.72
404.1	7.17	43.27	39.40	0.65	8.66	0.00	0.29	99.44
408.3	6.96	43.55	39.16	0.46	8.83	0.32	0.16	99.43
412.4	6.76	43.82	38.93	0.53	8.99	0.36	0.25	99.65
416.4	6.27	44.47	38.36	0.29	9.39	0.28	0.19	99.26
420.7	6.48	44.20	38.60	0.30	9.22	0.27	0.17	99.24
424.9	6.59	44.05	38.73	0.53	9.13	0.09	0.17	99.29
429.0	5.96	44.89	38.00	0.61	9.65	0.49	0.29	99.89
433.1	7.92	42.27	40.27	0.47	8.04	0.30	0.25	99.52
437.2	7.48	42.86	39.76	0.56	8.40	0.17	0.29	99.51
441.4	7.94	42.25	40.29	0.70	8.03	0.08	0.17	99.45

Pos. (μm)	Pos. (μm)	Pos. (μm)	87/86
631	0.70457	631	0.70353
643	0.70397	643	0.70354
654	0.70377	654	0.70403
666		666	0.70422
678	0.70434	678	0.70408
690	0.70372	690	0.70401
702		702	0.70372
714	0.70380	714	0.70433
726	0.70384	726	0.70417
738	0.70493	738	0.70332
750	0.70412	750	0.70384
762	0.70453	762	0.70398
773	0.70270	773	0.70465
785	0.70451	785	0.70466
797	0.70472	797	0.70342
809	0.70382	809	0.70509
821	0.70453	821	0.70462
833	0.70442	833	0.70380
845	0.70429	845	0.70460
857	0.70424	857	0.70427
869	0.70444	869	0.70394
881	0.70496	881	0.70410
892	0.70455	892	0.70404
904	0.70412	904	0.70269
916	0.70403	916	0.70343
928	0.70377	928	0.70308
940	0.70401	940	0.70328
952	0.70429		

Pos. (μm)	Na2O	Al2O3	SiO2	K2O	CaO	FeO	SrO	Total
445.5	8.11	42.02	40.49	0.70	7.89	0.08	0.27	99.55
449.5	7.76	42.48	40.08	0.23	8.17	0.03	0.16	98.92
453.7	7.55	42.77	39.84	0.60	8.35	0.18	0.30	99.58
457.7	7.77	42.47	40.09	0.42	8.17	0.22	0.23	99.37
461.8	8.24	41.85	40.63	0.50	7.78	0.45	0.15	99.60
465.9	8.49	41.52	40.92	0.60	7.58	0.01	0.19	99.29
470.0	8.62	41.34	41.07	0.38	7.47	0.27	0.20	99.34
474.2	9.01	40.81	41.53	0.48	7.15	0.22	0.26	99.45
478.3	8.92	40.94	41.41	0.67	7.23	0.21	0.20	99.57
482.6	8.44	41.58	40.86	0.70	7.62	0.29	0.27	99.76
486.6	8.16	41.96	40.54	0.79	7.85	0.16	0.28	99.74
490.7	8.13	41.99	40.51	0.22	7.87	0.39	0.22	99.32
495.0	8.26	41.82	40.66	0.40	7.76	0.29	0.26	99.46
499.2	8.10	42.03	40.48	0.78	7.89	0.33	0.26	99.87
503.6	7.46	42.89	39.73	0.75	8.42	0.25	0.22	99.72
507.8	5.46	45.55	37.43	0.57	10.06	0.38	0.22	99.67
512.1	5.62	45.34	37.61	0.72	9.93	0.32	0.22	99.76
516.3	6.20	44.56	38.29	0.34	9.45	0.15	0.21	99.19
520.7	6.09	44.72	38.15	0.79	9.54	0.08	0.20	99.57
525.0	6.64	43.98	38.79	0.25	9.09	0.49	0.30	99.54
529.2	7.23	43.19	39.47	0.51	8.61	0.47	0.27	99.74
533.4	7.59	42.71	39.89	0.30	8.31	0.25	0.24	99.29
537.7	7.06	43.41	39.28	0.57	8.74	0.07	0.25	99.40
542.0	6.98	43.52	39.19	0.25	8.81	0.03	0.27	99.05
546.2	6.98	43.52	39.18	0.64	8.81	0.17	0.26	99.57
550.5	8.03	42.12	40.40	0.68	7.95	0.22	0.25	99.65
554.8	7.73	42.53	40.05	0.52	8.20	0.31	0.17	99.51
559.2	6.19	44.58	38.27	0.29	9.46	0.17	0.25	99.22
563.5	6.10	44.71	38.16	0.49	9.54	0.31	0.19	99.49
567.8	6.34	44.38	38.45	0.45	9.34	0.35	0.24	99.54
572.0	5.51	45.48	37.49	0.61	10.01	0.22	0.30	99.63
576.3	5.78	45.13	37.79	0.33	9.80	0.25	0.18	99.26
580.9	6.47	44.21	38.59	0.24	9.23	0.14	0.17	99.05
585.3	7.10	43.37	39.32	0.38	8.71	0.32	0.18	99.38
589.7	6.83	43.72	39.01	0.69	8.93	0.41	0.17	99.77
593.9	7.15	43.30	39.38	0.49	8.67	0.07	0.29	99.36
598.0	7.00	43.50	39.21	0.76	8.79	0.24	0.19	99.69
602.1	6.47	44.20	38.60	0.52	9.23	0.46	0.28	99.77
606.5	6.58	44.07	38.72	0.33	9.14	0.25	0.23	99.31
610.7	6.70	43.90	38.86	0.40	9.04	0.38	0.17	99.45
615.0	6.72	43.87	38.88	0.42	9.02	0.15	0.19	99.26
619.3	6.64	43.98	38.79	0.50	9.09	0.00	0.26	99.26
623.5	7.02	43.48	39.22	0.66	8.78	0.45	0.29	99.90
627.7	7.18	43.26	39.41	0.55	8.65	0.20	0.28	99.53
632.1	6.95	43.57	39.15	0.53	8.84	0.14	0.27	99.44
636.5	6.71	43.88	38.88	0.27	9.03	0.12	0.16	99.04
640.9	7.12	43.33	39.35	0.45	8.69	0.41	0.22	99.58
645.3	7.25	43.17	39.49	0.25	8.59	0.10	0.20	99.05
649.5	7.74	42.51	40.06	0.34	8.19	0.50	0.29	99.63
653.9	8.03	42.13	40.39	0.65	7.95	0.50	0.16	99.81
658.2	8.41	41.62	40.83	0.54	7.64	0.39	0.19	99.62
662.6	8.55	41.44	40.99	0.33	7.53	0.05	0.30	99.17
666.9	8.34	41.71	40.75	0.22	7.70	0.24	0.18	99.14
671.1	7.77	42.47	40.10	0.53	8.16	0.30	0.21	99.53
675.5	7.39	42.98	39.66	0.39	8.47	0.13	0.23	99.25
679.7	7.86	42.35	40.20	0.55	8.09	0.18	0.25	99.47
683.9	6.34	44.38	38.44	0.27	9.34	0.29	0.20	99.27

Pos. (μm)	Pos. (μm)	Pos. (μm)	87/86

Pos. (μm)	Na2O	Al2O3	SiO2	K2O	CaO	FeO	SrO	Total
688.1	6.27	44.47	38.37	0.27	9.39	0.05	0.29	99.11
692.3	7.01	43.49	39.22	0.79	8.79	0.33	0.19	99.81
696.5	7.20	43.23	39.44	0.52	8.63	0.14	0.29	99.46
700.8	7.30	43.10	39.55	0.76	8.55	0.32	0.18	99.76
705.0	7.86	42.35	40.20	0.64	8.09	0.48	0.21	99.82
709.2	6.96	43.55	39.16	0.28	8.83	0.21	0.23	99.22
713.4	7.42	42.94	39.69	0.43	8.45	0.03	0.21	99.17
717.7	7.92	42.27	40.27	0.38	8.04	0.40	0.29	99.57
722.0	7.77	42.48	40.09	0.22	8.17	0.09	0.17	98.98
726.1	7.59	42.71	39.89	0.32	8.31	0.48	0.22	99.53
730.4	7.50	42.83	39.79	0.60	8.38	0.31	0.18	99.60
734.6	5.58	45.40	37.57	0.46	9.96	0.50	0.23	99.69
738.9	4.21	47.22	35.99	0.64	11.08	0.21	0.23	99.58
743.0	6.71	43.89	38.87	0.53	9.04	0.48	0.16	99.67
747.1	7.57	42.74	39.86	0.32	8.33	0.40	0.20	99.43
751.4	7.65	42.64	39.95	0.31	8.27	0.34	0.24	99.39
755.7	7.48	42.86	39.76	0.29	8.40	0.24	0.19	99.22
760.0	5.56	45.43	37.54	0.52	9.98	0.22	0.18	99.42
764.3	6.98	43.52	39.19	0.47	8.81	0.18	0.21	99.36
768.5	7.68	42.60	39.99	0.32	8.24	0.15	0.20	99.17
772.7	7.82	42.41	40.15	0.37	8.12	0.04	0.21	99.11
776.9	7.71	42.56	40.02	0.66	8.22	0.20	0.25	99.60
781.0	7.12	43.34	39.34	0.34	8.70	0.45	0.28	99.56
785.2	6.89	43.65	39.08	0.58	8.89	0.38	0.23	99.69
789.4	5.45	45.57	37.42	0.39	10.07	0.48	0.15	99.52
793.6	4.81	46.42	36.68	0.61	10.59	0.39	0.19	99.69
797.9	5.17	45.94	37.10	0.47	10.29	0.19	0.24	99.40
802.2	4.90	46.31	36.78	0.76	10.52	0.47	0.26	99.99
806.4	3.34	48.39	34.98	0.51	11.80	0.47	0.18	99.66
810.7	4.73	46.53	36.59	0.76	10.65	0.41	0.18	99.85
815.5	3.72	47.88	35.42	0.60	11.48	0.40	0.26	99.76
819.7	5.05	46.10	36.96	0.52	10.39	0.43	0.18	99.62
823.9	4.90	46.30	36.78	0.22	10.52	0.22	0.23	99.16
828.0	4.32	47.08	36.11	0.27	10.99	0.09	0.25	99.11
832.3	6.08	44.72	38.15	0.55	9.55	0.11	0.22	99.39
836.6	6.38	44.33	38.49	0.77	9.30	0.39	0.26	99.92
840.8	4.33	47.06	36.13	0.77	10.98	0.23	0.19	99.69
845.0	6.88	43.66	39.07	0.39	8.89	0.44	0.28	99.61
849.1	7.31	43.09	39.56	0.52	8.54	0.29	0.24	99.55
853.4	6.92	43.60	39.11	0.59	8.86	0.01	0.17	99.27
857.8	7.36	43.02	39.62	0.40	8.50	0.36	0.23	99.49
857.8	6.86	43.68	39.05	0.56	8.91	0.13	0.18	99.37
862.0	7.53	42.79	39.82	0.22	8.36	0.06	0.29	99.07
866.1	7.46	42.88	39.74	0.70	8.42	0.31	0.26	99.76
870.1	7.24	43.18	39.48	0.24	8.60	0.19	0.29	99.21
874.4	7.17	43.27	39.40	0.39	8.66	0.14	0.29	99.33
878.6	4.28	47.13	36.07	0.46	11.03	0.37	0.26	99.59
882.9	5.86	45.02	37.89	0.50	9.73	0.23	0.16	99.39
887.0	3.98	47.53	35.72	0.77	11.27	0.36	0.22	99.84
891.1	5.01	46.16	36.91	0.49	10.43	0.28	0.25	99.52
895.3	5.24	45.84	37.18	0.30	10.24	0.07	0.24	99.10
899.5	5.91	44.96	37.94	0.47	9.69	0.08	0.16	99.21
903.7	6.96	43.55	39.16	0.22	8.82	0.36	0.28	99.36
907.8	6.55	44.10	38.69	0.65	9.16	0.08	0.18	99.40
912.0	7.44	42.91	39.71	0.61	8.43	0.31	0.16	99.58
916.2	7.27	43.14	39.51	0.40	8.58	0.42	0.22	99.54
920.4	7.30	43.11	39.55	0.38	8.55	0.38	0.18	99.45

Pos. (μm)	Pos. (μm)	Pos. (μm)	87/86

Pos. (µm)	Na2O	Al2O3	SiO2	K2O	CaO	FeO	SrO	Total
924.5	7.64	42.64	39.95	0.40	8.27	0.24	0.21	99.35
928.6	7.75	42.50	40.07	0.28	8.18	0.41	0.26	99.45
932.8	7.68	42.59	39.99	0.53	8.24	0.05	0.22	99.31
937.0	7.44	42.91	39.71	0.71	8.43	0.06	0.21	99.48
941.2	7.09	43.38	39.31	0.37	8.72	0.11	0.15	99.13
945.3	6.92	43.61	39.11	0.62	8.86	0.26	0.26	99.64
949.5	7.23	43.19	39.47	0.24	8.61	0.30	0.22	99.25
953.6	17.74	29.18	51.58	0.33	0.00	0.15	0.26	99.24
957.7	7.61	42.69	39.91	0.25	8.30	0.08	0.16	98.99
961.9	7.68	42.59	39.99	0.79	8.24	0.41	0.16	99.87
966.1	7.69	42.58	40.00	0.21	8.23	0.02	0.26	98.99
970.1	7.88	42.32	40.22	0.76	8.07	0.06	0.26	99.58
974.3	7.48	42.86	39.75	0.63	8.41	0.34	0.22	99.70
978.3	7.14	43.31	39.37	0.39	8.68	0.49	0.22	99.60
982.4	6.35	44.36	38.46	0.42	9.32	0.33	0.20	99.46
986.5	7.64	42.65	39.94	0.61	8.27	0.35	0.24	99.70
990.6	7.38	42.99	39.64	0.33	8.49	0.44	0.26	99.53
994.6	7.46	42.89	39.73	0.64	8.42	0.35	0.25	99.74
998.8	7.39	42.98	39.65	0.61	8.48	0.04	0.17	99.32
1002.8	7.33	43.05	39.59	0.56	8.52	0.41	0.18	99.64
1006.9	6.42	44.28	38.53	0.23	9.27	0.24	0.28	99.25
1011.0	6.80	43.77	38.97	0.80	8.96	0.28	0.21	99.79
1015.1	5.94	44.91	37.99	0.35	9.66	0.20	0.16	99.21
1019.3	6.47	44.20	38.60	0.28	9.23	0.37	0.26	99.41
1023.3	6.83	43.72	39.01	0.33	8.93	0.13	0.17	99.13

Pos. (µm)	Pos. (µm)	Pos. (µm)	87/86

Unit: El Chichon E
Thin Section: CHI-9516
Crystal: F

Microprobe analyses

Pos. (μm)	Na2O	Al2O3	SiO2	K2O	CaO	FeO	SrO	Total
0	5.93	26.60	54.69	0.53	8.93	0.18	0.22	97.09
9.900505	5.97	27.17	55.34	0.47	9.25	0.17	0.18	98.54
19.80025	6.21	27.46	56.05	0.46	9.04	0.20	0.26	99.69
29.80017	6.39	26.97	55.78	0.46	9.07	0.24	0.24	99.16
29.90017	5.90	26.95	55.86	0.47	9.14	0.20	0.27	98.79
39.90013	6.59	26.78	56.28	0.50	8.48	0.17	0.17	98.97
50.1001	6.74	26.51	56.62	0.52	8.33	0.21	0.20	99.12
60.10008	6.72	26.42	56.96	0.55	8.26	0.18	0.21	99.28
70.10007	6.61	26.91	56.44	0.56	8.36	0.22	0.22	99.33
80.10006	6.92	26.43	56.69	0.57	8.34	0.18	0.20	99.33
90.10006	6.70	26.55	56.59	0.54	8.46	0.19	0.23	99.26
100.1	6.57	26.63	55.93	0.52	8.55	0.17	0.22	98.58
110.1	7.07	26.50	56.76	0.56	8.16	0.19	0.24	99.48
120.1	6.51	26.71	56.25	0.48	8.69	0.19	0.23	99.05
130.1	6.26	27.15	55.95	0.47	9.13	0.24	0.19	99.38
140.1	6.43	26.68	55.36	0.48	8.99	0.15	0.33	98.40
149.8	5.90	27.34	54.20	0.43	9.57	0.26	0.17	97.87
160.1	5.96	27.64	54.99	0.38	9.57	0.30	0.24	99.09
170.1	6.15	27.73	55.43	0.46	9.40	0.20	0.21	99.59
180.1	6.27	27.59	55.51	0.44	9.35	0.18	0.20	99.54
190.1	6.35	26.87	55.81	0.50	8.78	0.25	0.22	98.78
200.1	6.61	27.05	56.03	0.48	8.91	0.20	0.16	99.45
210.1	6.13	27.33	55.50	0.45	9.31	0.23	0.19	99.15
220.1	6.27	27.35	55.47	0.47	9.26	0.29	0.24	99.35
230.2	6.01	27.74	55.47	0.43	9.51	0.26	0.24	99.66
240.3	6.40	27.19	55.97	0.49	8.81	0.14	0.27	99.26
250.1	6.02	27.73	55.44	0.42	9.52	0.25	0.23	99.61
260.3	6.05	27.29	54.04	0.42	9.46	0.21	0.20	97.66
270.3	6.37	27.11	55.34	0.47	8.97	0.26	0.24	98.77
280.3	6.36	26.62	56.35	0.46	8.80	0.23	0.24	99.05
290.3001	6.47	26.55	56.78	0.52	8.39	0.24	0.25	99.21
300.3	6.44	26.71	55.93	0.52	8.62	0.22	0.25	98.70
310.4	6.74	26.61	56.58	0.49	8.38	0.12	0.25	99.17
320.4	6.19	26.99	55.33	0.44	9.13	0.14	0.30	98.51
330.4	6.27	27.03	55.64	0.45	8.96	0.20	0.23	98.77
340.4	6.69	26.51	56.80	0.54	8.31	0.17	0.24	99.25
350.4	6.89	26.49	56.79	0.57	8.34	0.20	0.19	99.48
360.4	6.59	26.62	56.89	0.53	8.26	0.24	0.22	99.34
370.4	6.65	26.37	56.67	0.58	8.09	0.24	0.22	98.82
380.4	6.56	26.43	56.97	0.54	8.37	0.22	0.24	99.34
390.4	6.75	26.51	56.47	0.54	8.19	0.16	0.28	98.90
400.4	6.49	25.95	54.23	0.48	10.02	0.14	0.24	97.55
410.3	6.69	26.91	55.70	0.50	8.81	0.16	0.28	99.04
420.2	6.76	25.93	56.76	0.57	8.32	0.13	0.25	98.73
430.3	7.18	25.77	57.94	0.61	7.65	0.18	0.26	99.58
440.2	7.10	25.70	57.94	0.63	7.60	0.23	0.32	99.52
450.2	7.01	26.03	57.32	0.61	7.74	0.24	0.24	99.19
460.1	6.49	24.45	54.62	0.64	7.38	0.20	0.21	93.98
469.9	7.25	26.09	57.30	0.57	7.93	0.19	0.29	99.61

ICP-MS

Pos. (μm)	87/86
0	0.70486
5	0.70420
10	0.70389
15	0.70331
20	0.70400
25	0.70335
30	0.70369
35	0.70498
40	0.70430
45	0.70430
50	0.70311
55	0.70466
60	0.70276
65	0.70387
70	0.70349
75	0.70499
80	0.70321
85	0.70422
90	0.70416
95	0.70427
100	0.70559
105	0.70296
110	0.70394
115	0.70463
120	0.70330
125	0.70417
130	0.70507
135	0.70298
140	0.70394
145	0.70407
150	0.70451
155	0.70565
160	0.70443
165	0.70433
170	0.70443
175	0.70478
180	0.70378
185	0.70447
190	0.70420
195	0.70358
200	0.70425
205	0.70407
210	0.70398
215	0.70440
220	0.70306
225	0.70413
230	0.70312
235	0.70361
240	0.70433

Pos. (µm)	Na2O	Al2O3	SiO2	K2O	CaO	FeO	SrO	Total	Pos. (µm)	Pos. (µm)
480.1	6.58	26.62	57.50	0.53	8.44	0.18	0.27	100.12	245	0.70410
490.1	6.72	26.13	56.76	0.51	8.24	0.17	0.28	98.81	250	0.70445
500.1	6.83	26.27	56.64	0.55	8.20	0.22	0.23	98.95	255	0.70363
510.1	6.93	25.98	57.26	0.56	8.01	0.19	0.21	99.14	260	0.70340
520.1	6.03	24.85	53.74	0.55	8.16	0.21	0.27	93.81	265	0.70398
529.8	6.17	27.42	54.97	0.42	9.47	0.21	0.24	98.89	270	0.70429
540.1	6.37	27.05	55.60	0.44	9.26	0.24	0.25	99.20	275	0.70471
550.1	6.50	26.46	56.50	0.51	8.52	0.21	0.21	98.91	280	0.70370
560.1	7.08	25.79	57.84	0.63	7.63	0.11	0.28	99.35	285	0.70363
570.1	6.90	25.60	57.65	0.60	7.66	0.26	0.24	98.90	290	0.70557
								0.00	295	0.70407
589.9	7.35	6.21	57.98	0.66	7.20	0.20	0.24	79.84	300	
600.1	7.39	25.34	58.27	0.69	7.20	0.22	0.23	99.34	305	
610.1	7.02	25.86	57.87	0.62	7.60	0.26	0.28	99.51	310	
620.1	7.12	25.54	57.39	0.62	7.52	0.12	0.30	98.60	315	
630.1	7.46	26.19	59.05	0.68	7.27	0.22	0.25	101.12	320	
640.1	7.32	24.94	58.12	0.72	6.95	0.18	0.19	98.41	325	
649.6	7.41	25.21	58.42	0.73	7.05	0.17	0.24	99.22	330	
660.1	7.43	25.15	58.03	0.70	6.86	0.20	0.29	98.67	335	
670.1	6.87	25.80	57.37	0.58	7.89	0.24	0.25	98.99	340	
680.1	6.80	26.27	56.93	0.55	8.28	0.25	0.26	99.33	345	
690.1	7.19	25.42	58.16	0.68	7.22	0.20	0.26	99.13	350	
700.1001	6.68	25.45	57.35	0.65	7.55	0.18	0.26	98.11	355	
710.1001	7.23	25.62	57.87	0.64	7.30	0.22	0.22	99.10	360	
720.1001	7.11	25.56	57.73	0.64	7.56	0.17	0.24	99.00	365	
730.1001	7.00	25.74	56.73	0.59	7.84	0.21	0.24	98.34	370	
740.1001	6.28	26.52	55.65	0.49	8.87	0.26	0.28	98.35	375	
750.1001	6.71	25.61	57.37	0.56	7.74	0.16	0.21	98.36	380	
760.2001	6.92	25.47	58.10	0.66	7.36	0.15	0.23	98.90	385	
770.2001	6.43	24.44	53.63	0.57	7.83	0.20	0.23	93.31	390	
780.2001	6.70	26.00	56.61	0.58	8.03	0.22	0.21	98.34	395	
790.2001	6.95	25.76	57.14	0.63	7.83	0.16	0.19	98.65	400	
800.3001	7.05	25.60	58.35	0.63	7.56	0.13	0.25	99.57	405	
810.3001	7.28	25.22	58.06	0.63	7.38	0.25	0.24	99.04	410	
820.3001	7.27	26.10	57.35	0.57	7.94	0.23	0.21	99.67	415	
830.3001	6.47	26.06	56.13	0.52	8.36	0.17	0.30	98.01	420	
840.3001	6.81	25.63	57.34	0.61	7.71	0.22	0.22	98.54	425	
850.3001	7.00	26.18	56.80	0.55	8.16	0.23	0.30	99.21	430	
860.4001	6.86	26.36	56.66	0.49	8.27	0.24	0.23	99.11	435	0.70320
869.9001	6.43	26.12	56.13	0.52	8.62	0.18	0.23	98.22	440	0.70430
880.4001	6.00	25.60	55.53	0.55	8.16	0.21	0.19	96.24	445	0.70402
890.4001	6.55	26.17	56.70	0.55	8.27	0.29	0.20	98.74	450	0.70277
900.4	6.61	26.32	56.46	0.56	8.39	0.23	0.22	98.80	455	0.70351
910.4001	6.78	26.41	56.67	0.53	8.60	0.26	0.20	99.44	460	0.70398
920.4	6.73	26.40	56.36	0.50	8.52	0.23	0.26	99.01	465	0.70292
930.5	6.25	26.69	55.93	0.46	8.84	0.19	0.16	98.50	470	0.70392
940.5001	6.76	26.27	56.72	0.54	8.33	0.23	0.24	99.08	475	0.70395
950.5001	5.97	27.57	54.85	0.43	9.54	0.22	0.28	98.86	480	0.70333
960.5001	6.14	26.67	55.50	0.43	9.11	0.12	0.23	98.20	485	0.70435
970.5001	5.75	25.22	51.87	0.51	8.09	0.26	0.18	91.88	490	0.70487
980.5001	6.37	26.00	56.09	0.51	8.68	0.18	0.24	98.07	495	0.70262
990.5001	6.99	26.03	57.07	0.54	8.03	0.16	0.23	99.05	500	0.70467
1000.5	6.99	25.41	57.53	0.63	7.48	0.18	0.28	98.52	505	0.70445
1010.5	6.70	26.12	56.13	0.52	8.29	0.19	0.23	98.18	510	0.70455

Pos. (μm)	Na2O	Al2O3	SiO2	K2O	CaO	FeO	SrO	Total	Pos. (μm)	Pos. (μm)
1020.5	6.96	25.80	56.62	0.56	8.17	0.25	0.19	98.55	515	0.70381
1030.4	6.80	25.54	56.99	0.58	8.01	0.22	0.20	98.34	520	0.70500
1040.5	7.16	25.64	57.71	0.61	7.65	0.18	0.16	99.10	525	0.70277
1050.5	6.85	25.33	57.05	0.62	7.65	0.20	0.18	97.88	530	0.70377
1060.6	7.22	25.62	57.33	0.61	7.77	0.24	0.22	99.00	535	0.70352
1070.5	7.15	25.27	57.20	0.66	7.44	0.20	0.20	98.12	540	0.70346
1080.6	6.84	25.66	57.08	0.59	7.69	0.17	0.15	98.18	545	0.70467
1090.6	6.59	25.97	56.63	0.53	8.36	0.23	0.28	98.58	550	0.70543
1100.6	7.03	25.52	56.91	0.59	7.84	0.25	0.18	98.31	555	0.70313
1110.6	6.97	25.72	56.11	0.56	8.18	0.25	0.25	98.03	560	0.70425
1120.5	6.86	26.30	55.74	0.51	8.57	0.15	0.21	98.34	565	0.70357
1130.5	6.99	25.65	56.73	0.58	7.82	0.15	0.17	98.09	570	0.70377
1140.5	7.07	25.27	57.15	0.62	7.73	0.17	0.20	98.22	575	0.70442
1150.5	7.27	25.25	57.57	0.66	7.43	0.19	0.17	98.54	580	0.70364
1160.5	7.67	25.09	58.44	0.69	7.12	0.23	0.20	99.44	585	0.70354
1170.5	6.53	24.46	57.70	0.58	7.91	0.26	0.17	97.61	590	0.70372
1180.5	6.25	26.65	55.12	0.49	9.00	0.20	0.27	97.97	595	0.70408
1190.4	6.48	26.04	56.09	0.52	8.60	0.27	0.26	98.26	600	0.70402
1200.5	6.60	24.72	56.56	0.63	7.78	0.18	0.28	96.75	605	
1210.5	7.02	25.86	57.61	0.63	7.64	0.20	0.19	99.14	610	
1220.5	3.37	17.35	40.11	0.58	6.73	0.18	0.18	68.51	615	
1230.5	6.78	24.74	55.37	0.63	7.61	0.27	0.23	95.62	620	0.70330
1240.5	6.22	26.58	55.53	0.46	9.04	0.23	0.33	98.38	625	0.70287
1250.5	6.49	26.71	56.00	0.51	8.75	0.28	0.25	98.98	630	0.70367
1260.5	6.15	26.31	55.77	0.54	8.67	0.21	0.25	97.90	635	0.70396
1270.5	6.48	27.03	50.85	0.55	8.76	0.31	0.19	94.16	640	0.70468
1280.6	6.45	27.00	56.08	0.51	9.04	0.32	0.24	99.65	645	0.70532
1290.6	5.99	26.71	54.52	0.44	9.47	0.25	0.26	97.64	650	0.70349
1300.6	5.78	27.35	54.30	0.38	9.83	0.19	0.29	98.11	655	0.70527
1310.6	5.20	28.44	52.82	0.31	11.23	0.23	0.17	98.39	660	0.70483
1320.6	4.92	28.38	52.98	0.32	10.74	0.29	0.25	97.87	665	0.70454
1330.5	6.13	27.25	55.00	0.43	9.21	0.27	0.28	98.56	670	0.70352
1340.6	6.38	26.43	55.12	0.50	8.81	0.14	0.25	97.63	675	0.70470
1350.6	6.01	25.71	54.32	0.48	8.91	0.25	0.27	95.94	680	0.70449
1360.6	7.22	25.84	56.69	0.48	7.98	0.17	0.26	98.64	685	0.70423
1370.6	3.63	14.89	34.83	0.30	4.87	0.12	0.14	58.79	690	0.70367
1380.6	6.21	25.67	54.58	0.53	8.65	0.29	0.25	96.17	695	0.70509
1390.6	6.65	25.96	55.70	0.51	8.55	0.24	0.27	97.88	700	0.70373
1400.6	6.60	26.08	56.07	0.55	8.46	0.32	0.29	98.37	705	0.70380
1410.7	8.17	26.80	59.33	0.67	7.48	0.25	0.25	102.95	710	0.70406
1420.7	7.02	25.06	57.27	0.66	7.48	0.23	0.22	97.93	715	0.70433
1430.7	7.33	24.94	56.91	0.61	7.61	0.19	0.28	97.87	720	0.70550
1440.9	7.09	25.26	56.88	0.61	7.77	0.25	0.26	98.11	725	
1450.9	6.44	26.30	55.33	0.49	8.79	0.31	0.27	97.94	730	
1461.1	6.06	27.40	54.15	0.39	9.96	0.28	0.21	98.45	735	
1470.6	6.63	25.91	56.10	0.50	8.50	0.25	0.22	98.10	740	
1481.1	6.94	25.35	56.82	0.60	8.01	0.23	0.31	98.26	745	
1491.3	6.87	25.78	56.44	0.57	8.42	0.21	0.28	98.56	750	
1501.4	6.18	24.28	57.61	0.54	8.33	0.23	0.27	97.45	755	
1511.4	6.27	26.74	54.50	0.42	9.26	0.22	0.28	97.70	760	0.70502
1521.4	5.81	26.92	54.63	0.41	9.65	0.29	0.29	98.01	765	0.70422
1531.4	5.55	27.88	53.59	0.33	10.54	0.23	0.24	98.37	770	0.70419
1541.5	5.54	27.58	53.94	0.37	10.21	0.25	0.26	98.15	775	
1551.5	6.04	27.33	53.88	0.37	9.99	0.32	0.30	98.22	780	0.70458

Pos. (μm)	Na2O	Al2O3	SiO2	K2O	CaO	FeO	SrO	Total
1561.5	5.81	27.25	54.27	0.40	9.68	0.23	0.27	97.90
1571.5	6.64	26.23	55.81	0.50	8.64	0.27	0.34	98.42
1581.5	6.54	26.45	56.17	0.51	8.56	0.27	0.29	98.79
1591.5	6.73	26.14	56.57	0.53	8.45	0.29	0.37	99.08
1601.5	6.77	26.25	55.95	0.50	8.54	0.20	0.18	98.38

Pos. (μm)	Pos. (μm)
785	
790	
795	0.70390
800	0.70483
805	0.70386
810	0.70409
815	0.70410
820	0.70399
825	0.70361
830	0.70389
835	0.70419
840	0.70423
845	0.70396
850	0.70376
855	0.70445
860	0.70364
865	0.70421
870	0.70444
875	0.70472
880	0.70455
885	0.70529
890	0.70454
895	0.70347
900	0.70429
905	0.70427
910	0.70482
915	0.70529
920	0.70413
925	0.70402
930	0.70403
935	0.70309
940	0.70339
945	0.70459
950	0.70373
955	0.70428
960	0.70397
965	
970	
975	
980	
985	
990	0.70435
995	0.70300
1000	0.70451
1005	0.70465
1010	0.70382
1015	0.70501
1020	0.70326
1025	0.70396
1030	
1035	
1040	
1045	0.70290
1050	0.70419

Pos. (μm)	Na2O	Al2O3	SiO2	K2O	CaO	FeO	SrO	Total

Pos. (μm)	Pos. (μm)
1055	0.70343
1060	0.70489
1065	0.70388
1070	0.70269
1075	0.70476
1080	0.70360
1085	0.70290
1090	0.70430
1095	0.70341
1100	
1105	
1110	
1115	
1120	
1125	
1130	
1135	
1140	0.70333
1145	0.70375
1150	0.70509
1155	0.70385
1160	0.70492
1165	0.70358
1170	0.70356
1175	0.70501
1180	0.70412
1185	0.70320
1190	0.70460
1195	0.70446
1200	0.70408
1205	0.70404
1210	0.70392
1215	0.70343
1220	0.70388
1225	0.70453
1230	0.70397
1235	0.70369
1240	0.70467
1245	0.70404
1250	0.70358
1370	
1375	0.70418
1380	0.70381
1385	0.70490
1390	
1395	
1400	
1405	
1410	
1415	
1420	
1425	0.70380
1430	0.70393

Pos. (µm)	Na2O	Al2O3	SiO2	K2O	CaO	FeO	SrO	Total

Pos. (µm)	Pos. (µm)
1435	0.70493
1440	0.70369
1445	0.70574
1450	0.70422
1455	0.70390
1460	0.70365
1465	0.70450
1470	0.70409
1475	0.70498
1480	0.70396
1485	0.70379
1490	0.70447
1495	0.70476
1500	0.70426
1505	0.70370
1510	0.70385
1515	0.70351
1520	0.70432
1525	0.70441
1530	0.70555
1535	0.70479
1540	0.70482
1545	0.70414
1550	0.70480
1555	0.70471
1560	0.70453
1565	0.70478
1570	0.70378
1575	0.70400
1580	0.70359
1585	0.70404
1590	0.70336
1595	0.70454
1600	0.70472
1605	0.70495
1610	0.70537
1615	0.70437
1620	0.70488
1625	0.70410
1630	0.70378
1635	0.70288
1640	0.70446
1645	0.70341
1650	0.70374
1655	0.70293
1660	0.70475
1665	0.70402
1670	0.70536
1675	0.70552
1680	0.70352
1685	0.70355
1690	0.70374
1695	0.70314
1700	0.70358

Pos. (μm)	Na2O	Al2O3	SiO2	K2O	CaO	FeO	SrO	Total

Pos. (μm)	Pos. (μm)
1705	0.70340
1710	0.70474
1715	0.70360
1720	0.70325
1725	0.70393
1730	0.70494
1735	0.70384
1740	0.70454
1745	0.70374
1750	0.70357
1755	0.70354

Unit: El Chichon E
Thin Section: CHI-9516
Crystal: G

Microprobe analyses

Pos. (µm)	Na2O	Al2O3	SiO2	K2O	CaO	FeO	SrO	Total
0.0	5.61	27.42	54.25	0.35	10.19	0.27	0.20	98.29
10.0	6.58	25.17	57.16	0.38	8.16	0.27	0.21	97.93
20.0	5.99	26.25	55.14	0.41	9.31	0.30	0.22	97.62
30.0	6.22	26.96	55.05	0.45	9.40	0.31	0.28	98.68
40.2	6.53	26.11	55.99	0.49	8.68	0.30	0.25	98.35
50.2	6.41	26.47	55.63	0.49	9.01	0.35	0.21	98.57
60.2	6.52	26.29	55.77	0.52	8.56	0.19	0.30	98.16
70.3	6.29	26.03	55.99	0.51	8.60	0.26	0.25	97.93
80.3	6.56	25.74	55.77	0.55	8.47	0.33	0.23	97.64
90.4	6.48	25.93	56.37	0.53	8.56	0.23	0.34	98.43
100.4	6.27	26.55	55.38	0.50	9.11	0.27	0.25	98.33
110.4	6.61	25.72	56.27	0.55	8.24	0.30	0.27	97.97
120.4	6.75	26.02	56.15	0.53	8.27	0.29	0.27	98.28
150.5	6.18	27.09	54.73	0.42	9.47	0.25	0.22	98.37
160.5	6.40	25.81	56.37	0.57	8.39	0.20	0.23	97.96
170.5	6.56	26.32	56.07	0.52	8.44	0.26	0.21	98.37
180.5	6.76	26.08	56.20	0.52	8.64	0.27	0.19	98.65
190.5	6.81	25.86	56.55	0.51	8.41	0.26	0.24	98.62
200.5	6.91	25.82	56.65	0.58	8.04	0.22	0.21	98.42
210.5	6.73	25.91	56.69	0.59	8.16	0.25	0.36	98.68
220.5	6.84	26.04	56.24	0.55	8.35	0.26	0.26	98.54
230.6	6.55	26.56	56.21	0.50	8.85	0.27	0.26	99.18
240.6	6.35	26.32	55.77	0.47	8.78	0.26	0.20	98.16
250.6	6.56	25.97	56.84	0.51	8.88	0.26	0.33	99.33
260.6	6.30	26.23	55.66	0.50	8.94	0.33	0.27	98.23
270.6	6.65	26.31	56.16	0.55	8.42	0.30	0.23	98.62
280.6	6.33	26.19	55.27	0.47	9.02	0.23	0.27	97.77
290.6	6.62	26.15	55.95	0.48	8.76	0.39	0.22	98.56
300.6	6.52	25.86	56.03	0.51	8.54	0.23	0.24	97.92
310.6	6.34	25.86	56.18	0.51	8.53	0.31	0.30	98.03
320.6	6.36	26.21	55.74	0.51	8.66	0.25	0.20	97.93
330.6	6.64	25.58	56.86	0.55	8.21	0.24	0.24	98.32
340.6	6.84	25.72	56.62	0.56	8.15	0.23	0.16	98.28
350.5	6.79	25.60	56.75	0.56	8.06	0.32	0.25	98.33
360.5	6.69	25.83	55.96	0.53	8.51	0.24	0.27	98.03
370.5	6.54	25.90	55.32	0.51	8.84	0.26	0.19	97.55
380.5	6.82	25.80	55.95	0.55	8.63	0.24	0.25	98.24
390.5	5.46	24.48	51.38	0.49	8.11	0.31	0.29	90.52
400.5	5.10	18.76	64.34	8.87	0.65	0.21	0.05	97.97
410.5	4.89	17.55	59.04	8.14	0.50	0.24	0.10	90.45
420.5	6.22	26.92	54.87	0.45	9.25	0.37	0.26	98.34
430.5	6.64	25.94	55.80	0.49	8.53	0.29	0.29	97.98
440.6	6.48	26.04	56.26	0.52	8.45	0.26	0.26	98.27
450.6	6.69	25.77	56.15	0.51	8.50	0.31	0.25	98.18
460.6	6.53	25.66	56.09	0.56	8.36	0.31	0.33	97.84
470.7	4.24	29.32	51.04	0.22	12.64	0.30	0.26	98.02
480.7	4.83	28.97	51.76	0.28	11.94	0.36	0.25	98.38
490.7	4.67	27.63	52.50	0.27	11.25	0.33	0.24	96.90
500.7	5.17	27.60	52.84	0.32	10.64	0.30	0.25	97.11

ICP-MS

Pos. (µm)	87/86	87/86

Pos. (μm)	Na2O	Al2O3	SiO2	K2O	CaO	FeO	SrO	Total
510.7	5.32	27.92	53.09	0.30	10.78	0.26	0.25	97.91
520.7	6.10	26.40	55.31	0.52	8.76	0.39	0.27	97.75
530.7	7.16	25.30	56.59	0.59	7.87	0.23	0.33	98.06
540.7	6.75	25.82	56.21	0.54	8.29	0.28	0.29	98.19
550.8	6.65	26.02	55.76	0.53	8.50	0.23	0.28	97.97
560.8	7.04	25.01	57.16	0.61	7.68	0.33	0.29	98.11
580.3	6.57	25.69	56.32	0.58	8.03	0.23	0.29	97.70
591.2	6.93	25.03	57.21	0.61	7.62	0.37	0.29	98.07
601.2	6.55	25.80	56.04	0.56	8.33	0.24	0.31	97.83
611.3	7.12	24.96	57.02	0.65	7.56	0.24	0.25	97.78
621.4	7.32	25.12	57.06	0.63	7.68	0.35	0.26	98.43
631.4	7.23	24.67	57.56	0.65	7.40	0.24	0.21	97.96
641.5	7.08	24.72	57.46	0.66	7.36	0.26	0.29	97.82
651.6	7.10	25.37	56.88	0.63	7.83	0.30	0.29	98.40
661.7	6.68	25.71	55.98	0.57	8.35	0.27	0.28	97.84
671.7	6.71	25.83	56.19	0.55	8.29	0.33	0.30	98.21
681.9	5.78	23.30	52.12	0.57	7.51	0.21	0.22	89.71
692.0	6.64	25.45	56.21	0.52	8.24	0.27	0.26	97.60
702.4	6.62	25.51	56.90	0.57	7.94	0.29	0.27	98.11
712.4	7.16	25.51	56.61	0.57	7.98	0.23	0.25	98.30
722.5	6.97	25.21	56.81	0.62	7.69	0.19	0.28	97.76
732.6	6.99	25.12	57.13	0.65	7.67	0.19	0.28	98.03
742.7	7.20	24.76	57.95	0.71	7.15	0.27	0.27	98.31
752.7	7.02	25.27	57.11	0.64	7.56	0.27	0.21	98.07
762.7	7.10	24.67	58.04	0.70	7.18	0.21	0.25	98.15
772.9	7.11	24.94	57.63	0.69	7.47	0.23	0.21	98.28
783.0	7.06	24.89	58.01	0.66	7.33	0.32	0.24	98.51

Pos. (μm)	Pos. (μm)	Pos. (μm)

Unit: El Chichon E
Thin Section: CHI-9516
Crystal: H

Microprobe analyses

Pos. (μm)	Na2O	Al2O3	SiO2	K2O	CaO	FeO	SrO	Total
0	7.21	25.55	57.29	0.59	7.61	0.16	0.26	98.67
10.1	7.44	25.39	56.63	0.63	7.56	0.24	0.23	98.12
20	7.53	24.88	57.06	0.61	7.31	0.20	0.21	97.79
30.1	7.40	25.04	57.12	0.66	7.41	0.25	0.21	98.09
40	7.40	25.40	57.89	0.65	7.23	0.16	0.26	98.99
50.1	7.46	24.97	57.49	0.67	7.20	0.19	0.21	98.20
60.1	7.49	25.13	57.59	0.67	7.22	0.17	0.28	98.54
70.2	7.63	24.74	57.76	0.69	6.81	0.18	0.19	97.99
80.2	7.86	24.67	58.05	0.65	6.83	0.20	0.27	98.54
90.2	7.79	24.64	57.95	0.69	6.53	0.17	0.24	97.99
100.2	7.98	24.67	58.38	0.71	6.46	0.16	0.24	98.61
110.2	7.56	24.52	57.77	0.67	6.70	0.25	0.26	97.73
120.1	7.43	24.80	57.27	0.64	6.92	0.21	0.23	97.49
130.1	7.24	25.08	57.18	0.59	7.16	0.16	0.30	97.70
140.1	7.10	25.13	56.90	0.60	7.28	0.17	0.22	97.40
150.1	7.33	25.19	56.47	0.58	7.47	0.19	0.29	97.51
160.2	7.11	25.32	56.35	0.57	7.39	0.16	0.23	97.13
170.2	6.87	25.43	55.68	0.53	7.91	0.30	0.29	97.01
180.2	5.61	28.02	53.07	0.35	10.26	0.27	0.30	97.87
190.2	5.64	27.16	53.20	0.37	9.80	0.21	0.27	96.65
200.2	5.63	25.27	44.85	0.38	8.14	0.24	0.16	84.67
210.3	6.41	25.90	54.16	0.44	8.57	0.26	0.27	96.01
220.2	6.80	25.96	56.01	0.54	8.16	0.16	0.29	97.93
230.3	7.21	25.25	56.23	0.60	7.43	0.22	0.30	97.23
240.3	7.25	24.98	57.18	0.68	7.22	0.23	0.26	97.80
250.1	7.66	24.49	57.63	0.71	6.74	0.27	0.25	97.75
260.3	8.06	24.20	58.14	0.76	6.51	0.24	0.28	98.19
270.2	7.42	25.27	56.69	0.64	7.24	0.22	0.23	97.71
280.1	7.00	25.64	56.03	0.57	7.90	0.19	0.20	97.53
290.2	6.98	25.25	56.44	0.59	7.30	0.28	0.25	97.09
300.3	7.25	24.58	57.26	0.64	6.95	0.21	0.24	97.11
310.3	7.62	23.84	57.90	0.79	6.27	0.22	0.26	96.89
320.4	7.97	23.75	59.16	0.91	5.64	0.30	0.25	97.97
330.4	8.02	23.94	58.72	0.87	6.03	0.28	0.26	98.13
340.5	7.51	24.48	57.92	0.70	6.63	0.28	0.28	97.79
350.5	7.30	24.94	57.06	0.62	7.03	0.27	0.25	97.46
360.5	7.43	24.89	57.24	0.64	7.08	0.28	0.23	97.78
370.5	7.80	23.87	58.12	0.79	6.18	0.27	0.21	97.26
380.4	7.36	24.78	56.79	0.62	7.12	0.31	0.27	97.27
390.4	7.05	25.09	56.76	0.60	7.41	0.23	0.21	97.34
400.5	7.30	24.69	57.24	0.67	7.05	0.22	0.25	97.42
410.5	7.54	24.60	57.74	0.68	6.76	0.31	0.23	97.85
420.5	7.37	25.10	56.92	0.62	7.11	0.28	0.21	97.61
430.3	6.85	25.08	56.85	0.61	7.35	0.28	0.17	97.19
440.5	7.38	25.70	56.65	0.55	7.59	0.31	0.24	98.42
450.5	7.40	25.25	56.86	0.61	7.29	0.26	0.29	97.94
460.4	7.12	25.17	57.31	0.62	7.08	0.25	0.28	97.83
470.5	8.01	24.84	57.72	0.62	6.57	0.34	0.24	98.35
480.4	6.87	25.61	56.86	0.54	7.51	0.31	0.25	97.95

ICP-MS

Pos. (μm)	87/86	87/86
15	0.70076	0.70305
30	0.70289	0.70552
45	0.70663	0.70450
60	0.70511	0.70432
80	0.70425	0.70517
100	0.70620	0.70225
120	0.70392	0.70328
140	0.70620	0.70718
155	0.70433	0.70230
170	0.70460	0.70458
185	0.70265	0.70420
200	0.70393	0.70127
215	0.70378	0.70296
230	0.70402	0.70449
245	0.70321	0.70460
260	0.70421	0.70351
275	0.70250	0.70422
290	0.70288	0.70185
305	0.70285	0.70398
320	0.70238	0.70427
335	0.70418	0.70327
350	0.70251	0.70280
365	0.70589	0.70456
380	0.70363	0.70395
395	0.70418	0.70411
410	0.70414	0.70319
425	0.70540	0.70400
440	0.70429	0.70209
455	0.70442	0.70308
470	0.70337	0.70320
485	0.70371	0.70418
500	0.70421	0.70180
515	0.70422	0.70458
530	0.70309	0.70377
545	0.70450	0.70405
560	0.70375	0.70405
575	0.70375	

Pos. (µm)	Na2O	Al2O3	SiO2	K2O	CaO	FeO	SrO	Total
490.5	7.43	25.01	56.70	0.63	7.17	0.24	0.31	97.49
500.5	7.35	24.93	56.99	0.57	7.16	0.28	0.22	97.49
510.5	7.64	25.04	56.87	0.57	7.15	0.25	0.23	97.74
520.5	6.87	23.97	55.73	0.62	7.03	0.24	0.20	94.66
530.5	7.36	24.74	56.45	0.59	7.16	0.31	0.28	96.91
540.5	7.16	25.44	56.62	0.56	7.40	0.29	0.28	97.75
550.5	7.40	25.21	55.48	0.57	7.12	0.22	0.31	96.29
560.5	7.65	24.99	57.54	0.63	6.72	0.21	0.23	97.96

Pos. (µm)	87/86	87/86

Unit: El Chichon F
Thin Section: CHI-9372
Crystal: A

85 μm diameter spot
"pos." indicates center

Microprobe analyses

Pos. (μm)	Na2O	Al2O3	SiO2	K2O	CaO	FeO	SrO	Total
0.0	12.08	36.72	45.07	0.45	4.63	0.08	0.19	99.22
5.6	10.99	38.18	43.80	0.48	5.53	0.09	0.22	99.29
11.2	11.03	38.12	43.85	0.71	5.49	0.16	0.18	99.54
16.7	7.37	43.00	39.64	0.39	8.49	0.24	0.30	99.43
22.3	9.00	40.83	41.52	0.65	7.15	0.33	0.26	99.73
27.9	7.64	42.65	39.94	0.61	8.27	0.34	0.29	99.74
33.5	8.92	40.94	41.41	0.49	7.23	0.16	0.26	99.41
39.1	10.80	38.43	43.59	0.49	5.68	0.20	0.28	99.46
44.6	9.59	40.05	42.19	0.53	6.68	0.40	0.19	99.62
50.2	9.99	39.51	42.65	0.53	6.35	0.31	0.22	99.56
55.8	9.85	39.69	42.50	0.78	6.46	0.30	0.28	99.85
61.4	10.85	38.37	43.64	0.23	5.64	0.15	0.19	99.07
66.9	12.45	36.23	45.49	0.57	4.33	0.34	0.21	99.61
72.5	10.53	38.79	43.28	0.69	5.90	0.36	0.20	99.75
78.1	11.12	38.00	43.96	0.34	5.42	0.12	0.22	99.18
83.7	17.10	30.03	50.85	0.24	0.52	0.02	0.21	98.97
89.3	11.40	37.64	44.27	0.58	5.19	0.30	0.17	99.55
94.8	11.58	37.39	44.48	0.32	5.04	0.38	0.28	99.49
100.4	11.44	37.58	44.33	0.78	5.16	0.44	0.27	99.99
106.0	12.22	36.53	45.23	0.62	4.52	0.17	0.26	99.55
111.6	9.50	40.17	42.08	0.62	6.75	0.06	0.18	99.36
117.2	11.26	37.82	44.12	0.35	5.31	0.11	0.30	99.26
122.7	11.44	37.58	44.33	0.63	5.16	0.33	0.18	99.64
128.3	11.30	37.76	44.17	0.23	5.27	0.00	0.30	99.03
133.9	12.18	36.59	45.17	0.36	4.55	0.15	0.26	99.28
139.5								
145.1	10.85	38.37	43.64	0.73	5.64	0.29	0.26	99.78
150.6	12.13	36.66	45.12	0.30	4.59	0.17	0.22	99.19
156.2	11.30	37.76	44.17	0.48	5.27	0.41	0.19	99.58
161.8	12.22	36.53	45.23	0.33	4.52	0.10	0.20	99.13
167.4	11.21	37.88	44.06	0.31	5.34	0.15	0.20	99.16
172.9	11.95	36.90	44.91	0.70	4.74	0.16	0.16	99.52
178.5	12.36	36.35	45.39	0.62	4.40	0.00	0.16	99.29
184.1								
189.7	10.80	38.43	43.59	0.47	5.68	0.00	0.18	99.15
195.3	11.90	36.96	44.86	0.34	4.78	0.45	0.27	99.57
200.8	11.72	37.21	44.64	0.41	4.93	0.14	0.16	99.21
206.4	11.58	37.39	44.48	0.43	5.04	0.49	0.15	99.57
212.0	11.62	37.33	44.54	0.71	5.01	0.13	0.24	99.58
217.6	11.49	37.51	44.38	0.64	5.12	0.01	0.30	99.45
223.2	11.99	36.84	44.96	0.64	4.71	0.49	0.21	99.85
228.7	11.99	36.84	44.96	0.29	4.71	0.25	0.18	99.21
234.3	12.22	36.53	45.23	0.41	4.52	0.42	0.26	99.59
239.9	11.62	37.33	44.54	0.44	5.01	0.05	0.18	99.16
245.5	11.76	37.15	44.70	0.57	4.89	0.19	0.28	99.54
251.1	10.35	39.03	43.07	0.72	6.05	0.40	0.30	99.91
256.6	13.76	34.49	47.00	0.39	3.26	0.09	0.26	99.23
262.2	11.53	37.45	44.43	0.29	5.08	0.10	0.25	99.14
267.8	11.85	37.02	44.80	0.60	4.82	0.27	0.18	99.55

ICP-MS

Pos. (μm)	87/86	2 s.e.
45	0.70469	0.00066
205	0.70457	0.00091
275	0.70396	0.00078
318	0.70551	0.00075
407	0.70406	0.00054
483	0.70392	0.00056
507	0.70506	0.00038

Pos. (μm)	Na2O	Al2O3	SiO2	K2O	CaO	FeO	SrO	Total
273.4	12.08	36.72	45.07	0.20	4.63	0.19	0.20	99.09
278.9	11.81	37.09	44.75	0.22	4.86	0.19	0.26	99.17
284.5								
290.1	12.04	36.78	45.01	0.65	4.67	0.31	0.27	99.72
295.7	13.20	35.23	46.35	0.62	3.72	0.45	0.23	99.80
301.3	11.62	37.33	44.54	0.37	5.01	0.27	0.28	99.42
306.8	10.80	38.43	43.59	0.79	5.68	0.01	0.22	99.52
312.4	10.80	38.43	43.59	0.38	5.68	0.29	0.26	99.42
318.0	11.21	37.88	44.06	0.33	5.34	0.26	0.25	99.34
323.6	9.94	39.57	42.60	0.39	6.38	0.33	0.21	99.43
329.2	12.36	36.35	45.39	0.80	4.40	0.34	0.28	99.92
334.7	11.35	37.70	44.22	0.68	5.23	0.44	0.19	99.81
340.3	11.81	37.09	44.75	0.55	4.86	0.31	0.23	99.59
345.9	12.27	36.47	45.28	0.39	4.48	0.34	0.15	99.38
351.5	11.40	37.64	44.27	0.46	5.19	0.40	0.18	99.54
357.1	11.03	38.12	43.85	0.76	5.49	0.28	0.23	99.77
362.6	11.85	37.02	44.80	0.56	4.82	0.22	0.24	99.52
368.2	11.49	37.51	44.38	0.32	5.12	0.46	0.19	99.47
373.8	13.71	34.55	46.94	0.28	3.30	0.27	0.22	99.26
379.4	10.71	38.55	43.49	0.38	5.75	0.43	0.20	99.51
384.9	10.94	38.24	43.75	0.34	5.57	0.24	0.27	99.35
390.5	11.62	37.33	44.54	0.61	5.01	0.37	0.29	99.77
396.1	10.44	38.91	43.17	0.29	5.98	0.35	0.26	99.40
401.7	10.80	38.43	43.59	0.50	5.68	0.08	0.26	99.34
407.3	10.99	38.18	43.80	0.70	5.53	0.21	0.29	99.70
412.8	12.69	35.92	45.76	0.59	4.14	0.27	0.28	99.64
418.4	12.82	35.73	45.92	0.62	4.02	0.40	0.29	99.81
424.0	12.04	36.78	45.01	0.54	4.67	0.49	0.29	99.81
429.6	10.80	38.43	43.59	0.37	5.68	0.45	0.29	99.61
435.2	11.08	38.06	43.91	0.43	5.46	0.28	0.20	99.41
440.7	14.13	33.98	47.43	0.38	2.95	0.22	0.22	99.32
446.3	11.44	37.58	44.33	0.60	5.16	0.49	0.21	99.81
451.9	10.49	38.85	43.22	0.68	5.94	0.37	0.24	99.79
457.5	11.76	37.15	44.70	0.76	4.89	0.03	0.24	99.53
463.1	12.55	36.10	45.60	0.26	4.25	0.35	0.18	99.29
468.6	10.40	38.97	43.12	0.43	6.01	0.33	0.17	99.43
474.2	13.24	35.17	46.40	0.61	3.68	0.19	0.22	99.52
479.8	14.23	33.86	47.54	0.52	2.87	0.32	0.19	99.53
485.4								
490.9	14.51	33.48	47.87	0.66	2.64	0.13	0.16	99.46
496.5	11.99	36.84	44.96	0.29	4.71	0.20	0.17	99.15
502.1	12.13	36.66	45.12	0.71	4.59	0.38	0.24	99.82
507.7	14.94	32.91	48.36	0.53	2.29	0.23	0.22	99.49
513.3	12.92	35.61	46.03	0.66	3.95	0.43	0.15	99.74
518.8	12.55	36.10	45.60	0.53	4.25	0.29	0.22	99.54
524.4	10.99	38.18	43.80	0.57	5.53	0.35	0.23	99.65
530.0	12.27	36.47	45.28	0.22	4.48	0.48	0.19	99.39
535.6	12.41	36.29	45.44	0.59	4.37	0.38	0.18	99.65
541.2	11.58	37.39	44.48	0.28	5.04	0.44	0.17	99.39
546.7	11.62	37.33	44.54	0.44	5.01	0.09	0.28	99.32
552.3	12.87	35.67	45.97	0.75	3.99	0.17	0.26	99.69
557.9	12.78	35.79	45.87	0.25	4.06	0.39	0.19	99.32
563.5	11.81	37.09	44.75	0.52	4.86	0.32	0.22	99.56
569.1	12.59	36.04	45.65	0.27	4.21	0.19	0.27	99.24

Pos. (μm)	Na2O	Al2O3	SiO2	K2O	CaO	FeO	SrO	Total
574.6	12.87	35.67	45.97	0.32	3.99	0.28	0.23	99.33
580.2	11.62	37.33	44.54	0.31	5.01	0.10	0.17	99.08
585.8	13.52	34.80	46.73	0.70	3.45	0.44	0.23	99.87
591.4	12.27	36.47	45.28	0.43	4.48	0.21	0.28	99.43
596.9	13.38	34.99	46.57	0.42	3.57	0.39	0.26	99.57
602.5	12.36	36.35	45.39	0.75	4.40	0.36	0.27	99.88
608.1	12.45	36.23	45.49	0.31	4.33	0.11	0.30	99.22
613.7	11.90	36.96	44.86	0.27	4.78	0.19	0.21	99.17
619.3	11.90	36.96	44.86	0.60	4.78	0.38	0.29	99.76
624.8	12.69	35.92	45.76	0.67	4.14	0.14	0.20	99.50
630.4	10.71	38.55	43.49	0.27	5.75	0.46	0.17	99.40
636.0	11.76	37.15	44.70	0.66	4.89	0.08	0.16	99.40
641.6	11.62	37.33	44.54	0.51	5.01	0.05	0.17	99.23
647.2	11.03	38.12	43.85	0.34	5.49	0.02	0.15	99.01
652.7	10.49	38.85	43.22	0.59	5.94	0.12	0.18	99.39
658.3	13.52	34.80	46.73	0.45	3.45	0.04	0.23	99.21
663.9	11.58	37.39	44.48	0.58	5.04	0.30	0.21	99.59
669.5	9.41	40.29	41.98	0.26	6.82	0.41	0.18	99.36
675.1	10.67	38.61	43.43	0.79	5.79	0.10	0.21	99.60
680.6	10.40	38.97	43.12	0.48	6.01	0.05	0.28	99.31
686.2	12.59	36.04	45.65	0.80	4.21	0.29	0.19	99.78
691.8	11.85	37.02	44.80	0.28	4.82	0.23	0.26	99.28
697.4	12.32	36.41	45.33	0.41	4.44	0.17	0.29	99.36
702.9	12.04	36.78	45.01	0.34	4.67	0.30	0.20	99.35
708.5	11.49	37.51	44.38	0.51	5.12	0.05	0.26	99.32
714.1	12.96	35.54	46.08	0.21	3.91	0.39	0.24	99.34
719.7	12.45	36.23	45.49	0.53	4.33	0.22	0.24	99.49
725.3	16.91	30.28	50.63	0.57	0.68	0.32	0.28	99.67
730.8	12.27	36.47	45.28	0.45	4.48	0.23	0.25	99.43
736.4	11.90	36.96	44.86	0.35	4.78	0.07	0.17	99.09
742.0	10.89	38.30	43.70	0.28	5.61	0.08	0.30	99.16
747.6	13.06	35.42	46.19	0.27	3.83	0.16	0.20	99.13
753.2	11.99	36.84	44.96	0.56	4.71	0.32	0.23	99.62
758.7	12.04	36.78	45.01	0.77	4.67	0.39	0.29	99.96
764.3	11.95	36.90	44.91	0.62	4.74	0.23	0.16	99.51
769.9	10.99	38.18	43.80	0.73	5.53	0.13	0.19	99.56
775.5	12.13	36.66	45.12	0.27	4.59	0.37	0.28	99.42
781.1	11.21	37.88	44.06	0.51	5.34	0.06	0.26	99.33
786.6	11.44	37.58	44.33	0.75	5.16	0.24	0.21	99.69
792.2	13.85	34.36	47.11	0.33	3.18	0.50	0.30	99.63
797.8	11.35	37.70	44.22	0.73	5.23	0.34	0.16	99.73
803.4	12.59	36.04	45.65	0.68	4.21	0.19	0.24	99.62
808.9	10.40	38.97	43.12	0.57	6.01	0.43	0.16	99.66
814.5	9.09	40.71	41.62	0.24	7.08	0.35	0.27	99.35
820.1	11.81	37.09	44.75	0.55	4.86	0.18	0.22	99.45
825.7	8.12	42.01	40.50	0.77	7.88	0.07	0.28	99.62
831.3								
836.8	10.76	38.49	43.54	0.38	5.72	0.03	0.19	99.10
842.4	10.12	39.33	42.81	0.62	6.24	0.25	0.18	99.56
848.0	10.35	39.03	43.07	0.50	6.05	0.38	0.27	99.65
853.6	11.53	37.45	44.43	0.51	5.08	0.41	0.20	99.63
859.2	12.08	36.72	45.07	0.33	4.63	0.01	0.21	99.05
864.7	11.26	37.82	44.12	0.35	5.31	0.12	0.26	99.23
870.3	11.76	37.15	44.70	0.54	4.89	0.01	0.17	99.21

Pos. (μm)	Na2O	Al2O3	SiO2	K2O	CaO	FeO	SrO	Total
875.9	10.17	39.27	42.86	0.55	6.20	0.13	0.25	99.43
881.5	11.99	36.84	44.96	0.38	4.71	0.32	0.29	99.50
887.1	11.21	37.88	44.06	0.44	5.34	0.43	0.26	99.63
892.6	16.67	30.61	50.35	0.74	0.88	0.35	0.29	99.89
898.2	11.40	37.64	44.27	0.32	5.19	0.14	0.19	99.15
903.8	11.95	36.90	44.91	0.40	4.74	0.21	0.30	99.41
909.4	11.49	37.51	44.38	0.24	5.12	0.41	0.17	99.33
914.9	10.80	38.43	43.59	0.28	5.68	0.08	0.27	99.14
920.5	12.59	36.04	45.65	0.72	4.21	0.36	0.27	99.85
926.1	11.12	38.00	43.96	0.43	5.42	0.44	0.26	99.62
931.7	12.32	36.41	45.33	0.69	4.44	0.30	0.30	99.78
937.3	11.08	38.06	43.91	0.59	5.46	0.08	0.21	99.38
942.8	10.80	38.43	43.59	0.50	5.68	0.27	0.25	99.53
948.4	11.99	36.84	44.96	0.41	4.71	0.17	0.16	99.24
954.0	11.12	38.00	43.96	0.65	5.42	0.04	0.29	99.48
959.6	10.53	38.79	43.28	0.40	5.90	0.43	0.20	99.52
965.2	9.99	39.51	42.65	0.51	6.35	0.45	0.28	99.74
970.7	12.04	36.78	45.01	0.59	4.67	0.26	0.21	99.55
976.3	9.99	39.51	42.65	0.33	6.35	0.37	0.17	99.37
981.9	10.62	38.67	43.38	0.41	5.83	0.27	0.28	99.46
987.5	11.44	37.58	44.33	0.33	5.16	0.40	0.26	99.49
993.1	11.95	36.90	44.91	0.47	4.74	0.03	0.24	99.24
998.6	10.26	39.15	42.96	0.74	6.12	0.22	0.25	99.71
1004.2	9.18	40.59	41.72	0.37	7.01	0.32	0.25	99.44
1009.8	9.18	40.59	41.72	0.68	7.01	0.10	0.19	99.46
1015.4	11.95	36.90	44.91	0.23	4.74	0.13	0.20	99.06

Unit: El Chichon F
Thin Section: CHI-9372
Crystal: B

85 μm diameter spot
"pos." indicates center

Microprobe analyses

Pos. (μm)	Na2O	Al2O3	SiO2	K2O	CaO	FeO	SrO	Total
0.0	10.40	38.97	43.12	0.65	6.01	0.32	0.28	99.76
5.9	11.72	37.21	44.64	0.64	4.93	0.14	0.27	99.56
11.7	11.17	37.94	44.01	0.73	5.38	0.20	0.17	99.60
17.6	11.26	37.82	44.12	0.43	5.31	0.23	0.22	99.38
23.4	9.45	40.23	42.03	0.60	6.79	0.44	0.20	99.74
29.3	11.67	37.27	44.59	0.64	4.97	0.12	0.16	99.42
35.1	11.21	37.88	44.06	0.46	5.34	0.07	0.16	99.19
41.0	10.35	39.03	43.07	0.77	6.05	0.25	0.25	99.76
46.9	12.13	36.66	45.12	0.20	4.59	0.47	0.16	99.34
52.7	10.35	39.03	43.07	0.56	6.05	0.30	0.29	99.64
58.6	10.99	38.18	43.80	0.48	5.53	0.12	0.25	99.35
64.4	12.45	36.23	45.49	0.31	4.33	0.16	0.17	99.14
70.3	9.54	40.11	42.13	0.21	6.71	0.26	0.21	99.17
76.1	10.62	38.67	43.38	0.64	5.83	0.28	0.17	99.59
82.0	12.45	36.23	45.49	0.50	4.33	0.03	0.16	99.19
87.9	13.01	35.48	46.13	0.21	3.87	0.23	0.19	99.14
93.7	12.32	36.41	45.33	0.50	4.44	0.35	0.26	99.61
99.6	12.59	36.04	45.65	0.70	4.21	0.44	0.17	99.81
105.4	13.10	35.36	46.24	0.21	3.80	0.29	0.25	99.26
111.3	10.89	38.30	43.70	0.78	5.61	0.20	0.17	99.65
117.1	12.55	36.10	45.60	0.34	4.25	0.36	0.17	99.37
123.0	12.27	36.47	45.28	0.55	4.48	0.09	0.17	99.30
128.9	11.95	36.90	44.91	0.66	4.74	0.34	0.28	99.78
134.7	13.71	34.55	46.94	0.33	3.30	0.04	0.16	99.04
140.6								
146.4	10.85	38.37	43.64	0.58	5.64	0.00	0.23	99.32
152.3	11.62	37.33	44.54	0.54	5.01	0.31	0.27	99.63
158.1	10.17	39.27	42.86	0.25	6.20	0.00	0.28	99.03
164.0	11.12	38.00	43.96	0.50	5.42	0.42	0.25	99.68
169.9	10.58	38.73	43.33	0.46	5.87	0.33	0.24	99.53
175.7	9.94	39.57	42.60	0.46	6.38	0.42	0.29	99.67
181.6	11.67	37.27	44.59	0.45	4.97	0.43	0.29	99.66
187.4	11.72	37.21	44.64	0.64	4.93	0.40	0.17	99.71
193.3	10.22	39.21	42.91	0.44	6.16	0.42	0.29	99.64
199.1	10.58	38.73	43.33	0.56	5.87	0.29	0.17	99.52
205.0	9.81	39.75	42.45	0.24	6.49	0.35	0.19	99.27
210.9	11.72	37.21	44.64	0.31	4.93	0.36	0.22	99.40
216.7	10.85	38.37	43.64	0.57	5.64	0.05	0.27	99.39
222.6	11.90	36.96	44.86	0.62	4.78	0.01	0.25	99.38
228.4	10.12	39.33	42.81	0.64	6.24	0.08	0.21	99.43
234.3	12.32	36.41	45.33	0.69	4.44	0.16	0.22	99.57
240.1	9.59	40.05	42.19	0.54	6.68	0.03	0.15	99.23
246.0	12.08	36.72	45.07	0.73	4.63	0.17	0.20	99.60
251.9								
257.7	11.17	37.94	44.01	0.63	5.38	0.17	0.23	99.53
263.6	12.73	35.85	45.81	0.29	4.10	0.02	0.24	99.06
269.4	12.18	36.59	45.17	0.71	4.55	0.06	0.21	99.48
275.3	12.55	36.10	45.60	0.49	4.25	0.11	0.16	99.26
281.1	10.31	39.09	43.02	0.26	6.09	0.19	0.16	99.11

ICP-MS

Pos. (μm)	87/86	2 s.e.
43	0.70466	0.00089
124	0.70445	0.00065
184	0.70564	0.00078
228	0.70557	0.00100
302	0.70413	0.00068

Pos. (μm)	Na2O	Al2O3	SiO2	K2O	CaO	FeO	SrO	Total
287.0	11.62	37.33	44.54	0.77	5.01	0.34	0.19	99.80
292.9	10.58	38.73	43.33	0.68	5.87	0.29	0.30	99.76
298.7	12.04	36.78	45.01	0.35	4.67	0.24	0.25	99.34
304.6	12.08	36.72	45.07	0.69	4.63	0.39	0.16	99.75
310.4	12.36	36.35	45.39	0.64	4.40	0.41	0.27	99.82
316.3	12.36	36.35	45.39	0.34	4.40	0.26	0.24	99.33
322.1	11.30	37.76	44.17	0.28	5.27	0.40	0.17	99.35
328.0	10.53	38.79	43.28	0.40	5.90	0.14	0.20	99.24
333.9	10.94	38.24	43.75	0.49	5.57	0.21	0.28	99.48
339.7	11.30	37.76	44.17	0.65	5.27	0.04	0.24	99.42
345.6	9.94	39.57	42.60	0.69	6.38	0.44	0.23	99.86
351.4	10.85	38.37	43.64	0.79	5.64	0.36	0.24	99.90
357.3								
363.1	12.45	36.23	45.49	0.53	4.33	0.00	0.22	99.25
369.0	11.49	37.51	44.38	0.51	5.12	0.42	0.21	99.64

Unit: El Chichon F
Thin Section: CHI-9372
Crystal: E

85 μm diameter spot
"pos." indicates center

Microprobe analyses

Pos. (μm)	Na2O	Al2O3	SiO2	K2O	CaO	FeO	SrO	Total
0.0	11.53	37.45	44.43	0.66	5.08	0.35	0.28	99.79
4.8	12.36	36.35	45.39	0.49	4.40	0.08	0.24	99.31
9.6	10.99	38.18	43.80	0.47	5.53	0.14	0.27	99.38
14.5	11.99	36.84	44.96	0.52	4.71	0.06	0.23	99.32
19.3	11.35	37.70	44.22	0.74	5.23	0.37	0.27	99.88
24.1	11.12	38.00	43.96	0.78	5.42	0.32	0.28	99.88
28.9	12.82	35.73	45.92	0.32	4.02	0.43	0.15	99.40
33.7	9.05	40.77	41.57	0.73	7.12	0.46	0.16	99.85
38.6	10.03	39.45	42.70	0.77	6.31	0.32	0.27	99.86
43.4	9.32	40.41	41.88	0.26	6.90	0.04	0.28	99.08
48.2	11.30	37.76	44.17	0.21	5.27	0.44	0.24	99.39
53.0	14.56	33.42	47.92	0.44	2.60	0.30	0.22	99.46
57.8	12.78	35.79	45.87	0.58	4.06	0.37	0.17	99.62
62.7	11.72	37.21	44.64	0.23	4.93	0.43	0.28	99.44
67.5	12.04	36.78	45.01	0.35	4.67	0.18	0.25	99.28
72.3	10.40	38.97	43.12	0.46	6.01	0.15	0.20	99.32
77.1	11.76	37.15	44.70	0.78	4.89	0.40	0.18	99.85
81.9	11.08	38.06	43.91	0.49	5.46	0.08	0.28	99.35
86.8	11.21	37.88	44.06	0.58	5.34	0.23	0.21	99.51
91.6	13.52	34.80	46.73	0.46	3.45	0.43	0.24	99.63
96.4	10.49	38.85	43.22	0.66	5.94	0.20	0.20	99.57
101.2	10.49	38.85	43.22	0.42	5.94	0.45	0.19	99.57
106.0	11.90	36.96	44.86	0.41	4.78	0.13	0.22	99.25
110.9								
115.7	11.40	37.64	44.27	0.29	5.19	0.44	0.17	99.40
120.5	10.58	38.73	43.33	0.24	5.87	0.21	0.26	99.21
125.3	11.81	37.09	44.75	0.44	4.86	0.16	0.16	99.26
130.1	11.21	37.88	44.06	0.63	5.34	0.19	0.20	99.51
134.9	12.92	35.61	46.03	0.53	3.95	0.07	0.18	99.28
139.8	12.08	36.72	45.07	0.50	4.63	0.48	0.20	99.68
144.6	12.87	35.67	45.97	0.31	3.99	0.35	0.22	99.38
149.4	12.27	36.47	45.28	0.20	4.48	0.35	0.24	99.29
154.2	12.04	36.78	45.01	0.42	4.67	0.27	0.15	99.34
159.0	13.29	35.11	46.46	0.69	3.64	0.46	0.25	99.90
163.9	11.85	37.02	44.80	0.53	4.82	0.01	0.21	99.25
168.7	13.52	34.80	46.73	0.22	3.45	0.17	0.27	99.16
173.5	11.72	37.21	44.64	0.44	4.93	0.14	0.28	99.36
178.3	12.27	36.47	45.28	0.68	4.48	0.28	0.28	99.75
183.1	14.42	33.61	47.76	0.58	2.72	0.45	0.18	99.71
188.0	11.72	37.21	44.64	0.51	4.93	0.34	0.27	99.62
192.8	11.35	37.70	44.22	0.30	5.23	0.10	0.18	99.08
197.6	14.13	33.98	47.43	0.66	2.95	0.31	0.29	99.75
202.4	13.06	35.42	46.19	0.63	3.83	0.39	0.16	99.68
207.2								
212.1								
216.9	12.78	35.79	45.87	0.33	4.06	0.41	0.20	99.44
221.7	13.34	35.05	46.51	0.73	3.60	0.28	0.28	99.79
226.5	11.58	37.39	44.48	0.30	5.04	0.22	0.26	99.28
231.3	12.36	36.35	45.39	0.78	4.40	0.36	0.19	99.83

ICP-MS

Pos. (μm)	87/86	2 s.e.
52	0.70528	0.00058
169	0.70564	0.00038
281	0.70534	0.00053
516	0.70471	0.00054

Pos. (μm)	Na2O	Al2O3	SiO2	K2O	CaO	FeO	SrO	Total
236.2	12.45	36.23	45.49	0.47	4.33	0.28	0.16	99.40
241.0	12.50	36.16	45.55	0.51	4.29	0.28	0.22	99.51
245.8	12.18	36.59	45.17	0.42	4.55	0.23	0.18	99.33
250.6	10.89	38.30	43.70	0.63	5.61	0.46	0.24	99.83
255.4	12.96	35.54	46.08	0.74	3.91	0.20	0.29	99.74
260.3	16.33	31.06	49.96	0.40	1.15	0.49	0.16	99.55
265.1	14.70	33.23	48.08	0.73	2.49	0.26	0.27	99.76
269.9	13.24	35.17	46.40	0.61	3.68	0.40	0.22	99.73
274.7	9.90	39.63	42.55	0.42	6.42	0.46	0.21	99.59
279.5	11.08	38.06	43.91	0.50	5.46	0.47	0.28	99.75
284.4	11.30	37.76	44.17	0.69	5.27	0.44	0.25	99.88
289.2	12.36	36.35	45.39	0.24	4.40	0.34	0.28	99.37
294.0	10.62	38.67	43.38	0.37	5.83	0.35	0.24	99.46
298.8	13.38	34.99	46.57	0.59	3.57	0.37	0.15	99.62
303.6	14.65	33.29	48.03	0.61	2.53	0.26	0.23	99.60
308.5	12.50	36.16	45.55	0.72	4.29	0.06	0.18	99.46
313.3	11.40	37.64	44.27	0.64	5.19	0.11	0.29	99.54
318.1	11.49	37.51	44.38	0.26	5.12	0.08	0.25	99.09
322.9	12.69	35.92	45.76	0.71	4.14	0.05	0.22	99.47
327.7	11.72	37.21	44.64	0.79	4.93	0.13	0.19	99.60
332.6								
337.4								
342.2	9.41	40.29	41.98	0.43	6.82	0.04	0.24	99.21
347.0	12.87	35.67	45.97	0.39	3.99	0.09	0.26	99.25
351.8	11.90	36.96	44.86	0.29	4.78	0.00	0.27	99.06
356.6								
361.5								
366.3	10.71	38.55	43.49	0.24	5.75	0.04	0.27	99.05
371.1	13.66	34.61	46.89	0.32	3.34	0.11	0.18	99.11
375.9	12.04	36.78	45.01	0.27	4.67	0.30	0.17	99.24
380.7	10.67	38.61	43.43	0.71	5.79	0.38	0.26	99.85
385.6	12.08	36.72	45.07	0.78	4.63	0.18	0.17	99.63
390.4	11.85	37.02	44.80	0.37	4.82	0.07	0.25	99.19
395.2	13.15	35.30	46.30	0.24	3.76	0.07	0.18	98.98
400.0	13.48	34.86	46.67	0.62	3.49	0.19	0.21	99.52
404.8	11.85	37.02	44.80	0.33	4.82	0.38	0.16	99.38
409.7	11.72	37.21	44.64	0.23	4.93	0.08	0.27	99.08
414.5	12.27	36.47	45.28	0.76	4.48	0.16	0.27	99.68
419.3	16.52	30.80	50.18	0.46	1.00	0.47	0.22	99.64
424.1	11.67	37.27	44.59	0.25	4.97	0.40	0.21	99.36
428.9	11.62	37.33	44.54	0.67	5.01	0.19	0.17	99.53
433.8	12.82	35.73	45.92	0.60	4.02	0.41	0.16	99.68
438.6	12.41	36.29	45.44	0.55	4.37	0.43	0.23	99.71
443.4	11.72	37.21	44.64	0.58	4.93	0.20	0.28	99.55
448.2	10.35	39.03	43.07	0.57	6.05	0.09	0.20	99.35
453.0	11.99	36.84	44.96	0.25	4.71	0.42	0.17	99.34
457.9	11.58	37.39	44.48	0.70	5.04	0.33	0.25	99.78
462.7	13.20	35.23	46.35	0.42	3.72	0.00	0.28	99.20
467.5	11.21	37.88	44.06	0.44	5.34	0.31	0.15	99.40
472.3	10.40	38.97	43.12	0.61	6.01	0.36	0.17	99.63
477.1	10.31	39.09	43.02	0.36	6.09	0.02	0.22	99.10
482.0	8.92	40.94	41.41	0.75	7.23	0.46	0.26	99.97
486.8	10.85	38.37	43.64	0.30	5.64	0.37	0.19	99.36
491.6	8.52	41.48	40.95	0.34	7.55	0.11	0.24	99.19

Pos. (µm)	Na2O	Al2O3	SiO2	K2O	CaO	FeO	SrO	Total
496.4	7.46	42.89	39.74	0.72	8.42	0.27	0.29	99.78
501.2	10.53	38.79	43.28	0.58	5.90	0.41	0.16	99.64
506.1	9.14	40.65	41.67	0.36	7.04	0.40	0.17	99.43
510.9	8.83	41.06	41.31	0.77	7.30	0.21	0.17	99.65
515.7	7.59	42.71	39.89	0.61	8.31	0.12	0.22	99.44
520.5	8.12	42.01	40.50	0.32	7.88	0.47	0.24	99.52
525.3	9.05	40.77	41.57	0.58	7.12	0.31	0.23	99.62
530.2	10.08	39.39	42.76	0.51	6.27	0.06	0.17	99.23
535.0	11.03	38.12	43.85	0.36	5.49	0.21	0.26	99.33
539.8	10.22	39.21	42.91	0.64	6.16	0.49	0.25	99.88
544.6	6.50	44.16	38.63	0.55	9.20	0.48	0.28	99.80
549.4	11.12	38.00	43.96	0.38	5.42	0.30	0.15	99.33
554.3	9.32	40.41	41.88	0.42	6.90	0.20	0.23	99.35
559.1	8.30	41.77	40.70	0.54	7.73	0.17	0.18	99.38
563.9	7.46	42.89	39.74	0.60	8.42	0.11	0.30	99.51
568.7	11.67	37.27	44.59	0.55	4.97	0.40	0.24	99.70
573.5	9.45	40.23	42.03	0.27	6.79	0.46	0.18	99.41
578.3	8.38	41.65	40.80	0.57	7.66	0.20	0.17	99.44
583.2	8.96	40.88	41.47	0.54	7.19	0.19	0.23	99.45
588.0	11.90	36.96	44.86	0.47	4.78	0.46	0.24	99.67
592.8	15.32	32.40	48.80	0.67	1.98	0.27	0.24	99.68
597.6								
602.4	9.76	39.81	42.39	0.30	6.53	0.19	0.28	99.27
607.3	8.61	41.36	41.06	0.40	7.48	0.33	0.26	99.49
612.1	7.20	43.24	39.43	0.45	8.63	0.42	0.27	99.64
616.9	7.29	43.12	39.53	0.41	8.56	0.19	0.19	99.28
621.7	12.64	35.98	45.71	0.72	4.18	0.09	0.30	99.62
626.5	10.35	39.03	43.07	0.72	6.05	0.16	0.23	99.61
631.4	10.31	39.09	43.02	0.69	6.09	0.38	0.29	99.87
636.2	7.33	43.06	39.58	0.50	8.53	0.47	0.27	99.73
641.0	4.96	46.22	36.85	0.63	10.47	0.17	0.19	99.49
645.8	8.30	41.77	40.70	0.72	7.73	0.46	0.28	99.96
650.6	7.99	42.18	40.34	0.72	7.99	0.02	0.28	99.53
655.5	8.74	41.18	41.21	0.60	7.37	0.44	0.20	99.74
660.3	7.81	42.42	40.14	0.51	8.13	0.43	0.21	99.65
665.1	5.81	45.08	37.84	0.52	9.77	0.06	0.25	99.32
669.9	8.78	41.12	41.26	0.77	7.34	0.47	0.19	99.94
674.7	8.61	41.36	41.06	0.27	7.48	0.14	0.17	99.07
679.6	7.72	42.53	40.04	0.48	8.20	0.28	0.22	99.47
684.4	9.27	40.47	41.83	0.71	6.93	0.14	0.29	99.64
689.2	8.78	41.12	41.26	0.58	7.34	0.24	0.19	99.51
694.0	6.81	43.76	38.98	0.55	8.95	0.35	0.18	99.58
698.8	8.12	42.01	40.50	0.62	7.88	0.27	0.22	99.61
703.7	9.81	39.75	42.45	0.62	6.49	0.06	0.21	99.39
708.5	9.90	39.63	42.55	0.72	6.42	0.48	0.21	99.91
713.3	10.85	38.37	43.64	0.49	5.64	0.45	0.15	99.59
718.1								
722.9	11.40	37.64	44.27	0.45	5.19	0.29	0.16	99.40
727.8	8.83	41.06	41.31	0.26	7.30	0.10	0.23	99.08
732.6	11.99	36.84	44.96	0.67	4.71	0.41	0.17	99.75
737.4	10.53	38.79	43.28	0.28	5.90	0.34	0.29	99.41
742.2	10.94	38.24	43.75	0.27	5.57	0.22	0.22	99.21
747.0	9.90	39.63	42.55	0.30	6.42	0.11	0.21	99.13
751.9	12.08	36.72	45.07	0.26	4.63	0.13	0.17	99.06

Pos. (μm)	Na2O	Al2O3	SiO2	K2O	CaO	FeO	SrO	Total
756.7	10.26	39.15	42.96	0.52	6.12	0.04	0.23	99.30
761.5	11.30	37.76	44.17	0.52	5.27	0.09	0.27	99.37
766.3								
771.1	11.53	37.45	44.43	0.71	5.08	0.48	0.20	99.89
776.0	10.99	38.18	43.80	0.29	5.53	0.44	0.30	99.53
780.8	9.72	39.87	42.34	0.38	6.57	0.35	0.19	99.42
785.6	9.50	40.17	42.08	0.27	6.75	0.33	0.23	99.33

Unit: El Chichon F
Thin Section: CHI-9372
Crystal: F

85 μm diameter spot
"pos." indicates center

Microprobe analyses

Pos. (μm)	Na2O	Al2O3	SiO2	K2O	CaO	FeO	SrO	Total
0.0	6.72	43.87	38.88	0.50	9.03	0.38	0.18	99.56
10.0	5.34	45.71	37.29	0.40	10.15	0.27	0.24	99.41
19.9	7.15	43.29	39.38	0.42	8.67	0.14	0.21	99.27
29.9	5.90	44.97	37.94	0.55	9.70	0.30	0.23	99.58
39.8	8.30	41.77	40.70	0.70	7.73	0.03	0.24	99.47
49.8	8.61	41.36	41.06	0.74	7.48	0.11	0.20	99.55
59.8	7.20	43.24	39.43	0.43	8.63	0.49	0.16	99.59
69.7	4.96	46.22	36.85	0.42	10.47	0.27	0.25	99.44
79.7	5.68	45.25	37.69	0.41	9.87	0.49	0.21	99.60
89.6	7.81	42.42	40.14	0.73	8.13	0.26	0.15	99.64
99.6	8.65	41.30	41.11	0.25	7.44	0.48	0.24	99.48
109.6	9.23	40.53	41.77	0.75	6.97	0.17	0.17	99.58
119.5	9.09	40.71	41.62	0.72	7.08	0.16	0.29	99.66
129.5	9.50	40.17	42.08	0.48	6.75	0.46	0.30	99.74
139.4	9.81	39.75	42.45	0.75	6.49	0.31	0.28	99.84
149.4	9.32	40.41	41.88	0.69	6.90	0.19	0.18	99.56
159.4								
169.3	8.74	41.18	41.21	0.43	7.37	0.36	0.22	99.51
179.3	9.76	39.81	42.39	0.66	6.53	0.21	0.22	99.59
189.2	9.63	39.99	42.24	0.76	6.64	0.27	0.17	99.70
199.2	9.32	40.41	41.88	0.68	6.90	0.16	0.15	99.49
209.2	9.63	39.99	42.24	0.21	6.64	0.06	0.26	99.03
219.1	9.36	40.35	41.93	0.79	6.86	0.21	0.23	99.73
229.1	11.44	37.58	44.33	0.24	5.16	0.04	0.23	99.00
239.0	11.58	37.39	44.48	0.71	5.04	0.36	0.19	99.76
249.0	10.58	38.73	43.33	0.50	5.87	0.01	0.22	99.22
259.0	11.72	37.21	44.64	0.33	4.93	0.21	0.27	99.31
268.9								
278.9	10.31	39.09	43.02	0.25	6.09	0.27	0.30	99.32
288.8	10.08	39.39	42.76	0.26	6.27	0.38	0.18	99.32
298.8	11.49	37.51	44.38	0.66	5.12	0.38	0.18	99.72
308.8	10.62	38.67	43.38	0.67	5.83	0.34	0.26	99.77
318.7	10.40	38.97	43.12	0.25	6.01	0.08	0.16	98.99
328.7	10.58	38.73	43.33	0.51	5.87	0.43	0.18	99.63
338.6	10.67	38.61	43.43	0.48	5.79	0.34	0.28	99.60
348.6	10.80	38.43	43.59	0.54	5.68	0.38	0.26	99.68
358.6	9.45	40.23	42.03	0.71	6.79	0.15	0.25	99.61
368.5	9.50	40.17	42.08	0.63	6.75	0.01	0.23	99.37
378.5	8.96	40.88	41.47	0.76	7.19	0.47	0.23	99.96
388.4	10.22	39.21	42.91	0.69	6.16	0.34	0.20	99.73
398.4	9.68	39.93	42.29	0.26	6.60	0.14	0.17	99.07
408.4	9.72	39.87	42.34	0.59	6.57	0.28	0.22	99.59
418.3	9.36	40.35	41.93	0.54	6.86	0.18	0.24	99.46
428.3	8.65	41.30	41.11	0.62	7.44	0.32	0.23	99.68
438.2	10.80	38.43	43.59	0.33	5.68	0.04	0.21	99.08
448.2	9.76	39.81	42.39	0.68	6.53	0.19	0.28	99.65
458.2	9.94	39.57	42.60	0.20	6.38	0.45	0.22	99.37
468.1	10.12	39.33	42.81	0.78	6.24	0.17	0.28	99.73
478.1	9.50	40.17	42.08	0.28	6.75	0.04	0.20	99.02

ICP-MS

Pos. (μm)	87/86	2 s.e.
90	0.70448	0.00114
121	0.70489	0.00045
178	0.70483	0.00065
206	0.70573	0.00056
214	0.70565	0.00068
241	0.70407	0.00056
306	0.70420	0.00067
354	0.70386	0.00053

Pos. (μm)	Na2O	Al2O3	SiO2	K2O	CaO	FeO	SrO	Total
488.0	10.94	38.24	43.75	0.26	5.57	0.25	0.27	99.28
498.0	9.27	40.47	41.83	0.57	6.93	0.38	0.22	99.67
508.0	8.74	41.18	41.21	0.48	7.37	0.31	0.22	99.51
517.9	13.90	34.30	47.16	0.66	3.14	0.15	0.17	99.48
527.9	12.96	35.54	46.08	0.70	3.91	0.34	0.16	99.70
537.8	11.62	37.33	44.54	0.48	5.01	0.17	0.28	99.43
547.8	9.59	40.05	42.19	0.28	6.68	0.32	0.22	99.31
557.7	8.74	41.18	41.21	0.79	7.37	0.18	0.23	99.71
567.7	11.17	37.94	44.01	0.32	5.38	0.26	0.17	99.24
577.7	10.85	38.37	43.64	0.49	5.64	0.19	0.18	99.36
587.6	10.71	38.55	43.49	0.68	5.75	0.50	0.18	99.86
597.6	10.12	39.33	42.81	0.34	6.24	0.36	0.26	99.46
607.5	10.99	38.18	43.80	0.26	5.53	0.47	0.18	99.42
617.5	10.22	39.21	42.91	0.29	6.16	0.10	0.17	99.06
627.5	9.18	40.59	41.72	0.70	7.01	0.01	0.29	99.50
637.4	8.74	41.18	41.21	0.49	7.37	0.45	0.19	99.63
647.4	8.16	41.95	40.55	0.74	7.84	0.45	0.28	99.97
657.3	9.41	40.29	41.98	0.77	6.82	0.09	0.28	99.64

Unit: El Chichon C
Thin Section: CHI-9521
Crystal: A

85 μm diameter spot
"pos." indicates center

Microprobe analyses

Pos. (μm)	Na2O	Al2O3	SiO2	K2O	CaO	FeO	SrO	Total
0.0	10.18	39.25	42.88	0.74	6.19	0.17	0.30	99.70
8.7	10.06	39.41	42.74	0.65	6.28	0.41	0.29	99.86
17.5	10.37	39.01	43.09	0.53	6.04	0.48	0.27	99.78
26.2	10.34	39.05	43.05	0.61	6.06	0.20	0.28	99.59
34.9	9.71	39.89	42.32	0.50	6.58	0.35	0.23	99.58
43.6	14.88	33.00	48.28	0.60	2.34	0.12	0.29	99.52
52.4	10.64	38.65	43.40	0.39	5.82	0.35	0.25	99.48
61.1	12.16	36.62	45.16	0.53	4.57	0.23	0.18	99.44
69.8	9.35	40.37	41.91	0.37	6.87	0.15	0.24	99.26
78.6	10.82	38.41	43.61	0.27	5.67	0.23	0.22	99.22
87.3	9.91	39.61	42.57	0.26	6.41	0.09	0.16	99.01
96.0	9.05	40.77	41.57	0.37	7.12	0.06	0.18	99.11
104.7	9.23	40.53	41.77	0.70	6.97	0.36	0.28	99.85
113.5	9.79	39.77	42.43	0.61	6.51	0.30	0.18	99.59
122.2	9.41	40.29	41.98	0.28	6.82	0.00	0.25	99.03
130.9	11.37	37.68	44.24	0.66	5.22	0.01	0.22	99.39
139.6	11.34	37.72	44.20	0.60	5.24	0.24	0.28	99.61
148.4	10.37	39.01	43.09	0.71	6.04	0.46	0.15	99.83
157.1	10.34	39.05	43.05	0.31	6.06	0.22	0.27	99.30
165.8	11.15	37.96	43.99	0.35	5.39	0.44	0.26	99.56
174.6	9.94	39.57	42.60	0.30	6.38	0.24	0.21	99.26
183.3	10.55	38.77	43.29	0.60	5.89	0.36	0.16	99.62
192.0	10.91	38.28	43.71	0.73	5.59	0.47	0.29	99.99
200.7	9.20	40.57	41.74	0.59	6.99	0.03	0.28	99.40
209.5	9.41	40.29	41.98	0.60	6.82	0.47	0.15	99.72
218.2	8.43	41.59	40.85	0.67	7.63	0.08	0.18	99.43
226.9	10.64	38.65	43.40	0.36	5.82	0.46	0.19	99.51
235.7	10.25	39.17	42.95	0.44	6.14	0.11	0.20	99.25
244.4	10.67	38.61	43.43	0.60	5.79	0.17	0.22	99.49
253.1	11.15	37.96	43.99	0.37	5.39	0.40	0.25	99.52
261.8	11.73	37.19	44.66	0.34	4.92	0.20	0.19	99.23
270.6	9.62	40.01	42.22	0.70	6.65	0.08	0.22	99.49
279.3	11.18	37.92	44.03	0.32	5.37	0.13	0.16	99.11
288.0	10.91	38.28	43.71	0.72	5.59	0.05	0.21	99.48
296.7	10.37	39.01	43.09	0.20	6.04	0.21	0.29	99.20
305.5	9.47	40.21	42.05	0.25	6.78	0.05	0.16	98.96
314.2	10.40	38.97	43.12	0.62	6.01	0.09	0.28	99.48
322.9	8.16	41.95	40.55	0.76	7.84	0.13	0.27	99.67
331.7	6.21	44.55	38.30	0.42	9.44	0.13	0.30	99.35
340.4	9.35	40.37	41.91	0.56	6.87	0.42	0.30	99.78
349.1	10.76	38.49	43.54	0.42	5.72	0.42	0.21	99.55
357.8	9.05	40.77	41.57	0.74	7.12	0.24	0.25	99.74
366.6	8.75	41.16	41.23	0.54	7.36	0.42	0.20	99.67
375.3	9.47	40.21	42.05	0.57	6.78	0.33	0.17	99.57
384.0	10.06	39.41	42.74	0.31	6.28	0.44	0.29	99.54
392.8	10.79	38.45	43.57	0.50	5.69	0.32	0.28	99.60
401.5	11.03	38.12	43.85	0.61	5.49	0.17	0.30	99.57
410.2	10.52	38.81	43.26	0.76	5.91	0.06	0.19	99.52
418.9	11.30	37.76	44.17	0.75	5.27	0.26	0.18	99.68

ICP-MS

Pos. (μm)	87/86	2 s.e.
31	0.70440	0.00046
96	0.70449	0.00056
168	0.70424	0.00052
243	0.70359	0.00063
270	0.70404	0.00048
314	0.70426	0.00056
369	0.70349	0.00050
432	0.70482	0.00036
519	0.70315	0.00051

Pos. (μm)	Na2O	Al2O3	SiO2	K2O	CaO	FeO	SrO	Total
427.7	9.71	39.89	42.32	0.64	6.58	0.27	0.23	99.63
436.4	9.35	40.37	41.91	0.39	6.87	0.48	0.23	99.60
445.1	9.32	40.41	41.88	0.30	6.90	0.11	0.26	99.17
453.8	10.79	38.45	43.57	0.31	5.69	0.09	0.28	99.18
462.6	8.02	42.14	40.38	0.59	7.96	0.43	0.18	99.70
471.3	7.99	42.18	40.34	0.24	7.99	0.43	0.20	99.37
480.0	11.49	37.51	44.38	0.49	5.12	0.06	0.24	99.29
488.8	9.50	40.17	42.08	0.45	6.75	0.31	0.22	99.47
497.5	9.74	39.85	42.36	0.63	6.55	0.41	0.26	99.79
506.2	17.09	30.05	50.83	0.61	0.53	0.10	0.23	99.44
514.9	8.61	41.36	41.06	0.40	7.48	0.36	0.25	99.52
523.7	11.27	37.80	44.13	0.58	5.29	0.00	0.23	99.32
532.4	11.15	37.96	43.99	0.72	5.39	0.34	0.22	99.77
541.1	7.05	43.43	39.27	0.33	8.75	0.30	0.16	99.29
549.9	7.23	43.20	39.47	0.80	8.61	0.11	0.28	99.68
558.6	9.23	40.53	41.77	0.36	6.97	0.19	0.26	99.30
567.3	10.28	39.13	42.98	0.22	6.11	0.40	0.20	99.33
576.0	9.97	39.53	42.64	0.67	6.36	0.32	0.29	99.78
584.8	8.66	41.28	41.12	0.41	7.43	0.08	0.23	99.22
593.5	9.29	40.45	41.84	0.36	6.92	0.44	0.15	99.45
602.2	10.18	39.25	42.88	0.53	6.19	0.07	0.28	99.39
611.0	8.13	41.99	40.51	0.62	7.87	0.02	0.23	99.37
619.7	8.22	41.87	40.61	0.28	7.79	0.25	0.30	99.33
628.4	9.20	40.57	41.74	0.56	6.99	0.07	0.22	99.34
637.1	7.81	42.42	40.14	0.47	8.13	0.33	0.24	99.54
645.9	13.49	34.84	46.69	0.32	3.48	0.04	0.18	99.03
654.6	9.41	40.29	41.98	0.31	6.82	0.37	0.23	99.41
663.3	10.52	38.81	43.26	0.28	5.91	0.02	0.25	99.05
672.0	10.06	39.41	42.74	0.73	6.28	0.44	0.26	99.93
680.8	9.79	39.77	42.43	0.23	6.51	0.17	0.22	99.12
689.5	10.09	39.37	42.77	0.78	6.26	0.31	0.22	99.82
698.2	9.44	40.25	42.01	0.32	6.80	0.07	0.19	99.08
707.0	12.56	36.08	45.62	0.23	4.24	0.40	0.27	99.40
715.7	9.88	39.65	42.53	0.51	6.43	0.14	0.17	99.33
724.4	9.05	40.77	41.57	0.41	7.12	0.32	0.28	99.51
733.1	9.44	40.25	42.01	0.42	6.80	0.34	0.26	99.53
741.9	9.82	39.73	42.46	0.55	6.48	0.29	0.22	99.55
750.6	9.94	39.57	42.60	0.38	6.38	0.43	0.27	99.57
759.3	10.91	38.28	43.71	0.34	5.59	0.33	0.26	99.44
768.1	10.43	38.93	43.16	0.63	5.99	0.06	0.22	99.41
776.8	11.70	37.23	44.63	0.37	4.94	0.48	0.23	99.58
785.5	11.00	38.16	43.82	0.52	5.52	0.44	0.25	99.70
794.2	10.79	38.45	43.57	0.22	5.69	0.39	0.22	99.33
803.0	11.09	38.04	43.92	0.67	5.44	0.14	0.21	99.52
811.7	10.25	39.17	42.95	0.64	6.14	0.43	0.29	99.87
820.4	13.15	35.30	46.30	0.24	3.76	0.20	0.29	99.23
829.1								
837.9	9.65	39.97	42.26	0.73	6.63	0.31	0.30	99.84
846.6	8.52	41.48	40.95	0.27	7.55	0.02	0.17	98.95
855.3	10.25	39.17	42.95	0.23	6.14	0.34	0.18	99.25
864.1	8.66	41.28	41.12	0.34	7.43	0.21	0.18	99.22
872.8	8.75	41.16	41.23	0.42	7.36	0.32	0.19	99.43
881.5	8.31	41.75	40.72	0.79	7.72	0.35	0.24	99.88
890.2	9.47	40.21	42.05	0.78	6.78	0.28	0.27	99.83

Pos. (µm)	Na2O	Al2O3	SiO2	K2O	CaO	FeO	SrO	Total
899.0	9.59	40.05	42.19	0.32	6.68	0.12	0.15	99.09
907.7	8.58	41.40	41.02	0.23	7.50	0.19	0.16	99.08
916.4	8.43	41.59	40.85	0.36	7.63	0.39	0.23	99.48
925.2	8.96	40.88	41.47	0.75	7.19	0.43	0.26	99.94
933.9	9.56	40.09	42.15	0.50	6.70	0.26	0.26	99.52
942.6	9.35	40.37	41.91	0.57	6.87	0.20	0.18	99.45
951.3	9.32	40.41	41.88	0.46	6.90	0.43	0.28	99.66
960.1	9.62	40.01	42.22	0.53	6.65	0.14	0.15	99.31
968.8	10.09	39.37	42.77	0.58	6.26	0.10	0.27	99.45
977.5	9.41	40.29	41.98	0.53	6.82	0.43	0.22	99.69
986.2	16.02	31.47	49.61	0.42	1.40	0.16	0.26	99.34
995.0	10.28	39.13	42.98	0.80	6.11	0.04	0.28	99.63
1003.7	7.61	42.69	39.90	0.68	8.30	0.14	0.29	99.61
1012.4	9.26	40.49	41.81	0.24	6.95	0.29	0.18	99.22
1021.2	10.22	39.21	42.91	0.43	6.16	0.21	0.19	99.33
1029.9	9.56	40.09	42.15	0.58	6.70	0.39	0.24	99.71
1038.6	8.61	41.36	41.06	0.64	7.48	0.14	0.18	99.46
1047.3	10.00	39.49	42.67	0.32	6.33	0.12	0.23	99.17
1056.1	9.35	40.37	41.91	0.57	6.87	0.35	0.29	99.71
1064.8	8.25	41.83	40.65	0.48	7.77	0.47	0.23	99.69
1073.5	11.85	37.02	44.80	0.23	4.82	0.32	0.21	99.26
1082.3	9.62	40.01	42.22	0.67	6.65	0.07	0.23	99.47
1091.0	6.01	44.81	38.07	0.78	9.60	0.11	0.26	99.65
1099.7	5.02	46.15	36.92	0.46	10.42	0.46	0.17	99.60
1108.4	9.05	40.77	41.57	0.22	7.12	0.25	0.26	99.23
1117.2	7.99	42.18	40.34	0.29	7.99	0.36	0.21	99.36
1125.9	6.33	44.39	38.43	0.22	9.34	0.38	0.20	99.30
1134.6	6.56	44.09	38.70	0.45	9.16	0.31	0.18	99.43
1143.3	6.53	44.12	38.67	0.35	9.18	0.13	0.29	99.27
1152.1	7.40	42.96	39.67	0.57	8.47	0.41	0.29	99.76
1160.8	9.14	40.65	41.67	0.49	7.04	0.40	0.23	99.62
1169.5	8.19	41.91	40.58	0.29	7.82	0.07	0.16	99.03
1178.3	9.05	40.77	41.57	0.59	7.12	0.01	0.26	99.36
1187.0	8.63	41.32	41.09	0.78	7.46	0.19	0.22	99.70
1195.7	8.78	41.12	41.26	0.45	7.34	0.21	0.25	99.40

Unit: El Chichon M
Thin Section: CHI-9521
Crystal: C

85 μm diameter spot
"pos." indicates center

Microprobe analyses

Pos. (μm)	Na2O	Al2O3	SiO2	K2O	CaO	FeO	SrO	Total
0.0	12.07	36.74	45.05	0.55	4.64	0.29	0.26	99.61
4.9	10.85	38.37	43.64	0.50	5.64	0.04	0.17	99.21
9.8	11.58	37.39	44.48	0.42	5.04	0.40	0.21	99.52
14.7	11.70	37.23	44.63	0.74	4.94	0.31	0.15	99.70
19.5	10.76	38.49	43.54	0.79	5.72	0.32	0.19	99.79
24.4	9.88	39.65	42.53	0.52	6.43	0.34	0.19	99.56
29.3	16.99	30.18	50.72	0.45	0.61	0.31	0.21	99.47
34.2	13.68	34.59	46.91	0.21	3.32	0.32	0.29	99.32
39.1	10.43	38.93	43.16	0.77	5.99	0.25	0.24	99.77
44.0	11.03	38.12	43.85	0.80	5.49	0.22	0.26	99.78
48.8	11.55	37.43	44.45	0.55	5.07	0.40	0.18	99.63
53.7	11.34	37.72	44.20	0.77	5.24	0.03	0.16	99.46
58.6	11.43	37.60	44.31	0.22	5.17	0.18	0.26	99.15
63.5	11.73	37.19	44.66	0.34	4.92	0.43	0.25	99.53
68.4	11.70	37.23	44.63	0.34	4.94	0.46	0.28	99.58
73.3	13.31	35.09	46.48	0.65	3.63	0.29	0.27	99.70
78.1	12.04	36.78	45.01	0.60	4.67	0.22	0.22	99.54
83.0	10.00	39.49	42.67	0.62	6.33	0.36	0.17	99.65
87.9	10.97	38.20	43.78	0.41	5.54	0.23	0.21	99.35
92.8	11.24	37.84	44.10	0.61	5.32	0.46	0.21	99.77
97.7	10.79	38.45	43.57	0.67	5.69	0.40	0.27	99.83
102.6	10.18	39.25	42.88	0.56	6.19	0.46	0.25	99.77
107.5	10.64	38.65	43.40	0.79	5.82	0.45	0.22	99.95
112.3	10.43	38.93	43.16	0.41	5.99	0.43	0.18	99.52
117.2	11.52	37.47	44.41	0.79	5.09	0.40	0.24	99.93
122.1	11.27	37.80	44.13	0.36	5.29	0.08	0.22	99.16
127.0	11.12	38.00	43.96	0.25	5.42	0.30	0.26	99.31
131.9	10.15	39.29	42.84	0.54	6.21	0.25	0.17	99.47
136.8	11.21	37.88	44.06	0.35	5.34	0.09	0.17	99.11
141.6	11.67	37.27	44.59	0.43	4.97	0.35	0.23	99.51
146.5	9.94	39.57	42.60	0.57	6.38	0.42	0.17	99.66
151.4	11.58	37.39	44.48	0.26	5.04	0.49	0.25	99.50
156.3								
161.2	11.34	37.72	44.20	0.49	5.24	0.22	0.21	99.42
166.1	13.15	35.30	46.30	0.65	3.76	0.29	0.26	99.69
171.0	11.49	37.51	44.38	0.68	5.12	0.14	0.25	99.56
175.8	11.21	37.88	44.06	0.39	5.34	0.19	0.27	99.36
180.7	11.21	37.88	44.06	0.32	5.34	0.14	0.17	99.13
185.6	11.55	37.43	44.45	0.31	5.07	0.01	0.24	99.06
190.5	11.37	37.68	44.24	0.78	5.22	0.03	0.23	99.54
195.4	10.58	38.73	43.33	0.80	5.87	0.05	0.19	99.54
200.3	11.12	38.00	43.96	0.49	5.42	0.16	0.25	99.40
205.1	10.76	38.49	43.54	0.27	5.72	0.35	0.28	99.41
210.0	9.91	39.61	42.57	0.75	6.41	0.13	0.16	99.54
214.9	11.55	37.43	44.45	0.37	5.07	0.01	0.20	99.08
219.8	9.97	39.53	42.64	0.22	6.36	0.46	0.18	99.37
224.7	11.12	38.00	43.96	0.63	5.42	0.45	0.19	99.78
229.6	11.12	38.00	43.96	0.43	5.42	0.31	0.25	99.48
234.4	10.82	38.41	43.61	0.29	5.67	0.20	0.23	99.22

ICP-MS

Pos. (μm)	87/86	2 s.e.
0	0.70368	0.00077
180	0.70466	0.00054
221	0.70357	0.00093
272	0.70339	0.00061
317	0.70415	0.00061
377	0.70435	0.00058

Pos. (µm)	Na2O	Al2O3	SiO2	K2O	CaO	FeO	SrO	Total
239.3	12.35	36.37	45.37	0.52	4.42	0.11	0.23	99.36
244.2	10.28	39.13	42.98	0.32	6.11	0.42	0.18	99.41
249.1	9.38	40.33	41.95	0.68	6.85	0.29	0.23	99.71
254.0	11.06	38.08	43.89	0.54	5.47	0.02	0.23	99.28
258.9	10.25	39.17	42.95	0.41	6.14	0.01	0.20	99.12
263.8	12.28	36.45	45.30	0.36	4.47	0.23	0.19	99.28
268.6	10.88	38.33	43.68	0.35	5.62	0.24	0.16	99.24
273.5	11.85	37.02	44.80	0.63	4.82	0.37	0.17	99.67
278.4	12.25	36.49	45.26	0.72	4.49	0.05	0.17	99.44
283.3	10.97	38.20	43.78	0.78	5.54	0.09	0.23	99.60
288.2	11.98	36.86	44.94	0.56	4.72	0.05	0.16	99.28
293.1	10.58	38.73	43.33	0.49	5.87	0.29	0.27	99.55
297.9	11.64	37.31	44.56	0.58	4.99	0.18	0.21	99.47
302.8	11.89	36.98	44.84	0.79	4.79	0.40	0.29	99.98
307.7	13.46	34.88	46.65	0.80	3.50	0.25	0.23	99.77
312.6	11.82	37.07	44.77	0.39	4.84	0.18	0.20	99.28
317.5	11.46	37.55	44.34	0.22	5.14	0.49	0.20	99.41
322.4	11.67	37.27	44.59	0.74	4.97	0.31	0.27	99.82
327.3	11.24	37.84	44.10	0.47	5.32	0.27	0.28	99.52
332.1	10.28	39.13	42.98	0.74	6.11	0.34	0.19	99.77
337.0	10.43	38.93	43.16	0.22	5.99	0.45	0.28	99.45
341.9	11.82	37.07	44.77	0.46	4.84	0.39	0.27	99.62
346.8	10.73	38.53	43.50	0.42	5.74	0.16	0.25	99.32
351.7	10.97	38.20	43.78	0.22	5.54	0.04	0.22	98.98
356.6	10.55	38.77	43.29	0.79	5.89	0.07	0.28	99.64
361.4	11.98	36.86	44.94	0.64	4.72	0.12	0.27	99.52
366.3	12.19	36.57	45.19	0.70	4.54	0.46	0.26	99.93
371.2	10.00	39.49	42.67	0.30	6.33	0.05	0.25	99.09
376.1	9.47	40.21	42.05	0.23	6.78	0.27	0.28	99.27
381.0	11.09	38.04	43.92	0.61	5.44	0.12	0.24	99.48
385.9	11.27	37.80	44.13	0.44	5.29	0.15	0.30	99.39
390.7	11.52	37.47	44.41	0.38	5.09	0.18	0.25	99.31
395.6	9.65	39.97	42.26	0.31	6.63	0.16	0.26	99.23
400.5	10.85	38.37	43.64	0.68	5.64	0.05	0.20	99.43
405.4	11.43	37.60	44.31	0.69	5.17	0.30	0.21	99.70
410.3	11.58	37.39	44.48	0.42	5.04	0.29	0.18	99.39
415.2	10.97	38.20	43.78	0.79	5.54	0.14	0.25	99.69
420.1	9.56	40.09	42.15	0.28	6.70	0.05	0.22	99.05
424.9	8.75	41.16	41.23	0.46	7.36	0.18	0.28	99.42
429.8	8.69	41.24	41.16	0.66	7.41	0.42	0.23	99.80
434.7	9.41	40.29	41.98	0.46	6.82	0.13	0.22	99.31
439.6	9.20	40.57	41.74	0.55	6.99	0.31	0.16	99.53
444.5	9.53	40.13	42.12	0.27	6.73	0.07	0.21	99.05
449.4	11.37	37.68	44.24	0.38	5.22	0.47	0.18	99.53
454.2	9.88	39.65	42.53	0.61	6.43	0.13	0.28	99.52
459.1	10.79	38.45	43.57	0.61	5.69	0.44	0.28	99.83
464.0	9.74	39.85	42.36	0.45	6.55	0.30	0.15	99.41
468.9	8.81	41.08	41.29	0.39	7.31	0.42	0.16	99.47
473.8	8.84	41.04	41.33	0.56	7.29	0.27	0.23	99.56
478.7	10.82	38.41	43.61	0.59	5.67	0.35	0.28	99.72
483.6	10.25	39.17	42.95	0.51	6.14	0.02	0.30	99.33
488.4	10.06	39.41	42.74	0.38	6.28	0.49	0.21	99.57
493.3	9.11	40.69	41.64	0.61	7.07	0.13	0.28	99.53
498.2	10.06	39.41	42.74	0.60	6.28	0.27	0.26	99.63

Pos. (μm)	Na2O	Al2O3	SiO2	K2O	CaO	FeO	SrO	Total
503.1	12.69	35.92	45.76	0.46	4.14	0.00	0.23	99.19
508.0	12.84	35.71	45.94	0.41	4.01	0.26	0.29	99.46
512.9	11.49	37.51	44.38	0.47	5.12	0.28	0.25	99.50
517.7	10.58	38.73	43.33	0.41	5.87	0.44	0.30	99.65
522.6	11.30	37.76	44.17	0.22	5.27	0.01	0.27	99.00
527.5	9.91	39.61	42.57	0.74	6.41	0.18	0.27	99.68
532.4	10.97	38.20	43.78	0.80	5.54	0.15	0.24	99.68
537.3	11.46	37.55	44.34	0.36	5.14	0.23	0.20	99.29
542.2	10.12	39.33	42.81	0.42	6.24	0.32	0.25	99.49
547.0	10.58	38.73	43.33	0.78	5.87	0.16	0.29	99.73
551.9	10.31	39.09	43.02	0.40	6.09	0.50	0.24	99.64
556.8	11.73	37.19	44.66	0.31	4.92	0.24	0.24	99.29
561.7								
566.6	11.06	38.08	43.89	0.70	5.47	0.08	0.23	99.50
571.5	10.18	39.25	42.88	0.21	6.19	0.44	0.21	99.36
576.4	11.24	37.84	44.10	0.61	5.32	0.44	0.22	99.78
581.2	10.61	38.69	43.36	0.73	5.84	0.22	0.18	99.63
586.1	9.79	39.77	42.43	0.77	6.51	0.12	0.19	99.59
591.0	10.58	38.73	43.33	0.30	5.87	0.11	0.26	99.17

Unit: El Chichon M
Thin Section: CHI-9521
Crystal: D

85 μm diameter spot
"pos." indicates center

Microprobe analyses

Pos. (μm)	Na2O	Al2O3	SiO2	K2O	CaO	FeO	SrO	Total
0.0	11.89	36.98	44.84	0.39	4.79	0.14	0.18	99.20
5.4	11.85	37.02	44.80	0.26	4.82	0.03	0.17	98.96
10.9	12.84	35.71	45.94	0.41	4.01	0.39	0.24	99.55
16.3	12.78	35.79	45.87	0.35	4.06	0.25	0.27	99.37
21.8	11.12	38.00	43.96	0.28	5.42	0.17	0.22	99.17
27.2	11.27	37.80	44.13	0.24	5.29	0.47	0.21	99.42
32.7	11.30	37.76	44.17	0.39	5.27	0.30	0.30	99.49
38.1	11.98	36.86	44.94	0.25	4.72	0.12	0.22	99.09
43.6	11.73	37.19	44.66	0.79	4.92	0.22	0.30	99.81
49.0	10.61	38.69	43.36	0.51	5.84	0.01	0.21	99.23
54.5	10.22	39.21	42.91	0.59	6.16	0.32	0.25	99.67
59.9	11.58	37.39	44.48	0.70	5.04	0.34	0.26	99.81
65.4	11.89	36.98	44.84	0.61	4.79	0.12	0.28	99.51
70.8	13.06	35.42	46.19	0.50	3.83	0.22	0.21	99.43
76.3	10.89	38.30	43.70	0.28	5.61	0.13	0.17	99.08
81.7								
87.2	14.28	33.80	47.59	0.67	2.84	0.18	0.25	99.60
92.6								
98.1	12.32	36.41	45.33	0.43	4.44	0.05	0.25	99.24
103.5	12.13	36.66	45.12	0.41	4.59	0.08	0.23	99.23
109.0								
114.4	12.93	35.59	46.05	0.21	3.94	0.10	0.24	99.04
119.9	11.92	36.94	44.87	0.24	4.77	0.36	0.22	99.33
125.3	11.67	37.27	44.59	0.47	4.97	0.01	0.20	99.18
130.8	10.46	38.89	43.19	0.41	5.96	0.33	0.30	99.53
136.2	11.46	37.55	44.34	0.61	5.14	0.46	0.17	99.74
141.7	10.49	38.85	43.22	0.62	5.94	0.16	0.20	99.48
147.1	11.12	38.00	43.96	0.39	5.42	0.10	0.17	99.16
152.6	11.24	37.84	44.10	0.44	5.32	0.47	0.29	99.71
158.0	11.12	38.00	43.96	0.28	5.42	0.24	0.21	99.23
163.5	11.15	37.96	43.99	0.51	5.39	0.02	0.30	99.33
168.9	10.91	38.28	43.71	0.37	5.59	0.48	0.23	99.58
174.4	12.16	36.62	45.16	0.50	4.57	0.10	0.19	99.29
179.8	11.21	37.88	44.06	0.56	5.34	0.31	0.15	99.52
185.3	10.52	38.81	43.26	0.51	5.91	0.47	0.16	99.64
190.7	11.64	37.31	44.56	0.78	4.99	0.11	0.15	99.54
196.2	10.15	39.29	42.84	0.70	6.21	0.45	0.23	99.88
201.6	11.21	37.88	44.06	0.27	5.34	0.14	0.30	99.21
207.1	11.95	36.90	44.91	0.68	4.74	0.50	0.17	99.85
212.5	10.76	38.49	43.54	0.69	5.72	0.14	0.30	99.63
218.0	11.61	37.35	44.52	0.24	5.02	0.36	0.26	99.36
223.4	10.94	38.24	43.75	0.58	5.57	0.28	0.23	99.60
228.9	11.61	37.35	44.52	0.61	5.02	0.49	0.22	99.82
234.3	10.61	38.69	43.36	0.39	5.84	0.27	0.28	99.44
239.8	12.16	36.62	45.16	0.67	4.57	0.04	0.21	99.43
245.2	12.90	35.63	46.01	0.68	3.96	0.05	0.26	99.49
250.7	10.76	38.49	43.54	0.67	5.72	0.49	0.23	99.88
256.1	11.67	37.27	44.59	0.21	4.97	0.36	0.17	99.23
261.6	11.85	37.02	44.80	0.71	4.82	0.38	0.21	99.80

ICP-MS

Pos. (μm)	87/86	2 s.e.
33	0.70441	0.00061
90	0.70312	0.00097
147	0.70413	0.00078
238	0.70444	0.00066
329	0.70398	0.00074
377	0.70307	0.00182
448	0.70333	0.00073
510	0.70516	0.00090
576	0.70486	0.00075

Pos. (µm)	Na2O	Al2O3	SiO2	K2O	CaO	FeO	SrO	Total
267.0	13.21	35.21	46.37	0.77	3.71	0.45	0.21	99.93
272.5	13.37	35.01	46.55	0.75	3.58	0.47	0.15	99.87
277.9	13.40	34.96	46.58	0.46	3.55	0.18	0.15	99.30
283.4	11.76	37.15	44.70	0.27	4.89	0.36	0.20	99.32
288.8	11.09	38.04	43.92	0.63	5.44	0.34	0.26	99.73
294.3	11.49	37.51	44.38	0.30	5.12	0.42	0.22	99.44
299.7	11.43	37.60	44.31	0.27	5.17	0.30	0.18	99.25
305.2	11.92	36.94	44.87	0.67	4.77	0.43	0.15	99.76
310.6	10.09	39.37	42.77	0.80	6.26	0.21	0.22	99.72
316.1	10.97	38.20	43.78	0.34	5.54	0.27	0.16	99.28
321.5	12.44	36.25	45.48	0.55	4.34	0.27	0.17	99.48
327.0	10.67	38.61	43.43	0.69	5.79	0.23	0.22	99.65
332.4	10.91	38.28	43.71	0.59	5.59	0.25	0.28	99.62
337.9	10.91	38.28	43.71	0.49	5.59	0.39	0.18	99.55
343.3	12.22	36.53	45.23	0.29	4.52	0.15	0.27	99.21
348.8	12.13	36.66	45.12	0.27	4.59	0.32	0.26	99.35
354.2	11.82	37.07	44.77	0.65	4.84	0.38	0.26	99.79
359.7	10.03	39.45	42.70	0.78	6.31	0.12	0.15	99.55
365.1	11.30	37.76	44.17	0.64	5.27	0.20	0.19	99.54
370.6	11.15	37.96	43.99	0.33	5.39	0.00	0.18	99.02
376.0	12.62	36.00	45.69	0.23	4.19	0.28	0.22	99.23
381.5	12.16	36.62	45.16	0.44	4.57	0.49	0.22	99.66
386.9	12.90	35.63	46.01	0.41	3.96	0.44	0.20	99.54
392.4	11.30	37.76	44.17	0.70	5.27	0.46	0.16	99.82
397.8	11.61	37.35	44.52	0.71	5.02	0.22	0.19	99.62
403.3	10.82	38.41	43.61	0.20	5.67	0.37	0.28	99.36
408.7	10.40	38.97	43.12	0.43	6.01	0.39	0.22	99.53
414.2	10.88	38.33	43.68	0.42	5.62	0.14	0.17	99.23
419.6	10.37	39.01	43.09	0.75	6.04	0.46	0.20	99.92
425.1	11.52	37.47	44.41	0.34	5.09	0.42	0.20	99.46
430.5	11.92	36.94	44.87	0.49	4.77	0.34	0.24	99.58
436.0	11.79	37.11	44.73	0.39	4.87	0.48	0.15	99.52
441.4	11.43	37.60	44.31	0.63	5.17	0.10	0.21	99.44
446.9	11.55	37.43	44.45	0.69	5.07	0.25	0.22	99.67
452.3	10.97	38.20	43.78	0.47	5.54	0.37	0.29	99.63
457.8	11.26	37.82	44.12	0.27	5.31	0.19	0.27	99.23
463.2	11.76	37.15	44.70	0.38	4.89	0.07	0.29	99.24
468.7	11.30	37.76	44.17	0.48	5.27	0.02	0.25	99.25
474.1	12.25	36.49	45.26	0.72	4.49	0.49	0.24	99.95
479.6	11.24	37.84	44.10	0.43	5.32	0.05	0.25	99.24
485.0	12.50	36.16	45.55	0.25	4.29	0.06	0.23	99.05
490.5	12.07	36.74	45.05	0.77	4.64	0.11	0.23	99.61
495.9	11.67	37.27	44.59	0.73	4.97	0.22	0.18	99.64
501.4	11.12	38.00	43.96	0.39	5.42	0.14	0.16	99.19
506.8	11.64	37.31	44.56	0.63	4.99	0.26	0.23	99.62
512.3	12.10	36.70	45.09	0.72	4.62	0.50	0.29	100.00
517.7	12.50	36.16	45.55	0.46	4.29	0.04	0.22	99.22
523.2	11.43	37.60	44.31	0.77	5.17	0.14	0.30	99.71
528.6	11.73	37.19	44.66	0.52	4.92	0.02	0.24	99.28
534.1	11.00	38.16	43.82	0.35	5.52	0.31	0.16	99.32
539.5	10.40	38.97	43.12	0.50	6.01	0.45	0.29	99.75
545.0	11.70	37.23	44.63	0.44	4.94	0.42	0.17	99.53
550.4	12.16	36.62	45.16	0.54	4.57	0.36	0.19	99.59
555.9	9.82	39.73	42.46	0.78	6.48	0.48	0.25	100.00

Pos. (µm)	Na2O	Al2O3	SiO2	K2O	CaO	FeO	SrO	Total
561.3	8.63	41.32	41.09	0.63	7.46	0.37	0.27	99.77
566.8	8.99	40.84	41.50	0.42	7.17	0.21	0.19	99.31
572.2	9.68	39.93	42.29	0.51	6.60	0.41	0.16	99.58
577.7	9.44	40.25	42.01	0.28	6.80	0.11	0.24	99.14
583.1	10.22	39.21	42.91	0.27	6.16	0.42	0.21	99.40
588.6	9.20	40.57	41.74	0.22	6.99	0.13	0.27	99.12
594.0	10.76	38.49	43.54	0.70	5.72	0.14	0.23	99.57
599.5	11.24	37.84	44.10	0.56	5.32	0.38	0.19	99.63
604.9	10.61	38.69	43.36	0.25	5.84	0.21	0.23	99.18
610.4	10.88	38.33	43.68	0.66	5.62	0.07	0.24	99.47
615.8	10.34	39.05	43.05	0.33	6.06	0.06	0.27	99.17
621.3	10.00	39.49	42.67	0.57	6.33	0.17	0.16	99.40
626.7	9.82	39.73	42.46	0.32	6.48	0.10	0.28	99.20
632.2	11.06	38.08	43.89	0.22	5.47	0.39	0.17	99.29
637.6	9.94	39.57	42.60	0.36	6.38	0.09	0.22	99.16
643.1	11.95	36.90	44.91	0.68	4.74	0.40	0.21	99.79
648.5	10.88	38.33	43.68	0.25	5.62	0.48	0.20	99.43
654.0	9.88	39.65	42.53	0.41	6.43	0.02	0.25	99.18
659.4	11.00	38.16	43.82	0.74	5.52	0.26	0.21	99.70
664.9	10.97	38.20	43.78	0.31	5.54	0.17	0.30	99.28
670.3	10.97	38.20	43.78	0.31	5.54	0.11	0.27	99.19
675.8	10.73	38.53	43.50	0.74	5.74	0.32	0.19	99.75
681.2	11.30	37.76	44.17	0.73	5.27	0.32	0.22	99.77
686.7	9.26	40.49	41.81	0.23	6.95	0.42	0.28	99.43
692.1	10.00	39.49	42.67	0.69	6.33	0.30	0.26	99.74
697.6	9.68	39.93	42.29	0.53	6.60	0.40	0.22	99.66
703.0	10.52	38.81	43.26	0.65	5.91	0.33	0.21	99.68
708.5	10.70	38.57	43.47	0.22	5.77	0.03	0.20	98.94
713.9	9.76	39.81	42.39	0.71	6.53	0.47	0.23	99.91
719.4	11.49	37.51	44.38	0.60	5.12	0.42	0.29	99.81
724.8	11.43	37.60	44.31	0.71	5.17	0.29	0.23	99.73
730.3	10.43	38.93	43.16	0.21	5.99	0.14	0.27	99.12
735.7	9.85	39.69	42.50	0.76	6.46	0.25	0.27	99.78
741.2	11.24	37.84	44.10	0.71	5.32	0.25	0.27	99.73
746.6								
752.1	9.47	40.21	42.05	0.39	6.78	0.21	0.21	99.32
757.5	9.56	40.09	42.15	0.55	6.70	0.46	0.24	99.75
763.0	6.91	43.62	39.10	0.53	8.87	0.16	0.20	99.40
768.4	7.87	42.34	40.21	0.63	8.08	0.30	0.17	99.60
773.9	9.50	40.17	42.08	0.23	6.75	0.24	0.17	99.14
779.3	7.87	42.34	40.21	0.70	8.08	0.03	0.26	99.49
784.8	6.39	44.32	38.50	0.54	9.30	0.28	0.22	99.54
790.2	8.16	41.95	40.55	0.46	7.84	0.48	0.26	99.70
795.7	9.05	40.77	41.57	0.42	7.12	0.14	0.20	99.25
801.1	7.11	43.35	39.33	0.53	8.70	0.27	0.25	99.56
806.6	9.23	40.53	41.77	0.75	6.97	0.36	0.25	99.86
812.0	9.68	39.93	42.29	0.53	6.60	0.09	0.16	99.27
817.5	10.34	39.05	43.05	0.60	6.06	0.01	0.19	99.30
822.9	11.30	37.76	44.17	0.64	5.27	0.15	0.16	99.45
828.4	9.71	39.89	42.32	0.45	6.58	0.05	0.27	99.27
833.8	7.49	42.85	39.77	0.67	8.39	0.03	0.24	99.44
839.3	7.52	42.81	39.80	0.59	8.37	0.41	0.22	99.72
844.7	8.75	41.16	41.23	0.62	7.36	0.34	0.21	99.67
850.2	7.78	42.46	40.11	0.62	8.16	0.40	0.28	99.81

Pos. (μm)	Na2O	Al2O3	SiO2	K2O	CaO	FeO	SrO	Total
855.6	8.34	41.71	40.75	0.34	7.70	0.04	0.20	99.08
861.1	8.46	41.56	40.89	0.29	7.60	0.36	0.29	99.43
866.5	7.72	42.53	40.04	0.69	8.20	0.31	0.17	99.67
872.0	7.93	42.26	40.28	0.61	8.04	0.36	0.25	99.72
877.4	8.90	40.96	41.40	0.31	7.24	0.40	0.18	99.39
882.9	8.81	41.08	41.29	0.42	7.31	0.41	0.17	99.50
888.3	8.84	41.04	41.33	0.30	7.29	0.38	0.18	99.36
893.8	8.05	42.10	40.41	0.58	7.94	0.14	0.22	99.44
899.2	7.49	42.85	39.77	0.20	8.39	0.30	0.17	99.17
904.7	10.03	39.45	42.70	0.20	6.31	0.01	0.22	98.94
910.1	8.63	41.32	41.09	0.45	7.46	0.01	0.23	99.20
915.6	9.91	39.61	42.57	0.45	6.41	0.48	0.21	99.63
921.0	10.06	39.41	42.74	0.48	6.28	0.07	0.24	99.29
926.5	10.03	39.45	42.70	0.75	6.31	0.06	0.27	99.58
931.9	10.79	38.45	43.57	0.46	5.69	0.00	0.29	99.25
937.4	9.65	39.97	42.26	0.33	6.63	0.22	0.19	99.25
942.8	11.58	37.39	44.48	0.23	5.04	0.04	0.19	98.96
948.3	9.85	39.69	42.50	0.22	6.46	0.12	0.24	99.08
953.7	10.61	38.69	43.36	0.61	5.84	0.27	0.30	99.68
959.2	10.58	38.73	43.33	0.24	5.87	0.02	0.29	99.05
964.6	9.26	40.49	41.81	0.58	6.95	0.25	0.16	99.48
970.1	10.00	39.49	42.67	0.78	6.33	0.14	0.15	99.58
975.5	9.47	40.21	42.05	0.65	6.78	0.23	0.20	99.58
981.0	9.44	40.25	42.01	0.67	6.80	0.36	0.22	99.76
986.4	9.26	40.49	41.81	0.63	6.95	0.40	0.16	99.68
991.9	10.31	39.09	43.02	0.40	6.09	0.26	0.17	99.33
997.3	10.73	38.53	43.50	0.64	5.74	0.03	0.23	99.40
1002.8	9.08	40.73	41.60	0.34	7.09	0.09	0.18	99.11
1008.2	12.72	35.88	45.80	0.31	4.11	0.46	0.30	99.57
1013.7	10.31	39.09	43.02	0.61	6.09	0.26	0.27	99.63
1019.1	10.12	39.33	42.81	0.65	6.24	0.40	0.24	99.79
1024.6	9.68	39.93	42.29	0.79	6.60	0.40	0.17	99.86
1030.0	10.76	38.49	43.54	0.42	5.72	0.34	0.15	99.41
1035.4	10.61	38.69	43.36	0.75	5.84	0.32	0.29	99.86
1040.9	11.06	38.08	43.89	0.62	5.47	0.32	0.20	99.65
1046.3	10.31	39.09	43.02	0.22	6.09	0.48	0.29	99.48
1051.8	10.85	38.37	43.64	0.45	5.64	0.38	0.28	99.60
1057.2	10.94	38.24	43.75	0.40	5.57	0.16	0.19	99.25
1062.7								
1068.1								
1073.6								
1079.0								
1084.5								
1089.9	12.13	36.66	45.12	0.39	4.59	0.11	0.26	99.26
1095.4	9.32	40.41	41.88	0.28	6.90	0.41	0.18	99.37
1100.8	10.49	38.85	43.22	0.23	5.94	0.11	0.27	99.11
1106.3	9.41	40.29	41.98	0.74	6.82	0.09	0.18	99.50
1111.7	9.56	40.09	42.15	0.54	6.70	0.10	0.19	99.33
1117.2	10.43	38.93	43.16	0.39	5.99	0.44	0.29	99.62
1122.6	10.18	39.25	42.88	0.38	6.19	0.40	0.29	99.58
1128.1	10.34	39.05	43.05	0.63	6.06	0.00	0.27	99.40
1133.5	10.15	39.29	42.84	0.38	6.21	0.30	0.21	99.39
1139.0	9.38	40.33	41.95	0.30	6.85	0.35	0.16	99.30
1144.4	12.16	36.62	45.16	0.78	4.57	0.11	0.23	99.61

Pos. (µm)	Na2O	Al2O3	SiO2	K2O	CaO	FeO	SrO	Total
1149.9	10.52	38.81	43.26	0.51	5.91	0.21	0.20	99.42
1155.3	10.79	38.45	43.57	0.74	5.69	0.18	0.17	99.59
1160.8	10.12	39.33	42.81	0.42	6.24	0.18	0.26	99.36
1166.2	11.52	37.47	44.41	0.32	5.09	0.25	0.21	99.28
1171.7	11.46	37.55	44.34	0.66	5.14	0.27	0.30	99.73
1177.1	10.37	39.01	43.09	0.27	6.04	0.05	0.27	99.09
1182.6	10.70	38.57	43.47	0.76	5.77	0.02	0.19	99.47
1188.0	10.58	38.73	43.33	0.49	5.87	0.11	0.20	99.31
1193.5	9.76	39.81	42.39	0.29	6.53	0.40	0.29	99.48
1198.9	10.28	39.13	42.98	0.62	6.11	0.42	0.24	99.78
1204.4	10.37	39.01	43.09	0.39	6.04	0.37	0.16	99.42
1209.8	12.08	36.72	45.07	0.37	4.63	0.29	0.18	99.34
1215.3	12.41	36.29	45.44	0.37	4.37	0.11	0.17	99.16
1220.7	10.40	38.97	43.12	0.67	6.01	0.20	0.30	99.67
1226.2	13.09	35.38	46.22	0.26	3.81	0.41	0.26	99.44
1231.6	10.94	38.24	43.75	0.66	5.57	0.12	0.24	99.52
1237.1	9.97	39.53	42.64	0.79	6.36	0.17	0.25	99.70
1242.5	10.15	39.29	42.84	0.49	6.21	0.15	0.18	99.32
1248.0	11.09	38.04	43.92	0.22	5.44	0.03	0.22	98.96
1253.4	9.26	40.49	41.81	0.79	6.95	0.39	0.21	99.89
1258.9	8.69	41.24	41.16	0.36	7.41	0.01	0.29	99.17
1264.3	13.15	35.30	46.30	0.49	3.76	0.22	0.29	99.50
1269.8	9.82	39.73	42.46	0.23	6.48	0.10	0.26	99.10
1275.2	11.46	37.55	44.34	0.78	5.14	0.41	0.15	99.84
1280.7	10.00	39.49	42.67	0.29	6.33	0.12	0.28	99.19
1286.1	10.06	39.41	42.74	0.24	6.28	0.30	0.18	99.22
1291.6	9.05	40.77	41.57	0.56	7.12	0.27	0.25	99.58
1297.0	10.97	38.20	43.78	0.42	5.54	0.27	0.19	99.38
1302.5								
1307.9								
1313.4	11.85	37.02	44.80	0.34	4.82	0.29	0.22	99.35
1318.8	6.97	43.55	39.17	0.78	8.82	0.40	0.16	99.84
1324.3	7.96	42.22	40.31	0.28	8.01	0.40	0.28	99.46
1329.7	8.99	40.84	41.50	0.58	7.17	0.26	0.29	99.63
1335.2	9.41	40.29	41.98	0.56	6.82	0.04	0.23	99.33
1340.6	8.07	42.07	40.44	0.41	7.91	0.23	0.30	99.45
1346.1	10.28	39.13	42.98	0.68	6.11	0.14	0.27	99.59
1351.5	10.12	39.33	42.81	0.74	6.24	0.28	0.24	99.76
1357.0	10.46	38.89	43.19	0.42	5.96	0.22	0.26	99.40
1362.4	9.47	40.21	42.05	0.49	6.78	0.18	0.26	99.43
1367.9	8.78	41.12	41.26	0.74	7.34	0.14	0.30	99.68

Appendix 3: Ksudach KS_1 Sample Locations and Analyses

Sample locations are shown in Figure A3.1. Detailed descriptions of deposit stratigraphy are given in Andrews et al. (2007) and Andrews (2004).

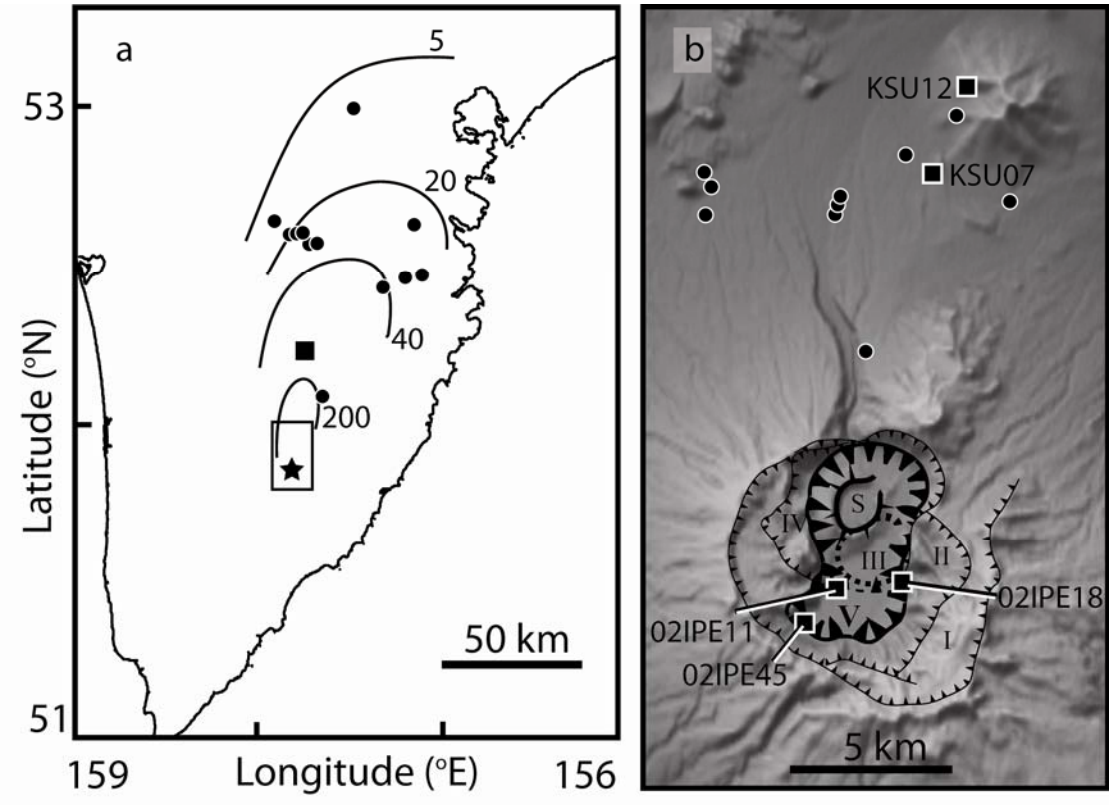

Figure A3.1. Ksudach sample locations. a) Kamchatka peninsula with KS_1 cumulative deposit isopachs indicated with in mm. Locations of KSU23 and Ksudach are indicated with a black square and star respectively. b) Ksudach Caldera V is the youngest of 5 nested calderas. Locations of sites KSU07 and KSU12 and samples 02IPE11, 02IPE18, and 02IPE45 are indicated with black boxes. Locations used in previous work (Andrews et al., 2007) are indicated with black circles.

Analyses were collected using JEOL JXA-8200 and Cameca SX-50 electron microprobes at The University of Texas at Austin and University of Alaska Fairbanks, respectively. FTIR analyses of dissolved water in glass inclusions were conducted using a ThermoElectron Nicolet Nexus 670 FTIR in the Department of Geological Sciences in the University of Oregon. All analyses are reported as weight percent oxides.

Table A3.1. Electron microprobe standards and secondary standards.

	Na2O	MgO	Al2O3	SiO2	K2O	CaO	TiO2
Glass	Albite	Kak. Hbl.	VG	LPGL	Orthoclase	VG2	Ilmenite
Plagioclase	Albite	--	An50	Orthoclase	Orthoclase	An100	--
Pyroxene	Kak. Hbl.	Enstatite	K412	Enstatite	Kak. Hbl.	K412	Kak. Hbl.
Fe-Ti Oxide	--	Chromite	Chromite	--	--	--	Ilmenite

	MnO	Cr2O3	FeO	SO3	Cl	Secondary
Glass	Ilmenite	--	VG2	Pyrite	Scapolite	KN18
Plagioclase	--	--	Fayalite	--	--	An50
Pyroxene	Mn Garnet	--	Fayalite	--		Enstatite & K411
Fe-Ti Oxide	Mn Garnet	Chromite	Ilmenite	--	--	Ilmenite

Sample: Ksudach
Phase: Matrix Glass

Conditions: 15 kV, 10 nA, 10 μm

Sample	Na2O	MgO	Al2O3	SiO2	K2O	CaO	TiO2	MnO	FeO	Total
Uncertainty	0.05	0.02	0.09	0.23	0.03	0.03	0.02	0.04	0.17	
02IPE45	4.72	0.62	12.94	71.44	1.32	2.43	0.23	0.12	2.67	96.49
02IPE45	5.22	0.59	13.20	72.58	1.27	2.45	0.37	0.15	2.84	98.69
02IPE45	4.16	0.51	12.50	71.49	1.32	2.03	0.36	0.12	2.51	94.99
02IPE45	6.20	0.47	13.52	73.68	1.52	2.28	0.29	0.18	2.68	100.82
02IPE45	5.40	0.50	13.51	73.37	1.42	2.09	0.34	0.15	3.17	99.95
02IPE45	5.09	0.40	12.91	71.51	1.36	2.00	0.37	0.10	2.58	96.33
02IPE45	5.13	0.42	13.60	71.90	1.47	2.06	0.22	0.10	2.44	97.33
02IPE45	4.83	0.40	13.66	73.31	1.41	2.21	0.36	0.17	2.73	99.09
02IPE45	4.15	0.38	13.02	73.20	1.35	2.03	0.31	0.10	2.11	96.64
KSU-23A	5.29	0.56	12.82	71.74	1.45	2.13	0.51	0.10	2.86	97.45
KSU-23A	5.35	0.64	13.07	71.89	1.23	2.27	0.35	0.13	3.30	98.25
KSU-23A	4.45	0.62	13.03	72.22	1.34	2.12	0.27	0.15	3.24	97.43
KSU-23A	5.28	0.64	13.36	70.82	1.35	2.16	0.42	0.17	2.98	97.19
KSU-23A	5.37	0.61	13.01	70.33	1.27	2.26	0.45	0.14	2.71	96.14
KSU-23A	4.00	0.49	13.57	73.43	1.34	2.46	0.35	0.17	2.68	98.50
KSU-23A	4.16	0.49	13.03	75.13	1.41	2.16	0.34	0.09	2.75	99.56
KSU-23A	4.58	0.41	13.02	71.89	1.40	1.98	0.29	0.10	2.20	95.88
KSU-23A	5.06	0.30	13.10	72.07	0.89	4.08	0.23	0.09	1.83	97.65

Sample: Ksudach
Phase: Glass Inclusions

Conditions: 15 kV, 10 nA, 10 μm

Sample	Na2O	MgO	Al2O3	SiO2	K2O	CaO	TiO2	MnO	FeO	SO3	Cl	H2O	Total
	0.05	0.02	0.09	0.23	0.03	0.03	0.02	0.04	0.17	0.00	0.01		
White													
02IPE45	3.01	0.13	12.01	69.72	1.15	1.65	0.10	0.21	2.44	0.47	0.18	1.50	92.56
02IPE45	3.01	0.13	12.01	69.72	1.15	1.65	0.10	0.21	2.44	0.47	0.18	1.52	92.58
02IPE45	8.24	0.13	12.01	69.72	1.15	1.65	0.10	0.21	2.44	0.47	0.18	1.52	97.82
02IPE45	8.24	0.13	12.01	69.72	1.15	1.65	0.10	0.21	2.44	0.47	0.18	1.52	97.82
02IPE45	3.45	0.44	11.74	64.34	1.34	1.93	0.24	0.17	2.41	0.16	0.15	5.11	91.51
02IPE45	3.52	0.42	11.33	64.81	1.29	1.76	0.11	0.11	2.28	0.17	0.10	5.87	91.75
02IPE45	3.52	0.42	11.33	64.81	1.29	1.76	0.11	0.11	2.28	0.17	0.10	4.66	90.55
02IPE45	2.84	0.35	11.21	59.45	1.23	1.83	0.61	0.07	2.05	0.02	0.08	7.88	87.62
02IPE45	2.84	0.35	11.21	59.45	1.23	1.83	0.61	0.07	2.05	0.02	0.08	7.20	86.94
02IPE45	2.70	0.08	14.52	67.90	1.18	1.47	0.14	0.08	1.73	0.07	0.18	3.56	93.61
02IPE45	2.90	0.06	12.55	72.31	1.17	1.73	0.10	0.13	1.76	0.02	0.13	3.56	96.42
02IPE45	3.21	0.23	12.34	70.25	1.23	1.50	0.41	0.12	2.34	0.06	0.13	4.44	96.26
02IPE45	3.21	0.23	12.34	70.25	1.23	1.50	0.41	0.12	2.34	0.06	0.13	4.41	96.23
02IPE45	3.27	0.13	11.72	67.78	1.12	1.59	0.26	0.07	1.96	0.10	0.17	4.43	92.58
02IPE45	3.29	0.11	12.56	71.36	1.23	1.66	0.61	0.11	4.12	0.32	0.17	2.49	98.04
Gray													
02IPE18	2.80	0.30	12.57	70.50	1.06	1.89	0.20	0.10	2.86	0.07	0.23	3.75	96.31
02IPE18	2.77	0.25	12.41	70.53	1.02	1.97	0.71	0.17	2.90	0.17	0.26	2.03	95.18
02IPE18	2.53	0.27	12.15	71.37	1.07	1.79	0.51	0.13	2.66	0.09	0.18	2.03	94.79
02IPE18	3.11	0.35	12.13	70.93	1.22	1.72	0.41	0.11	2.03	0.01	0.15	2.71	94.86
02IPE18	3.11	0.35	12.13	70.93	1.22	1.72	0.41	0.11	2.03	0.01	0.15	3.01	95.17
02IPE18	3.11	0.35	12.13	70.93	1.22	1.72	0.41	0.11	2.03	0.01	0.15	3.00	95.16
02IPE18	3.35	0.24	12.63	71.38	1.28	1.68	0.20	0.18	2.93	0.02	0.03	4.89	98.83
02IPE18	3.35	0.24	12.63	71.38	1.28	1.68	0.20	0.18	2.93	0.02	0.03	4.78	98.72
02IPE18	2.50	0.30	12.41	72.89	1.22	1.62	0.34	0.09	2.13	0.02	0.06	4.82	98.39
02IPE18	1.75	0.32	12.56	72.32	1.11	1.61	0.68	0.12	2.23	0.07	0.20	5.33	98.31
02IPE18	2.86	0.37	12.36	70.21	1.09	1.92	0.61	0.10	2.84	0.07	0.16	3.69	96.28
02IPE18	2.13	0.34	12.24	72.47	1.11	1.64	0.10	0.12	2.08	0.04	0.16	3.76	96.20
02IPE18	2.26	0.34	12.20	70.98	1.10	1.74	0.38	0.13	2.25	0.03	0.17	4.82	96.40
02IPE18	3.11	0.35	12.13	70.93	1.22	1.72	0.41	0.11	2.03	0.01	0.15	6.63	98.78
02IPE18	3.11	0.35	12.13	70.93	1.22	1.72	0.41	0.11	2.03	0.01	0.15	4.01	96.17

Sample: Ksudach
Phase: Plagioclase Phenocrysts

Conditions: 15 kV, 10 nA, focused beam

Sample	Na2O	Al2O3	SiO2	K2O	CaO	FeO	Total
White							
02IPE45	7.02	26.35	58.97	0.11	8.13	0.35	100.94
02IPE45	6.72	26.05	58.52	0.12	8.14	0.36	99.92
02IPE45	6.40	26.81	57.51	0.13	8.97	0.42	100.23
02IPE45	6.84	26.68	58.55	0.13	8.34	0.40	100.95
02IPE45	6.12	26.66	58.34	0.13	8.46	0.31	100.02
02IPE45	6.07	26.91	57.53	0.12	8.87	0.33	99.82
02IPE45	6.87	26.10	59.07	0.12	8.21	0.42	100.78
02IPE45	7.34	26.03	59.05	0.12	8.20	0.45	101.19
02IPE45	7.64	26.02	59.59	0.14	7.75	0.41	101.56
02IPE45	6.84	27.93	56.94	0.09	9.76	0.51	102.06
02IPE45	6.70	26.45	57.75	0.09	8.76	0.47	100.22
02IPE45	5.90	26.78	57.77	0.11	8.97	0.34	99.88
02IPE45	6.97	27.02	57.83	0.10	8.96	0.42	101.30
02IPE45	7.03	26.15	56.56	0.10	8.53	0.45	98.82
02IPE45	6.73	26.23	58.52	0.12	8.11	0.35	100.06
02IPE45	6.93	26.31	58.87	0.12	8.47	0.21	100.90
02IPE45	6.96	26.18	59.13	0.11	8.04	0.25	100.67
02IPE45	7.03	25.94	59.16	0.12	8.03	0.27	100.54
02IPE45	5.66	27.61	57.20	0.10	9.65	0.31	100.52
02IPE45	5.82	27.44	56.64	0.11	9.37	0.41	99.80
Gray							
KSU-23A	6.62	26.25	58.66	0.11	8.04	0.37	100.06
KSU-23A	6.36	27.02	57.52	0.09	8.91	0.30	100.20
KSU-23A	6.31	27.12	57.74	0.10	8.88	0.37	100.52
KSU-23A	6.30	27.02	58.46	0.12	8.72	0.36	100.97
KSU-23A	6.68	26.97	59.05	0.11	8.81	0.44	102.06
KSU-23A	6.63	26.56	58.73	0.13	8.47	0.42	100.95
KSU-23A	6.70	26.24	59.10	0.10	8.23	0.36	100.73
KSU-23A	6.80	26.58	58.82	0.11	8.31	0.32	100.94
KSU-23A	6.77	27.00	58.23	0.12	8.53	0.37	101.03
KSU-23A	6.34	26.70	58.88	0.10	8.57	0.39	100.96
KSU-23A	6.27	26.71	58.25	0.12	8.63	0.38	100.36
KSU-23A	6.28	26.75	58.66	0.10	8.58	0.32	100.70
KSU-23A	6.49	26.99	58.18	0.11	8.69	0.29	100.75
KSU-23A	6.56	26.77	57.95	0.11	8.65	0.29	100.34
KSU-23A	6.48	25.94	58.63	0.13	8.18	0.46	99.82
KSU-23A	6.68	26.37	58.49	0.13	8.32	0.31	100.30
KSU-23A	6.82	26.27	58.99	0.12	8.28	0.38	100.86
KSU-23A	7.00	26.23	58.44	0.13	8.22	0.32	100.33
KSU-23A	6.39	26.03	57.95	0.14	8.62	0.38	99.51

Sample: Ksudach
Phase: Pyroxene Phenocrysts

Conditions: 15 kV, 10 nA, focused beam

Sample	Na2O	MgO	Al2O3	SiO2	CaO	TiO2	MnO	FeO	Total
White -- 02IPE45									
CPX	0.301206	14.24539	1.239944	54.0141	20.25619	0.293319	0.464738	9.490784	100.3057
CPX	0.273611	14.61917	1.134045	54.40373	20.08006	0.242961	0.669765	10.00702	101.4304
CPX	0.282911	14.37511	1.035182	52.96405	20.07822	0.211442	0.465404	9.349888	98.76221
CPX	0.255379	14.57594	1.023847	53.21335	20.37074	0.24508	0.474852	9.606164	99.76535
CPX	0.217077	14.32277	1.164818	53.84111	19.87953	0.249441	0.482137	9.7336	99.89046
CPX	0.288569	14.14103	1.938402	53.05615	20.56811	0.485511	0.692551	10.40134	101.5717
CPX	0.266211	14.09102	1.358794	53.29396	20.46331	0.346058	0.510448	10.75667	101.0865
CPX	0.250895	14.41405	1.117732	53.06198	20.27793	0.283647	0.511968	10.60899	100.5272
CPX	0.340277	14.14697	1.270123	52.94902	19.93521	0.283492	0.502134	10.1396	99.56682
CPX	0.343027	13.58658	2.009267	52.65358	20.22631	0.438098	0.646837	10.369	100.2727
CPX	0.272709	14.0782	1.431054	52.4947	20.52216	0.273102	0.626922	10.0538	99.75264
CPX	0.293795	13.94775	1.294285	52.97044	19.83984	0.297289	0.417851	9.992062	99.05331
CPX	0.295464	14.50188	1.607865	53.15982	20.52623	0.364852	0.560855	10.63712	101.6541
OPX	0.013324	18.53374	0.874359	52.44729	1.352845	0.228923	1.736405	23.71293	98.89981
OPX	0.003337	19.08179	0.92511	53.38247	1.37658	0.234864	1.740901	24.16238	100.9074
OPX	0.01669	19.18231	0.608661	53.25685	1.376153	0.187989	1.577922	24.67839	100.885
OPX	0	19.42324	0.59158	52.97052	1.270418	0.131087	1.854245	24.01246	100.2535
OPX	0.053399	19.59171	0.594976	53.33901	1.333643	0.167608	1.912598	23.88519	100.8781
OPX	0.036868	19.79697	0.526861	53.14491	1.293531	0.165805	2.165582	24.24356	101.3741
OPX	0.020083	19.607	0.666083	52.69284	1.353655	0.149716	1.996452	24.07807	100.5639
OPX	0.010058	19.25755	0.736217	52.62299	1.350903	0.20097	1.890249	24.49562	100.5646
OPX	0.083967	19.43346	0.739335	52.65191	1.360608	0.238401	1.816625	24.88718	101.2115
OPX	0.050001	19.16486	0.522702	52.68286	1.389954	0.198516	1.883272	24.11145	100.0036
OPX	0.050003	19.26022	0.554271	52.65258	1.265811	0.170944	2.124699	23.33433	99.41284
OPX	0.080114	19.51738	0.633336	52.57918	1.423066	0.175406	1.712935	23.37023	99.49164
OPX	0.026685	19.38419	0.536299	52.42414	1.40087	0.144153	1.769215	23.79655	99.4821
OPX	0	19.58483	0.422655	52.61673	1.354092	0.154005	1.836365	23.60459	99.57326
OPX	0.010043	19.70352	0.393271	52.82361	1.343531	0.145546	1.879548	23.12352	99.42258
OPX	0	19.75822	0.527278	52.37317	1.334266	0.163731	1.833538	22.98541	98.97559
OPX	0.006674	19.44329	0.48628	51.85344	1.323163	0.182661	1.893973	24.01199	99.20148
OPX	0.046618	19.1435	0.505903	52.54752	1.494094	0.161309	1.74374	24.04723	99.68992
OPX	0	19.42102	0.510029	52.2432	1.326791	0.183876	1.94442	24.52555	100.1549
OPX	0.063716	19.67581	0.525114	52.35663	1.470691	0.116785	1.862963	25.34724	101.4189
OPX	0.010139	19.34	0.472613	52.63025	1.387941	0.151323	2.005365	25.29675	101.2944
OPX	0.073518	19.43957	0.45303	52.12938	1.389699	0.097429	1.929308	24.45151	99.96345
OPX	0.006707	19.17575	0.403126	52.28403	1.222379	0.139788	1.798441	25.00858	100.0388
OPX	0.01008	19.3446	0.433487	52.70052	1.349558	0.173546	2.161971	25.08973	101.2635
OPX	0	19.57141	0.4834	52.38366	1.372649	0.135302	1.966841	24.42085	100.3341
OPX	0.026797	18.91773	0.380477	52.4656	1.344649	0.173178	1.925388	24.86239	100.0962

Sample	Na2O	MgO	Al2O3	SiO2	CaO	TiO2	MnO	FeO	Total
Gray -- KSU-07b									
CPX	0.294079	13.35427	1.378284	53.503	18.48799	0.347578	1.241175	12.55496	101.1613
CPX	0.372983	13.46581	1.303489	53.21266	18.77455	0.274202	1.057495	12.80146	101.2627
CPX	0.295171	13.6553	1.356095	53.37585	18.82312	0.341112	1.076639	12.2243	101.1476
CPX	0.237815	13.45327	1.372946	53.33176	18.50818	0.252127	1.067219	12.06267	100.286
CPX	0.305303	13.53207	1.352708	53.00602	18.86423	0.265845	1.003646	12.11863	100.4484
CPX	0.404994	13.5744	1.311663	53.28554	18.80209	0.26102	1.139667	12.07842	100.8578
CPX	0.299111	13.29792	1.331459	52.87326	19.21219	0.222817	1.030592	12.20351	100.4709
CPX	0.276542	13.7774	0.966007	52.90479	19.09001	0.274006	1.0468	12.47036	100.8059
CPX	0.36343	13.34856	1.29068	52.5699	18.27062	0.287431	1.228819	12.39742	99.75686
CPX	0.321353	13.73288	1.286301	52.76555	18.13774	0.255618	1.189831	12.4879	100.1772
CPX	0.256971	13.82441	1.133576	53.62289	19.88524	0.248249	0.997015	11.44896	101.4173
CPX	0.375541	13.08536	1.821187	52.11774	20.29462	0.367618	0.816151	11.68183	100.56
CPX	0.415638	13.01346	1.863583	51.8922	19.96399	0.400863	0.862897	11.34707	99.75971
CPX	0.407046	12.98804	1.816442	52.06805	19.90861	0.385073	1.126441	11.66931	100.369
CPX	0.993109	12.01664	1.62254	47.40454	16.69106	0.359111	0.823143	8.597048	88.50719
CPX	0.407065	13.08443	1.890234	52.2146	19.91613	0.432153	1.203755	11.50489	100.6533
CPX	0.331849	13.13992	1.811591	52.10595	20.09342	0.334574	1.026899	11.62705	100.4713
CPX	0.391698	12.94611	2.029686	51.88734	20.24058	0.414519	0.721684	11.72303	100.3547
CPX	0.360289	12.92911	1.956409	51.71165	19.94004	0.439979	0.853674	11.87308	100.0642
OPX	0	19.78732	0.59104	52.8919	1.360292	0.190986	1.488672	23.5133	99.82352
OPX	0	20.30999	0.58324	53.04464	1.428446	0.141701	1.834043	23.49621	100.8383
OPX	0.036461	20.37158	0.552949	53.193	1.447927	0.227815	1.665918	23.74235	101.238
OPX	0.019796	20.14301	0.622365	53.75264	1.404623	0.129473	1.604249	23.73244	101.4086
OPX	0.039736	20.52237	0.601725	52.98201	1.367163	0.228597	1.668729	24.1958	101.6061
OPX	0.016462	20.4789	0.582342	53.66867	1.40992	0.19388	1.636093	23.15132	101.1376
OPX	0.059185	20.19458	0.607513	53.02189	1.334653	0.18088	1.817113	22.92943	100.1452
OPX	0.046336	20.82336	0.588979	52.96027	1.364672	0.150516	2.057115	24.04194	102.0332
OPX	0.00331	20.24696	0.626867	53.56944	1.364873	0.15143	1.704535	23.44167	101.1091
OPX	0.009984	20.17249	0.633784	53.33367	1.376856	0.205863	1.736666	24.54928	102.0186
OPX	0.056896	18.25813	0.687781	48.29766	1.315871	0.131024	1.715452	23.17604	93.63886

Sample: Ksudach
Phase: Fe-Ti Oxide Pairs

Conditions: 15 kV, 10 nA, focused beam

Sample	TiO2	Al2O3	Cr2O3	FeO	Fe2O3	MnO	MgO	Total	Ilm	ulv
White										
02IPE45	44.92	0.21	0.02	34.69	15.13	1.14	2.56	98.66	84.62	
	12.00	2.37	0.05	38.56	42.34	0.82	1.65	97.79		35.98
02IPE45	44.77	0.21	0.01	34.26	15.65	1.14	2.72	98.77	84.06	
	12.05	1.88	0.03	38.89	43.11	0.89	1.47	98.32		35.39
02IPE45	44.80	0.18	0.05	34.51	16.11	1.19	2.57	99.41	83.73	
	12.05	1.88	0.03	38.89	43.11	0.89	1.47	98.32		35.39
02IPE45	44.78	0.16	0.04	34.71	15.09	1.21	2.44	98.43	84.63	
	12.28	1.91	0.02	39.37	43.15	0.94	1.42	99.09		35.87
Gray										
02IPE11	45.19	0.18	0.03	34.93	14.88	1.23	2.51	98.96	84.92	
	12.24	2.06	0.03	39.21	43.23	0.88	1.58	99.23		35.73
02IPE11	44.96	0.15	0.05	34.65	14.95	1.12	2.61	98.50	84.77	
	12.24	2.06	0.03	39.21	43.23	0.88	1.58	99.23		35.73
02IPE18	40.77	0.31	0.03	30.15	23.27	0.83	3.19	98.55	76.05	
	11.78	1.91	0.05	38.65	43.64	0.91	1.48	98.42		34.59
02IPE18	40.77	0.31	0.03	30.15	23.27	0.83	3.19	98.55	76.05	
	12.12	1.96	0.02	39.55	44.48	0.96	1.50	100.58		34.78

Sample: Ksudach Equilibria Experiments
Phase: Glass (average compositions)

Conditions: 15 kV, 10 nA, 10 μm

Sample	Na2O	MgO	Al2O3	SiO2	K2O	CaO	TiO2	MnO	FeO	Total
Uncertainty	0.05	0.02	0.09	0.23	0.03	0.03	0.02	0.04	0.17	
K-1	4.12	0.51	13.60	72.96	1.29	2.71	0.37	0.20	2.51	98.27
K-2	4.36	0.40	13.04	76.64	1.39	2.09	0.27	0.14	2.14	100.47
K-1r	4.76	0.55	13.36	69.27	1.28	4.60	0.33	0.22	2.76	97.11
K-3	3.86	0.14	11.38	72.01	1.90	1.08	0.24	0.06	1.14	91.81
K-4	3.62	0.15	9.77	74.34	1.62	1.26	0.22	0.07	1.43	92.48
K-6	3.83	0.26	12.94	74.73	1.52	1.75	0.24	0.09	1.91	97.27
K-5	4.25	0.23	12.26	73.24	1.60	1.51	0.30	0.09	1.65	95.13
K-7	4.21	0.37	12.46	71.31	1.36	1.89	0.38	0.12	2.39	94.49
K-8	4.13	0.36	13.04	70.52	1.35	2.15	0.30	0.07	2.39	94.31
K-11B	4.30	0.61	12.95	69.47	1.24	2.34	0.41	0.14	2.69	94.15
K-12A	3.70	0.42	13.44	70.79	1.21	2.17	0.29	0.11	1.83	93.96
K-12B	4.49	0.37	12.91	73.55	1.40	1.74	0.28	0.12	1.72	96.57
K-14	4.87	0.29	12.30	75.34	1.55	1.60	0.33	0.09	2.12	98.48
K-13	5.14	0.26	13.62	71.53	1.66	1.56	0.31	0.12	1.72	95.92
K-15	3.77	0.13	12.51	77.34	1.79	2.41	0.21	0.08	1.53	99.75
K-16	3.20	0.40	13.25	67.44	1.31	2.23	0.24	0.12	1.88	90.08
K-18A	4.06	0.54	13.27	68.33	1.18	2.54	0.32	0.15	2.20	92.58
K-17A	4.12	0.46	12.80	69.95	1.31	2.07	0.31	0.12	2.25	93.40
K-19	3.67	0.50	12.93	69.49	1.01	2.03	0.27	0.13	2.14	92.18
K-20	3.50	0.13	11.99	76.89	1.51	1.99	0.22	0.18	1.76	98.17
K-22	4.30	0.67	13.52	68.67	1.26	2.74	0.38	0.12	1.85	93.53
K-23	3.44	0.58	13.29	70.03	1.40	2.25	0.32	0.13	1.48	92.91
K-24	4.25	0.29	13.63	71.89	1.66	1.73	0.15	0.12	0.98	94.69

Sample: Ksudach Phase Equilibria Experiments
Phase: Plagioclase

Conditions: 15 kV, 10 nA, focused beam

Sample	Na2O	Al2O3	SiO2	K2O	CaO	FeO	Total
K-1r	6.92	26.05	58.27	0.14	8.20	0.31	99.88
K-1r	6.55	26.55	56.81	0.12	9.04	0.46	99.53
K-1r	6.63	26.28	58.19	0.10	8.58	0.33	100.12
K-2	2.16	31.61	48.62	0.21	15.63	0.61	98.84
K-2	6.50	25.27	57.73	0.12	8.19	0.39	98.19
K-2	6.48	25.82	57.70	0.10	8.39	0.34	98.84
K-3	6.92	24.17	62.88	0.24	5.50	0.69	100.39
K-4	7.93	21.49	62.87	0.26	5.26	0.52	98.32
K-4	9.14	22.20	64.27	0.41	4.18	0.19	100.38
K-4	7.50	21.84	56.36	0.32	5.32	8.70	100.03
K-4	7.85	23.47	61.13	0.17	6.09	0.34	99.05
K-4	8.79	22.48	63.30	0.34	4.60	0.17	99.69
K-5	6.66	24.60	59.49	0.16	7.42	0.67	99.00
K-5	2.11	12.04	72.46	1.18	1.36	1.95	91.09
K-5	5.59	27.76	55.15	0.08	10.65	0.46	99.68
K-5	2.33	13.07	72.24	1.15	1.84	1.81	92.43
K-5	2.16	12.16	71.70	1.24	1.37	1.70	90.33
K-5	7.22	24.73	59.63	0.16	7.17	0.32	99.22
K-5	7.27	24.16	60.03	0.20	7.10	0.47	99.24
K-6	5.98	22.48	61.42	0.40	6.80	0.64	97.71
K-6	6.45	26.52	57.48	0.10	8.67	0.46	99.67
K-6	7.07	25.41	58.67	0.11	7.80	0.45	99.51
K-6	6.94	25.35	58.98	0.14	7.93	0.44	99.78
K-7	6.68	23.34	59.82	0.23	6.58	0.70	97.37
K-7	7.22	24.66	58.36	0.13	7.10	0.57	98.04
K-7	6.53	25.84	56.33	0.13	8.56	0.41	97.81
K-8	7.11	24.79	59.04	0.14	7.63	0.46	99.17
K-8	6.53	25.79	57.40	0.13	8.51	0.51	98.86
K-8	6.54	25.69	57.67	0.12	8.75	0.38	99.15
K-8	2.22	13.05	70.47	1.06	1.95	2.48	91.23
K-8	7.04	25.28	59.35	0.15	7.80	0.56	100.18
K-8	7.07	25.41	59.22	0.13	7.81	0.38	100.02
K-8	6.40	25.35	57.53	0.13	8.35	0.41	98.17
K-13	6.59	26.19	57.55	0.13	8.34	0.40	99.21
K-13	7.16	24.95	58.91	0.17	7.50	0.72	99.41
K-13	6.62	25.97	57.39	0.12	8.74	0.45	99.30
K-13	6.58	25.66	56.71	0.10	8.61	0.63	98.29
K-14	6.85	24.72	59.12	0.13	7.66	0.53	99.00
K-14	6.65	25.58	57.14	0.09	8.71	0.28	98.44
K-14	5.35	22.47	62.68	0.43	6.96	1.05	98.94
K-14	6.39	23.33	61.55	0.30	7.03	0.52	99.11
K-15	7.03	24.65	58.69	0.10	7.47	0.32	98.26
K-15	6.33	24.75	57.15	0.14	8.26	0.41	97.03
K-18B	6.93	25.91	58.16	0.12	8.40	0.40	99.93
K-18B	7.41	24.26	59.58	0.15	7.00	0.27	98.66
K-18B	5.74	23.91	59.25	0.25	7.76	0.71	97.61
K-18B	6.44	25.66	57.47	0.13	8.60	0.42	98.72
K-19	5.25	27.36	54.81	0.09	11.10	1.00	99.61
K-19	4.34	25.40	57.17	0.22	10.15	1.09	98.37
K-19	5.03	27.01	54.42	0.09	11.01	1.04	98.61
K-20	6.91	25.70	58.40	0.11	8.37	0.38	99.87
K-20	7.49	23.00	62.21	0.23	5.91	0.50	99.34
K-20	7.08	22.75	62.39	0.27	6.19	0.89	99.57
K-21	6.76	25.25	58.34	0.11	8.20	0.37	99.03
K-21	6.59	25.54	57.50	0.11	8.52	0.34	98.60

Sample	Na2O	Al2O3	SiO2	K2O	CaO	FeO	Total
K-22A	6.70	25.29	57.70	0.15	8.20	0.47	98.51
K-22A	6.43	23.80	61.08	0.18	8.10	1.04	100.61
K-22A	6.79	23.67	58.50	0.17	7.52	0.51	97.14
K-22A	6.49	25.74	57.57	0.14	8.67	0.47	99.08
K-22A	7.46	22.55	62.81	0.29	5.82	0.64	99.57
K-23	7.25	24.97	59.11	0.17	7.49	0.43	99.40
K-23	7.08	25.63	58.42	0.16	8.02	0.47	99.77
K-24	7.13	24.34	57.96	0.18	7.30	0.44	97.35
K-24	6.84	25.11	56.42	0.15	8.27	0.42	97.21
K-24	3.12	14.90	65.45	1.27	2.70	0.83	88.27

Appendix 4: Mount St. Helens Sample Locations and Granulometry

Samples of pyroclastic fall and flow deposits were collected from sites to the northeast and north of Mount St. Helens (Figure A4.1). Stratigraphic descriptions of those deposits are given at the end of this appendix.

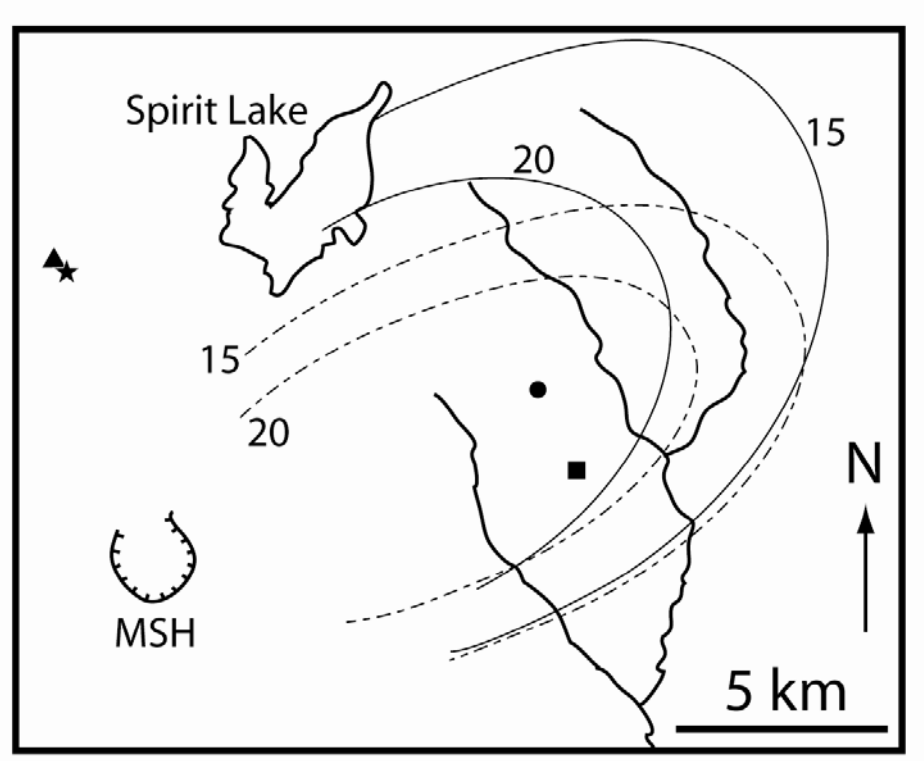

Figure A4.1. Fall deposit locations 05MSH-12 and 05MSH-16 are indicated with the black square and circle, respectively. Pyroclastic flow deposits 06 MSH-27 and 06MSH-28 are indicated with the black star and triangle, respectively. Lithic isopleths (in mm) of the B2 and B4 phases are indicated with solid and dashed lines, respectively (after Carey et al., 1990).

Grain size distributions and componentry of fall samples are presented in Figure A4.2. Grain size and componentry data of those samples is presented in full at the end of

this appendix. Samples were wet-sieved in 0.5 ϕ increments from the coarsest particles to 4 or 5 ϕ (63 or 32 μm). The size distributions of fines fractions were measured in o.5 f intervals to 9 ϕ using a Spectrex Laser Grain Size Analyzer.

Componentry of samples was determined by counting 300 particles from each size fraction 3 ϕ and coarser using a binocular microscope. Pumice, lithics, plagioclase, pyroxene, and amphibole were identified and counted as separated phases during analyses. Gray pumice only appeared in B3 and B4 deposits and composed <10 % of the pumice counted. White and gray pumice are grouped together as "pumice." The average masses of each phase were determined as a function of size by separating and weighing 50 particles at the 2, 1, 0 and -1 ϕ size fractions. Those average particle masses were then used to convert particle counts to mass fractions.

Estimated initial grain size distributions, GSD_o, are presented in Figure A4.2. Those distributions are calculated from Plinian fall deposit distributions using the expression

$$GSD_o = \sum_{\phi} \frac{S_{\phi o}}{v_{\phi}}$$

where particles, ϕ, vary in size and componentry, v_ϕ is the fall velocity specific to each component and size, and $S_{\phi o}$ is the initial sedimentation rate. The initial sedimentation rate is calculated, following (Sparks et al., 1992), as

$$S_{\phi o} = \frac{S_{\phi}}{exp\left(\frac{-\pi(r^2 - r_o^2)v_{\phi}}{Q}\right)}$$

where S_ϕ is the weight fraction of each grain size and component in a Plinian fall deposit, r and r_o are the radial distances of the sample location and plume corner from the vent, respectively, and Q is the buoyant volumetric eruption rate.

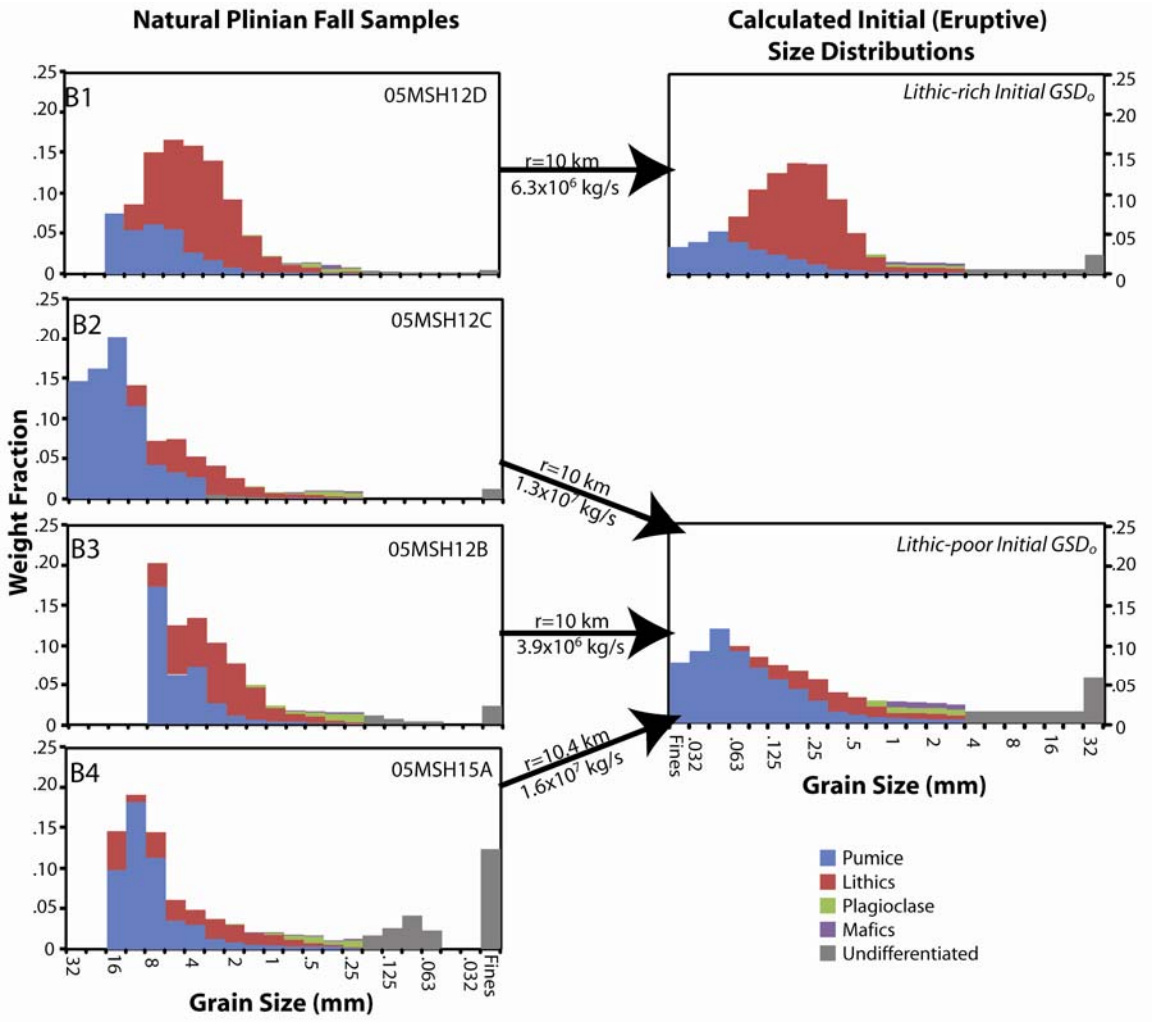

Figure A4.2. Plinian fall and initial grain size distributions.

Table A4.1. Parameters used to calculate GSD_o.

Phase	Mass flux (kg/s)	Q (m3/s)	r (km)	r_o (km)
B1	6.30E+06	2.86E+03	1.00E+01	5.00E+00
B2	1.30E+07	5.91E+03	1.00E+01	6.50E+00
B3	3.90E+06	1.77E+03	9.90E+00	5.00E+00
B4	1.60E+07	7.27E+03	1.00E+01	7.50E+00

Although the B1 phase Plinian fall deposits require a lithic-rich eruptive grain size distribution, a single, comparatively lithic-poor distribution can produce the B2, B3, and B4 Plinian fall deposits (Figure A4.2). This assumes that certain phases (e.g. lithics) do not preferentially partition into the pyroclastic flows.

Stratigraphic Descriptions

Location	05MSH-15			
	Unit	Thickness	Description	Sample
Top		<2 cm	gray, poorly-sorted sandy ash	
	B4	2 cm	coarse, white well-sorted pumcie fall	A
	B3	3 cm	poorly-sorted, pumice-bearing ash	B
	B2	10 cm	lithic-poor, well-sorted coarse white pumice fall	C
	B1	9 cm	lithic-rich, well-sorted pumice fall	D
	A3	4.5 cm	well-sorted greenish brown silty ash	
Base	Blast	>7 cm	dark gray, sandy, poorly-sorted ash	

Location	05MSH-12			
	Unit	Thickness	Description	Sample
		0.5	Gray silty ash	
	B4	2.5 cm	white pumice fall	A
	B3	3.0 cm	lithic-poor, poorly-sorted white pumice fall	B
	B2	5.0 cm	lithic-poor, well-sorted coarse white pumice fall	C
	B1	6.0 cm	lithic-rich, well-sorted pumice fall	D
	A3	6.5 cm	well-sorted greenish brown silty ash	
Base	Blast	>13 cm	dark gray, sandy, poorly-sorted ash	

Location	06MSH-27			
	Unit	Thickness	Description	Sample
top		2 m	Massive pumice-poor flow deposit	
		0.3 m	Pumice lens; grades laterally into laminated ash	E (lam. ash)
		2 m	Laminated ash; 10-30 cm thick layers	D
		0.3 m	Pumice lens; laterally discontinuous	
		2 m	Massive flow deposit	C
		0.5 m	Laminated ash; grades laterally into pumice lens	B
		3.5 m	Massive flow deposit	A
Base	cover			

Location	06MSH-28			
	Unit	Thickness	Description	Sample
		2 m	Massive flow deposit; contains pumice lenses	
		0.5 m	Lithic-rich flow deposit	C
		2 m	Massive flow deposit	
		0.3 m	Pumice lens	
		4.5 m	Massive flow deposit	A(base); B (mid)
Base	debris avalanche			

Sample **05 MSH 12B**

Mass Fraction

	FINES	**9**	**8.5**	**8**	**7.5**	**7**	**6.5**	**6**	**5.5**	**5**	**4.5**	**4**	**3.5**	**3**	**2.5**
Total	0.0225	0	0	0	0	0	0	0	0	0	0	0.003	0.0035	0.0059	0.0103
Pumice															
Lithics															
Plag															
Mafics															

	2	**1.5**	**1**	**0.5**	**0**	**-0.5**	**-1**	**-1.5**	**-2**	**-2.5**	**-3**	**-3.5**	**-4**	**-4.5**	**-5**
Total	0.0148	0.0139	0.0154	0.0162	0.0229	0.0488	0.0763	0.1021	0.1327	0.1231	0.201	0.1374	0.0501	0	0
Pumice	0.0002	0.0014	0.0008	0.0032	0.0035	0.005	0.0103	0.0259	0.0724	0.0624	0.1718	0	0		
Lithics	0.0015	0.0026	0.0085	0.0092	0.0163	0.0403	0.066	0.0761	0.0604	0.0608	0.0292	0	0		
Plag	0.011	0.0086	0.0054	0.0036	0.0031	0.0034	0	0	0	0	0	0	0		
Mafics	0.0021	0.0013	0.0007	0.0003	0	0	0	0	0	0	0	0	0		

Sample **05 MSH 12C**

Mass Fraction

	FINES	**9**	**8.5**	**8**	**7.5**	**7**	**6.5**	**6**	**5.5**	**5**	**4.5**	**4**	**3.5**	**3**	**2.5**
Total	0.0123	0	0	0	0	0	0	0	0	0	0	0.0015	0.0018	0.0031	0.0055
Pumice															
Lithics															
Plag															
Mafics															

	2	**1.5**	**1**	**0.5**	**0**	**-0.5**	**-1**	**-1.5**	**-2**	**-2.5**	**-3**	**-3.5**	**-4**	**-4.5**	**-5**
Total	0.0089	0.0104	0.0103	0.0081	0.0085	0.015	0.0259	0.0411	0.0521	0.074	0.0724	0.1405	0.2015	0.1614	0.1457
Pumice	0.0008	0.0007	0.0006	0.0012	0.0008	0.0014	0.0027	0.0042	0.0272	0.0333	0.0424	0.1148	0.2015	0.1614	0.1457
Lithics	0.0012	0.0025	0.0042	0.0053	0.0074	0.0133	0.0233	0.0369	0.0249	0.0407	0.0299	0.0257	0		
Plag	0.005	0.0062	0.005	0.0015	0.0004	0.0004	0	0	0	0	0	0	0		
Mafics	0.0019	0.001	0.0005	9E-05	0	0	0	0	0	0	0	0	0		

Sample **05 MSH 12D**

Mass Fraction

	FINES	**9**	**8.5**	**8**	**7.5**	**7**	**6.5**	**6**	**5.5**	**5**	**4.5**	**4**	**3.5**	**3**	**2.5**
Total	0.0052	0	0	0	0	0	0	0	0	0.0006	0.0009	0.0014	0.0015	0.0024	0.0039
Pumice															
Lithics															
Plag															
Mafics															

	2	**1.5**	**1**	**0.5**	**0**	**-0.5**	**-1**	**-1.5**	**-2**	**-2.5**	**-3**	**-3.5**	**-4**	**-4.5**	**-5**
Total	0.0079	0.0115	0.0142	0.0135	0.0225	0.0477	0.0923	0.1398	0.1587	0.1654	0.15	0.0858	0.0746	0	0
Pumice	0.0006	0.0003	0.002	0.0021	0.0016	0.0028	0.0081	0.0169	0.0269	0.0554	0.0619	0.054	0.0746	0	0
Lithics	0.0017	0.0018	0.0056	0.009	0.0198	0.0448	0.0842	0.123	0.1317	0.11	0.0881	0.0318	0		
Plag	0.0046	0.0034	0.0057	0.0023	0.0011	0.0001	0	0	0	0	0	0	0		
Mafics	0.001	0.006	0.0009	0.0002	0	0	0	0	0	0	0	0	0		

Sample **05 MSH 15A**

Mass Fraction

	FINES	**9**	**8.5**	**8**	**7.5**	**7**	**6.5**	**6**	**5.5**	**5**	**4.5**	**4**	**3.5**	**3**	**2.5**
Total	0.1233	0	0	0	0	0	0	0	0	0	0	0.0238	0.0417	0.0268	0.0176
Pumice															
Lithics															
Plag															
Mafics															

	2	**1.5**	**1**	**0.5**	**0**	**-0.5**	**-1**	**-1.5**	**-2**	**-2.5**	**-3**	**-3.5**	**-4**	**-4.5**	**-5**
Total	0.0129	0.0117	0.0174	0.0188	0.0216	0.0221	0.0318	0.0379	0.0491	0.0615	0.1448	0.1913	0.146	0	0
Pumice	0.0021	0.0041	0.0042	0.0038	0.0051	0.0067	0.0091	0.0131	0.0313	0.0359	0.1142	0.1817	0.0987		
Lithics	0.0015	0.0025	0.0043	0.0087	0.0134	0.0134	0.0224	0.0248	0.0178	0.0256	0.0306	0.0095	0.0473		
Plag	0.0076	0.0047	0.0078	0.0059	0.0024	0.0018	0.0003	0	0	0	0	0	0		
Mafics	0.0018	0.0004	0.001	0.0004	0.0007	0.0002	0	0	0	0	0	0	0		

Sample **05 MSH 15B**

Mass Fraction

	FINES	**9**	**8.5**	**8**	**7.5**	**7**	**6.5**	**6**	**5.5**	**5**	**4.5**	**4**	**3.5**	**3**	**2.5**
Total	0.0898									0.0073	0.0106	0.0217	0.0148	0.0055	0.0078
Pumice															
Lithics															
Plag															
Mafics															

	2	**1.5**	**1**	**0.5**	**0**	**-0.5**	**-1**	**-1.5**	**-2**	**-2.5**	**-3**	**-3.5**	**-4**	**-4.5**	**-5**
Total	0.0155	0.0236	0.0461	0.102	0.1213	0.0926	0.0831	0.0725	0.0669	0.081	0.0684	0.0586	0.0109	0	0
Pumice	0.0004	0.0015	0.0028	0.0073	0.0145	0.0276	0.0337	0.0437	0.0406	0.0481	0.0406	0.0492	0.0109		
Lithics	0.0035	0.0067	0.0217	0.0735	0.1033	0.065	0.0489	0.0288	0.0263	0.0329	0.0278	0.0094	0		
Plag	0.0094	0.0142	0.0195	0.0199	0.0025	0	0.0005	0	0	0	0	0	0		
Mafics	0.0022	0.0012	0.0021	0.0014	0.0011	0	0	0	0	0	0	0	0		

Sample **05 MSH 15C**

Mass Fraction

	FINES	**9**	**8.5**	**8**	**7.5**	**7**	**6.5**	**6**	**5.5**	**5**	**4.5**	**4**	**3.5**	**3**	**2.5**
Total	0									0	0	0.0016	0.0017	0.0023	0.0023
Pumice															
Lithics															
Plag															
Mafics															

	2	**1.5**	**1**	**0.5**	**0**	**-0.5**	**-1**	**-1.5**	**-2**	**-2.5**	**-3**	**-3.5**	**-4**	**-4.5**	**-5**
Total	0.003	0.0036	0.0076	0.0174	0.0357	0.0577	0.088	0.1075	0.1462	0.1967	0.1718	0.1369	0		
Pumice	0.0001	0.0003	0.0008	0.0008	0.0031	0.0093	0.0266	0.0564	0.1033	0.1547	0.1311	0.1488			
Lithics	0.0003	0.0005	0.0031	0.0128	0.0312	0.0484	0.0614	0.0511	0.0429	0.0421	0.0407	0			
Plag	0.0022	0.0026	0.0036	0.0037	0.0014	0	0	0	0	0	0	0			
Mafics	0.0004	0.0002	4E-05	0	0	0	0	0	0	0	0	0			

Sample **06 MSH 27A**

Mass Fraction

	FINES	**9**	**8.5**	**8**	**7.5**	**7**	**6.5**	**6**	**5.5**	5	4.5	4	3.5	3	2.5
Total	3E-05	0.0002	0.0005	0.0021	0.0026	0.0072	0.0078	0.0184	0.0292	0.0268	0.0259	0.0427	0.0551	0.0948	0.0805
Pumice														0.0061	0.0025
Lithics														0.0294	0.0205
Plag														0.0412	0.0378
Mafics														0.0182	0.0196

	2	**1.5**	**1**	**0.5**	**0**	**-0.5**	**-1**	**-1.5**	**-2**	**-2.5**	**-3**	**-3.5**	**-4**	**-4.5**	**-5**
Total	0.0879	0.0754	0.0764	0.0496	0.0476	0.0436	0.0412	0.0375	0.0375	0.0244	0.0392	0.0115	0.0345	0	0
Pumice	0.0033	0.0053	0.0056	0.0037	0.0065	0.0033	0.0035	0.0029	0.0034	0.0032	0.011	0.0025	0		
Lithics	0.0386	0.0328	0.0457	0.0372	0.0384	0.0395	0.0377	0.0344	0.034	0.0212	0.0281	0.009	0.0345		
Plag	0.0399	0.0284	0.0239	0.0082	0.0022	0.0006	0	0.0002	0	0	0	0	0		
Mafics	0.0061	0.0089	0.0011	0.0005	0.0005	0.0001	0	0	0	0	0	0	0		

Sample **06 MSH 27B**

Mass Fraction

	FINES	**9**	**8.5**	**8**	**7.5**	**7**	**6.5**	**6**	**5.5**	5	4.5	4	3.5	3	2.5
Total	3E-05	0.0003	0.0008	0.005	0.0094	0.0289	0.03	0.0245	0	0	0	0.0375	0.0489	0.0691	0.0781
Pumice														0.0014	0.0021
Lithics														0.0226	0.0216
Plag														0.034	0.0391
Mafics														0.0111	0.0153

	2	**1.5**	**1**	**0.5**	**0**	**-0.5**	**-1**	**-1.5**	**-2**	**-2.5**	**-3**	**-3.5**	**-4**	**-4.5**	**-5**
Total	0.0891	0.0795	0.0775	0.0619	0.0542	0.0526	0.048	0.0447	0.0423	0.0478	0.0309	0.0391	0	0	0
Pumice	0.0064	0.0034	0.0059	0.0028	0.0055	0.0034	0.0045	0.0063	0.0053	0.0061	0	0.014	0		
Lithics	0.0358	0.0424	0.048	0.0487	0.0474	0.0484	0.0434	0.0384	0.0371	0.0416	0.0309	0.025	0		
Plag	0.0437	0.0297	0.0236	0.0102	0.0014	0.0007	0.0001	0	0	0	0	0	0		
Mafics	0.0033	0.0041	0	0.0002	0	0.0001	0	0	0	0	0	0	0		

Sample **06 MSH 27C**

Mass Fraction

	FINES	**9**	**8.5**	**8**	**7.5**	**7**	**6.5**	**6**	**5.5**	5	4.5	4	3.5	3	2.5
Total	1E-05	0.0001	0.0006	0.0028	0.0038	0.0088	0.0102	0.0084	0.0282	0.0154	0.0142	0.041	0.0475	0.0752	0.0847
Pumice														0.0028	0.0043
Lithics														0.0181	0.0275
Plag														0.0438	0.0418
Mafics														0.0106	0.0112

	2	**1.5**	**1**	**0.5**	**0**	**-0.5**	**-1**	**-1.5**	**-2**	**-2.5**	**-3**	**-3.5**	**-4**	**-4.5**	**-5**
Total	0.0968	0.0871	0.085	0.0648	0.0534	0.0498	0.0456	0.0432	0.0402	0.0407	0.0348	0.0177	0	0	0
Pumice	0.0042	0.0029	0.0065	0.0074	0.0074	0.0088	0.0059	0.0062	0.005	0.0069	0.0087	0.0022	0		
Lithics	0.0398	0.042	0.0474	0.0483	0.0441	0.041	0.0397	0.037	0.0352	0.0338	0.026	0.0156	0		
Plag	0.0405	0.0378	0.028	0.0091	0.0018	0	0	0	0	0	0	0	0		
Mafics	0.0122	0.0043	0.003	0	0	0	0	0	0	0	0	0	0		

Sample **06 MSH 27D**

Mass Fraction

	FINES	**9**	**8.5**	**8**	**7.5**	**7**	**6.5**	**6**	**5.5**	5	4.5	4	3.5	3	2.5
Total	0	1E-06	2E-05	0.0006	0.0026	0.0114	0.0087	0.0093	0.0168	0.0313	0.023	0.044	0.0558	0.0762	0.0762
Pumice														0.0027	0.0114
Lithics														0.0228	0.0212
Plag														0.039	0.0303
Mafics														0.0118	0.0133

	2	**1.5**	**1**	**0.5**	**0**	**-0.5**	**-1**	**-1.5**	**-2**	**-2.5**	**-3**	**-3.5**	**-4**	**-4.5**	**-5**
Total	0.1078	0.0889	0.0787	0.0528	0.0493	0.0459	0.0361	0.0358	0.0287	0.0318	0.031	0.0483	0.0091	0	0
Pumice	0.008	0.004	0.0022	0.0037	0.0053	0.0041	0.0029	0.0038	0.0039	0.004	0.0028	0.0037	0		
Lithics	0.0392	0.0471	0.0503	0.0425	0.0421	0.0415	0.0332	0.0321	0.0248	0.0278	0.0282	0.0446	0.0091		
Plag	0.043	0.0343	0.0254	0.0065	0.0019	0.0003	0	0	0	0	0	0	0		
Mafics	0.0177	0.0035	0.0008	0	0	0	0	0	0	0	0	0	0		

Sample **06 MSH 27E**

Mass Fraction

	FINES	**9**	**8.5**	**8**	**7.5**	**7**	**6.5**	**6**	**5.5**	5	4.5	4	3.5	3	2.5
Total	9E-07	8E-06	0.0001	0.0004	0.0008	0.0148	0.0055	0.0411	0.0141	0.0084	0.0078	0.0388	0.0475	0.0963	0.0745
Pumice														0.0113	0.0025
Lithics														0.0211	0.0142
Plag														0.04	0.0332
Mafics														0.024	0.0246

	2	**1.5**	**1**	**0.5**	**0**	**-0.5**	**-1**	**-1.5**	**-2**	**-2.5**	**-3**	**-3.5**	**-4**	**-4.5**	**-5**
Total	0.0882	0.0874	0.0804	0.0544	0.0468	0.0436	0.0423	0.0327	0.0335	0.0352	0.0412	0.064	0	0	0
Pumice	0.0052	0.0095	0.008	0.0055	0.0062	0.0067	0.007	0.0076	0.0146	0.0352	0.0412	0.064	0		
Lithics	0.0264	0.0382	0.0445	0.0396	0.0373	0.0366	0.0353	0.0251	0.0189	0	0	0	0		
Plag	0.0386	0.0323	0.0271	0.0083	0.0033	0.0003	0	0	0	0	0	0	0		
Mafics	0.018	0.0075	0.0008	0.001	0	0	0	0	0	0	0	0	0		

Sample **06 MSH 28A**

Mass Fraction

	FINES	**9**	**8.5**	**8**	**7.5**	**7**	**6.5**	**6**	**5.5**	5	4.5	4	3.5	3	2.5
Total	0	0	0	0	0.0009	0.0314	0.0375	0.0564	0.1696	0.0734	0.0192	0.0752	0.0751	0.0903	0.0754
Pumice														0.0022	0.0008
Lithics														0.0274	0.035
Plag														0.0485	0.0392
Mafics														0.0122	0.0004

	2	**1.5**	**1**	**0.5**	**0**	**-0.5**	**-1**	**-1.5**	**-2**	**-2.5**	**-3**	**-3.5**	**-4**	**-4.5**	**-5**
Total	0.0696	0.0617	0.0584	0.0396	0.0269	0.0205	0.0097	0.0092	0	0	0	0	0	0	0
Pumice	0.0018	0.0031	0.0025	0.0021	0.0057	0.0018	0.0008	0.0029	0	0	0	0	0		
Lithics	0.0393	0.0398	0.0477	0.0337	0.0198	0.0188	0.0089	0.0064	0	0	0	0	0		
Plag	0.0267	0.0185	0.0082	0.0039	0.0012	0	0	0	0	0	0	0	0		
Mafics	0.0019	0.0004	0	0	0.0002	0	0	0	0	0	0	0	0		

Sample **06 MSH 28B**

Mass Fraction

	FINES	**9**	**8.5**	**8**	**7.5**	**7**	**6.5**	**6**	**5.5**	5	4.5	4	3.5	3	2.5
Total	0	0	0	1E-05	0.0004	0.0029	0.0096	0.0256	0.1006	0.033	0.0344	0.0517	0.0668	0.0898	0.0885
Pumice														0.003	0.004
Lithics														0.0076	0.0231
Plag														0.0506	0.0462
Mafics														0.0287	0.0153

	2	**1.5**	**1**	**0.5**	**0**	**-0.5**	**-1**	**-1.5**	**-2**	**-2.5**	**-3**	**-3.5**	**-4**	**-4.5**	**-5**
Total	0.0991	0.0934	0.0824	0.0566	0.0535	0.0419	0.0338	0.0222	0.0068	0.007	0	0	0	0	0
Pumice	0.0021	0.0099	0.014	0.0087	0.0056	0.006	0.006	0.0075	0.0068	0.007	0	0	0		
Lithics	0.0333	0.0441	0.0482	0.0404	0.0461	0.0359	0.0278	0.0148	0	0	0	0	0		
Plag	0.0522	0.0369	0.0202	0.0074	0.0019	0	0	0	0	0	0	0	0		
Mafics	0.0115	0.0025	0	0	0	0	0	0	0	0	0	0	0		

Sample **06 MSH 28C**

Mass Fraction

	FINES	**9**	**8.5**	**8**	**7.5**	**7**	**6.5**	**6**	**5.5**	5	4.5	4	3.5	3	2.5
Total	0	0	0	0	0	6E-05	0.0021	0.0074	0.0264	0.012	0.0111	0.0154	0.0351	0.0578	0.0548
Pumice														0.0029	0.0029
Lithics														0.0121	0.0137
Plag														0.0323	0.031
Mafics														0.0105	0.0073

	2	**1.5**	**1**	**0.5**	**0**	**-0.5**	**-1**	**-1.5**	**-2**	**-2.5**	**-3**	**-3.5**	**-4**	**-4.5**	**-5**
Total	0.0797	0.0517	0.0878	0.0444	0.0362	0.0342	0.0273	0.0278	0.0249	0.0282	0.0332	0.0391	0.1899	0.0734	0
Pumice	0.0035	0.0032	0.0048	0.0023	0.0037	0.0028	0.0029	0.0031	0.0026	0.0007	0.0033	0.0012			
Lithics	0.0281	0.0226	0.047	0.034	0.0296	0.0312	0.0244	0.0247	0.0223	0.0275	0.0298	0.0379	0.1899	0.0734	
Plag	0.0413	0.0244	0.0337	0.0073	0.0025	0.0002	7E-05	0	0	0	0	0			
Mafics	0.0068	0.0015	0.0022	0.0008	0.0004	0	0	0	0	0	0	0			

Appendix 5: Mount St. Helens Length Scales and Velocity Fields

Eddy sizes were measured from photographs and individual video frames of the B2 and B3 eruption columns. Those sizes were measured as the lateral distances across the large cauliform structures on the column surface. Measurements were scaled using the 1.9 km crater rim visible along the bottom of each image. Representative photographs used for measurements of eddy size are presented in the following pages. Copyright restrictions prevent inclusion of video stills and image stacks in open appendices. For access to those files please contact the author or Dr. James Gardner.

The velocity field of the images was measured using the ImageJ plug-in FlowJ (Abramoff et al., 2000). That program measures the velocity field by tracking pixel intensities through a stack of images. The resulting velocity fields were then used to calculate the average velocity (u), deviatoric velocity (u'), and integral length scales (Λ). The procedures below describe my method of progressing from digitized video to calculations of u, u', and Λ.

1) Digitize VHS video.

2) Decimate video file and extract individual frames as ".tif" files. In this step, 30 frames per second (fps) video is decimated to 5 or 6 fps ".tif" images.

3) Convert the series of images to an image stack in ImageJ.

4) Measure velocity field using the Uras algorithm within the FlowJ plugin.

5) Calculate average velocity, u, as the average of all measured column velocities.

6) Calculate characteristic deviatoric velocity, *u'*, as the root mean squared value of velocity minus the average velocity.

7) Calculate the autocorrelation function, *R*, of the velocity field as a function of distance *r* using the expression

$$R = \frac{U(x,t)U(x+r,t)}{u(t)^2}$$

where *U* is the velocity measured at time *t* as a function of position *x*+*r*; *U* is the average velocity.

8) Measure the integral length scale, *Λ*, from the autocorrelation diagram as the distance at which the autocorrelation, *R*, decreases to 0.

Turbulence measurements of the B2 and B3 eruption column are presented in Table A5.1.

Gradient Richardson numbers, *Ri*, were calculated for the B2 and B3 eruption column margins using the expression

$$Ri = abs\left(\frac{g\frac{\rho-\alpha}{\Lambda}}{\alpha\left(\frac{u'}{\Lambda}\right)^2}\right)$$

where *g* is gravitational acceleration, ρ is the interior column density, α is atmospheric density, *u'* is the deviatoric velocity, and *L* is the integral length scale of the velocity field. For those calculations, atmospheric density was assumed as 1.25 kg/m^3, and column density was assumed to be 1 kg/m^3 during the B2 phase and 2 kg/m^3 during the B3 phase.

Table A5.1. Turbulent length scales and characteristic velocities of the Mount St. Helens 18 May 1980 B2 and B3 eruption columns.

Phase	Image Stack	u	u'	Λ
B2	B2-1	38.9576	42.42049	758
	B2-2	43.28622	82.24382	914
	B2-3	43.28622	61.46643	676
	B2-4	51.94346	86.57244	1008
	B2-5	53.67491	68.39223	931
	B2-6	50.21201	77.04947	657
	B2-7	53.67491	71.85512	900
B3	B3-2	50.21739	93.26087	390
	B3-3	50.86957	107.6087	285
	B3-4	56.08696	120	190
	B3-5	53.47826	74.34783	370
	B3-6	56.08696	95.21739	240
	B3-7	58.69565	94.56522	223

B2 Eruption Column

Photograph: Swanson, USGS

Eddy sizes (m)				
671	388	549	283	400
459	474	343	441	

Photograph: Post, USGS

Eddy sizes (m)				
602	455	582	475	656
395				

Photograph: Post, USGS

Eddy sizes (m)				
703	436	625	514	351
722	677	852	403	573

Photograph: Krimmel, USGS

Eddy sizes (m)				
405	445	427	374	458
489	449	396	436	596
587	356	570		

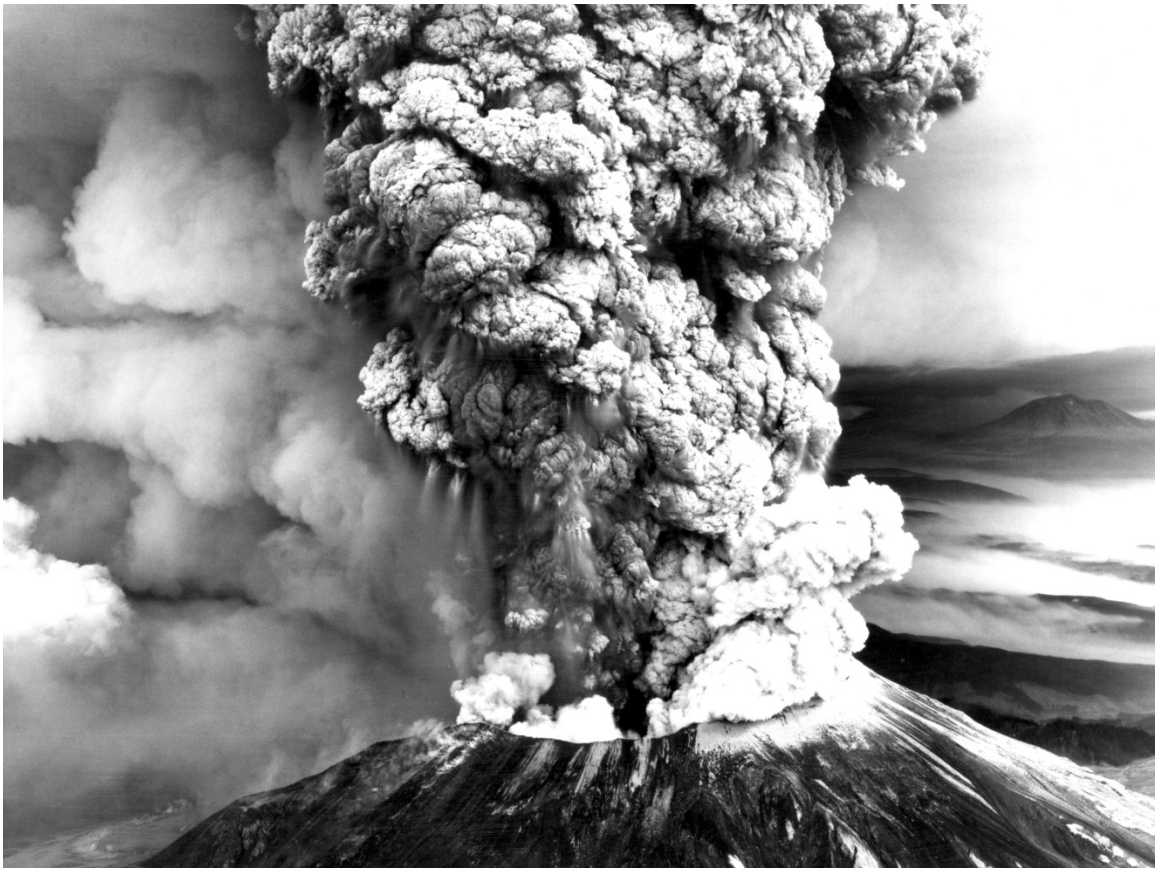

Photograph: Krimmel, USGS

Eddy sizes (m)				
633	441	560	534	376
572	614	614	798	679
737	330	560		

Photograph: USGS

Eddy sizes (m)				
496	564	551	537	1019
633	1046			

Photograph: Werth, Longview Daily News

Eddy sizes (m)				
518	570	484	345	587
570	484	345	380	

Photograph: Haller, Seattle Times

Eddy sizes (m)				
617	740	642	666	666
444	642	469	469	790

B3 Eruption Column

Photograph: Cloud and Aerosol Research Group, University of Washington

Eddy sizes (m)				
451	424	478	547	369
656	369	519	232	437

Photograph: USGS

Eddy sizes (m)				
538	382	478	335	406
287	526	370	741	299
275	358	394	418	382
526	335	299		

Photograph: Rose, USGS

Eddy sizes (m)				
559	320	261	484	365
373	730	566	507	283
536	663	551	596	313

Photograph: Post, USGS

Eddy sizes (m)				
272	352	566	235	283
181	219	368	251	213
187	208	208	229	390
181	342	310	224	342
213	278	246	213	336
411	171	213	219	

Photograph: National Park Service

Eddy sizes (m)				
450	711	669	661	443
570	479	535	457	605
725	493	486	704	584
556	739	556	415	

Photograph: National Park Service

Eddy sizes (m)				
393	377	228	178	238
436	456	360	149	324
317	370	406		

Photograph: USGS

Eddy sizes (m)				
222	459	412	412	301
253	190	364	317	301
459	301	523	491	333
222	364			

References

Abramoff, M.D., Niessen, W.J., and Viergever, M.A., 2000. Objective quantification of the motion of soft tissues. IEEE TMI. 2000, 19: 986-995.

Anderson, D.J. and Lindsley, D.H., 1988. Internally consistent solution models for Fe-Mg-Mn-Ti oxides. Am. Mineral., 73: 714-726.

Anderson, D.J., Lindsley, D.H., and Davidson, P.M., 1993. QUILF: a Pascal program to assess equilibria among Fe-Mg-Mn-Ti oxides, pyroxenes, olivine, and quartz. Computers and Geosciences, 19: 1333-1350.

Andrews, B.J., 2004. Eruption dynamics of the ca. 240 A.D. eruption of Ksudach Volcano, Kamchatka. M.S. Thesis, University of Alaska Fairbanks.

Andrews, B.J., J.E. Gardner, and T. Housh, 2005. Long-term magma recharge recorded in 87Sr/86Sr zonation in plagioclase phenocrysts, El Chichon, Mexico. EOS, American Geophysical Union Fall Meeting Supplement.

Andrews, B.J., Gardner, J.E., Tait, S., Ponomareva, V., and Melekestsev, I.V., 2007. Dynamics of the 1800 ^{14}C yr BP caldera-forming eruption of Ksudach Volcano, Kamchatka, Russia. Geophysical Monograph, 172: 325-342.

Andrews, B.J., J.E. Gardner, and T. Housh, 2008. Repeated recharge, assimilation, and hybridization n magmas erupted from El Chichón as recorded by plagioclase and amphibole phenocrysts. J. Volcanol. Geotherm. Res., 175: 415-426.

Bachman, O., and M.A. Dungan, 2002. Temperature-induced Al-zoning in hornblendes of the Fish Canyon magma, Colorado. American Mineralogist, 87, 1062-1076.

Bacon, C.R. and Hirschmann, M.M., 1988. Mg/Mn partitioning as a test for equilibrium between coexisting Fe-Ti oxides. Am. Mineral., 73: 57-61.

Bacon, C.R., 1983. Eruption history of Mount Mazama and Crater Lake caldera, Cascade Range, U.S.A. J. Volcanol. Geotherm. Res., 18: 57-115.

Beard, B.L., and F. Albarède, 2004. Analytical methods for non-traditional isotopes, in: Johnson, C.M., Beard, B.L., and Albarède, F. (Eds.). Geochemistry of Non-Traditional Stable Isotopes, Reviews in Mineralogy & Geochemistry. Mineralogical Society of America, vol. 55, pp. 113-152.

Belkin, H.E., J.J. McGee, and R.I. Tilling, 1984. Plagioclase zonation as an indicator of the magmatic history of El Chichón volcano, Chiapas, Mexico. Geological Society of America, Abstracts with Programs, 16: 442.

Bernard, P.S. and Wallace, J.M., 2002. *Turbulent Flow: Analysis, Measurement, and Prediction*. John Wiley and Sons, Hoboken.

Braitseva, O.A., Melekestsev, I.V., Ponomareva, V.V., and Kirianov, V.Yu., 1996. The caldera-forming eruption of Ksudach volcano about cal. A.D. 240: the greatest explosive event of our era in Kamchatka, Russia. J. Volcanol. Geotherm. Res., 70: 49-65.

Browne, B.L., J.E. Gardner, J. Larsen, 2003. Amphibole reaction rims in response to decompression compared to heating: an experimental approach. EOS, American Geophysical Union Fall Meeting Supplement.

Carey, S. and Sigurdsson, H., 1985. The May 18, 1980 eruption of Mount St. Helens: 2. Modeling of dynamics of the Plinian Phase. J. Geophys. Res., 90: 2948-2958.

Carey, S., Sigurdsson, H., Gardner, J.E., and Criswell, W., 1990. Variations in column height and magma discharge during the May 18, 1980 eruption of Mount St. Helens. J. Volcanol. Geoth. Res., 43: 99-112.

Carslaw, H.S. and J.C. Jaeger, 1959. Conduction of heat in solids. Clarendon Press, Oxford, 510 p.

Castro, J.M. and Gardner, J.E., 2008. Did magma ascent rate control the explosive-effusive transition at the Inyo volcanic chain, California? Geology, 36: 279-282.

Christiansen, R. L. and Peterson, D.W., 1981. Chronology of the 1980 activity of Mount Saint Helens, Washington. USGS Prof. Paper, 1250: 17-30.

Cortes, J.A., M. Wilson, E. Condliffe, L. Francalanci, and D.G. Chertkoff, 2005. The evolution of the magmatic system of Stromboli Volcano during the Vancori Period (26-13.8 k.y.). J. Volcanol. Geotherm. Res., 147: 1-38.

Costa, F., S. Chakraborty, and R. Dohmen, 2003. Diffusion coupling between trace and major elements and a model for calculation of magma residence times using plagioclase. Geochim. Cosmochim., 67: 2189-2200.

Criswell, W., 1987. Chronology and pyroclastic stratigraphy of the May 18, 1980, eruption of Mount St. Helens, Washington. J. Geophys. Res., 92 B10: 10,237-10,266.

Damon, P. and E. Montesinos, 1978. Late Cenozoic volcanism and metallogenesis over and active Benioff Zone in Chiapas, Mexico. Arizona Geological Society Digest, 11: 155-168.

Davidson, J., F.J. Tepley, Z. Palacz, and S. Meffan-Main, 2001. Magma recharge, contamination and residence times revealed by *in situ* laser ablation isotopic analysis of feldspar in volcanic rocks. Earth and Planetary Science Letters, 184: 427-442.

DePaolo, D.J., 1981. Trace element and isotopic effects of combined wallrock assimilation and fractional crystallization. Earth and Planetary Science Letters, 53: 189-202.

Druitt, T.H., and Sparks, R.S.J., 1984. On the formation of calderas during ignimbrite eruptions. Nature, 310: 679-681.

Duffield, W.A., R.I. Tilling, and R. Canul, 1984. Geology of El Chichón Volcano, Chiapas, Mexico. J. Volcanol. Geotherm. Res., 20: 117-132.

Espindola, J.M., J.L. Macias, R.I. Tilling, and M.F. Sheridan, 2000. Volcanic history of El Chichón Volcano (Chiapas, Mexico) during the Holocene, and its impact on human activity. Bull. Volcanol., 62: 90-104.

Galer, S.J.G., and W. Abouchami, 1998. Practical application of lead triple spiking for correction of instrumental mass discrimination. V.M. Goldschmidt Conference; extended abstracts. Mineralogical Magazine, 62A: 491-492.

Gardner, J.E. and Tait, S., 2000. The caldera-forming eruption of Volcano Ceboruco, Mexico. Bull. Volcanol., 62: 20-33.

Gardner, J.E., S. Carey, M.J. Rutherford, and H. Sigurdsson, 1995a. Petrologic diversity in Mount St. Helens dacites during the last 4,000 years; implications for magma mixing. Contributions to Mineralogy and Petrology, 119: 224-238.

Gardner, J.E., M Rutherford, S. Carey, and H Sigurdsson, 1995b. Experimental constraints on pre-eruptive water contents and changing magma storage Prior to explosive eruptions of Mount St. Helens Volcano. Bull. Volcanol., 57: 1-17.

Gilletti, B.J., and J.E.D. Casserly, 1994. Strontium diffusion kinetics in plagioclase feldspars. Geochim. Cosmochim., 58: 3785-3793.

Ginibre, C., A. Kronz, and G. Wörner, 2002. High-resolution quantitative imaging of plagioclase composition using accumulated backscattered electron images: new constraints on oscillatory zoning. Contributions to Mineralogy and Petrology, 142: 436-448.

Gioncada, A., R. Mazzuoli, and A.J. Milton, 2005. Magma mixing at Lipari (Aeolian Islands, Italy): Insights from textural and compositional features of phenocrysts. J. Volcanol. Geotherm. Res., 145: 97-118.

Gonnermann, H. and Manga, M., 2007. The fluid mechanics inside a volcano: Annual Review of Fluid Mechanics, 39: 321-356.

Hammer, J.E., Cashman, K.V., Hoblitt, R.P., and Newman, S., 1999. Degassing and microlite crystallization during pre-climactic events of the 1991 eruption of Mt. Pinatubo, Philippines. Bull. Volcanol., 60: 355-380.

Hildreth, W. and Mahood, G.A., 1986. Ring-fracture eruption of the Bishop Tuff. Geol. Soc. Am. Bull., 97:396-403.

Hildreth, W., 1983. The compositionally zoned eruption of 1912 in the valley of Ten Thousand Smokes, Katmai National Park, Alaska. J. Volcanol. Geotherm. Res., 18: 1-56.

Hinch, E.J. and Acrivos, A., 1980. Long slender drops in a simple shear flow. J. Fluid Mech., 98: 305-328.

Hobden, B.J., B.F. Houghton, J.P. Davidson, and S.D. Weaver, 1999. Small and short-lived magma batches at composite volcanoes; time windows at Tongariro Volcano, New Zealand. J. Geol. Soc. London, 156: 865-868.

Holland, T., and J. Blundy, 1994. Non-ideal interactions in calcite amphiboles and their bearing on amphibole-plagioclase thermometry. Contributions to Mineralogy and Petrology, 116: 433-447.

Holtz, F., H. Sato, J. Lewis, H. Behrens, and S. Nakada, 2005. Experimental petrology of the 1991-1995 Unzen dacite, Japan: Part I, phase relations, phase compositions and pre-eruptive conditions. J. Petrol., 46: 319-337.

Housh, T. and T.P. McMahon, 2000. Ancient isotopic characteristics of Neogene Potassic magmatism in western New Guinea (Irian Jaya, Indonesia). Lithos, 50: 217-239.

Huppert, H.E. and R.S.J. Sparks, 1980. The fluid-dynamics of a basaltic magma chamber replenished by influx of hot, dense ultrabasic magma. Contributions to Mineralogy and Petrology, 75: 279-289.

Jaupart, C., 2000. Magma ascent at shallow levels, in: Sigurdsson, H., Houghton, B.F., McNutt, S.R., Rymer, H., Stix, J. (Eds.), Encylopedia of Volcanoes, 237-248.

Kaminski, E., Tait, S., and Carazzo, G., 2005. Turbulent entrainment in jets with arbitrary buoyancy. J. Fluid Mech., 526: 361-376.

Klug, C. and Cashman, K.V., 1994. Vesiculation of May 18, 1980, Mount St. Helens magma. Geology, 22: 468-472.

Larsen, J.F., 2005. Experimental study of *plagioclase* rim growth around anorthite seed crystals in rhyodacitic melt. American Mineralogist, 90: 417-427.

LeBas, M.J., R.W. LeMaitre, A. Streckeisen, and B.A. Zanettin, 1986. Chemical classification of volcanic rocks based on the total alkali-silica diagram. J. Petrol., 27: 745-750.

Lipman, P.W., 2000. Calderas, in: Sigurdsson, H., Houghton, B.F., McNutt, S.R., Rymer, H., Stix, J. (Eds.), Encylopedia of Volcanoes, 643-662.

Macias, J.L., J.L. Arce, J.C. Mora, J.M. Espindola, R. Saucedo, and P. Manetti, 2003. A 550-year-old Plinian eruption at El Chichón Volcano, Chiapas, Mexico; explosive volcanism linked to reheating of the magma reservoir. J. Geophys. Res., 108: B12.

Mangan, M. and Sisson, T., 2005. Evolution of melt-vapor surface tension in silicic volcanic systems: Experiments with hydrous melts. J. Geophys. Res., 110, B01202: doi:10.1029/2004JB003215.

Mastin, L.G. and Ghiorso, M.S., 2000. A numerical program for steady-state flow of magma-gas mixtures through vertical eruption conduits. USGS Open-File Report 00-209.

Mastin, L.G., 2002. Insights into volcanic conduit flow from an open-source numerical model. Geochem. Geophys. Geosyst., 3(7), 10.1029/2001GC000192

McGee, J.J., R.I. Tilling, and W.A. Duffield, 1987. Petrologic characteristics of the 1982 and pre-1982 eruptive products of El Chichón Volcano, Chiapas, Mexico. Geofisica International, 26: 85-108.

McGimsey, R.G. and Dorava, J.M., 1994. Video of the August 18,1992, eruption of Crater Peak Vent on Spurr Volcano, Alaska. U.S. Geological Survey Open-File Report 94-614.

Moore, G., Vennemann, T., and Carmichael, I.S.E., 1998. An empirical model for the solubility of H_2O in magmas to 3 kilobars. Am. Mineral., 83: 36-42.

Nakamura, M. and S. Shimakita, 1998. Dissolution origin and syn-entrapment compositional change of melt inclusions in plagioclase. Earth and Planetary Science Letters, 161, 119-133.

Neri, A., Esposito Ongaro, T., Macedonio, G., and Gidaspow, D., 2003. Multiparticle simulation of collapsing volcanic columns and pyroclastic flow. J. Geophys. Res., 108, doi: 10.1029/2001JB000508.

Newman, S., Stolper, E.M., and Epstein, S., 1986. Measurements of water in rhyolitic glasses: calibration of an infrared spectroscopic technique. Am. Mineral., 71: 1527-1541.

Ogden, D.E., Glatzmaier, G.A., and Wohletz, K.H., 2008. Effects of vent overpressure on buoyant eruption columns: Implications for plume stability. Ear. Planet. Sci. Lett., 268: 283-292.

Pallister, J.S., Hoblitt, R.P., and Reynes, A.G., 1992. A basalt trigger for the 1991 eruptions of Pinatubo Volcano? Nature, 356: 426-428.

Pallister, J.S., Hoblitt, R.P., Meeker, G.P., Knight, R.J., and Siems, D.F., 1996. Magma mixing at Mount Pinatubo: petrographic and chemical evidence from the 1991 deposits, in: Newhall, C.G., Punongbayan, R.S. (Eds.), Fire and Mud: eruptions and lahars of Mount Pinatubo, Philippines, 687-731.

Ramos, F.C., J.A. Wolff, and D.L. Tollstrup, 2005. Sr isotopes disequilibrium in Columbia River flood basalts; evidence for rapid shallow-level open-system processes. Geology Boulder, 33: 457-460.

Roche, O., and Druitt, T.H., 2001. Onset of caldera collapse during ignimbrite eruptions. Earth Planet. Sci. Lett., 191: 191-202.

Rose, W.I., Jr., T.J. Bornhorst, S.P. Halsor, W.A. Capaul, P.S. Plumley, S. de la Cruz-Reyna, M. Mena, and R. Mota, 1984. Volcán El *Chichón*, Mexico; pre-1982 S-rich eruptive activity. J. Volcanol. Geotherm. Res., 23: 147-167.

Rust, A.C. and Manga, M., 2002. Bubble shapes and orientations in low Re simple shear flow. J. Colloid Int. Sci.., 249: 476-480.

Rutherford, M.J., Sigurdsson, H., Carey, S., and Davis, A., 1985. The May 18, 1980, eruption of Mount St. Helens; 1, Melt composition and experimental phase equilibria. J. Geophys. Res., 90: 2929-2947.

Scott, W.E., Hoblitt, R.P., Torres, R.C., Self, S., Martinez, M.M.L., and Nillos, T. Jr., 1996. Pyroclastic flows of the June 15, 1991, climactic eruption of Mount Pinatubo, in: Newhall, C.G., Punongbayan, R.S. (Eds.), Fire and Mud: eruptions and lahars of Mount Pinatubo, Philippines, 545-570. Univ. Washington Press, Seattle.

Sigurdsson, H., and Carey, S., 1989. Plinian and co-ignimbrite tephra fall from the 1815 eruption of Tambora volcano. Bull. Volcanol., 51: 243-270.

Snyder, D., 2000. Thermal effects of the intrusion of basaltic magma into a more silicic magma chamber and implications for eruption triggering. Earth and Planetary Science Letters, 175: 257-273.

Sparks, R.S.J., Sigurdsson, H., and Wilson, L., 1977. Magma mixing; a mechanism for triggering acid explosive eruptions. Nature, 267: 315-318.

Sparks, R.S. J., 1986. The dimensions and dynamics of volcanic eruption columns. Bull. Volcanol., 48: 3-15.

Sparks, R.S.J., Bursik, M.I., Thomas, R.M.E., and Carey, S.N., 1992. Sedimentation of tephra by volcanic plumes. Part 2: controls on thickness and grain-size variations of tephra fall deposits. Bull. Volcanol., 54: 685-695.

Spera, F.J. and W.A. Bohrson, 2004. Open-system magma chamber evolution: an energy-constrained geochemical model incorporating the effects of concurrent

eruption, recharge, variable assimilation and fractional crystallization (EC-E'RAχFC). J. Petrol., 45: 2459-2480.
Spera, F.J., 2000. Physical properties of magmas. in: Sigurdsson, H., Houghton, B.F., McNutt, S.R., Rymer, H., Stix, J. (Eds.), Encylopedia of Volcanoes, 171-190.
Stolper, E.M., 1982. Water in silicate glasses; an infrared spectroscopic study. Cont. Min. Petrol., 81: 1-17.
Stormer, J.C., 1983. The effects of recalculation on estimates of temperature and oxygen fugacity from analyses of multicomponent iron-titanium oxides. Am. Mineral., 68: 586-594.
Suzuki, Y.J., Koyaguchi, T., Ogawa, M., and Hachisu, I., 2005. A numerical study of turbulent mixing in eruption clouds using a three-dimensional fluid dynamics model. J. Geophys. Res., 110, doi: 10.1029/2004JB003460.
Suzuki-Kamata, K., Kamata, H., and Bacon, C.R., 1993. Evolution of the caldera-forming eruption at Crater Lake, Oregon, indicated by component analysis of lithic fragments. J. Geophys. Res., 98: 14059-14074.
Tepley, F.J., J. Davidson, and M.A. Clynne, 1999. Magmatic interactions recorded in plagioclase phenocrysts of Chaos Crags, Lassen Volcanic Center, California. J. Petrol., 40: 787-806.
Tepley, F.J., J. Davidson, R.I. Tilling, and J.G. Arth, 2000. Magma mixing, recharge and eruptive histories recorded in plagioclase phenocrysts from El Chichón Volcano, Mexico. J. Petrol. 41, 1397-1411.
Tilling, R.I., M. Rubin, H. Sigurdsson, S. Carey, W.A. Duffield, and W.I. Rose, 1984. Holocene eruptive activity of El Chichón volcano, Chiapas, Mexico. Science, 224: 747-749.
Tsuchiyama, A. and E. Takahashi, 1983. Melting kinetics of a plagioclase feldspar. Contributions to Mineralogy and Petrology, 84: 345-354.
Tsuchiyama, A., 1985. Dissolution kinetics of plagioclase in the melt of the system diopside-albite-anorthite, and origin of dusty plagioclase in andesites. Contributions to Mineralogy and Petrology, 89: 1-16.
Turcotte, D.L. and G. Schubert, 2002. Geodynamics. Cambridge University Press, New York, 456 p.
Volynets, O.N., V.V. Ponomareva, O.A. Braitseva, I.V. Melekestsev, and C.H. Chen, 1999. Holocene eruptive history of Ksudach volcanic massif, South Kamchatka; evolution of a large magmatic chamber. J. Volcanol. Geotherm. Res., 91: 23-42.
Waitt, R.B. and Dzurisi, D., 1981. Proximal air-fall deposits from the May 18 eruption – stratigraphy and field sedimentology. USGS Prof. Paper, 1250: 601-616.
Wilson, C.J.N., and Hildreth, W., 1997. The Bishop Tuff: new insights from eruptive stratigraphy. J. Geology, 105: 407-439.
Wombacher, F. and M. Rehkämper, 2003. Investigation of the mass discrimination of multiple collector ICP-MS using neodymium isotopes and the generalized power law. J. Analytical Atomic Spectroscopy, 18:1371-1375.

Woods, A., 1995. The dynamics of explosive volcanic eruptions. Rev. Geophys., 33: 495-530.

Zellmer, G.F., C. Annen, B.L.A. Charlier, R.M.M. George, S.P. Turner, and C.J. Hawkesworth, 2005. Magma evolution and ascent at volcanic arcs; constraining petrogenetic processes through rates and chronologies. J. Volcanol. Geotherm. Res., 140: 171-191.

Zellmer, G.F., R.S.J. Sparks, C.J. Hawkesworth, and M. Wiedenbeck, 2003. Magma emplacement and remobilization timescales beneath Montserrat: Insights from Sr and Ba zonation in plagioclase phenocrysts. J. Petrol., 44: 1413-1431.

Zhang, Y., Belcher, R., Ihinger, P.D., Wang, L., Xu, Z., and Newman, S., 1997. New calibration of infrared measurement of dissolved water in rhyolitic glasses. Geochim. Cosmochim., 61: 3089-3100.

Vita

Benjamin James Andrews attended Cleveland High School, Portland, Oregon. In 1998 he entered the University of Oregon Honors College in Eugene, Oregon. During 2001 he attended the University of Otago in Dunedin, New Zealand as an exchange student. He received the degree Bachelor of Science (Hon.) in Geology from the University of Oregon Honors College in March 2002. In August 2002 he entered the University of Alaska Fairbanks Graduate School and in August 2004 received a Master of Science in Geology. In September 2004, he entered the Graduate School at the University of Texas at Austin.

Permanent address: 2533 S.E. Taylor, Portland, OR 97214

This dissertation was typed by the author.